Universidade do Algarve

Paleoenvironmental and paleoceanographic changes recorded in the marine and nearshore sediments in the Lower Cretaceous Arrifes sequence, Albufeira, Algarve Basin, Portugal

Gabrielle Sofia Descamps

Tese

Mestrado de Sistemas Marítimos e Costeiros /
Marine and Coastal systems (MaCS)

Trabalho efetuado sob a orientação de:

Paulo Fernandes e Gilda Lopes

2021

Gabrielle Sofia Descamps

Paleoenvironmental and paleoceanographic changes recorded in the marine and nearshore sediments in the Lower Cretaceous Arrifes sequence, Albufeira, Algarve Basin, Portugal

Marine and Coastal Systems — Master thesis

Supervisor: Professor Paulo Fernandes

(FCT, Universidade do Algarve)

Co-supervisor: PhD Gilda Lopes

(FCT, Universidade do Algarve)



Universidade do Algarve

Faculdade de Ciências e Tecnologia

2021

Paleoenvironmental and paleoceanographic changes recorded in the marine and nearshore sediments in the Lower Cretaceous Arrifes sequence, Albufeira, Algarve Basin, Portugal

---

Declaração de autoria de trabalho/ Declaration of authorship of the work

Declaro ser a autora deste trabalho, que é original e inédito. Autores e trabalhos consultados estão devidamente citados no texto e constam da listagem de referências incluído.

I declare to be the author of this work, which is original and unprecedented. Consulted authors and works are rightfully cited in the text and are included in the list of references.

Gabrielle Sofia Descamps

Piriac-sur-mer 30 sept. 2021

Copyright

"A Universidade do Algarve tem o direito, perpétuo e sem limites geográficos, de arquivar e publicitar este trabalho através de exemplares impressos reproduzidos em papel ou de forma digital, ou por qualquer outro meio conhecido ou que venha a ser inventado, de o divulgar através de repositórios científicos e de admitir a sua cópia e distribuição com objetivos educacionais ou de investigação, não comerciais, desde que seja dado crédito ao autor e editor."

"The University of Algarve reserves the right, in accordance with the provisions of the Code of Copyright and Related Rights, to archive, reproduce and publish the work, regardless of the medium used, as well as to disseminate it through scientific and technical repositories and to admit its copy and distribution for purely educational or research and non-commercial purposes, as long as due credit is given to the respective author and editor."

Abstract

This project focuses on the Late Hauterivian to Late Barremian sedimentary succession that outcrops at Arrifes, southwest of Albufeira (southern Portugal). The aim is to study the forcing mechanisms (sedimentological, climatic, oceanographic and biological) that are recorded in the stratigraphic succession of Arrifes. A detailed stratigraphic log of the sequence was established to interpret the different sedimentary facies, their relations and evolution. This task was necessary to guide the sampling used for geochemical and palynological studies, including the study of palynofacies, and the biostratigraphic studies of dinoflagellate cysts. The latter study allowed dating of the Arrifes succession of Late Hauterivian to Late Barremian age. The depositional age constrained also the paleoenvironmental, paleoceanographic (including eustasy) and paleoclimatic changes observed in the Arrifes sequence. Geochemical analysis of whole-rock and carbon stable isotopes was also used to characterise paleoenvironmental and paleoclimatic conditions.

During Lower Cretaceous times, the Arrifes succession experienced shifts between wet climates in the Late Hauterivian, increasing aridity in the Early Barremian and again wet climates during the Late Barremian. Multiple sea-level fluctuations occurred during this time interval, but overall the depositional environments were of tide dominated nearshore carbonate environments. During the peak of transgressive phases, deep water offshore facies were also established. The $\delta^{13}C_{org}$ curve indicates the presence of several moderate negative excursions during Barremian times. These excursions are tentatively related to the deposition of marine organic-rich sediments, mainly induced by oceanographic conditions of sea-level rises or induced by climatic consequences such as density stratification or increased continental flows to the ocean, rather than deposition influenced by an Oceanic Anoxia Event (OAE), since no such event has been identified for Barremian age. However, the Late Hauterivian shows a strong negative values of $\delta^{13}C_{org}$, at the base of the stratigraphic succession, it could be tentatively related to the Faraoni OAE (F-OAE). Moreover, the sedimentology, age and geochemical features of the Arrifes succession are similar to the Salema and the Barrancão formations located in the western Algarve Basin, and can therefore be correlated which each other.

Keywords: *Algarve Basin; Early Cretaceous; Paleoclimate; Eustatism; Oceanic anoxia; Stratigraphy; Palynology; Geochemistry*

Resumo

O estudo do registo sedimentar permite a reconstrução das condições ambientais do passado relacionadas com as alterações climáticas globais e as variações eustáticas associadas. As sequências estratigráficas também fornecem informações sobre eventos marinhos anóxicos do passado, paleotemperaturas, actividade e evolução biológica. A sedimentação do Cretáceo Inferior na Bacia do Algarve, foi controlada principalmente por várias fases de alterações do nível do mar Este projecto irá concentrar-se na sucessão sedimentar de idade Hauteriviano a Barremiano superior que aflora entre a Praia da Baleeira e a Praia dos Arrifes a sudoeste de Albufeira (sul de Portugal). São investigados os mecanismos de forçamento (sedimentológico, climático, oceanográfico e biológico) e o seu registo na sucessão estratigráfica dos Arrifes.

Foi estabelecido um registo estratigráfico detalhado da sequência para interpretar as diferentes facetas sedimentares, as suas relações e evolução. Esta tarefa foi necessária para orientar a amostragem utilizada para estudos palinológicos e geoquímicos. Os estudos palinológicos, incluiu o estudo de palinofacies, e biostratigráficos de dinoflagelados. Este último permitiu a datação da sucessão dos Arrifes de idade Hauteriviano a Barremiano superior. A idade deposicional condicionou também as alterações paleoambientais, paleoceanográficas (incluindo as variações eustáticas) e paleoclimáticas observadas na sucessão dos Arrifes. As análises geoquímicas de rocha total e isotópos estávceis de carbono em matéria orgânica, foi também utilizada para caracterizar as condições paleo-ambientais e paleoclimáticas.

Os objectivos estabelecidos no início do projecto foram alcançados. Em primeiro lugar a datação palinológica de Mendes et al. (em preparação) foi necessária para a correcta idade geológica da sucessão permitindo fazer correlações mais precisas com a estratigrafia do Cretácico da Bacia do Algarve melhores conhecida e formalizada. Assim, a sequência podia ser dividida em três idades diferentes, desde a mais antiga até à mais nova: (1) Hauteriviano tardio ao Barremiano inferior; (2) Barremiano inferior ao Barremian médio; e (3) Barremian superior. Todas as técnicas analíticas eram complementares e permitiam conclusões gerais sobre as condições ambientais, paleoclimáticas e paleoceanográficas que controlavam a deposição da sequência estratigráfica de Arrifes.

Ambiente deposicional: A análise detalhada das litofácias permitiu o reconhecimento dos principais ambientes deposicionais, e como evoluíram ao longo do tempo de deposição. Os principais ambientes deposicionais são representados por sedimentos intertimareais de águas pouco profundas, representando 107,5m de espessura ou 55,5% da espessura total da sucessão de Arrifes. As condições offshore moderadamente profundas são as segundas mais dominantes (23%), seguidas pelas supramareais (17,1%), e finalmente, o domínio offshore

profundo representa apenas 3,4%. Assim, pode afirmar-se que a sequencia estratigráfica dos Arrifes, durante o Hauteriviano superior ao Barremiano superior, foi ambientes costeiros geralmente pouco profundo, incluindo alguns sedimentos de águas profundas relativamente associados ao pico das fases transgressivas (subida do nível do mar).

Paleoclima: Os dados geoquímicos de rocha total e complementados com o trabalho de Dinis et al. (2020), indicam que o clima foi relativamente quente, mas sofreu alterações do regime de humidade. Passou de relativamente húmido para árido na fronteira Hauteriviano - Barremiano (132,9My), marcado pela ocorrência e dominância de fitoclastos opacos, e depois mudou para condições mais húmidas durante o Barremiano superior. Estas podem ser correlacionadas com eventos geológicos regionais e globais descritos para este período de tempo geológico.

Paleoceanográfica e alterações associadas a variações do nível do mar: O nível do mar sofreu numerosas flutuações que tiveram um efeito profundo na sequência estratigrafica dos Arrifes. Os ambientes deposicionais oscilaram principalmente entre ambientes intertimareais - submareais e ambientes offshore ou supramareais-intermareais. O Hauterivian superior é marcado por uma fase transgressiva, enquanto o registo geológico do Barremiano inferior indica uma tendência regressiva, tal como descrito para este período a nível global. Contudo, o Barremiano superior foi o intervalo de tempo mais marcado por condições offshore, incluindo facies sedimentares indicadoras de maior profundidade (>50m de coluna de água), indicando uma tendência de aprofundamento e períodos prolongados em que os ambientes submareais dominaram.

Evento de Anoxia Oceânica (EAO): Poucos EOAs puderam ser detectadas nos Arrifes a sequência, e as suas origens diferem umas das outras. O EAO descrito no Hauteriviano superior está provavelmente relacionada com o evento de EAO global de Faraoni (F-OAE), que perturbou muitos ecossistemas marinhos à escala global. No Barremiano médio, o clima árido e a baixa precipitação abrandaram fortemente a circulação termohalina, causando estratificação da densidade da coluna de água e esgotamento do oxigénio dissolvido no fundo do mar. Quanto ao período húmido do Barremianao superior, as acumulações de matéria orgânica nos sedimentos não foram induzidas pelos mesmos mecanismos forçadores, com (1) condições de deposição offshore; (2) uma taxa de sedimentação excepcionalmente elevada de matéria orgânica, o que favoreceu a sua preservação nos sedimentos; (3) taxas elevadas de meteorização continental, aumentando os fluxos de nutrientes que provocaram a fenómenos de eutrofização em ambientes costeiros, aumentando fortemente a procura de oxigénio dissolvido, e consequentemente o seu esgotamento; ou (4) fases de transgressão criadas em bacias epicontinentais pouco

profundas, causando um crescimento excepcional das plataformas carbonatadas que também aumentaram a procura de oxigénio dissolvido na água.

Biodiversidade: Os ambientes marinhos pouco profundos e relativamente profundos de águas quentes carbonatadas, permitiram que muitas plataformas carbonatadas ricas em lamas carbonatadas se estabelecessem. Isto é particularmente verdade durante as fases de transgressão quando a subida do nível do mar inunda o continente, criando ambientes quentes relativamente profundos. Além disso, a presença recorrente de bioturbação e.g.pistas de Talassinóides, ndica que o substrato foi regularmente oxigenado, permitindo que os organismos bentónicos florescessem.

A sequência de Arrifes na Bacia do Algarve: A geoquímica de rocha total indicam condições semelhantes de meteorização e reciclagem sedimentar, entre a sucessão de Arrifes e as formações de Salema e Barrancão. Isto sugere contemporaneidade entre as duas sequencias, aspecto que é confirmado pela nova era palinológica. Esta correlação é ainda apoiada pelo facto de a Formação de Salema ser também caracterizada por carbonatos depositados em águas pouco profundas com influência da marés.

Palavras-chave: *Bacia do Algarve; Cretáceo pInferior; Paleoclima; Eustacia; Evento Oceânico Anóxico; Estratigrafia; Palinologia; Geoquímica*

Acknowledgements

This study was supported by the Centro de Investigação Marinha e Ambiental (CIMA, Center for Marine and Environmental Research) and the Laboratório Nacional de Energia e Geologia (LNEG, National Laboratory of Energy and Geology), which made it possible to obtain the necessary data for the project, as well as by the Universidade do Algarve (University of the Algarve), which offers the international Master's degree in Marine and Coastal Systems (MaCS).

I would like to warmly thank my thesis supervisor Paulo Manuel Carvalho Fernandes, for his availability, his know-how, his human qualities and his judicious advices which contributed to my reflection. I will remember with pleasure and nostalgia the field and laboratory days with him. Furthermore, I am very grateful to my co-supervisor Gilda Lopes, for being very available, for taking the time to explain many concepts and for providing multiple interpretative figures. Their knowledge, experience and corrections helped to push the work and writing of this thesis to a higher level.

In addition, I would like to express my gratitude to Márcia Mendes and Zélia Pereira, based at LNEG, who contributed greatly to the study by providing valuable palynological data.

Finally, I would like to thank my dear French friends Anicet, Emile and Marius for having accompanied me in this extraordinary adventure in the magnificent setting of the Ria Formosa. I also thank Alexandre, Ruben, Ruslan and Mama who joined us in this Faro community, as well as all the people I met, especially Catherine, Jacqueline, Rodrigue and so many others, for making these memories unforgettable. Many thanks to my parents who made this experience possible.

Thank you all for the advice, the continuous moral support and encouragement.

Indexes

List of contents

Abstract 1

Resumo 2

Acknowledgements 5

Indexes 6

List of contents 6

List of figures 8

List of tables 9

List of appendices....9

List of abbreviations 11

(Extra master thesis cover) 13

1. Introduction 14

1.1 Motivation for the topic 14

1.2 Main goals 15

2. State of the art - The Early Cretaceous 17

2.1 Paleogeography....17

2.2 Paleoclimate....19

2.3 Paleoceanography and eustatic sea-level....21

2.4 Oceanic Anoxia Events (OAEs)....25

2.5 Biodiversity....27

2.6 Algarve Basin during Early Cretaceous times 29

3. Study area 32

4. Methods and Materials 35

4.1 Sedimentology 35

4.2 Palynology 38

4.3 Geochemistry 40

5.Results 43
5.1 Sedimentology 43
5.1.1 Facies description 43
5.1.2 Arrifes stratigraphic succession description....48
5.2 Palynological description....57
5.2.1 Palynological dating 57
5.2.2 Palynofacies 58
5.3 Geochemistry 63
5.3.1 Whole-Rock geochemistry 63
5.3.2 Organic Carbon δ13C stable isotopes geochemistry 68
6. Discussion 71
6.1 The Age of the Arrifes stratigraphic succession....71
6.2 Paleoweathering, recycling and sediment sources 73
6.2.1 Paleoweathering indices....73
6.2.2 Paleoweathering conditions 79
6.2.3 Recycling 80
6.2.4 Source of sediments 81
6.3 Arrifes paleoenvironmental conditions 83
6.3.1 Age 1: Late Hauterivian to Early Barremian 86
6.3.2 Age 2: Early Barremian to earliest Late Barremian 87
6.3.3 Age 3: Late Barremian....89
7. Conclusions 93
References 97

List of figures

Figure 1.1.1. Geological Map of the World at 1:35000000, third edition (Bouysse et al., 2014).....15

Figure 2.1.1 Lower Cretaceous paleogeography (after Scotese 2014).....18

Figure 2.2.1 Cretaceous global average temperatures (after Hay and Floegel, 2012) 20

Figure 2.3.1 Characteristics of a storm-dominated shelf environment (after Nichols, 2009).....22

Figure 2.3.2 Facies distribution in a reef complex (after Nichols, 2009).....23

Figure 2.3.3 Stratigraphic time scale associated with the eustatic sea-level fluctuation curve and major Oceanic Anoxia Events (Baudin and Riquier, 2014) 24

Figure 2.4.1 Global paleogeographic distribution of the F-OAE level, its equivalents, and the black shales potentially correlated to this Faraoni event (Baudin and Riquier, 2014) 27

Figure 2.6.1 Algarve Basin location (after Ramos et al., 2016) 29

Figure 2.6.2 Simplified map showing major tectonic features, which have had different behaviour since the Late Triassic (after Ramos et al., 2016).....29

Figure 2.6.3 Map of Cretaceous outcrops in Algarve (in grey) (after Rey, 1986) 30

Figure 3.1 Location of the study area in the Algarve Basin (Google Earth pro, 2021) 32

Figure 3.2 Cross section of two onshore salt related structures including the Albufeira Diapir. Evaporite thickness is controlled by the extensional Algibre Fault; Restoration at Early Cretaceous times (after Ramos et al., 2017) 33

Figure 3.3 Field pictures.....34

Figure 4.1.1 Folk & Dunham carbonates textural classification (1962) (after Wardana, 2016) 36

Figure 4.1.2 Typical geologist's hammer (e.g.) (Estwing, 2021).....37

Figure 4.2.1 Isolated organic residues obtained for P126.1 after preparation 39

Figure 4.2.2 Dinocyst observed under UV light fluorescence 39

Figure 4.3.1 Key steps of protocol for whole-rock geochemistry analysis 41

Figure 5.1.1.1 Arrifes lithofacies and their associated depositional environments 47

Figure 5.1.2.1 Simplified stratigraphic log of Arrifes succession, associate legend and sampling strategy (P: palynology and G: geochemistry) 48

Figure 5.1.2.2 Some fossil pictures to illustrate the field work.....56

Figure 5.2.2.1 Palynofacies results plotted, SP/D data are from Mendes et al. (in preparation).....60

Figure 5.2.2.2 Some pictures to illustrate the microscope work (See Appendix 5 for more). 62

Figure 5.3.1.1.1 Normalised major elements plot, ratios UCC/PAAS, UCC/G1 and UCC/G2 64

Figure 5.3.1.1.2 Normalised trace elements plot, ratios UCC/PAAS, UCC/G1 and UCC/G2.....65

Figure 5.3.1.2.1 Normalised REE plot for G1 and G2 samples 67

Figure 5.3.2.1 Plotted results for organic Carbon δ13C stable isotopes geochemistry in ‰ and Total Organic Content (TOC) in %, the red bars delineate the four segments described below.....69

Figure 6.1.1 Age ranges attributed to Arrifes stratigraphic sequence; FO: First Occurence and LO: Last Occurrence; Leereveld (1997) 71

Figure 6.1.2 Lithostratigraphic scheme for the Lower Cretaceous Algarve Basin (Portugal) by Mendes et al. (in preparation), after Rey (2009) 72

Figure 6.2.1.1 Plotted CIX data, including data from Dinis et al. (2020) 75

Figure 6.2.1.2 Plotted Na2O/Sm data, including data from Dinis et al. (2020) 76

Figure 6.2.1.3 Plotted K2O/Th*1000 data, including data from Dinis et al. (2020) 77

Figure 6.2.1.4 Plotted and description Indices of element mobility (αAlE), including data from Dinis et al. (2020); the detailed data are available in the Appendix 6 78

Figure 6.2.2.1 Paleoweathering plot, including data from Dinis et al. (2020).....80

Figure 6.2.3.1 Sediment's recycling plot, including data from Dinis et al. (2020) 81

Figure 6.2.4.1 Sediments' source plot (1), including data from Dinis et al. (2020) 82

Figure 6.2.4.2 Sediments' source plot (2), including data from Dinis et al. (2020) 82

Figure 6.3.1 Paleoenvironmental reconstruction of the Arrifes stratigraphic sequence 84

Figure 6.3.2 Summary figure coupling the log of Arrifes stratigraphic sequence; the four main depositional environments (1) supratidal, (2) subtidal, (3) offshore, (4) deep offshore; Arrifes relative sea-level curve (R) regression, (T) transgression; the global eustatic sea-level is from Haq (2014); the SP/D ratio curve is from Mendes et al. (in preparation); organic δ13C and Total Organic Content curves from organic geochemistry 85

Figure 7.1.1 Proportion of the depositional environments in the Arrifes succession.....93

List of tables

Table 5.2.2.1 Palynofacies results obtained via microscopic observations, coupled with the SP/D ratio calculated by Mendes et al. (in preparation) 59

Table 5.3.1.1.1 Normalised major elements data, ratios UCC/PAAS, UCC/G1 and UCC/G2 64

Table 5.3.1.1.2 Normalised trace elements data, ratios UCC/PAAS, UCC/G1 and UCC/G2.....65

Table 5.3.1.2.1 Normalised Rare Earth Elements data for G1 and G2 samples 66

Table 5.3.2.1 Results for organic Carbon δ13Corg stable isotopes geochemistry 68

Table 6.2.1.1 Chemical weathering index (CIX), including data from Dinis et al. (2020) 75

Table 6.2.1.2 Na2O/Sm ratio data, including data from Dinis et al. (2020) 76

Table 6.2.1.3 K2O/Th*1000, including data from Dinis et al. (2020) 77

List of appendices

Appendix 1. The Geological Map of the World (Bouysse et al., 2014) 104

Appendix 2. International Chronostratigraphic Chart (Cohen et al., 2013; updated).....105

Appendix 3. Whole-rock geochemistry.....106
Appendix 4. Arrifes stratigraphic log — Details of the layers.....117
Appendix 5.1 Palynology including palynofacies analysis — P002.1 124
Appendix 5.2 Palynology including palynofacies analysis — P003.1 125
Appendix 5.3 Palynology including palynofacies analysis — P005.1 126
Appendix 5.4 Palynology including palynofacies analysis — P008.1 127
Appendix 5.5 Palynology including palynofacies analysis — P017.1 128
Appendix 5.6 Palynology including palynofacies analysis — P020.1 129
Appendix 5.7 Palynology including palynofacies analysis — P028.1 130
Appendix 5.8 Palynology including palynofacies analysis — P030.1 131
Appendix 5.9 Palynology including palynofacies analysis — P032.1 132
Appendix 5.10 Palynology including palynofacies analysis — P066.1 133
Appendix 5.11 Palynology including palynofacies analysis — P071.1 134
Appendix 5.12 Palynology including palynofacies analysis — P077.1 135
Appendix 5.13 Palynology including palynofacies analysis — P081.1 136
Appendix 5.14 Palynology including palynofacies analysis — P085.1 137
Appendix 5.15 Palynology including palynofacies analysis — P089.1 138
Appendix 5.16 Palynology including palynofacies analysis — P095.1 139
Appendix 5.17 Palynology including palynofacies analysis — P097.1 140
Appendix 5.18 Palynology including palynofacies analysis — P106.1 141
Appendix 5.19 Palynology including palynofacies analysis — P108.1 142
Appendix 5.20 Palynology including palynofacies analysis — P114.1 143
Appendix 5.21 Palynology including palynofacies analysis — P120.1 144
Appendix 5.22 Palynology including palynofacies analysis — P124.1 145
Appendix 5.23 Palynology including palynofacies analysis — P126.1 146
Appendix 5.24 Palynology including palynofacies analysis — P130.1 147
Appendix 5.25 Palynology including palynofacies analysis — P134.1 148
Appendix 5.26 Palynology including palynofacies analysis — P138.1 149
Appendix 5.27 Palynology including palynofacies analysis — P140.1 150
Appendix 5.28 Palynology including palynofacies analysis — P153.1 151
Appendix 5.29 Palynology including palynofacies analysis — P155.1 152
Appendix 5.30 Palynology including palynofacies analysis — P158.1 153
Appendix 5.31 Palynology including palynofacies analysis — P152.1 154
Appendix 5.32 Palynology including palynofacies analysis — P152.2 155
Appendix 5.33 Palynology including palynofacies analysis — P154.1 156

Appendix 5.34 Palynology including palynofacies analysis — P166.1 157
Appendix 5.35 Palynology including palynofacies analysis — P168.1 158
Appendix 5.36 Palynology including palynofacies analysis — P160.1 159
Appendix 5.37 Palynology including palynofacies analysis — P162.1 160
Appendix 5.38 Palynology including palynofacies analysis — P164.1 161
Appendix 5.39 Palynology including palynofacies analysis — P173.1 162
Appendix 5.40 Palynology including palynofacies analysis — P173.2 163
Appendix 5.41 Palynology including palynofacies analysis — P173.3 164
Appendix 5.42 Palynology including palynofacies analysis — P175.1 165
Appendix 5.43 Palynology including palynofacies analysis — P175.2 166
Appendix 5.44 Palynology including palynofacies analysis — P176.a 167
Appendix 5.45 Palynology including palynofacies analysis — P176.b 168
Appendix 5.46 Palynology including palynofacies analysis — P178.1 169
Appendix 5.47 Palynology including palynofacies analysis — P181.1 170
Appendix 5.48 Palynology including palynofacies analysis — P193.1 171
Appendix 6.1 Whole-rock geochemistry results 172
Appendix 6.2 Whole-rock geochemistry results 173
Appendix 6.3 Whole-rock geochemistry results 174

List of abbreviations

- **°C:** Celsius degree
- **%wt:** percentage of weight
- **∑REE:** Average of total (sum) of Rare Earth Elements (REEs)
- **αAlE:** Indices of element mobility
- **AOM:** Amorphous Organic Matter
- **As:** Arsenic
- **Al:** Aluminium
- **Al_2O_3:** Alumine *a.k.a.* Aluminium oxyde
- **Ba:** Barium
- **Bi:** Bismuth
- **^{12}C:** Carbon-12 stable isotope
- **^{13}C:** Carbon-13 stable isotope
- **C:** Carbon
- **$CaCO_3$:** Calcium carbonate
- **$[CaFe(CO_3)_2]$:** Ferrodolomite
- **CCD:** Calcite Compensation Depth
- **CFBP's:** Continental Flood Basalt Provinces
- **CH_4:** Methane
- **$[CaMg(CO_3)_2]$:** Dolomite
- **CaO:** Calcium oxyde
- **Cd:** Cadmium
- **CIMA:** Centro de Investigação Marinha e Ambiental
- **CIX:** Chemical weathering index
- **Co:** Cobalt
- **CO_2:** Carbon dioxyde
- **C_{org}:** Organic Carbon
- **Cr:** Chromium
- **Cs:** Cesium
- **Cu:** Copper
- **δ:** Delta (‰ deviation)

- **d:** Density
- **DIC:** Dissolved Inorganic Carbon
- **DOC:** Dissolved Organic Carbon
- **DO:** Dissolved Oxygen
- **Eu:** Europium
- **Fe_2O_3:** Iron oxyde
- **Fe_2O_3(T):** Total Iron oxyde
- **F-OAE:** Oceanic Anoxia Event of Faraoni
- **g:** Gram
- **H:** Hydrogene
- **HCS:** Hummocky-Cross-Stratification
- **HCl:** Hydrochloric acid
- **HF:** Hydrofluoric acid
- **Hf:** Hafnium
- **HFSE:** High Field Strength Elements
- **HREE:** Heavy Rare Earth Elements
- **K:** Potassium
- **K_2O:** Potassium oxyde
- **K-T:** Cretaceous-Tertiary boundary
- **km:** kilometer
- **Ky:** Thousands of years
- **LIP's:** Large Igneous Provinces
- **LNEG:** Laboratório Nacional de Energia e Geologia
- **LREE:** Light Rare Earth Elements
- **m:** Meter
- **MARE:** Centro de Ciências do Mar e do Ambiente
- **Mg:** Magnesium
- **MgO:** Magnesium oxyde
- **mL:** Milliliter
- **mm:** Millimeter
- **MnO:** Manganese oxyde
- **Mo:** Molybdenum
- **My:** Millions years
- **Na_2O:** Sodium oxyde
- **Nb:** Niobium
- **Ni:** Nickel
- **nm:** Nanometer
- **P_2O_5:** Phosphorus pentoxide
- **PAAS:** Post Archaen Australian Shales
- **Pb:** Lead
- **pCO_2:** Pressure carbon dioxyde
- **PDMSL:** Present Day Mean Sea-Level
- **PIA:** Plagioclase weathering index
- **P*xx.x*:** Sample code in this project
- **O:** Oxygene
- **OAE:** Oceanic Anoxia Event
- **OM:** Organic Matter
- **Rb:** Rubidium
- **REE:** Rare Earth Elements
- **S:** Sulfur
- **Sb:** Antimony
- **SiO_2:** Silicium dioxyde
- **Sm:** Samarium
- **SP/D:** Spore-Pollen/Dinokyste ratio
- **Sr:** Strontium
- **Th:** Thorium
- **Tl:** Thallium
- **TiO_2:** Titanium dioxyde
- **TOC:** Total Organic Content
- **µm:** Micrometer
- **U:** Uranium
- **UALG:** Universidade do Algarve
- **UCC:** Upper Continental Crust
- **UV:** Ultraviolet
- **V:** Vanadium
- **Y:** Yttrium
- **Zn:** Zinc
- **Zr:** Zirconium

Gabrielle Sofia Descamps

Paleoenvironmental and paleoceanographic changes recorded in the marine and nearshore sediments in the Lower Cretaceous Arrifes sequence, Albufeira, Algarve Basin, Portugal



Master thesis — 2021

Marine and Coastal Systems
Universidade do Algarve
Faculdade de Ciências e Tecnologia

Supervisor: Paulo Fernandes
(FCT, Universidade do Algarve)
Co-supervisor: Gilda Lopes
(FCT, Universidade do Algarve)

1. Introduction

1.1 Motivation for the topic

Actualism is a fundamental principle of Earth Science that postulates that past events can be explained in the same way as currently observable phenomena (Larousse, 2021). The Cretaceous period (145-66My) presents many environmental changes at the heart of current concerns about climate change, such as global warming, eustatic variations in sea-level or periods of oxygen depletion in the oceans. Indeed, the Cretaceous period experienced an intense prolonged greenhouse effect due to high levels of atmospheric CO_2, a long-term sea-level rise and some notable Oceanic Anoxic Events (OAEs). The latter are, for example, among the hottest topics of the last forty-five years in Sciences. All these phenomena have had, and still have today, influences on sedimentary cycles and biodiversity (Baudin, 2005; Wang et al. 2014; Föllmi, 2012; Hu et al. 2012; Spicer, 2003; Weissert et al. 1998). Thus, the study of Cretaceous sedimentary successions may be suitable for parameterising future climate models (Skelton, 2003).

Studies on this geological period are very abundant (more than one million studies referenced on Google Scholar with the keyword ''Cretaceous''), thanks to the numerous outcrops available around the globe on the continents and on the sea floor. Indeed, there is still a large Cretaceous geological record observable on the ocean floor, as shown on Figure 1.1.1, where Cretaceous rocks are in green. A preliminary study of the paleoclimatic conditions of the Lower Cretaceous Algarve Basin has already been made (Dinis et al., 2020). Rey and Ramalho (1974) compared the facies and stratigraphic position of the Arrifes succession and correlated it with the Luz Formation, dated Aptian-Albian. After a preliminary study of the terrain, it was impossible to make this correlation. Thus, samples were sent for dating *via palynology*, and were used to assign a Late Hauterivian to Late Barremian age. The study by Dinis et al. (2020) is deficient in that it does not discuss any dated sedimentary succession from this period for the central Algarve Basin. The stratigraphic sequence studied in this project meets these criteria and will therefore allow to fill the knowledge gap for this Iberian region.

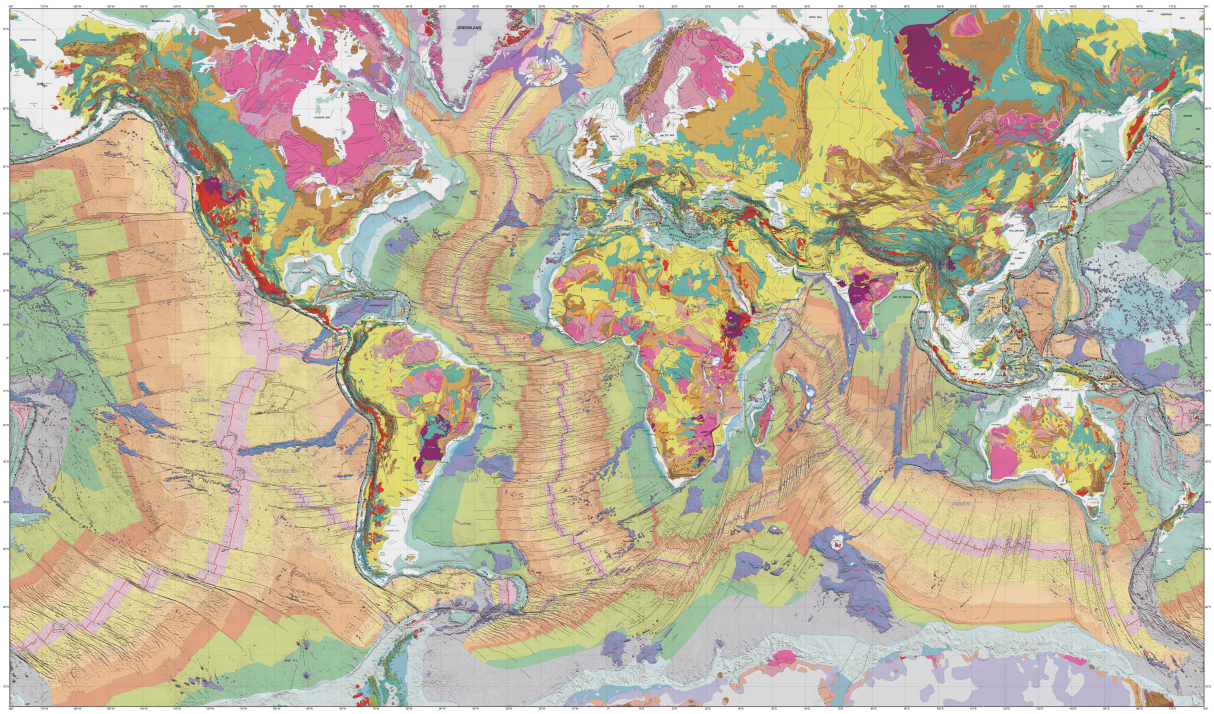


Figure 1.1.1. Geological Map of the World at 1:35000000, third edition (Bouysse et al., 2014)
Note: The full map is available in Appendix 1.

It would be interesting to correlate the knowledge already established for the Cretaceous with the observations and interpretations made in this project. In addition to contributing to the development of models on future climate change, this project could broaden and refine this geological period by providing additional information on the origin and implications of environmental changes on the sedimentary record and its biodiversity. Palynological and geochemical techniques will provide proxies that could allow future studies to adjust the accuracy of the Lower Cretaceous geological time scale.

1.2 Main goals

The main objective of this project is to reconstruct the climatic and oceanographic conditions of the Early Cretaceous Algarve Basin (Portugal) through the stratigraphic sequence that outcrops between Ponta da Baleeira and Praia dos Arrifes, southwest of Albufeira. To this end, a very detailed stratigraphic log was constructed to determine which intervals should be sampled for palynological and geochemical analyses. The latter are intended to complete and refine the first interpretations of the sedimentary environment.

The ultimate goal of this study is to determine the influence of sea-level fluctuations and periods of marine anoxia at this time.

Along with the main objectives, other parallel objectives are:

(1) To study the Lower Cretaceous sedimentary rocks of the Arrifes stratigraphic sequence;

(2) To recognise the sedimentary cyclicity and its relation with the eustatic curve of the period;

(3) To recognise in a broad coastal sedimentation context the manifestation of Oceanic Anoxic Events (OAEs) of the time, characterised by variations in ^{13}C stable carbon isotopes on sampled organic matter;

(4) To provide a detailed sedimentological log of the sequence;

(5) To attempt to date the stratigraphic succession accurately *via* palynology;

(6) To fill the geological knowledge gap of the Hauterivian-Barremian central Algarve.

To achieve these objectives, this study was divided into several phases:

(1) Field observation and construction of the detailed log of the Arrifes succession;

(2) First interpretations of the depositional environmental conditions based on these field observations;

(3) Establishment of a sampling strategy to collect marl and marly limestone samples;

(4) Laboratory work following standard sample preparation protocols for palynological and geochemical studies;

(5) Interpretation of the results of these analyses and their integration with the preliminary sedimentological interpretations;

(6) Proposal of a depositional model for the Arrifes stratigraphic sequence including environmental paleoconditions (climate, oceanography, sea-level variations, OAEs, *etc*).

2. State of the art - The Early Cretaceous

The sedimentary succession exposed at Praia dos Arrifes is dated to the Early Cretaceous (Rey and Ramalho, 1974). Therefore, this review will describe the most important geological events that characterise this geological time.

The Cretaceous is a well-known period in the history of Earth (Wang et al., 2014), during which conditions were very different from those we know today (Spicer, 2003). This geological epoch was so unique that Skelton (2003) named it ''The Cretaceous World''. It begins at the base of the Berriasian, 144.6(±0.8)My ago (Mahoney et al., 2005) and ends 66My ago at the Cenozoic boundary (*Cf.* Appendix 2 for the International Chronostratigraphic Chart, 2020). This boundary is marked by one of the most severe mass extinctions in Earth's history, the Cretaceous-Tertiary (K-T) crisis (Alvarez et al., 1980). During the Cretaceous, other significant geological events occurred, such as the renewal of the Pangea break-up with the opening of the South Atlantic Ocean, Oceanic Anoxic Events (OAEs), a prolonged greenhouse climate mode, carbon isotope excursions, significant volcanism associated with Large Igneous Provinces (LIPs) and Continental Flood Basalt Provinces (CFBPs), high nutrient availability in the oceans due to excessive rates of continental weathering and wet periods, ecological changes including some minor extinctions and the drowning of large carbonate shelves (Baudin and Riquier, 2014; Wang et al., 2014; Föllmi, 2012; Keller, 2008; Hu et al., 2012; Baudin, 2005; Spicer, 2003; Weissert et al., 1998).

2.1 Paleogeography

Since Wegener's theory of continental drift (1915), and later with the acceptance of plate tectonics in the 1960s and 1970s, geologists have attempted to reconstruct the paleogeography of landmasses and oceans throughout Earth's history. The spatial arrangement of continents and oceans on the globe essentially controls climate circulation and global ocean circulation, just as the Gulf Stream would not be without the current configuration of continents and oceans (Hay, 2017).

To understand the Lower Cretaceous world, we need to go back to 250My to the beginning of the Mesozoic Era. At the beginning of the Triassic, most of the landmasses were organised into the supercontinent Pangaea, surrounded by the vast ocean Panthalassa. At

the eastern margin of Pangea there was a large trench forming the Tethys Ocean in the intertropical belt. During Late Triassic times, Pangea began to break up, forming several continental rift basins. In the Early Jurassic, one of these initial rift basins became an oceanic ridge. Then, the first oceanic crust formed between North America and Europe, including the North and Central Atlantic Oceans. Towards the end of the Jurassic, the Central Atlantic Ocean widened and opened an arm of the sea connecting it to the Tethys Ocean (Baudin and Riquier, 2014; Föllmi, 2012; Badiola et al., 2008).

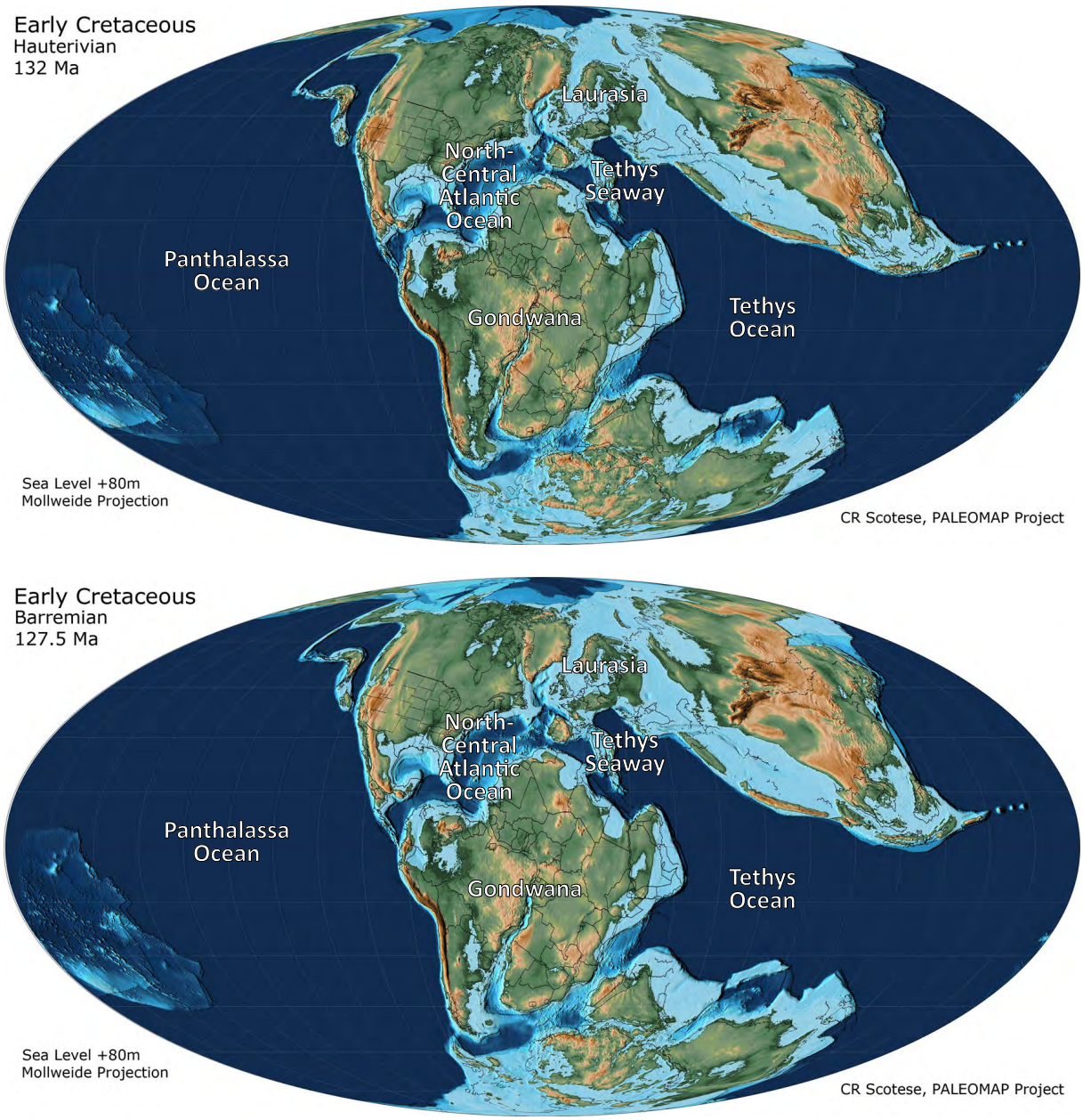


Figure 2.1.1 Lower Cretaceous paleogeography (after Scotese 2014)

In the Early Cretaceous (Figure 2.1.1), only 10-45% of the landmass was emergent compared to the present, and most landforms were no more than 1km high, especially in Europe and Africa (Skelton, 2003). The new seaway linking the young North Atlantic and the Tethys Ocean allowed significant physico-chemical fluxes between these water masses, including, for example, consequent climatic changes such as the modification of the Early Mesozoic mega-monsoonal Pangean climate to more zoned climate belts around this seaway (Weissert et al., 1998). At the same time, Gondwana began to break up to the south, and the South Atlantic Ocean formed between Africa and South America. Shallow waters submerged much of the continental shelves, and the climate was warm, favouring the establishment of vast carbonate platforms (Föllmi, 2012; Hu et al., 2012). The process of the break-up of Pangea led to major geomorphological, climatic and oceanographic changes on a global scale (Le Pichon and Huchon, 1984). These have had consequences for global biodiversity and sedimentation patterns in the Early Cretaceous.

2.2 Paleoclimate

Understanding and reconstructing the paleoclimate is achieved by studying geological formations and fossils that provide data on past atmospheric CO_2 concentrations. Indeed, this gas is one of the leading greenhouse gases and contributes significantly to global warming (Wang et al., 2014; Littler et al., 2011). It is common to retrace its concentrations through the sediments as it is regularly transformed into $CaCO_3$ for the shells or skeletons of carbonate organisms (Skelton, 2003). In the Cretaceous, atmospheric concentrations of CO_2 were higher than today, and global temperatures were also higher (Figure 2.2.1) (Föllmi, 2012; Hu et al., 2012; Litter et al., 2011). Indeed, the fragmentation of Pangea led to a series of prolonged episodes of volcanic activity, releasing significant amounts of CO_2 into the atmosphere (Föllmi, 2012; Weissert et al., 1998). Many authors suggest that these temperature increases through volcanic activity may have led to the establishment of Oceanic Anoxia Events such as The Weissert OAE, considered the first of the Cretaceous (Hu et al., 2012; Litter et al., 2011; Baudin, 2005). The Paraná-Etendeka volcanic activity (located in South Atlantic), is related to Gondwana rifting and is consistently described as an episode of enhanced Lower Cretaceous volcanism. It started 138My ago (Early Valanginian) until it peaked between 133 and 131My (Hauterivian) and then abruptly declined (Föllmi, 2012; Weissert et al., 1998).

Based on oxygen isotopes in marine fossils, Cretaceous paleoclimates can be divided into three episodes. An initial cooler episode in the Early Cretaceous was followed by a very warm Middle Cretaceous and a warm Late Cretaceous (Huber et al., 2012). Despite colder conditions from the Berriasian to the Barremian, the Early Cretaceous climate was warmer than today (Figure 2.2.1) (Littler et al., 2011). This period of relative coolness could be detected by evidence of ice in the poles, including dropstones, glendonites and diamictites at high paleoaltitude (Hu et al., 2012; Littler et al., 2011).

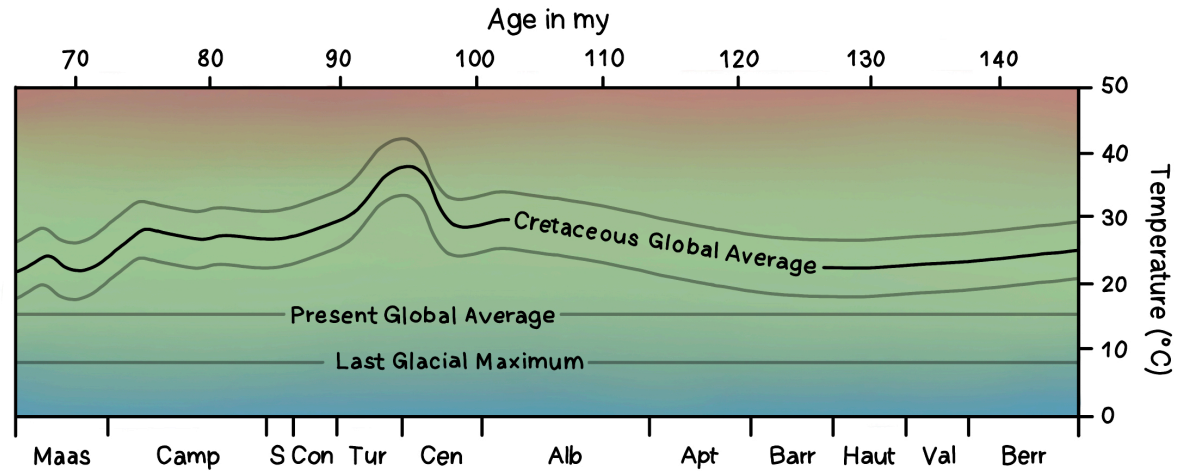


Figure 2.2.1 Cretaceous global average temperatures (after Hay and Floegel, 2012)

The Early Cretaceous climate has continuously oscillated between wet and dry regimes (Hallam, 1985). Föllmi (2012) explicitly described the Early Cretaceous climate at the Tithonian-Berriasian boundary (145My) as arid in a greenhouse climate model. Indeed, given the global spatial distribution of oceans and continents, climate models suggest that little moisture from the oceans reached the interior (Hay and Floegel, 2012). There are many examples of these conditions. In the absence of precipitation, evaporation is higher and biogeochemical weathering rates are lower and slower, resulting in less silica from weathering and fewer nutrients being transported from the continents toward the oceans. If these conditions are maintained for a long time, the ocean waters become stratified, and the bottom waters become depleted in oxygen (Baudin and Riquier, 2014).

The climate changed to a humid greenhouse, intensified by higher winds and precipitation at the Berriasian-Valanginian boundary (139.8My). Evidence for this change is based on increased biogeochemical weathering (*e.g.* presence of kaolinite), and increased

fluxes of nutrients and dissolved inorganic and organic carbon (DIC and DOC) to the oceans, resulting in increased primary productivity. In addition, this increased runoff from the continental shelves toward oceans has led to disturbances in carbonate production. The increase in humidity also allowed for an increase in vegetation cover, contributing to the decrease in pCO_2 of the atmosphere (Föllmi, 2012; Weissert et al., 1998).

The arid greenhouse climate was associated with a relatively low sea-level in the Early Berriasian. Transition to a wetter climate in the Valanginian is due to the gradual dispersion of landmasses with rising sea-levels (Skelton, 2003). A wetter climate can change the atmospheric circulation and cause, for example, more intense extreme weather events, such as tropical storms (Föllmi, 2012). This can be reflected by the presence of Hummocky-Cross-Stratification (HCS) in the sedimentary record (Boggs, 2006). These changes in atmospheric and oceanic circulation can be accompanied by eustatic sea-level rise. These conditions were maintained during the Early Hauterivian but reached a peak of humidity in the Middle-Late Hauterivian, possibly related to the strong Paraná-Etendeka volcanism (Föllmi, 2012).

The climate from the Late Hauterivian to the Early Barremian returned to a dry and warm regime. Indeed, the boundary between these two geological epochs (129.4My) is characterised by a climatic transition from humid Hauterivian to arid Barremian conditions (Föllmi, 2012; Masse and Fenerci-Masse, 2008). In addition, high temperatures favour lightning activity. In addition to a dry environment, the fire risk was high in the Cretaceous, especially observable in charcoal mesofossils from Portuguese Barremian-Aptian formations (Bond et al., 2010; Friis et al., 2010). However, palynological observations on *Classopolis* (coniferous) pollen have shown that their decreases in the Late Barremian sedimentary record induce a change from a warm and dry climate to a wetter one where temperatures were lower, and precipitation more frequent. This idea is reinforced by increasing in podocarpaceous and pinaceous pollens in the sedimentary record (Weissert et al., 1979).

2.3 Paleoceanography and eustatic sea-level

Eustasy refers to the absolute eustatic variations in sea-level as it rises in a transgressive phase or falls in a regressive phase (Nichols, 2009). Long-term sea-level fluctuates mainly (1) as a function of temperature, with higher temperatures leading to transgression due to thermal expansion of the ocean (Church et al., 1991), (2) as a function of the amount of ice present around the globe, with higher temperatures also leading to sea-

level rise due to less sequestration of ice by their melting (Haq, 2014; Hu et al., 2012), and (3) as a function of the volume available in ocean basins, *i.e.* the arrangement of continents, the activity and presence of ocean ridges, seamounts and submarine volcanoes (Haq, 2014). Hu et al. (2012) argue that Cretaceous eustatic fluctuations, with their amplitude of several tens of meters in less than a million years (*i.e.* short term in geology), can only be explained by the building and melting of ice sheets. However, some authors do not agree with this hypothesis because these Cretaceous periods are of the "extreme greenhouse effect" type (Föllmi, 2012; Ando et al., 2009). The latter would instead associate these rapid transgressions with major rifting phases and the formation of large submarine basaltic plateaus.

Sea-level fluctuations and the environmental energy control the positions of clastic sediments such as gravel, sand and mud (Nichols, 2009) or the position of carbonate sediments in a carbonate platform (Haq, 2014). Indeed, the structures and nature of sedimentary rocks provide information on the depth and position of the shoreline, as suggested in Figure 2.3.1 for terrigenous rocks. Beach facies are associated with the foreshore section (the depth of low tides defines its base), sandstones with current structures are associated with the shoreface. Secondly, fair-weather wave action has less influence with depth. The sandy mudstones, sometimes marked by storm energy, are found in the offshore transition zone, defined by the depths of the fair-weather wave base and the storm wave base, respectively. The offshore, is characterised by the deposition of mudstone deposits, showing relatively calm dynamics for particle settling. Thus, if the depth of the water column is estimated for each sedimentary layer, it will be possible to determine the fluctuations in the sea-level according to lithofacies changes (Nichols, 2009).

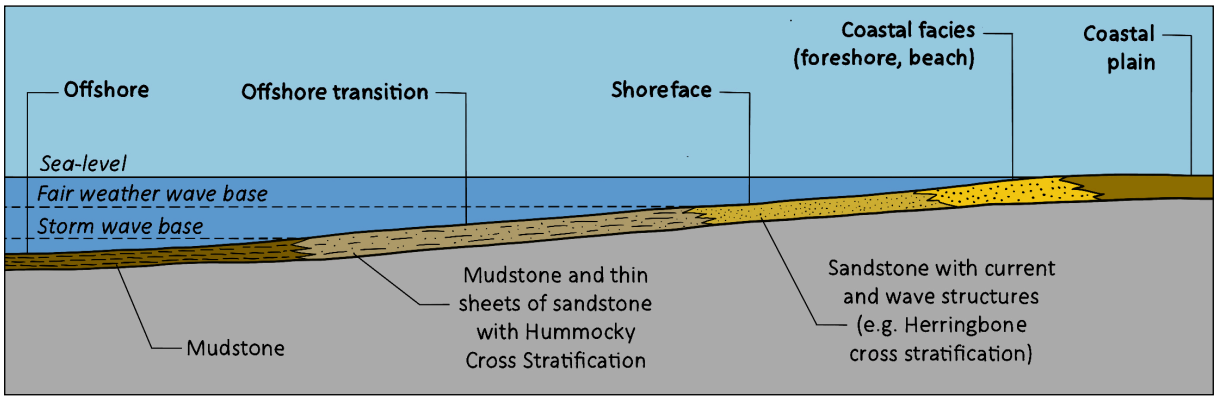


Figure 2.3.1 Characteristics of a storm-dominated shelf environment (after Nichols, 2009)

The principle is similar for carbonate platforms (Figure 2.3.2), where each ''type'' of a living organism is positioned according to the water depth and energy of the environment. For example, massive, encrusting corals are better adapted to withstand wave action than globular corals found in the calmer lagoon. This figure follows the carbonate classification of Folk and Dunham (1965) explained later in this work.

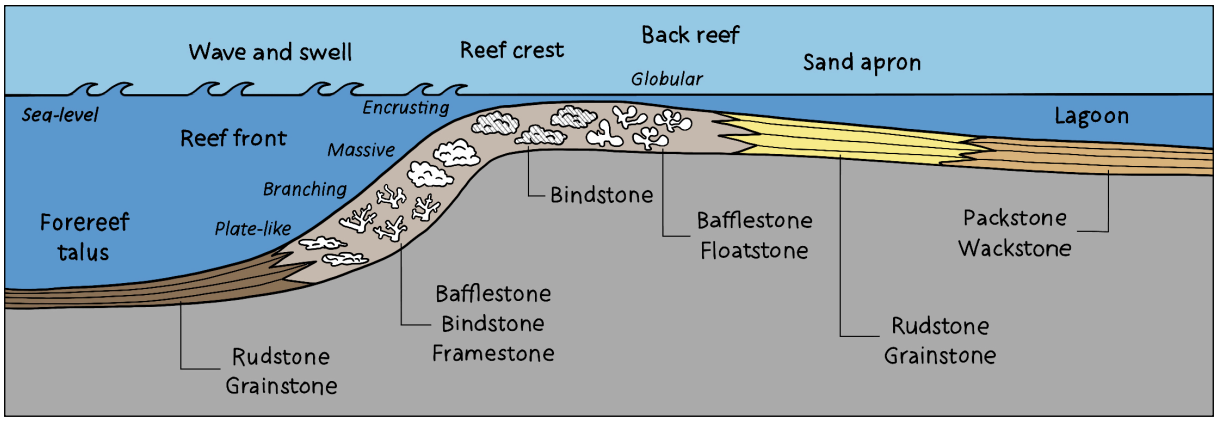
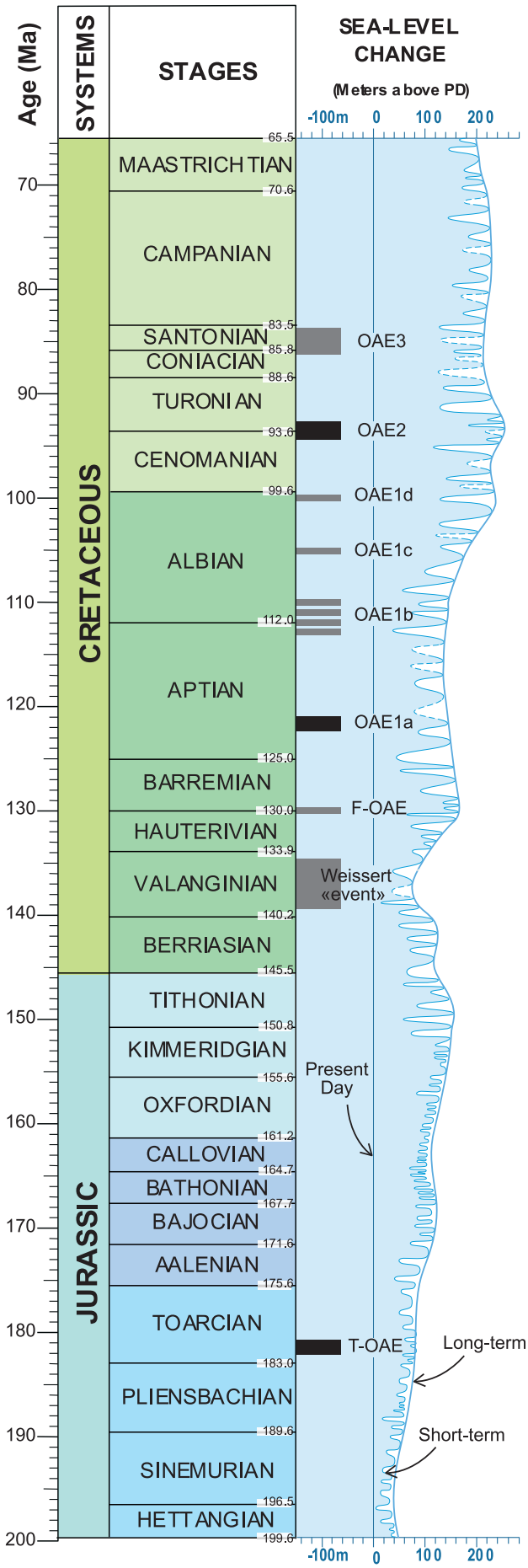


Figure 2.3.2 Facies distribution in a reef complex (after Nichols, 2009)

Given the geography and climatic trends of the Early Cretaceous, the physicochemical oceanographic conditions were very different from those we know today. Sedimentary records from deep marine environments and shallow carbonate platform successions suggest several transgression-regression cycles indicating, therefore, oscillations in mean sea-level throughout this period (Figure 2.3.3) (Baudin and Riquier, 2014; Haq, 2014). Although these fluctuations are second-order, if their intensity is large enough, they can disrupt environmental conditions. During the very Late Hauterivian, a major second-order transgression took place, changing the environmental conditions at the Hauterivian-Barremian boundary. Indeed, it allowed water mass exchanges that led to the cooling of the Tethys, illustrated, for example, by the presence of Boreal ammonites and dinoflagellates in southern Europe. Conversely, Tethyan *Nannoconus* in the boreal domain at the Hauterivian-Barremian boundary suggests a rise in temperature at the end of the Upper Hauterivian (Baudin and Riquier, 2014; Masse and Fenerci-Masse, 2008).

The long-term trend in eustasy indicates that sea-level rose during the Mesozoic and peaked in the Late Cretaceous (Skelton, 2003). Haq (2014) suggests that its level was 75m above present mean sea-level (PDMSL) in the middle Valanginian and 240-250m above



Present Day Maximum Sea-level (PDMSL) in the Early Turonian. This long transgression is called first-order, *i.e.* it is the general trend of a long-term period.

Figure 2.3.3 Stratigraphic time scale associated with the eustatic sea-level fluctuation curve and major Oceanic Anoxia Events (Baudin and Riquier, 2014)

In the Central Atlantic Ocean and Western Tethys, carbonate platforms were drowned by transgressions over large areas (Föllmi, 2012; Hu et al., 2012). The death of carbonate platform-building organisms contributed to the accumulation of organic matter (OM) and carbonates on the seabed. However, Weissert et al. (1998) pointed out that Calcite Compensation Depth (CCD) had shallowed in two stages during the Cretaceous, first during the Valanginian-Hauterivian and then in the Early Aptian. The dislocation of the CCD meant that calcite was dissolved entirely in oceanic waters at this time, resulting in the sedimentation of siliceous oozes (biogenic silica microfossils) and clays on the ocean floor.

In addition, the Lower Cretaceous oceanic circulations were highly disturbed by changing climatic conditions and their associated eustatic

variations and experienced intense periods of stratification. Indeed, their origins lie in climatic changes from cool and wet to warm and dry regimes, causing the collapse of the western Tethys thermohaline circulation and the cessation of upwellings during the Barremian, which was replaced by a density stratification (Weissert et al., 1979). As a result, Oceanic Anoxic Events were able to establish themselves in and above the seabed. However, these ''stagnant'' water conditions were regularly disrupted by renewed periods of circulation causing the formation of cyclic successions of organic-rich black shales (Baudin and Riquier, 2014; Wang et al., 2014; Weissert et al., 1979).

2.4 Oceanic Anoxia Events (OAEs)

Oceanic Anoxic Events impact marine ecological systems and can be detected in sediments and sedimentary rocks. They occur through a series of different possibilities: (1) when the amount of dissolved oxygen (DO) decreases in intermediate to deep waters, during periods of density stratification, for example; (2) when primary productivity is high (proliferating organisms consume the dissolved oxygen) or; (3) when the rate of sedimentation is high enough to ensure that organic matter is well-preserved in the sediments (Baudin and Riquier, 2014; Wang et al. 2014; Föllmi, 2012; Leckie et al., 2002; Weissert et al. 1998; Weissert et al. 1979).

These events result in ecological minor or major extinctions (Leckie et al., 2002) and geochemical perturbations of the global carbon cycle (Hu et al., 2012), which can be estimated by measuring stable isotope of H, C, O, N and S (Arthur et al., 1988). Consequently, during OAEs, fluxes of organic carbon (C_{org}) occur toward the seafloor, where they accumulate over large areas forming organic-rich dark sediments (*i.e.* ''black shales'') (Wang et al., 2014). In these characteristic sediments, some redox-sensitive trace metals may concentrate, such as As, Bi, Cd, Co, Cr, Cu, Mo, Ni, Sb, Tl, V and U in particular. Furthermore, enrichment of Ba, Ni, Zn and Cu in these black shales indicates bioaccumulation (Baudin and Riquier, 2014). With regard to isotopic data, increased C_{org} burial results in a positive excursion of $\delta^{13}C$ calculated from isotopic values of inorganic (or marine carbonate) carbon (^{12}C) and sedimentary organic carbon (Huck et al., 2013). In contrast, negative excursions in $\delta^{13}C$ can be explained by increased volcanic activity (releasing large amounts of ^{13}C-poor atmospheric CO_2) or by the release of CH_4 through dissociation of clathrates on the continental slope (Baudin and Riquier, 2014; Huck et al., 2013; Föllmi, 2012). Furthermore, if

geochemical analyses are done in organic matter rather that in inorganic carbonates, a negative excursion means that the light isotope was sequestrated, thus, with an increase in the carbon burial where the sediments become organic-rich (Sephton et al., 2002).

In the Early Cretaceous OAEs coincide with the geomorphological, climatic and oceanographic changes described above (Keller, 2008). To date, numerous main OAEs have been validated for this geological epoch: (1) Valanginian Weissert OAE; (2) Late Hauterivian Faraoni OAE; (3) Aptian-Albian OAE1a, 1b, 1c, 1d ; (4) Cenomanian-Turonian OAE2; and (5) Coniacian-Santonian OAE3 (Hu et al., 2012; Baudin, 2005). Ecologically and environmentally, these events caused minor extinction crises in carbonate platforms and other benthic and pelagic organisms contemporary with these events (Wang et al., 2014; Föllmi, 2012).

Weissert et al. (1979) suggested that positive Early Cretaceous carbonates $\delta^{13}C$ excursions were correlated with episodes of density stratification, episodes of increased organic carbon accumulation in sediments, and exceptional growths of carbonate platforms influenced by nutrient input from rivers in wet climates, the idea of ''climatic eutrophication''. More generally, other authors suggest that the primary forcing for OAEs was a rapid increase in temperature inherited from the extensive volcanic activities of the time. The increase in primary productivity was supported by increased terrestrial nutrient fluxes (*e.g.* nitrate and phosphate) that resulted from these rapid and intense climatic warmings (Baudin and Riquier, 2014; Hu et al., 2012; Baudin, 2005). In addition, OAEs are often linked to transgression events that flood specific parts of carbonate platforms. These rises in sea-level flooded the land, creating epicontinental seas where primary productivity can increase, increasing the demand for dissolved oxygen in the water masses (Baudin and Riquier, 2014; Baudin, 2005; Weissert, 1998).

In more detail for the Faraoni OAE or F-OAE (Figure 2.4.1) (Late Hauterivian ≈131My during ≈100 ky), this episode has been correlated with the Paraná-Etendenka volcanism (133-131My), a distinct heat peak and a major second-order transgression, both contemporaneous with this same epoch (Baudin and Riquier, 2014; Haq, 2014; Föllmi, 2012; Masse and Fenerci-Masse, 2008; Baudin, 2005; Weissert et al., 1998). Traces of this event have been detected in various areas (Figure 2.4.1) such as the Mediterranean Tethys, Sicily, the North Sea and the eastern Central Atlantic Ocean, including Portugal (Baudin and Riquier, 2014; Baudin, 2005).

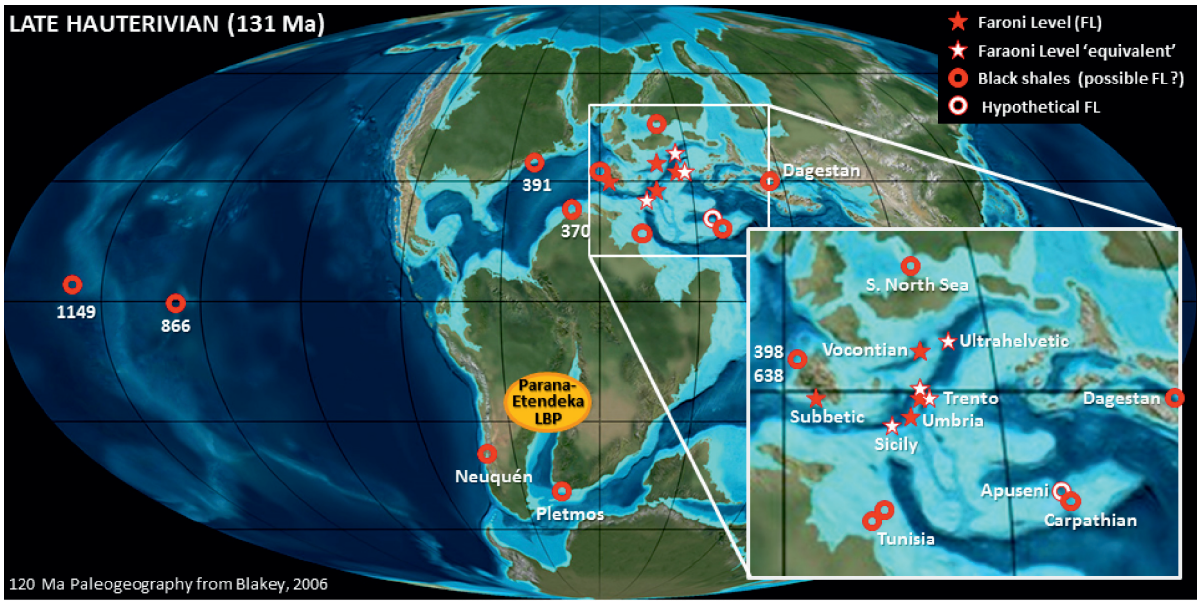


Figure 2.4.1 Global paleogeographic distribution of the F-OAE level, its equivalents, and the black shales potentially correlated to this Faraoni event (Baudin and Riquier, 2014)

2.5 Biodiversity

Marine and terrestrial organisms are, depending on the species, more or less sensitive to environmental changes. Therefore, their study can provide relevant clues to the ecology and environmental conditions of the places and times they live. Ammonites and belemnites are the most common fossils used for dating Cretaceous strata. The increasing proportions of families found in Cretaceous sedimentary rocks have led to estimates of a long-term increase in biodiversity (Skelton, 2003).

The break-up of Pangea into Gondwana and Laurasia at the end of the Jurassic divided many of the land populations. However, the creation of archipelagos in the Lower Cretaceous allowed terrestrial tetrapods to move between the landmasses of Laurasia, in particular during phases of low sea-level. These ''bridges'' make this period fascinating from the point of view of the evolution of vertebrate faunas (including mammals) and their geographical distribution (Badiola et al., 2008; Skelton et al., 2003).

During this period, the most significant event in terrestrial populations was the end of the non-avian dinosaur era (Alvarez et al., 1980) and the advent of flowering plants. Angiosperms appeared in the Early Cretaceous (Valanginian-Hauterivian detected in Helez, Israel) in a humid tropical climate and proliferated to become ecologically dominant in the Late Cretaceous, constituting today the most prevalent group of terrestrial autotrophs (Friis

et al., 2010; Wing and Boucher, 1998; Brenner, 1996). Although their biomass was minor compared to other plants until the Middle Cretaceous (Bond et al., 2010), they made possible an explosion in predator diversity, from insects to insectivorous birds, lizards and mammals (Strickson et al., 2016). We should also note the strength of the ecological interaction of angiosperms with their environment, notably *via* pollinating insects or the various animals used in seed dispersal (Badiola et al., 2008).

Until the mid-Cretaceous, angiosperms were characterised by shrubs or small understory trees, as well as grasses (Bond et al., 2010). The Barremian was mainly composed of grasses, ferns, bennettites, conifers (in large numbers) and magnoliaceous trees growing in a warm, dry climate (Coiffard et al., 2007; Wing and Boucher, 1998). However, during the Late Barremian, *Classopollis* conifer pollens decreased in abundance, favouring a wetter climate. Conversely, this change to cooler and wetter environmental conditions tended to increase Podocarpaceae and Pinaceae pollens (Weissert et al., 1979).

In the Early Cretaceous, populations of calcareous organisms, phytoplankton and other marine plankton changed. For example, (1) *Bivalvia* and *Hippuritacea* rudists on carbonate platforms evolved; (2) groups of ammonites underwent renewal, *Crioceratites Pseudothurmannia* lineage or the genera *Neolissoceras* and *Plesiospitidiscus* disappeared during Late Hauterivian and were replaced by typical Barremian groups *Barremites* and the first *Holcodiscinae*, *Leptoceratoidinae* and *Silesitidae;* (3) radiolarians underwent an extinction phase; and (4) a group of planktonic elongated chambered foraminifera (*Hedbergella roblesae* and *Hedbergella semielongata*) underwent the first radiation just before the F-OAE (Föllmi, 2012; Masse and Fenerci-Masse, 2008; Coccioni et al., 2006; Company et al., 2005; Weissert et al., 1998). Corals resemble too those of the Late Jurassic to the Valanginian. Others appear and are typical of the Lower Cretaceous, such as the genera *Eugyra*, *Myakosmilia*, *Microseris*, *Hydnomorphomeandra* and *Felixigyra*. The shallow margins of the Tethys Basin played a major role in their geographic distribution by serving as a corridor for coral larvae (Bond et al., 2010).

Extensive carbonate platforms have characterised the Cretaceous seas due to the persistence of warm shallow waters but are considered the most vulnerable in the Early Cretaceous biosphere. However, they have a relatively rapid recovery capacity of several million years (Baudin and Riquier, 2014; Haq, 2014). The Late Cretaceous eustasy maximum and associated marine transgression drowned most of these carbonate platforms during other transgression episodes and associated OAE such as F-OAE at the end of the

Hauterivian. The organisms that build them died due to the lack of light and nutrients. (Baudin and Riquier, 2014; Föllmi, 2012; Weissert et al., 1998). This F-OAE episode also allowed exchanges between the boreal and Tethyan domains, with species migrating in both directions (Baudin and Riquier, 2014).

2.6 Algarve Basin during Early Cretaceous times

The Algarve Basin is located at the southwestern end of the Iberian Peninsula, in the south of Portugal. This Meso-Cenozoic basin (Figure 2.6.1 and 2.6.2) has undergone two major tectonic events that give it its elongated east-west shape over 136km.

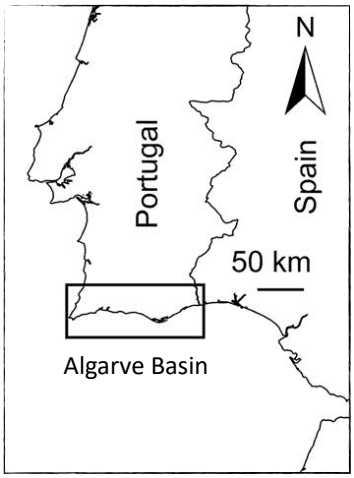


Figure 2.6.1 Algarve Basin location (after Ramos et al., 2016)

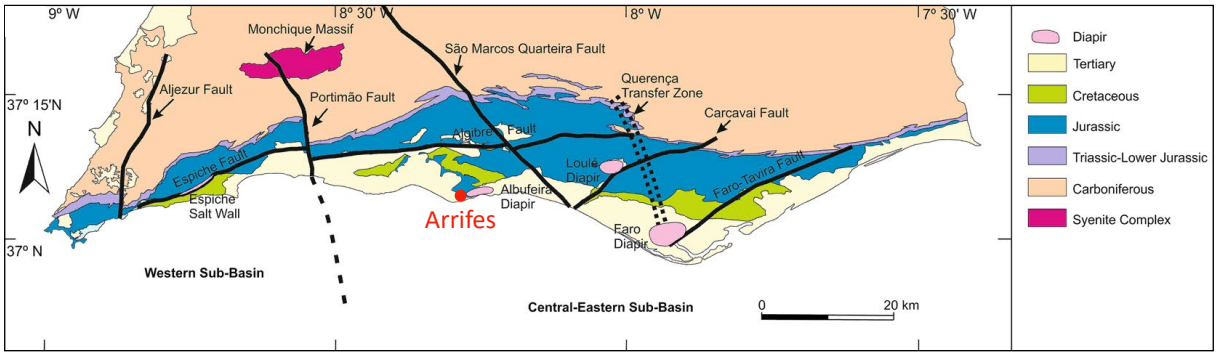


Figure 2.6.2 Simplified map showing major tectonic features, which have had different behaviour since the Late Triassic (after Ramos et al., 2016)

Note: The Arrifes sequence Cretaceous is thin, the authors chose not to represent it.

The Algarve Basin formation is related to the initial break-up and rifting of the supercontinent Pangaea in the Late Triassic, whose sedimentation (*i.e.* continental red beds and evaporites) unconformably overlies Upper Carboniferous Flysch formations of the Variscan South Portuguese Zone (SPZ). Extensional tectonics dominated the Algarve Basin until the Early Cretaceous, creating rift basins that evolved into passive margin basins. The second major geodynamic event is the Alpine Orogeny, characterised by compressional movements that inverted the Algarve Basin and exposed its land part. Salt tectonics resulted

from the Alpine Orogeny with the coexisting extrusion of saline diapirs, which also controlled the region's geology. Notably the extrusion of the Albufeira diapir passively folded the adjacent sedimentary strata and verticalised the Early Cretaceous succession at Praia dos Arrifes, which is the area of this study (Dinis et al., 2020; Ramos et al., 2017; Ramos et al., 2016; Fernandes et al., 2013; Trindade et al., 2010; Terrinha, 1998; Oliveira, 1990).

The Early Cretaceous Algarve Basin is divided into western, central and eastern sectors (Figure 2.6.3), where lithostratigraphic units have been studied for each. The central part was one of the main depocentres of the Algarve Basin, with continuous sedimentation from the Upper Triassic to the Early Cretaceous, reaching a thickness of about 3km. The Upper Cretaceous strata form an essential part of this sedimentary pile, reaching a maximum thickness of 1.5km, consisting mainly of marine carbonates and siliciclastic rocks. Due to Alpine tectonics, the Neogene carbonate fossil beds are unconformably overlapping the Cretaceous formations. This hiatus is probably due to tectonic inversion and uplift of the Mesozoic basin due to diapirism in the region (Ramos et al., 2016; Fernandes., 2013; Trindade et al., 2010; Rey, 1983).

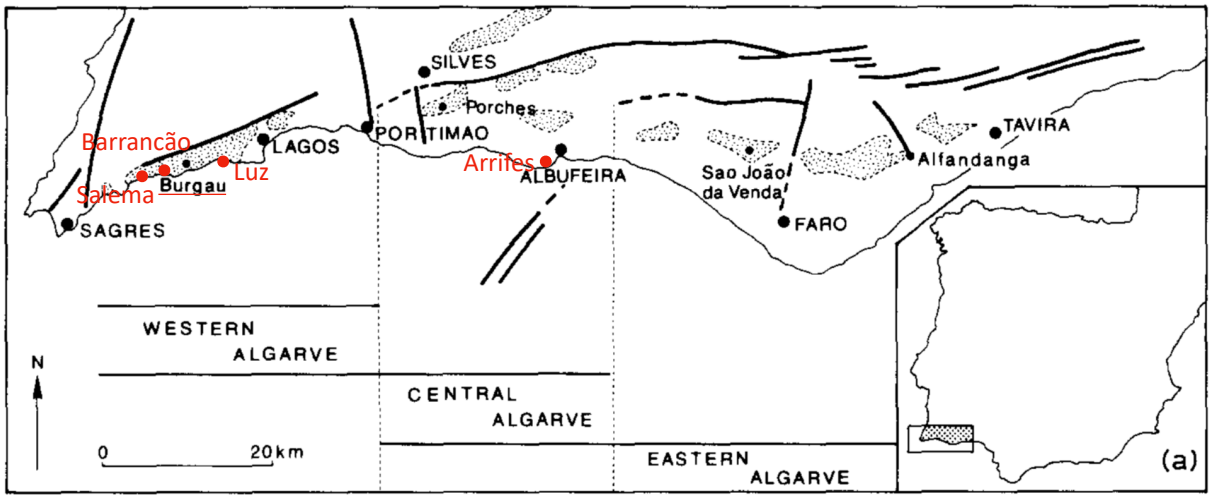


Figure 2.6.3 Map of Cretaceous outcrops in Algarve (in grey) (after Rey, 1986)

Note: In red are the five stratigraphic formations that are mentioned in this project; and again, the Arrifes sequence Cretaceous is thin, the author chose not to represent it.

The Early Cretaceous sedimentary rocks of the Algarve Basin were mainly deposited in coastal environments, from coastal lagoons and marine shelf carbonates under the influence of waves, tides and storm processes (Dinis et al., 2020; Fernandes et al., 2013;

Santos et al., 2013; Friis et al., 2010; Trindade et al., 2006; Rey, 1983). Due to the proximity of coastal environments, sea-level oscillations, sometimes disturbed by tectonic events, were the main factors controlling sedimentation (Trindade et al., 2010). In more detail for the central Algarve Basin, the rate of subsidence was relatively low and limited from Berriasian to Late Barremian, although it was more important during the Jurassic (especially Kimmeridgian) and latest Early (from Aptian) to Late Cretaceous (Ramos et al., 2017; Terrinha, 1998; Rey, 1986; Wilson, 1975). Moreover, rifting movements and their isostatic adjustments (*i.e.* subsidence or uplift) were more felt on the very western passive margin of Iberia (*e.g.* Lusitanian Basin or Alentejo Basin), affecting little of this central part of the Algarve (Dinis et al., 2010; Alves et al., 2009). Thus, the sea-level variations recorded in the sedimentary deposits were unlikely to be due to local tectonics. Therefore, Early Cretaceous sedimentation was mainly controlled by relative sea-level changes, and may be related to global eustatic cycles (Rey, 1986).

There are also traces of continental organisms in this basin, such as the presence of angiosperms showing flourishing vegetation in the Early Cretaceous (Föllmi, 2012; Heimhofer et al., 2007), and dinosaur footprints showing the existence of episodic bridges linking central and southern Europe when terrestrial sediments were prograding to form extensive intertidal plains (Santos et al., 2013; Diedrich, 2011). Moreover, the frequent presence of kaolinite in the sedimentary rocks of the Lower Cretaceous Algarve Basin indicates the predominance of humid tropical to subtropical climates, where intense geochemical weathering prevailed (Trindade et al., 2013).

3. Study area

The Arrifes stratigraphic sequence is located between Praia dos Arrifes (west) and Praia da Baleeira (east), southwest of the Albufeira region, central Algarve basin (Figure 3.1).



Figure 3.1 Location of the study area in the Algarve Basin (Google Earth pro, 2021)

The studied outcrops consist of a succession of 187 layers for a total thickness of 193.8m. Rey and Ramalho (1974) attributed an Aptian age to it by their field observations, and Berthou et al. (1983) assigned a late Aptian age to it due to the foraminifera *Orbitulina parva*. However, the palynological results of this work proved that the sediments of the sequence were deposited during the Late Hauterivian to Late Barremian interval (Lower Cretaceous). The stratigraphic sequence youngs westwards and ends at the angular unconformity (90°) between the Barremian vertical layers and the horizontal Lower Miocene carbonate rocks (Kullberg, 1992).

The rock sequence outcrops along the sea cliffs and is formed by vertical layers due to the salt movements of the Albufeira diapir during the Late Cretaceous and Paleogene (Fernandes et al., 2013; Terrinha et al., 2013). This salt structure is located south of the extensive Algibre Fault. It was mainly fed by Upper Triassic-Hettangian evaporites. Figure 3.2 shows that this salt layer reached the surface as far back as the upper Jurassic, since limestones dating from this period cover it. It was only during the Alpine compression (mostly Cenozoic) that the diapir was reactivated and compressed (Ramos et al., 2017) causing the important tilting of the Early Cretaceous sedimentary layers of the Arrifes stratigraphic sequence.

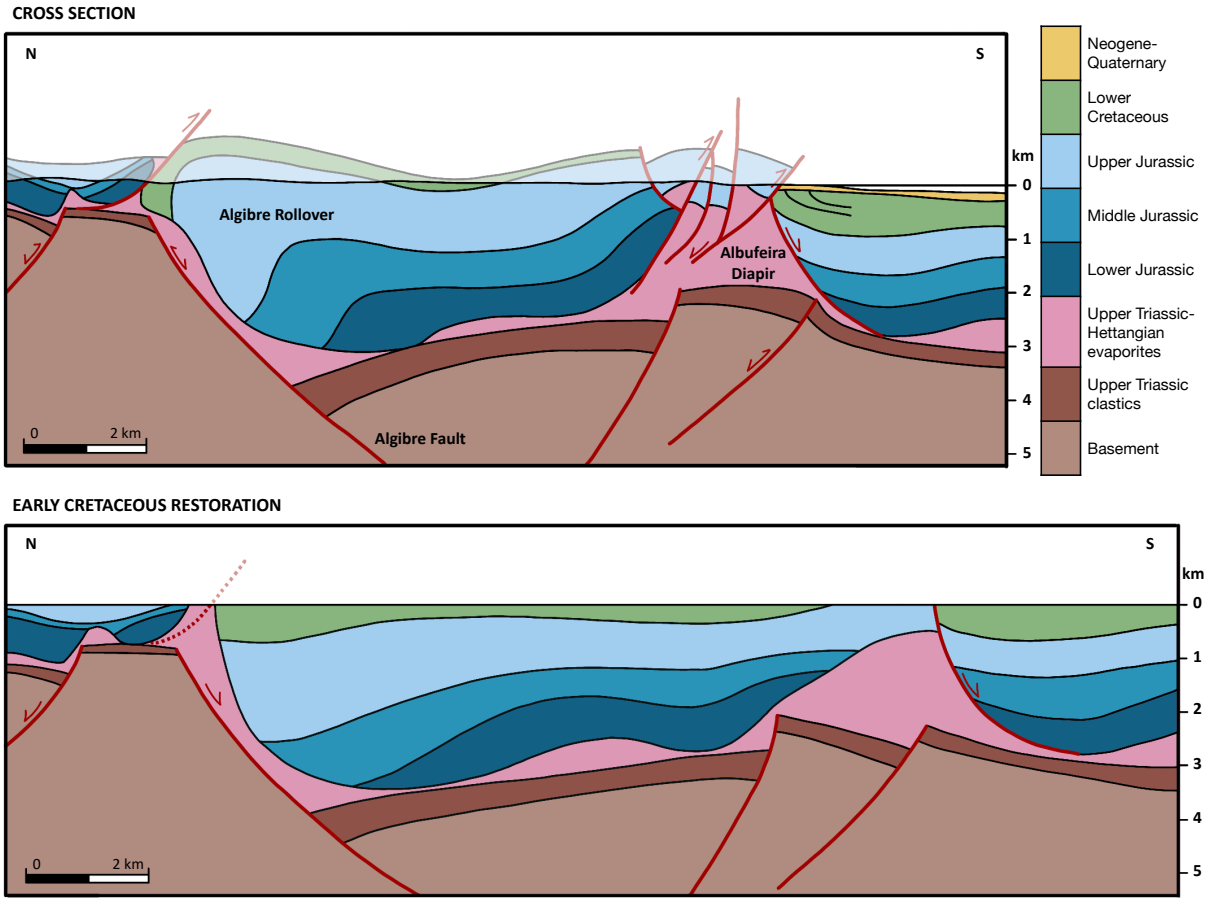


Figure 3.2 Cross section of two onshore salt related structures including the Albufeira Diapir. Evaporite thickness is controlled by the extensional Algibre Fault; Restoration at Early Cretaceous times (after Ramos et al., 2017)

Arrifes sequence consists of mixed lithologies including sandstones, limestones and mudstones showing all kinds of shallow and deepwater sedimentary structures such as herringbone-cross-stratifications, Hummocky-Cross-Stratifications (HCS), and graded bedding

or cross-bedding, for example. Moreover, the succession is fossiliferous since it is also possible to observe gastropod and bivalve shells, foraminifera, plant debris, traces of dinosaurs or traces of benthic biological disturbances (which are mainly *Thalassinoids* burrows of lobsters, crabs or shrimps). Finally, some rocks in the field suggest anoxic conditions (*e.g.* dark marls filled with organic matter).

Although Correia (1989) associated these sedimentary deposits with a long-term transgressive phase throughout the section, this sequence has not been described in detail, and no comprehensive sedimentological study has been attempted. Consequently, there is still much to be known and discovered about the basic geology of the Lower Cretaceous sequence at Arrifes.



(a) Overview of the Arrifes stratigraphic sequence



(b) Vertical layers of Arrifes stratigraphic sequence



(c) Bed n°1 Very coarse reddish-brown conglomerate



(d) Sampling process (sample P081.1)

Figure 3.3 Field pictures

4. Methods and Materials

This work used several methodologies. The methods used include sedimentology, palynology, as well as both inorganic and organic geochemistry. The data acquired was essential for reconstructing the paleoenvironmental, paleoclimatic and paleoceanographic conditions in this part of the Algarve Basin in the Early Cretaceous. These and the associated tasks followed an order during the project, based on its multidisciplinary approach. The first task was observing and recording the lithologies and their sedimentary features to make preliminary interpretations of the depositional environments, past physicochemical and oceanographic processes (*e.g.* eustatism and anoxia). Palynological and geochemical studies followed the last task to have more insight into the depositional conditions and the overall paleoenvironmental conditions of the Algarve Basin in Lower Cretaceous times. In the next sub-parts, each technique used is going to be described in detail.

4.1 Sedimentology

The sedimentological data will first be presented in a detailed stratigraphic log that records the succession of the different sedimentary rocks and the present structures. This graphic tool allows the perception of the various geological entities in terms of their time order. A measured lithological log is also essential for the organisation of the different stages of the project.

A lithological-sedimentological log is constructed by measuring the successive layers' thickness and plotting it in graph paper at a convenient scale. Together with the thickness, the type of lithologies and sedimentary structures shown are also recorded. Other geological information can also be added to the log, such as the grain size, the rocks' colour, the fossil content, trace fossils, weathering features, *etc*. Because most of the lithologies were carbonates, the classification used to identify and classify carbonate rocks is after Folk and Dunham (1962) (Figure 4.1.1).

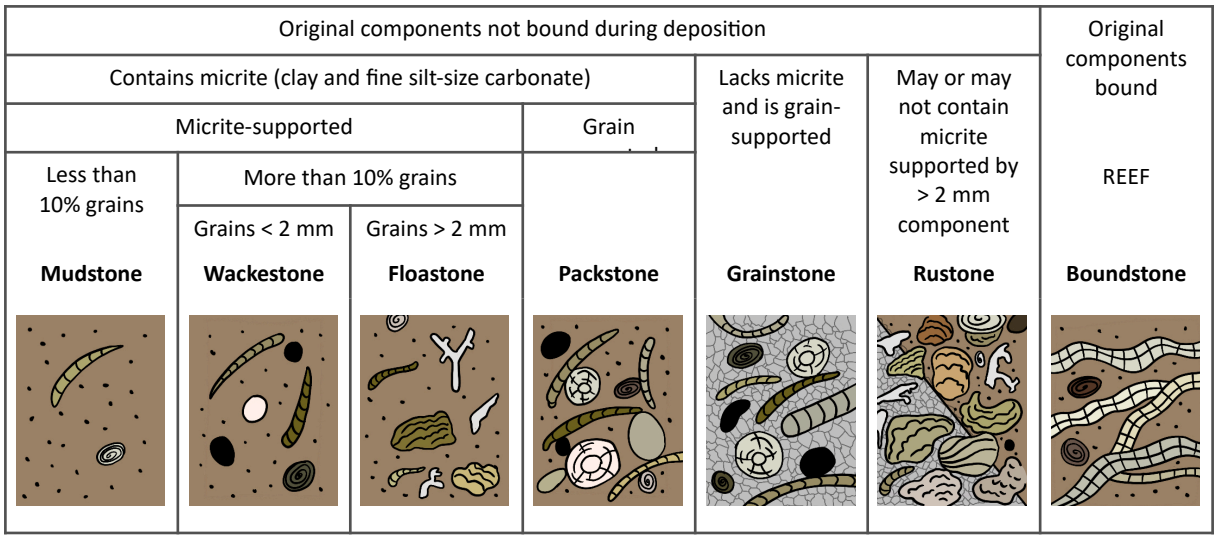


Figure 4.1.1 Folk & Dunham carbonates textural classification (1962) (after Wardana, 2016)

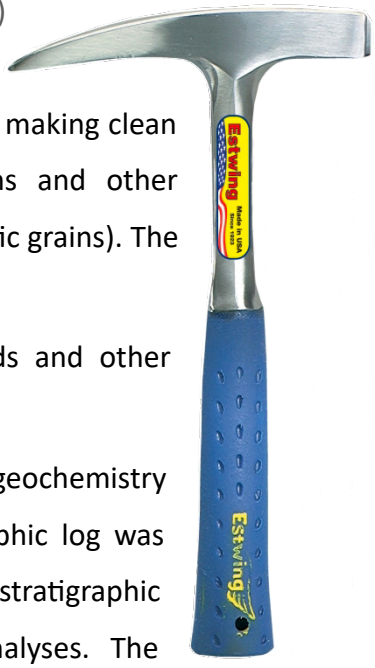
The sedimentological data is collected initially during fieldwork. The tides have defined the working hours because part of the stratigraphic succession is only safely accessed during low tide. However, if stranded by the rising tide, some identified escape routes to the cliff tops can be used and left without danger. Once on-site, a starting point is defined, and logging of the succession process towards the youngest beds, *i.e.* going westward. At the end of the day's fieldwork, the last observation point is recorded. It will become the starting point for the field day and so on until the stratigraphic sequence is fully completed. The field material used was:

(1) The **field notebook** is the most essential and indispensable item of any geologist doing fieldwork. It contains all the sketches, diagrams, notes and observations of the studied outcrops. It also includes the draft stratigraphic log. Indeed, the geological informations gathered during fieldwork, were recorded in a provisional log with a very detailed vertical scale.

(2) A **base map** (topographic or aerial photograph) provides information on the type of terrain and geomorphologic features of the study region. Additionally, and if available, a **geological map** is also relevant. The latter provides information of outcrops and sub-surface rocks, as well as information on the different lithologies, associated ages, tectonic structures, the spatial organisation of the rocks as well as the strike and dip of planar and linear geological structures (bedding, faults, joints, lineations, *etc.*).

(3) A **compass/clinometer** for measuring the strike and dip of planar and linear geologic features.

Figure 4.1.2 Typical geologist's hammer (*e.g.*) (Estwing, 2021)



(4) A **hammer** made of hard steel was used to break rocks and making clean surfaces to observe and better identify minerals grains and other components (*e.g.* fossils and types of cement between clastic grains). The hammer is also necessary for sampling.

(5) A **measuring tape** to measure the thickness of the beds and other distances between geological features.

(6) **Sample plastic bags** to carry samples for palynology and geochemistry studies. Sampling was only performed after the stratigraphic log was completed and finished. This allowed us to select the best stratigraphic intervals and the most suitable lithologies for the analyses. The lithologies targeted were marls and marly limestone. It is essential to reference the samples to precisely situate them in the stratigraphic sequence.

(7) A **pocket magnifying glass** (10X or 20X) to observe the rocks in detail and to help ascertain the identification of mineral grains, the grain size of clasts, small fossils (*e.g.* foraminifera), to recognise the nature of the binder between the carbonate constituents, which can be made of mud (micrite) or cement (sparite).

(8) **Hydrochloric acid (HCl)** was diluted to 10%, to detect carbonate minerals in a rock sample. Indeed, a chemical reaction of effervescence occurs in contact with the carbonated material. The acid reacts with the $CaCO_3$, releasing CO_2 and thus creating the bubbles (Santschi and Rossi, 2006).

(9) **Alizarin Red-S** is a dye used to distinguished calcite from dolomite minerals. After scratching and cleaning the sample's surface with HCl and water, the rock is soaked in a solution of alizarin red-S, and observe the absence or presence of colours. Calcite ($CaCO_3$) will give a pinkish-red colour, while dolomite [$CaMg(CO_3)_2$] and ferrodolomite [$CaFe(CO_3)_2$] will not change the rock original colour (Dickson, 1965).

A detailed stratigraphic log must provide sufficient information to make a primary interpretation of the depositional environments, including in the case of marine sedimentary rocks, the paleoceanographic dynamics and processes that have affected the area under

study. When presented, a curve relating the lithologies to sea-level variations interpreted from the sedimentary successions provide critical information regarding the last process.

Three complementary and independent analyses were planned for a more in-depth understanding of the depositional environments and theirs dynamics and relations with other natural processes active during deposition. The sedimentary rocks to be sampled were defined in advance. Sampling aims to target organic-rich mudstones for palynological and organic geochemistry of carbon stable isotopes, whereas carbonates were sampled for whole-rock inorganic geochemistry. Indeed, as the environment controls their production and preservation, proxies based on organic matter and inorganic geochemistry help reconstruct marine environments and past climates (Meyers, 1997).

4.2 Palynology

Palynology is the study of palynomorphs mainly represented by (1) pollens; (2) spores (these two are also called sporomorphs); (3) dinoflagellate cysts or dinocysts; (4) acritarchs; (5) chitinozoans; (6) foraminiferal linings; (7) marine algae; and (8) prasinophytes. Palynomorphs have an acid-resistant organic wall and are found in large quantities in fine-grained mudstones, as well as in some sandstones or limestones (Priyanka et al. 2015; Atta-Petters and Kyorju, 2013). Furthermore, the study of palynofacies refers to the study of palynomorphs, and also to organic components of sediments such as Amorphous Organic Matter (AOM), and palynodebris. Palynofacies are divided into three distinct groups (1) palynomorphs; (2) Amorphous Organic Matter; and (3) black opaque or translucent debris (or phytoclasts) (Atta-Petters and Kyorju, 2013). Palynological studies allow comparison between fresh, brackish and fully marine waters, as well as oxygenated and anoxic environments (Piasecky, 1986), and are used for dating stratigraphic succession, as well as in paleoecological and paleoenvironmental studies.

A total of forty-eight samples directly collected from Arrifes stratigraphic succession were prepared and analysed to reconstruct its history. For these palynological and palynofacies studies, the laboratory methodology for sample preparation was entirely carried out in the laboratory facilities of the Marine and Environmental Research Centre (CIMA) of the Universidade do Algarve (UALG). The laboratory methodology for isolating organic matter involved, in the first step, crushing the rock (1-2mm) and reserving 100g in a 500mL vial. Then, HCl diluted to 10% was added to the flask to eliminate the carbonate minerals. After a

few hours, the vial was checked to see if it was still reacting with the HCl by replacing it. If the reaction was complete, the content of the vial was neutralised by decanting several times with distilled water. After neutralisation, hydrofluoric acid (HF) diluted to 40% was added to the vial to dissolve the silicates and then left to react for two to four days. After the silicate materials were completely dissolved, the vial was decanted several times with distilled water to neutralise the organic residue. Once all the inorganic components have been removed, if any minerals remain, the organic material was separated by adding zinc chloride of density d=2 to the vial. The minerals sinked in the heavy liquid, while the organic matter float. The latter was isolated by sieving it through a 15µm mesh sieve with distilled water.

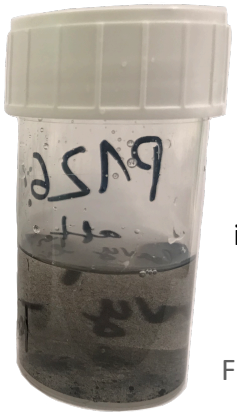
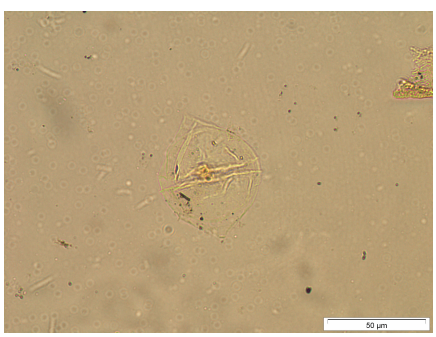


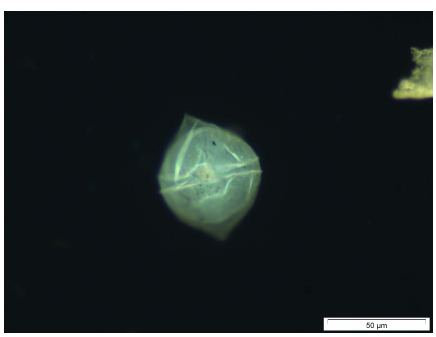
Figure 4.2.1 Isolated organic residues obtained for P126.1 after preparation

Due to the age uncertainty of Arrifes, part of the organic residue was sent to Laboratório Nacional de Energia e Geologia (LNEG) at Porto for palynostratigraphic studies (*i.e.* dating using palynomorphs, more specific using dinocysts). Dating was done by the first occurrence of dinoflagellate species whose biozonation was based on the interval zones of Leereveld (1997) which allow the dating of Lower Cretaceous Tethyan of southern Europe.

The remaining part of the organic residues were mounted on slides using resin Estellan® as mounting medium. The palynological slides were studied using an Olympus BX-51 transmitted light microscope equipped with a Cite Series 120Q metal halide lamp fluorescence unit and a +12 violet and blue filter block that generates a wavelength in the UV band (390-490nm). The UV fluorescence of the organic material allows the distinction of different organic constituents. For example, dinocysts are easier to identify under UV light fluorescent than under transmitted light (Priyanka et al., 2015).



Dinocyst under transmitted light (P155.1)



Dinocyst under UV fluorescence (P155.1)

Figure 4.2.2 Dinocyst observed under UV light fluorescence

After identifying 250 organic residues (*i.e.* the different palynomorphs, phytoclasts and AOMs), their abundances (in %) were calculated together with the ratio between continental *versus* marine palynomorphs to determine sea-level fluctuations. Indeed, marine palynomorphs are more abundant under marine conditions associated with transgression phases, whereas continental palynomorphs are more abundant during regression periods. However, looking at the too-high proportion of unidentified palynomorphs in the palynofacies task, we considered it was more accurate to use the spore-pollen/dinoflagellate cysts ratios (SP/D) ratios calculated by Mendes et al. (in preparation).

4.3 Geochemistry

This work employed two different geochemical studies, whole-rock lithogeochemistry and stable carbon isotopes performed in organic matter, obtained by the palynological techniques. Critical geochemical parameters such as the Chemical Index of Alteration (CIX), obtained from the whole-rock inorganic geochemistry of marls and marly limestones, reflect past climatic conditions (Dinis et al., 2020). The mineralogy of these lithologies is in equilibrium with conditions that prevailed during their sedimentation and can be used as proxies of past climatic conditions. Furthermore, in carbonates, calcite may be found in shells of invertebrate fauna or may precipitate inorganically directly onto the seafloor. However, in both situations, calcite precipitation takes place in equilibrium with seawater. In addition, the organic geochemistry of ^{13}C stable isotopes on marine organic matter, allows retrieving past oceanographic and climatic conditions by detecting, for example Oceanic Anoxic Events or episodes of enhanced volcanic activity (Godet et al., 2006; Huck et al., 2013).

The sedimentary layers sampled for geochemical studies were selected once the stratigraphic log was completed and interpreted. Dinis et al. (2020) has diagnosed the major climatic trends in the Algarve Basin during Early Cretaceous. The information gathered from the bibliography was contradictory regarding the age of the Arrifes section. Rey and Ramalho (1974) correlated it with the Luz Formation dated Aptian. In contrast, the geological maps of the Portuguese Geological Survey indicate a Hauterivian to Barremian age (Geological maps of the Portuguese survey). Therefore, one of the project's initial aims was to complement the Dinis et al. (2020) study by incorporating the older Arrifes section, having a more comprehensive range of ages (from Hauterivian to late Aptian). The geochemical analysis and the methodologies applied in this work are similar to the Dinis et al. (2020) study.

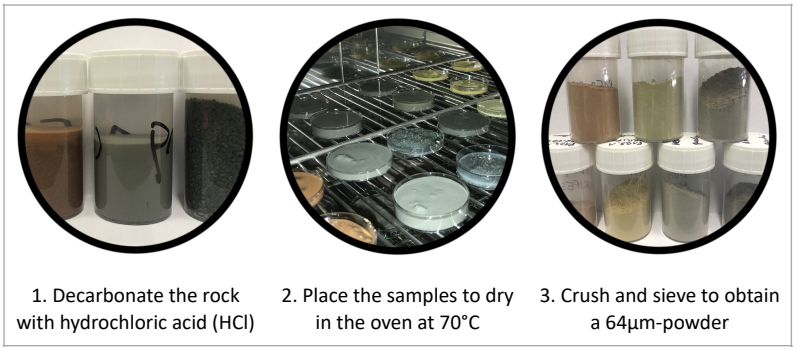


Figure 4.3.1 Key steps of protocol for whole-rock geochemistry analysis

From the forty-eight samples collected, twenty-two were selected for whole-rock inorganic geochemistry study. The first part of the laboratory preparation was carried out in the CIMA laboratory facilities of UALG. Approximately 100g of marls and marly limestones were pulverised using an agate mortar, and decarbonated by adding 10% diluted HCl to the powder. When the dissolution reaction was complete, the samples were neutralised and placed in an oven at 70°C until they were dry and moisture-free. Then, the samples showed some cohesion, they were passed again in the mechanical mortar to produce a powder, which was passed through a 64µm sieve (Figure 4.3.1). 10g of this very fine powder is reserved and stratigraphically referenced before being sent for geochemical analysis.

The samples were analysed for major and trace elements and Rare Earth Elements (REEs) at Actlabs (Canada). The analytical procedures used were inductively coupled plasma-optical emission spectrometry (ICP-OES) for major elements analysis of Ba, Sr and Zr, and inductively coupled plasma-mass spectrometry (ICP-MS) for the majority of trace elements. Alkaline dissolution with lithium metaborate/tetraborate followed by nitric acid dissolution was performed for all analyses, except for the determination of Cu, Ni and Zn, for which acid digestion was carried out. The standards used were: NIST 694, DNC-1, BIR-1, FK-N, NIST 1633b, SY-3, W-2, NIST 696, JSD-3, CTA-AC-1, WMG-1, GXR-1, MICA-FE, GXR-2, LKSD-3 and MAG-1. Appendix 3 shows the analyses for three standard reference materials (BIR-1, W-2a and DNC-1) and detection limits for each element. The calculated reproducibility is better than 3% for major element contents (SiO_2, TiO_2, Al_2O_3; Fe_2O_3, MnO, MgO, CaO, Na_2O, K_2O and P_2O_5), ≈4% for Rare Earth Elements and ≈5% for High Field Strength Elements (HFSE). Additional information on analytical procedures is available at *http://www.actlabs.com*.

Once the results were available, the major and Rare Earth Elements values were used in various discriminating graphs. Non-mobile REE ratios such as K/Cs, Th/Sc, Cr/Th and Th/Co were calculated as they are relevant to sediment provenance and sediment recycling studies. Other ratios such as Na_2O/Sm and K_2O/Th were also calculated. When they decrease, the prevailing climate is humid, associated with high chemical weathering rates, whereas the

increase reflects an arid climate with low precipitation and moderate chemical weathering rates (Dinis et al., 2020; Jorge et al., 2013). Weathering conditions can be reflected in the calculated values of certain paleoclimatic indices, such as the chemical weathering index (CIX) or the Chemical Index of Alteration (CIA). The latter varies from 50, slightly weathered, to 100, highly weathered, including the presence of kaolinite (which results from strong chemical weathering of the soil and parent rock). The degree of weathering was calculated using the plagioclase weathering index (PIA) based on the degree of conversion of feldspar to clay (Fedo et al., 1995). All these values and ratios were analysed, and interpretations were based on the proxies and knowledge already established on geochemical techniques concerning the study of past environmental conditions.

Stable carbon isotope analysis ($\delta^{13}C_{org}$) was completed for twenty-nine marl samples. The organic material analysed was the palynological residues obtained during palynological laboratory preparation. According to the methodology, the samples were decarbonated so that only C_{org} was analysed. The palynological residues of the selected samples were dried in an oven at 300°C, and 1g of the dry residue was weighted and stored in an *Eppendorf* vial. The $\delta^{13}C_{org}$ and Total Organic Content (TOC) analyses were performed by the stable isotope laboratory at the MARE research centre (Centro de Ciências do Mar e do Ambiente) of the University of Coimbra. The carbon isotopic composition of the samples was determined using a Flash EA 1112 Series elemental analyser coupled on line *via* Finningan ConFlo III interface to a Thermo delta V S mass spectrometer. The carbon isotope ratios are expressed in delta notation (δ), defined as the parts per thousand (‰), a deviation from a standard material (PDB limestone for $\delta^{13}C$): $\delta^{13}C$ (Rsample/Rstandard)−1]×1000, where $R=^{13}C/^{12}C$. The precision in the overall preparation and analysis was better than 0.1‰ for $\delta^{13}C$.

The variation of $\delta^{13}C_{org}$ along the Arrifes stratigraphic succession aims to detect changes in the burial of organic carbon related to the evolution of marine environments (Godet et al., 2006). In organic matter, negative excursions of $\delta^{13}C_{org}$ can be linked to OAEs or, to a certain degree, to oceans stratification, transgression phases or enhance primary activity (both mainly climate-induced) that causes a decrease in dissolved oxygen in the water, favouring an increase in the flux of organic matter (and therefore ^{13}C) towards the ocean floor and its preservation. However, some external factors such as the atmosphere-ocean exchange of CO_2 linked to prolonged or extensive volcanic activity or the release of CH_4 by the dissociation of clathrates in the continental slopes can disturb these geochemical processes (Godet et al., 2006; Huck et al. 2013; Weissert, 1989).

5.Results

The fieldwork allowed constructing a (1) sedimentological stratigraphic log through observations of the different lithological types, rock colours, sedimentary figures, structures and fossils. Forty-eight samples were collected to refine the interpretations. All samples were used for (2) palynological studies, including dating and palynofacies analysis; twenty-two samples were used for (3) whole-rock inorganic geochemistry, and twenty-nine for (4) $^{13}C_{org}$ stable isotope organic geochemistry. The correlation of these four techniques allows for a better interpretation of the environmental, climatic and oceanographic conditions that governed the depositional conditions during the emplacement of Arrifes succession.

5.1 Sedimentology

Several days of fieldwork were required to observe the entire outcrop in detail. This involved travelling to Albufeira, more specifically to the Praia dos Arrifes, located about forty minutes from the Gambelas Campus of the Universidade do Algarve by car. The weather conditions were generally good and the tide schedules allowed for about six hours of work before the beaches were completely submerged by the rising tide.

The sequence comprises a total of 187 layers (including a break) and is 193.8m long. Some layers have a code number higher than 187 because after the fieldwork, we had identified a duplicate portion of beds. Once deleted, we did not change the code of the sedimentary layers despite the gap (*e.g.* layer n°194 corresponds to the 187th layer). The lithologies mainly found are marl, marly limestone, limestone, sandstone, some conglomerate and calcarenite (*i.e.* limestone made of carbonated sand). The main fossils are fragmented or well-preserved bivalve shells, biological disturbances such as burrows of benthic organisms, and plant material.

5.1.1 Facies description

A lithofacies is an attribute of the sedimentary layers representing similar lithologies, sedimentary features and similar paleontological content. As a rule, beds showing the same type of lithofacies represent similar depositional environments.

FACIES A - Medium to coarse-grained conglomerates

Description: This facies is represented by conglomerate beds. The clasts are of gravel size (granule to pebble) that show rounded to sub-rounded surfaces, and are clasts to matrix supported. Most of the clasts composition consists of quartz. The base of the layers can show erosional features and are normal graded bedding.

Interpretation: During deposition, an energetic environment is necessary for the transport of large grains (Nichols, 2009). Thus, the depositional environment is attributed to a near-shore supratidal beach environment.

FACIES B - Medium to coarse-grained sandstones

Description: This facies consists of medium to coarse-grained sandstones. The beds show normal graded bedding, parallel lamination, herringbone cross-stratification, and wave cross-laminae.

Interpretation: Like Facies A, deposition requires a relatively energetic environment, *i.e.* close to the coast. The sedimentary structures indicate deposition in the shelf zone under the influence of waves and tides, most likely the shoreface or inner continental shelf zone above the fair weather wave base (Nichols, 2009).

FACIES C - Medium to very fine-grained sandstones

Description: This lithofacies is composed of medium to very fine-grained sandstone beds. They can show erosional bases, normal grading, parallel lamination and Hummocky-Cross-Stratifications (HCS).

Interpretation: The fine-grained sandstones implies calmer conditions than the previous clastic lithofacies. However, the presence of HCS indicates a depositional environment affected by storm events. Thus, the depositional conditions are characteristic of the intermediate continental shelf, which stands for the offshore zone below the average depth of fair weather waves (Nichols, 2009; Boggs, 2006).

FACIES D - Red marls and marly limestones

Description: This facies consists of marls and marly limestones that are orange-reddish in colour. Sedimentary structures are very scarce, apart from bioturbation, where *Thalassinoids* burrows are the more common ichnogenus.

Interpretation: The characteristic red colours is due to the oxidation of the sediments. The origin of this oxygenation may come from the fact that the sediments are regularly exposed to the open air. Thus, the environment would be located close to the coastline, subject to tidal action and therefore regularly exposed and submerged corresponding, therefore, to intertidal zones where the energy is sometimes calm enough for the tiny particles to settle (Fan, 2013).

FACIES E - Fossiliferous marls and marly limestones

Description: This facies includes marls and marly limestones that are beige to light grey. Bioclasts (broken shells) are common, and well-preserved invertebrate shells are rare. Marls often show plant material and impressions, wood debris (probably charcoal), and *Thalassinoids* burrows.

Interpretation: The presence of invertebrate shells indicates and environments were carbonate organisms would flourish, indicating fully marine conditions. The presence of broken shells may indicate reworking of the carbonate sediments due the waves, storms or predator biological activity. Moreover, the frequent presence of plants debris indicates that the depositional system was still relatively close to a vegetated shoreline. Thus, a shallow water lagoon-type carbonate depositional environment is assigned to this facies.

FACIES F - Red limestones and calcarenites

Description: This lithofacies consists of thick bioclastic limestones and calcarenites beds showing pinkish-red colours. Some limestone beds show rare wave cross-laminae. Bioturbation is common with both horizontal and vertical burrows.

Interpretation: The depositional environment of these limestones was on a shallow water zone of a carbonate platform, above fair weather wave base. The thick bedded limestones may indicate high carbonate productivity during the deposition of this lithofacies. Although, the depositional site were very similar to the previous facies, what distinguished

the two facies was the carbonate productivity. The presence of marls in Facies E suggests terrigenous input into the carbonate platform, and less carbonate production.

FACIES G - Dark marls and marly limestones

Description: This facies consists of interbedded layers of dark brown and dark grey, sometimes almost black, marls and marly limestones. Shelly faunas are rare, as well as traces of bioturbation, and plant material.

Interpretation: The dark overall colour of this facies, together with the scarcity of traces of biota living on the sediment floor, or above, suggest deposition in a ''near-offshore'' environment, *i.e.* the intermediate shelf zone, the offshore environment where the sea floor was below the photic zone, but probably the water column did not exceed *ca*. fifty meters.

FACIES H - Light colour bioclastic limestones and calcarenites

Description: This facies is composed by light-coloured (beige, yellow, light grey) hard bioclastic limestones and calcarenites (packstone to grainstone), which are very fossiliferous. The main fossil groups represented are bivalves and gastropods, and foraminifera for one bed. The shells show various degrees of preservation from well-preserved to moderately broken. Other traces of marine life may be present in these formations such as burrows.

Interpretation: The environmental deposition was fully marine and the sea floor was in the photic zone. The well-preserved shells also indicate that the depositional environment was quiet and do not show many evidences that the carbonate sediments were reworked by bottom currents, thus it is most likely located in the offshore zone of the carbonate shelf.

FACIES I - Dark grey to black marls and marly limestones

Description: This facies consists of interbedded very dark grey or black marls and marly limestones. What makes it different from Facies G is that the beds have an undisturbed aspect with very rare evidences of shell fauna and trace fossils. When broken, they may have a fetid smell due the presence of organic matter.

Interpretation: The lithologies and sedimentary features suggest deposition in the outer shelf with relatively deeper waters below the photic zone. The oxygenation of the

sediments was defective, dysoxic to anoxic conditions established on the sea floor or above it. The water column probably exceeded fifty meters in depth.

Nine lithofacies were identified along the Arrifes stratigraphic sequence. Their association reflect four main sedimentary depositional environments of this Lower Cretaceous carbonate platform: (1) the proximal (relative to the coastline) supratidal zone, most exposed region together with the upper intertidal zone, including Facies A and D; (2) the shallow water lower intertidal to subtidal zone, including Facies B, E and F; (3) the offshore zone below wave base and in the photic zone, entirely marine with evidences of life, including Facies C, G and H; and (4) the offshore zone without evidences of life, where the water depth is greatest and below the photic zone, representing the more distal zone of the carbonate platform, including Facies I only (Figure 5.1.1.1).

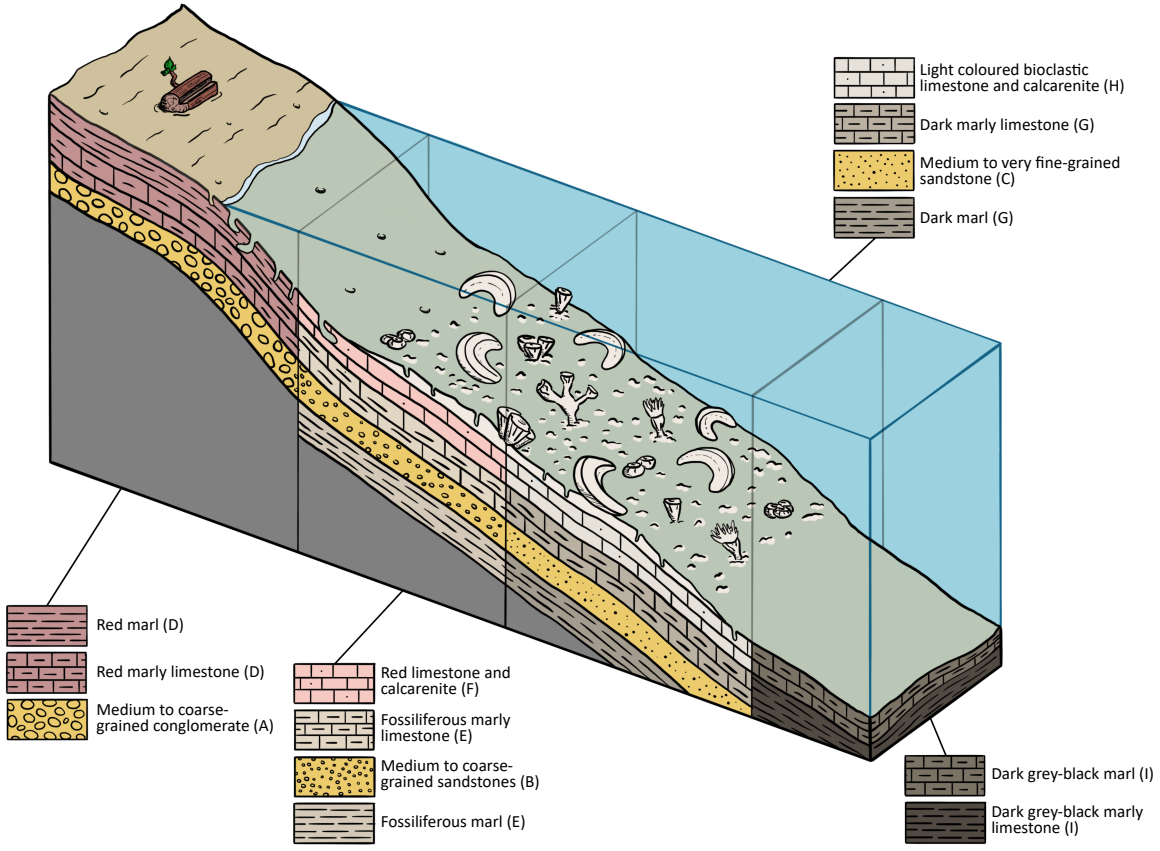
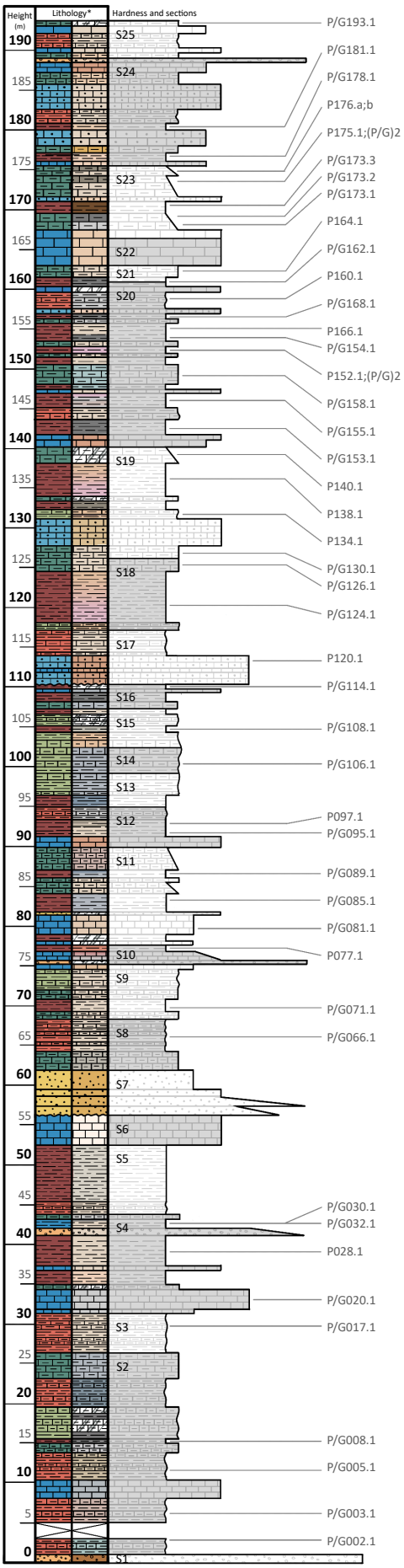


Figure 5.1.1.1 Arrifes lithofacies and their associated depositional environments

Note: The different lithologies appear to be superimposed, but this is not to be interpreted. It is only a graphic representation to show which lithology belongs to which environment.



5.1.2 Arrifes stratigraphic succession description

The stratigraphic sequence described starts at the eastern part of Arrifes at the first vertical bed unconformably cover by Miocene (23-5.3My) conglomeratic beach deposit (Kullberg et al., 1992). Figure 5.1.2.1 is a simplified stratigraphic log of the Arrifes succession.

More detailed information is available in Appendix 4. In this description, the entire succession is divided into several sections formed (1) by beds of one lithofacies type or, (2) by beds of different lithofacies previously described, that may show a sedimentary trend and environmental continuity. This allows a simpler visualisation of the results, while mentioning the characteristic layers.

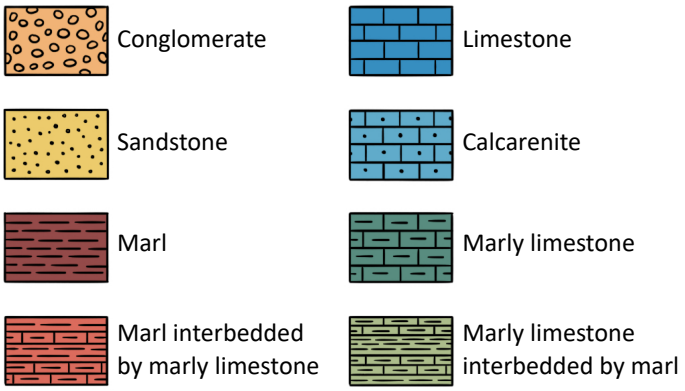


Figure 5.1.2.1 Simplified stratigraphic log of Arrifes succession, associate legend and sampling strategy (P: palynology and G: geochemistry)

Note: The lithology* is divided into two column (1) left is the lithology and (2) right is the colour of the sedimentary layers observed in the field; S(…) refers to the sections that are described below, from 1 to 25.

SECTION 1: Facies A | Layer n°1 for 1m

The stratigraphic sequence at Arrifes begins with a very coarse carbonate conglomerate (or breccia) composed of limestone and dolomite clasts typical of Facies A. Two scenarios may have been put forward for the deposition of this strata: (1) a tectonic event allowed the transport of the material, or (2) the carbonate were deposited in a shallow proximal environment, exposed and then karstified, and the voids created were eventually filled by the conglomeratic matrix. Assumption (2) is more likely as the rock has a rusty aspect and reddish colour, evidence of oxidation, and therefore possibly exposure.

SECTION 2: Facies E - F | Layers n°2 to 16 for 25.85m

This section is relatively thick and is represented by fifteen layers characteristic of Facies E and F. Bed n°5 shows evidence of burrows and bed n°16 birdseye structures, which both are intertidal sedimentary figures (Shinn, 1968). There are also marly limestones with broken oyster shells (bed n°10) or layers showing coal, wood debris and other plant material (beds n°4, 7, 10, 11, 12). The depositional environment was controlled by the influence of the tidal action in a shallow environment close to the continent.

SECTION 3: Facies G | Layers n°17 and 18 for 4.95m

This section is characterised by two layers with alternating dark marl, beige-grey marly limestone and light grey limestone. These beds are probably related to offshore conditions, which is to be confirmed with the palynological study.

SECTION 4: Facies B - E - F | Layers n°19 to 35 for 10.05m

Section n°4 is represented by all the facies that are characteristic of shallow water environments in the Arrifes succession. These conditions are evident in some strata such as two grey to pinkish limestones (beds n°19 and 21) showing wave patterns and parallel current laminations respectively, and a coarse-grained sandstone showing both of these sedimentary structures (bed n°29). The other layers in this section are various limestones, marlstones and marly limestones of relatively light, sometimes pinkish colours.

SECTION 5: Facies D | Layers n°36 and 37 for 8.7m

This section is composed of only two layers, a succession of marl and marly limestone, and a 7m thick marl. Both formations exhibit pinkish colours indicating a possible exposure phase, suggesting a foreshore environment, subject to tidal action and therefore regularly exposed and submerged (Fan, 2013). The oxidation of the sediments is proven by the red colours and the presence of benthic animal burrows.

SECTION 6: Facies H | Layer n°38 for 3.9m

Section n°6 is represented by a thick, compact, light grey limestone. In the top part of this limestone bed, khaki-brown nodules of iron oxides and calcite were observed. This bed was probably deposited in relatively deep offshore conditions.

SECTION 7: Facies A - B - C | Layers n°39 to 47 for 5.7m

This section is lithological different from the others because it is composed solely of siliciclastics. All these formations have a yellow-orange colour and the beds are attributed to Facies A, then B, then C. This section starts by an erosive surface marked by a conglomerate bed (n°39) composed of centimetric quartz pebbles, grading upwards to granules and coarse sand clasts size. The presence of large clasts suggests a high energy coastal deposition, allowing this layer to be related to an ancient beach deposit (Nichols, 2009).

There are then three coarse to medium-grained sandstones characteristic of Facies B (beds n°40, 41 and 42). These beds show normal grading parallel laminations, currents laminations, and herringbone cross-stratification (*i.e.* tidal current). The depositional environment was near coastal where the water column was not deeply influenced by tidal action (Boggs, 2006).

The top layers of section n°7 are characterised by Facies C (beds n°43 to 47). Four of the six beds show evidence of bioturbation, and two exhibit Hummocky-Cross-Stratification (HCS), which are storm structures that are known to form in the distal offshore transition zone (Boggs, 2006).

SECTION 8: Facies D | Layers n°48 to 55 for 6.35m

This section is composed of marl and marly limestone typical of Facies B, exhibiting reddish colours and rusty levels, indicating phases of exposure of the sediments. The environment was therefore intertidal.

SECTION 9: Facies E - F | Layers n°56 to 62 for 7m

Section n°9 is characterised by a greater proportion of marly limestones and a 0.7m limestone bed. The layers forming this section show light, sometimes pinkish colours and are interpreted as tidal to intertidal deposits.

SECTION 10: Facies A - D | Layers n°63 to 66 for 2.15m

This section is composed of layers of Facies A and D indicating beach and tidal flat deposits, most of which are red in colour.

SECTION 11: Facies B - E - F | Layers n°67-93 for 13.2m

The beds forming section n°11 are attributed to Facies B, E and F. Some of these strata are fossiliferous such as beds n°72, 74, 90, 91 and 93 show *Thalassinoids* burrows. Bed n°73 show plant material. The facies association of this section indicate deposition in shallow water proximal conditions under tidal influences.

SECTION 12: facies G - H | Layers n°94 to 100 for 4.45m

This section is composed by layers showing features attributed to Lithofacies G and H. It begins with a limestone bed (bed n°94), composed almost exclusively of *Orbitolins*, which are benthic foraminifera with an agglutinated test that only lived in the Cretaceous (Maru et al., 2007). Relatively dark marls containing very fine and dark laminations (possible OAE?) can then be observed. Furthermore, the carbonate formations (limestones and marly limestones) are all composed of bivalve debris (*e.g.* oysters) in large quantities. Most of the beds also show *Thalassinoids* burrows. Thus, the combined observations made suggest an offshore environment but still within the photic zone, which allowed many marine organisms, plankton, crustaceans, bivalves and carbonate platforms to flourish.

SECTION 13: Facies I | Layers n°101 to 103 for 3.95m

This section comprises two dark ''pure'' marls and alternating marl-marly limestones cycles, also relatively dark. The latter show very few oyster shells compared to the underlying layers (*cf.* Section n°12), indicating less favourable conditions for life in a more offshore area where the water column was above fifty meters.

SECTION 14: Facies G | Layers n°104 and 105 for 3.9m

In this section, the two beds of marly limestone and marl are rich in bivalves (oysters and clams). In addition, bed n°105 shows traces of burrows and lumpy limestone balls. These formations are therefore characteristic of a quiet and shallow environment, ideal for the establishment of muddy carbonate platform.

SECTION 15: Facies E | Layers n°106 to 110 for 4.35m

The beds of this section are referenced to Facies E, and indicate deposition in shallow waters carbonate platform. The presence of plant debris (beds n°106 and 108) indicates again, the preponderant continental influence.

SECTION 16: Facies G - H | Layers n°111 to 114 for 3.1m

Section n°16 is represented by relatively dark marl and highly fossiliferous carbonate rocks. Indeed, layers n°111 and 113 are composed of more than 50% of tiny fragments of shells. The sedimentary deposition took place in a well-established carbonate platform in a shallow and quiet environment within the photic zone.

SECTION 17:Facies E - F | Layers n°115 to 122 for 6.9m

The layers of section n°17 are typical of Facies D and F. Three calcarenites and a reddish limestone (beds n°115, 116, 117 and 119) indicating a well-oxygenated environment within the photic zone. Beds are very fossiliferous and contain well-preserved and broken gastropod and oyster shells. In addition, parallel laminations are observable in layer n°116, indicating proximity to an energetic environment (Nichols, 2009). Thus, the depositional conditions for these strata occurred in a shallow intertidal to subtidal environment.

SECTION 18: Facies D | Layers n°123 to 126 for 9.1m

The lithologies that make up the whole of section n°18 are marls and marly limestones. The 6.5m thick marl (bed n°124), with a reddish-purple to beige colour, stands out among the layers of the Arrifes sequence. It contains clasts of jet (coal) and white concretions of mixed calcite and dolomite (paleosoil). A supratidal to intertidal environment is suggested, and is supported by the presence of a large wood log impression.

SECTION 19: Facies G - H | Layer n°127 to 140 for 13.85m

Including layer n°138 (Facies D)

All the strata in this section are characterised by facies G and H, with the exception of layer n°138 which is attributed to Facies D, as it is similar to layer n°124. Although, their interpretations are the same, *i.e.* the depositional environment is supratidal.

Concerning the rest of the section, except for a very bioturbated calcarenite (bed n°131), the formations are relatively dark marl and grey-beige marly limestones. In the latter beds, *Thalassinoids* burrows are common (beds n°137 and 140), vertical burrows (bed n°129), well-preserved gastropods (bed n°139), and broken bivalve shells (bed n°140). The sediment deposition took place in an offshore environment with a depth not exceeding that of the photic zone.

SECTION 20: Facies E - F | Layer n°141 to 163 for 19.65m

Two beds differ from the overall lithofacies of this section: a limestone with wave ripples (bed n°146) and a bioturbated calcarenite with broken shells (bed n°159). The majority of the beds of this section consists of marls and marly limestones. Overall, they form a 19.65m thick succession where the colours vary from light to dark grey-beige, passing to purple and red. Many layers contain shell fragments (beds n°148, 155 and 159) as well as large (beds n°148 and 151) and smaller (beds n°155, 159, 160, 161 and 163) T*halassinoids* burrows. Hence, the environment is suggested as intertidal to subtidal shallow water. Note also the presence of a very thin dark layer in layer n°145, that appears to be organic-rich.

SECTION 21: facies D | Layers n°164 and 165 for 1.1m

A marl and then a marly limestone characteristic of Facies D make up this section. The latter has three so-called ''positive'' footprints of two species of terrestrial dinosaurs. Since they are positive, this shows that these sauropod and tridactyl (Santos et al., 2016) walked on the underlying marl and that the ''holes'' left under their weight were filled in by the deposition of the marly limestone. Furthermore, the elongated, curved shape of the claws indicates that the dinosaurs were ''skating'' as they moved across the muddy ground (Figure 5.1.2.1—e), indicating a tidal flat depositional environment exposed to the open air.

SECTION 22: facies E - F | Layers n°166 to 169 for 3.6m

This section is represented by Facies E and F, notably by the presence of a pinkish marl, a grey-beige marly limestone and particularly the presence of two bioturbated bioclastic limestones (beds n°166 and 168), one of the beds exhibit unidirectional cross stratification, probably formed by the action of tidal currents (Nichols, 2009). Thus, the depositional environment for these four strata is an intertidal to subtidal shallow water.

SECTION 23: facies G - H | Layers n°170 to 176 for 9.1m

Including layers n°172 and 173 (Facies I)

This section is mainly composed of layers related to Facies G and H, with the exception of beds n°172 and 173. The later two beds are dark in colour with rare traces of bioturbation suggesting distal conditions, possibly below fifty meters depth.

The majority of the layers are assigned to Facies G and H and characterise offshore depositional conditions. A competent limestone (bed n°170) and a calcarenite (bed n°174) with T*halassinoids* burrows may indicate two short episodes of shallow water deposition.

SECTION 24: facies B - E - F | Layers n°177 to 188 for 13.3m

The sedimentary layers that make up this section are assigned to Facies B, E and F. Excepting layers n°181 and 188, all the other layers show invertebrate fossils or trace fossils, indicating that the sea floor was well-oxygenated. The environmental conditions of deposition were characterised by a shallow and energetic environment under tidal influence

to supratidal environments. This idea is supported by the presence of sedimentary structures such as parallel current laminations, rip-up clasts or tepees structures (Nichols, 2009).

SECTION 25: facies G - H | Layers n°189 to 194 for 4.8m

Including n°193 (Facies D)

The last section of the Arrifes stratigraphic sequence is represented by facies G and H, with the exception of layer n°193, which exhibits features assigned to Facies D. Indeed, by showing desiccation cracks, this dark marl implies a phase of subaerial exposure allowing the formation of these particular sedimentary structures (El Hajjar et al., 2019).

Otherwise, the formations are mainly composed of carbonates. Some are bioclastic (beds n°190 and 192). In addition, the presence of bioturbation indicates that the conditions were favourable for benthic organisms. All of these evidences suggests offshore environment below wave base, but within the photic zone.

The succession is now described, allowing first interpretations to be done according to the lithofacies observations, as well as establishing the sampling strategy for palynology and geochemistry analyses.



(a) Large *Thalassinoids* burrows



(b) Well-preserved gastropod shell



(c) *Thalassinoids* burrows



(d) Wood log print



(e) Dinosaur footprint; burrows all around



(f) Clasts of coal

Figure 5.1.2.2 Some fossil pictures to illustrate the field work

5.2 Palynological description

A detailed palynological description was carried out using the palynological residues of forty-eight marl and marly limestone samples. These residues were observed under the microscope for organic matter and palynomorphs recognition, and the different organic constituents were also counted. Palynological studies are widely used for high resolution biostratigraphic correlations and paleoenvironmental interpretations. Palynofacies in this study were used to assess the depositional environments and its correlation to the other techniques used, namely sedimentology, and geochemistry.

After preliminary visualisation of organic residues, it was found that many were rich in palynomorphs, especially dinoflagellate cysts. In view of the uncertainty regarding the age of the Praia dos Arrifes succession (*cf.* "1.Introduction"), the organic residues were divided in two, and one of the halves was sent to Laboratório Nacional de Energia e Geologia (LNEG, Porto) for palynology and biostratigraphy. The dating was essentially focused on the dinoflagellate cysts. These studies were made by the LNEG researchers Márcia Mendes and Zélia Pereira, and the results are reported here. The main reason for this procedure is having an accurate time frame, to facilitate the discussion regarding the evidences and geological relationships obtained by the different methods used to understand the depositional environments of the Arrifes succession. The temporal frame allows correlations with the regional geology and with worldwide geological events characteristic of the ages obtained.

5.2.1 Palynological dating

Palynological dating attributed three different ages for the Arrifes succession. The different ages are based on the Lower Cretaceous dinocysts biozones of Leereveld (1997). The attribution of the different ages were based on the first occurrence of selected dinoflagellate species, and the abundance of selected taxa. Accordingly, the three ages identified were, from older to younger: (1) Late Hauterivian to Early Barremian; (2) Early Barremian to earliest Late Barremian; and (3) Late Barremian (Mendes et al., in preparation).

The Late Hauterivian to Early Barremian age correspond to the beds from the bottom of the succession until sample P017.1, at 31.35m above the base of the log. The dinoflagellate species that dates this part of the succession is *Subtilisphaera perlucid*a. From samples P028.1 to P085.1, presence of the dinoflagellate species *Subtilisphaera*

scabrata attribute this part of the succession from the Early Barremian to the earliest Late Barremian. The younger dinocyst assemblage is of Late Barremian age, and is defined by the presence of dinoflagellates of the *Odontochitina* genus, in particular the species *Odontochitina operculata*. The samples expressing this age are from samples P095.1 to P176.b, constituting the upper part of the stratigraphic sequence. There are some gaps in the chronostratigraphy because some samples were barren (no palynomorphs, or too few) and therefore did not allow precise dating (Figure 5.2.2.1).

5.2.2 Palynofacies

Organic residues of the forty-eight samples collected along the stratigraphic column, were observed under the microscope for the identification and counting of their organic constituents. The latter were divided into three groups (1) palynomorphs; (2) phytoclasts; and (3) Amorphous Organic Matter (AOM) (Atta-Peters and Kyorju, 2013). Palynomorphs group was subdivided into terrestrial derived palynomorphs (sporomorphs: spores and pollens), and marine derived palynomorphs (dinocysts and other marine: foraminifera innerlinings and algae). Organic particles that were clearly palynomorphs but with doubtful origin, were counted as unidentified palynomorphs. The phytoclasts group was subdivided into opaque and translucent. They respectively correspond (2.a) to all black-opaque organic matter that mainly include particles of woody origin, and (2.b) to all recognisable plant material of woody origin. AOM corresponds to all organic matter that visually is unorganized, structureless, and which may be finely disseminated or coagulated into fluffy masses.

The use of UV fluorescence microscopy was very useful in the palynofacies task, due to the fluorescence properties of palynomorphs, helping to distinguishing the different constituents of the palynomorphs groups. For each sample a total of 250 organic particles were counted. The results are summarised in Table 5.2.2.1 and plotted in Figure 5.2.2.1. The individual number of each organic particle has been converted in percentages.

In more detail for the palynofacies study, the abundances of continental palynomorphs on one hand, and marine palynomorphs on the other, allow us to determine whether the depositional environment was terrestrial or marine dominated. Indeed, a greater proportion of sporomorphs indicates a stronger continental influence, whereas a greater proportion of dinoflagellate cysts indicates an oceanic domination. For this purpose, the calculation is the following: (1) continental = (total spore+pollen)/total dinocyst; and (2)

marine = total dinocyst/(total spore+pollen). However, we used the (SP/D) ratios calculated by M. Mendes and Z. Pereira from LNEG. The reason for using this ratio is related to its greater precision and accuracy, as it was carried out by more experienced palynological researchers. Further information on Palynofacies is available in Appendix 5 which provides colour photos of the different palynofacies groups for each sample.

Table 5.2.2.1 Palynofacies results obtained *via* microscopic observations, coupled with the SP/D ratio calculated by Mendes et al. (in preparation)

Note: In yellow are the dominant organic matter groups, height is from the base of the sequence.

Layer n°	Height (m)	Sample code	Palynomorphe					Phytoclast		AOM	Palynofacies		
			Spore	Pollen	Dinocyst	Other marine	Unidentified	Opaque	Translucide		Continental	Marine	SP/D ratio
2	3	**P002.1**	0,0	7,4	1,6	9,0	21,2	29,0	3,9	27,9	41,1	58,9	-
4	8	**P003.1**	0,8	18,4	7,7	2,3	27,2	26,8	6,5	10,4	65,8	34,2	0.99
6	13,8	**P005.1**	1,5	6,0	7,1	35,1	19,1	7,5	9,0	14,9	15,1	84,9	0.93
8	15,5	**P008.1**	0,0	0,0	0,0	0,0	0,0	77,1	23,0	0,0	Barren		-
17	31,35	**P017.1**	0,0	11,1	4,0	0,4	0,0	80,5	1,5	2,6	71,6	28,4	0.28
20	32,85	**P020.1**	0,0	0,0	0,0	0,0	1,0	75,1	16,0	8,0	Barren		-
28	41,05	**P028.1**	0,8	5,9	4,3	0,0	3,5	73,8	3,9	7,8	60,9	39,1	-
30	42,05	**P030.1**	0,0	0,0	0,0	0,0	0,0	44,4	17,9	37,8	Barren		-
32	42,95	**P032.1**	0,0	0,0	0,0	0,0	0,0	52,4	28,3	19,4	Barren		-
53	66,3	**P066.1**	0,0	0,9	0,0	0,0	0,0	86,9	9,6	2,6	Not relevant		-
59	70,85	**P071.1**	7,4	7,0	3,2	0,0	1,0	72,6	1,9	7,0	81,8	18,2	-
66	77,45	**P077.1**	0,0	0,0	0,0	0,0	0,0	39,0	18,0	43,0	Barren		-
71	79,85	**P081.1**	1,1	36,3	11,8	0,4	13,5	15,7	2,5	18,9	75,4	24,6	0.69
76	81,95	**P085.1**	1,5	9,4	10,5	10,9	30,1	24,1	8,6	4,9	33,7	66,3	0.96
89	87,1	**P089.1**	0,0	0,4	1,4	0,7	4,6	66,0	15,6	11,4	16,0	84,0	-
95	91,95	**P095.1**	1,5	21,5	27,3	3,1	7,7	24,3	2,3	12,3	43,1	56,9	0.35
97	93	**P097.1**	1,1	1,5	31,7	0,8	21,3	18,7	14,9	10,1	7,4	92,6	0.33
106	103,15	**P106.1**	1,6	14,3	34,8	0,4	14,7	23,6	8,1	2,7	31,1	68,9	0.58
108	105,2	**P108.1**	1,1	7,1	6,0	4,1	33,2	32,9	10,1	5,6	44,8	55,2	-
114	110,4	**P114.1**	0,4	0,7	0,0	0,0	5,4	74,6	13,8	5,1	Not relevant		-
118	112,35	**P120.1**	0,0	1,0	1,0	0,0	4,0	84,1	10,0	0,0	50,0	50,0	-
124	124,6	**P124.1**	0,0	0,0	0,0	0,0	2,0	81,1	17,0	0,0	Barren		-
126	126,4	**P126.1**	0,4	10,4	22,6	0,4	18,8	26,5	17,3	3,8	32,0	68,0	0.88
130	127,85	**P130.1**	0,0	8,5	28,7	0,4	28,0	12,0	14,0	8,5	22,6	77,4	0.3
134	132,05	**P134.1**	0,8	9,4	35,2	0,0	26,2	14,3	9,7	4,5	22,5	77,5	0.46
138	138,25	**P138.1**	0,0	0,0	0,0	0,0	3,0	86,1	6,0	5,0	Barren		-
140	140,25	**P140.1**	0,0	0,0	0,0	0,0	1,6	29,5	9,3	59,7	Barren		-
143	143,7	**P153.1**	0,8	11,8	33,0	1,8	18,5	25,2	6,3	2,6	26,6	73,4	0.66
145	147.1	**P155.1**	0,4	16,0	36,7	1,6	24,2	10,2	3,9	7,0	30,0	70,0	0.69
148	149	**P158.1**	0,8	17,5	16,4	2,0	20,7	13,3	17,1	12,4	49,9	50,1	-
152	152.4	**P152.1**	0,0	0,0	0,0	0,0	1,0	22,0	6,0	71,1	Barren		-
152	152.9	**P152.2**	0,0	0,0	0,0	0,0	1,0	17,5	19,4	62,2	Barren		-
154	154	**P154.1**	0,0	0,0	0,0	0,0	0,0	28,9	21,2	50,0	Barren		-
156	155,9	**P166.1**	0,0	0,0	0,0	0,0	0,0	22,0	9,0	69,1	Barren		-
158	157.1	**P168.1**	0,0	0,0	0,0	0,0	0,0	70,1	30,0	0,0	Barren		-
160	159.9	**P160.1**	0,0	0,0	0,0	0,0	0,0	96,1	4,0	0,0	Barren		-
162	161,3	**P162.1**	0,4	10,0	31,1	4,6	22,6	11,5	15,0	5,0	22,6	77,4	0.41
164	162,4	**P164.1**	0,0	0,0	0,0	0,0	0,0	92,1	8,0	0,0	Barren		-
171	168,6	**P173.1**	0,0	1,0	0,0	0,0	1,0	88,1	10,0	0,0	Not relevant		-
172	170,3	**P173.2**	0,6	12,3	33,3	1,9	13,5	18,9	17,66	1,9	26,8	73,2	0.21
173	171,2	**P173.3**	1,2	17,5	28,2	0,8	14,3	15,1	20,3	2,8	39,2	60,8	-
175	173,4	**P175.1**	3,5	7,6	38,9	6,5	23,5	12,4	3,5	4,1	19,6	80,4	0.38

175	174,4	**P175.2**	0,4	11,2	25,5	8,6	27,7	9,4	7,5	9,7	25,4	74,6	0.77
176	175	**P176.a**	0,4	17,0	21,1	0,4	26,8	3,8	24,9	5,7	44,7	55,3	0.66
176	175,7	**P176.b**	0,0	20,9	19,8	1,2	18,6	20,4	13,4	5,8	49,9	50,1	0.39
178	177,2	**P178.1**	0,0	0,0	0,0	0,0	0,0	79,1	21,0	0,0	Barren		-
181	180,9	**P181.1**	0,0	0,0	0,0	0,0	0,0	29,0	44,0	27,0	Barren		-
193	193,5	**P193.1**	0,0	0,0	0,0	0,0	3,0	46,0	31,0	20,0	Barren		-

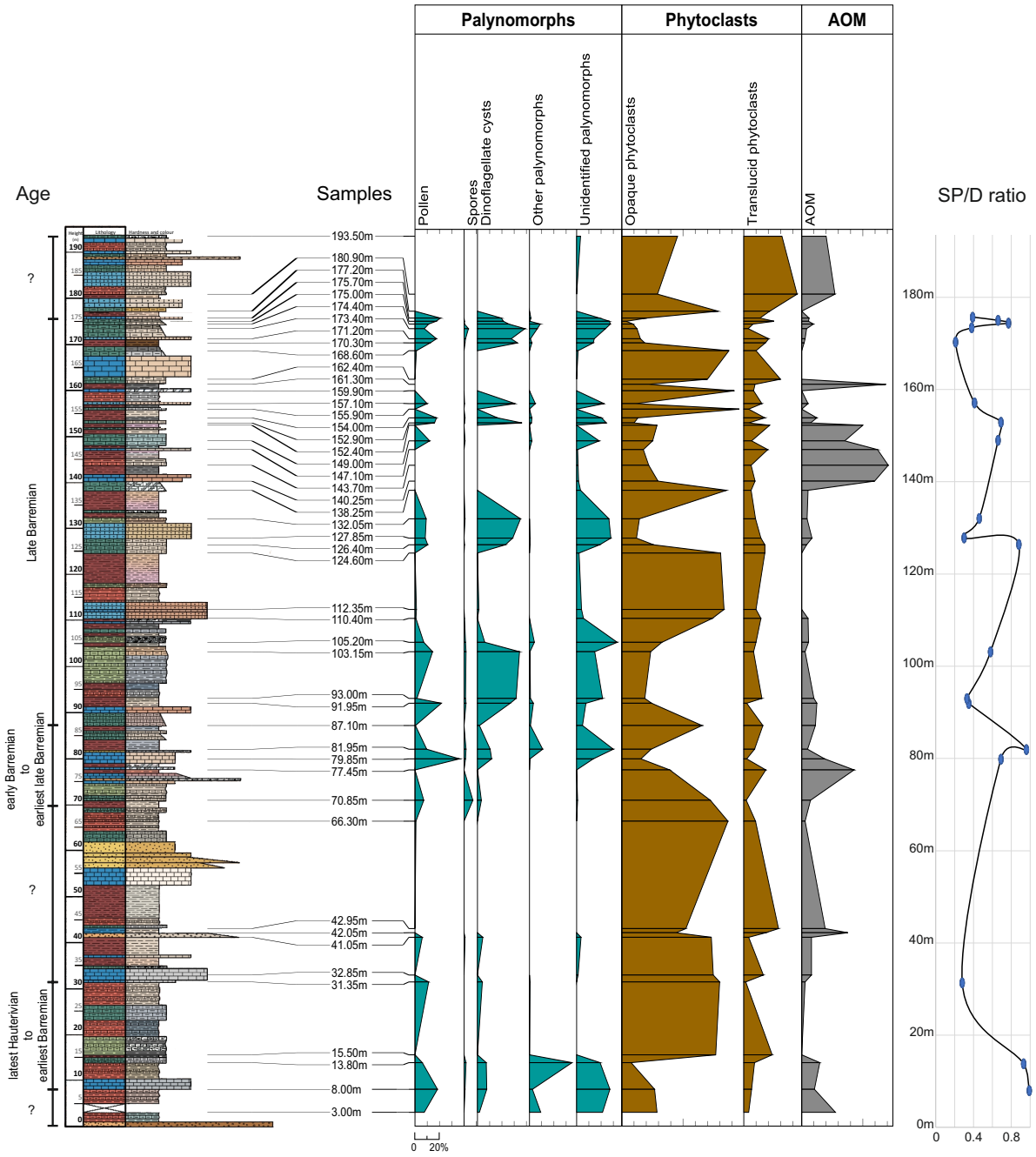


Figure 5.2.2.1 Palynofacies results plotted, SP/D data are from Mendes et al. (in preparation)

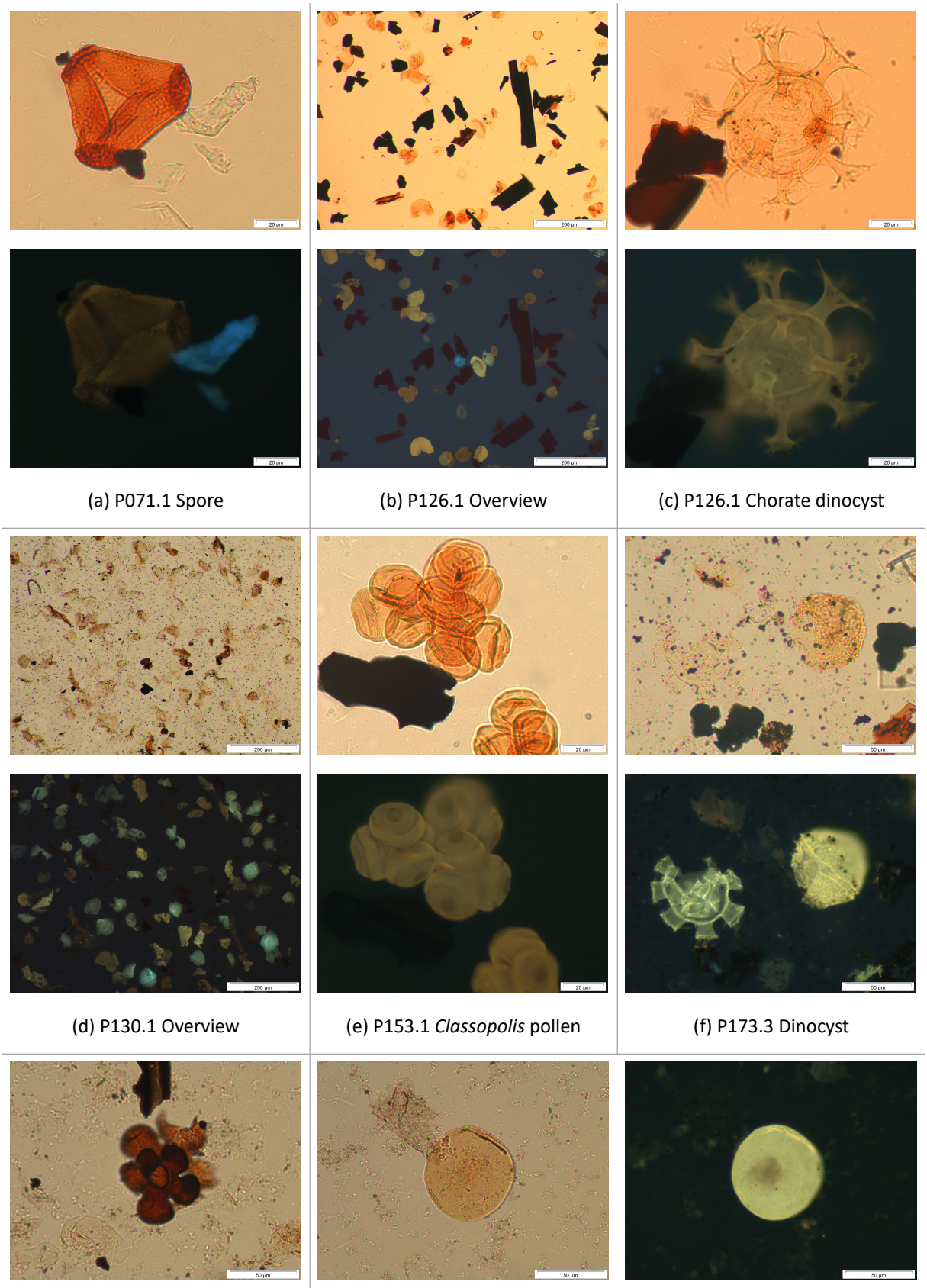
Twenty-two samples, from the forty-eight studied, have higher percentages of palynomorphs over phytoclasts and AOM groups. Looking at the abundances of

sporomorphs, it is possible to see that pollens are always more abundant than spores, the only exception is sample P071.1. The same trend was observed for dinoflagellate cysts, which occur in greater proportion than the other marine palynomorphs; with the exception of samples P002.1, P005.1 and P085.1. Furthermore, of the forty-eight samples, twenty-one are dominated by the phytoclasts group, four by AOM and one sample (P154.4) has an equal-value (50%) between the two latter groups of organic matter. In addition to this, opaque phytoclasts were observed in all samples, and the majority of the samples (forty samples) show higher abundances of opaque than translucent phytoclasts.

Twenty-one samples did not yielded palynomorphs and could not be used in the analysis of palynofacies that uses the SP/D ratio. Regarding the samples that yielded palynomorphs, only five have higher proportion of continental than marine palynomorphs, including the maximum value of 81.8% in sample P071.1. Samples with these characteristics are located in the first 71m of the stratigraphic sequence, from samples P002.1 to P071.1, and indicate a great influence of the continental derived organic matter on the carbonate platform. Conversely, twenty samples exhibit a more significant marine influence and are located in the upper part of the sequence. As for samples P120.1, P158.1 and P176.b, they show an equal abundance of continental and marine derived palynomorphs.

It should be noted, however, that compared to the results of Mendes et al. (in preparation), the dominant environmental influences observed are similar for only half of the samples. Indeed, the results are in agreement for samples P003.1, P081.1, P095.1, P097.1, P130.1, P134.1, P162.2, P173.2 and P175.1. For P005.1, P017.1, P085.1, P106.1, P126.1, P153.1, P155.1, P175.2 and P176.a the influences are opposite, *i.e.* the palynofacies data showed a continental influence while Mendes et al. (in preparation) rather detected a marine dominance, or *vice versa*. Moreover, contrary to the palynofacies observations, the terrestrial influence is not only restricted to the beginning of the Arrifes succession. It is possible to observe that the dominant environmental conditions fluctuated throughout the depositional period. These differences are explained by the fact that, compared to the LNEG researchers, I am inexperienced in the recognition of palynomorphs and probably confused some of them. That is why we used their SP/D values for the discussion.

The results will be used to describe the evolution of the Arrifes stratigraphic sequence. Indeed, palynofacies were a useful tool to discern whether the depositional environments were showing landward or seaward trends, *i.e.* regressions and transgression trends respectively, and if similar lithologies were deposited under the same conditions.



(a) P071.1 Spore

(b) P126.1 Overview

(c) P126.1 Chorate dinocyst

(d) P130.1 Overview

(e) P153.1 *Classopolis* pollen

(f) P173.3 Dinocyst

(g) P175.2 Foraminifer innerlining

(h) P175.2 Marine algae

Figure 5.2.2.2 Some pictures to illustrate the microscope work (See Appendix 5 for more).

5.3 Geochemistry

Two types of analyses were carried out for geochemical studies, on two distinct groups of samples. Firstly, whole-rock lithogeochemistry allows for the general chemical characterisation of the sediments, including the values of the major and trace elements, as well as Rare Earth Elements (REEs). The results were used to trace the history of the sediments in terms of provenance and recycling, and thus gain insight into paleoclimatic trends during the time of deposition (Dinis et al., 2020). Whole-rock lithogeochemistry analysis were performed on decarbonated rock powder of carbonated rocks, and required the elimination of carbonate minerals before analysis.

The second geochemical analysis performed was the measure of δ^{13}Corg in the palynological residues. The values obtained by this technique, were used to have a more insight view on the evolution of the Arrifes sedimentary record in terms of the local and global response to the carbon biogeochemical cycle; for example, it can help to detect Oceanic Anoxic Events (OAEs) in the sedimentary record.

5.3.1 Whole-Rock geochemistry

To describe and discuss the geochemical results of the twenty-two samples analysed, the latter were divided into two distinct groups according to their stratigraphic position (thus, their age) in Arrifes succession. Indeed, group G1 includes samples dated to Late Hauterivian to Early Barremian interval (samples P002.1 to P089.1); and group G2 includes samples from Mid to Late Barremian (samples P106.1 to P193.1). The main goals of this task were to understand the sources and recycling of sediments during these two time intervals, and how this may be related to Lower Cretaceous paleoclimates and environmental changes, such as transitions from wet to dry climates and *vice versa* (Dinis et al., 2020; Jorge et al., 2013).

5.3.1.1 Major and trace elements

Major and trace elements values were calculated and normalised to the Post Archaen Australian Shales (PAAS) used for fine-grained clastic sediments and the average composition of the Upper Continental Crust (UCC). They are standardised mean values used to compare the sediments with the mean igneous rocks of the upper continental crust (McLennan, 2001). In table 5.3.1.1.1, G1 and G2 correspond to the average of all samples that were

included in these two geochemical and stratigraphic groups. The major elements values are very similar between G1 and G2 (Table 5.3.1.1.1 and Figure 5.3.1.1.1). When compared to PAAS, G1 and G2 have similar compositions, with the exception of MnO, CaO, Na_2O and P_2O_5, where G1 and G2 are slightly impoverished. When compared with each other, G1 and G2 MnO, CaO, Na_2O and P_2O_5 are in various degrees depleted, whereas the oxides SiO_2, TiO_2, Al_2O_3, MgO and K_2O show a relative constancy.

Table 5.3.1.1.1 Normalised major elements data, ratios UCC/PAAS, UCC/G1 and UCC/G2

%wt	SiO_2	TiO_2	Al_2O_3	$Fe_2O_3(T)$	MnO	MgO	CaO	Na_2O	K_2O	P_2O_5
PAAS	0,95	2,00	1,25	1,60	1,57	1,00	0,31	0,31	1,09	0,80
G1	0,84	2,08	1,25	1,53	0,54	0,97	0,12	0,09	1,56	0,29
G2	0,85	2,03	1,27	1,40	0,32	0,80	0,07	0,06	1,36	0,19

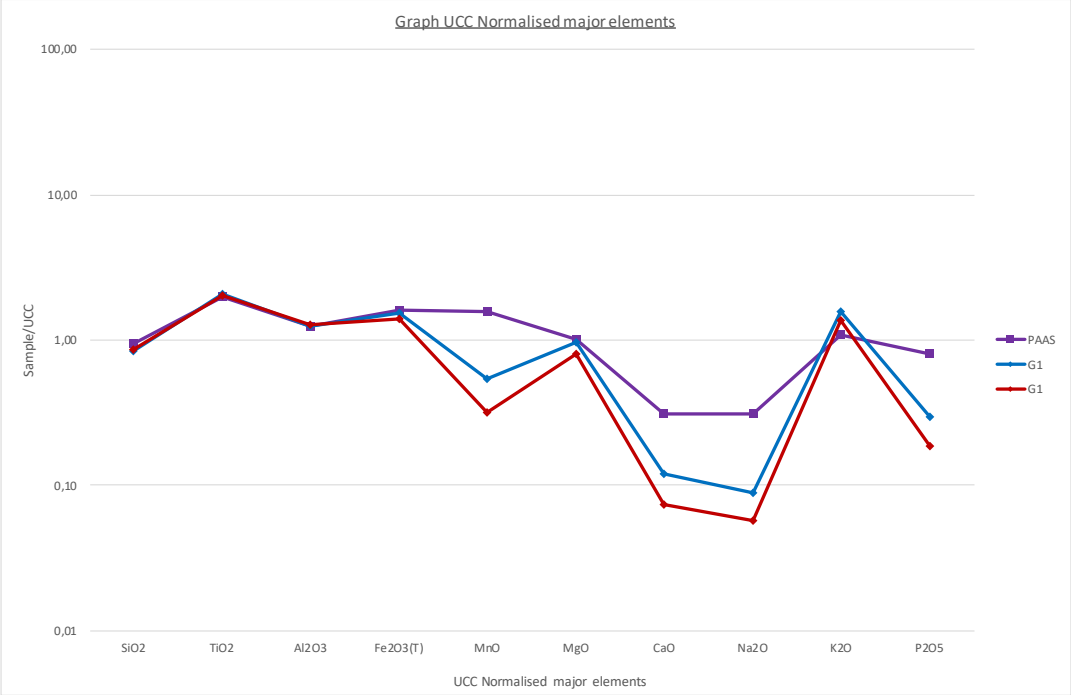


Figure 5.3.1.1.1 Normalised major elements plot, ratios UCC/PAAS, UCC/G1 and UCC/G2

The trace elements of G1 and G2 groups do not show notable variations in their composition when compare to PAAS. When compared to the UCC, elements such as V, Cr, Co, Ni and Rb show various degrees of increase in G1 and G2, whereas Sr is strongly depleted in those groups. Elements Y, Zr, Nb, Ba, Hf, Pb, Th and U do not show any notable degree of

variation to the UCC composition. Actually, the values of these elements in G1 and G1 groups is similar to their composition in the UCC.

Table 5.3.1.1.2 Normalised trace elements data, ratios UCC/PAAS, UCC/G1 and UCC/G2

%wt	V	Cr	Co	Ni	Rb	Sr	Y	Zr	Nb	Ba	Hf	Pb	Th	U
PAAS	2,50	3,14	2,30	2,75	1,43	0,57	0,45	1,11	0,76	1,18	0,86	1,00	1,36	1,11
G1	2,20	3,42	1,65	2,14	1,95	0,21	0,76	1,00	0,72	0,64	0,83	1,13	0,82	1,10
G2	2,29	3,21	1,31	1,91	1,72	0,14	0,84	1,06	0,65	0,55	0,84	0,69	0,71	1,04

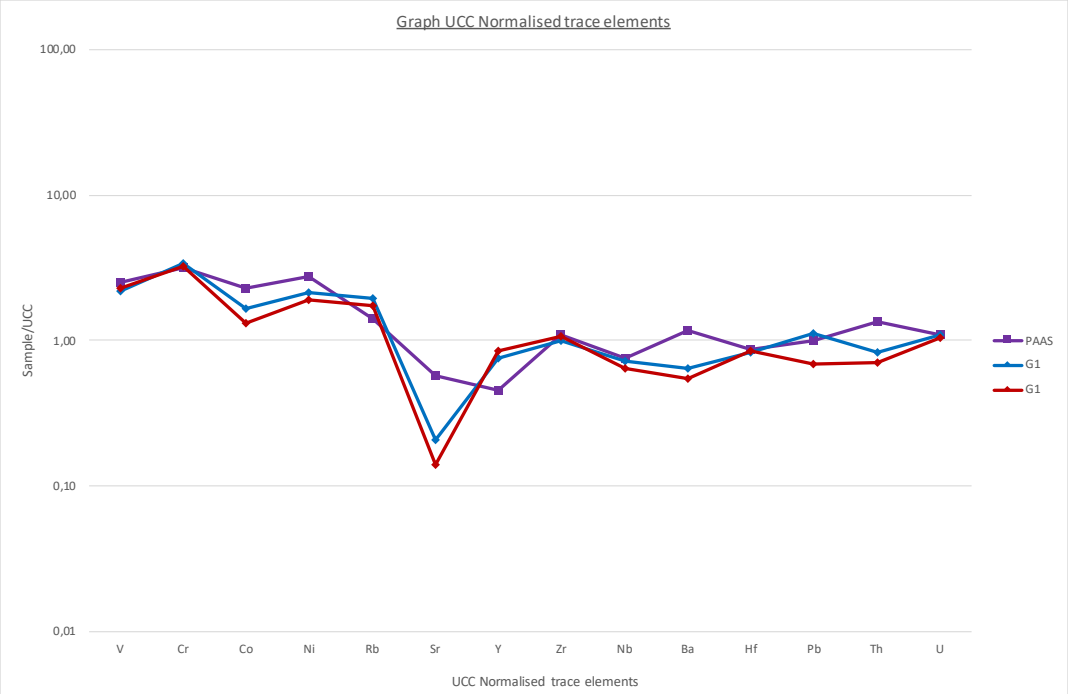


Figure 5.3.1.1.2 Normalised trace elements plot, ratios UCC/PAAS, UCC/G1 and UCC/G2

5.3.1.2 Rare Earth Elements (REEs)

The Rare Earth Element (REEs) values were calculated and normalised according to the chondrite database (McDonough and Sun, 1995). The average of total of REE (∑REE) contents for G1 and G2 (105 and 115ppm, respectively) are less than the UCC (146.4ppm; Taylor and McLennan, 1985). As illustrated in Figure 5.3.1.2.1, average chondrite-normalised REEs patterns (Taylor and McLennan, 1985) of analysed rocks are enriched in light REE (LREE), with the flattened patterns of heavy REE (HREE). The Europium or Eu anomaly (Eu/Eu*) is variable. For G1, Eu/Eu* value is 0.69 ±0.05, and for G2 the value is 0.67 ±0.03.

Table 5.3.1.2.1 Normalised Rare Earth Elements data for G1 and G2 samples

G1 from Late Hauterivian to Early Barremian (n=7)														
%wt	**La**	**Ce**	**Pr**	**Nd**	**Sm**	**Eu**	**Gd**	**Tb**	**Dy**	**Ho**	**Er**	**Tm**	**Yb**	**Lu**
P002.1	84,74	60,40	47,08	32,21	18,61	9,89	10,88	9,66	10,00	9,05	9,52	10,39	10,65	11,00
P003.1	66,76	46,50	36,06	25,46	14,29	8,30	8,69	8,10	8,01	7,52	7,91	8,62	8,67	9,34
P017.1	55,59	39,39	30,66	21,80	12,38	6,39	7,39	7,41	7,95	7,64	7,71	8,37	8,23	8,32
P020.1	58,86	41,38	32,48	21,94	12,64	6,24	7,84	7,24	7,59	7,29	7,31	8,06	8,06	7,85
P032.1	49,05	34,38	26,42	18,42	10,74	6,02	7,68	7,07	7,43	7,17	7,55	8,17	7,66	7,77
P085.1	67,85	45,77	35,26	24,47	13,20	7,34	7,45	7,07	7,19	6,93	7,19	7,89	7,98	8,14
P089.1	69,21	49,01	39,42	27,85	15,50	8,56	8,82	8,62	8,48	8,11	8,39	8,68	9,19	9,53
G2 from mid to Late Barremian (n=15)														
%wt	**La**	**Ce**	**Pr**	**Nd**	**Sm**	**Eu**	**Gd**	**Tb**	**Dy**	**Ho**	**Er**	**Tm**	**Yb**	**Lu**
P106.1	62,94	42,95	34,45	22,78	13,38	7,07	8,07	6,90	6,88	6,46	7,07	7,70	7,98	8,40
P108.1	59,40	41,59	32,48	23,77	13,55	7,45	8,43	7,76	7,38	7,40	7,71	8,37	8,06	8,27
P124.1	39,51	28,74	22,55	16,32	9,83	4,95	6,83	7,24	7,53	7,76	8,59	9,78	9,84	10,37
P126.1	63,22	46,50	36,93	27,00	15,50	8,07	9,18	8,79	9,03	8,23	8,84	9,97	10,00	10,00
P152.1	101,09	74,92	60,88	45,43	22,81	11,49	12,97	11,90	11,13	9,87	10,68	11,26	11,41	11,76
P152.2	67,30	47,54	37,30	25,60	15,50	7,98	9,74	8,62	8,43	7,87	8,43	9,19	8,91	8,79
P153.1	72,21	50,47	40,36	27,29	15,80	8,67	9,08	9,14	8,71	8,23	8,67	9,58	9,35	9,40
P154.1	76,57	54,75	44,16	31,79	19,00	9,57	10,49	10,86	10,18	9,75	9,92	10,42	9,96	10,16
P162.1	66,76	48,80	39,49	26,86	15,32	8,25	9,51	8,79	8,19	8,11	8,51	8,68	8,71	8,69
P173.1	79,84	57,99	45,55	32,49	18,48	9,34	11,63	11,03	10,42	9,64	9,96	10,56	10,08	9,97
P173.2	91,55	67,92	54,16	38,82	21,86	10,82	13,24	12,24	11,52	10,69	11,33	11,54	11,17	11,08
P173.3	64,31	45,45	35,99	25,18	13,94	7,41	8,07	7,59	7,66	7,05	7,63	7,89	7,70	8,48
P175.2	65,67	47,54	38,32	26,72	15,32	8,16	9,28	8,97	8,45	7,99	8,76	8,54	8,67	9,00
P181.1	58,04	42,84	33,94	24,05	14,24	6,95	8,43	7,76	7,48	7,29	7,51	8,68	8,39	8,66
P193.1	65,12	47,75	37,52	26,58	14,55	8,01	8,89	8,10	7,66	7,29	7,75	8,37	8,47	8,45

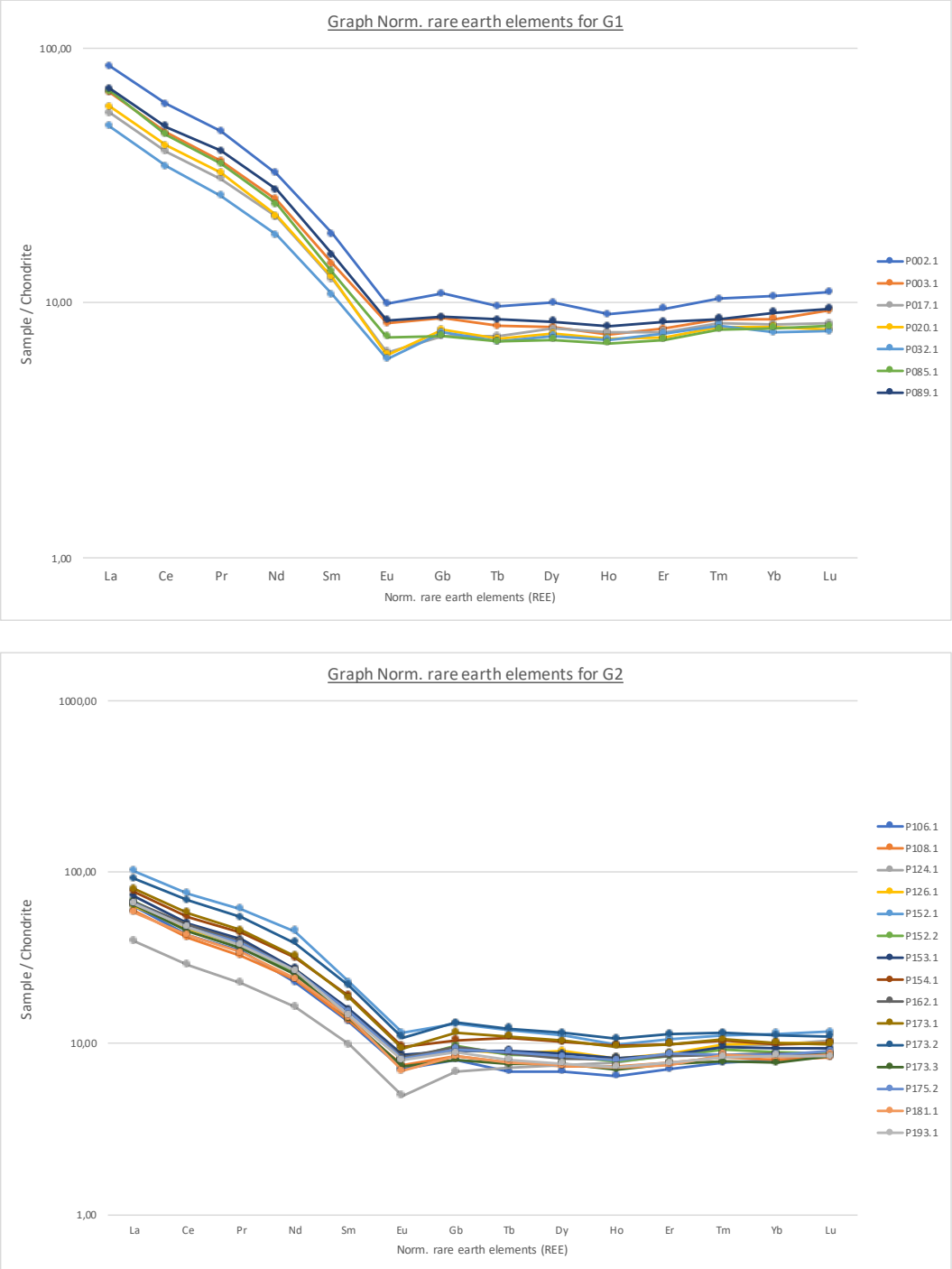


Figure 5.3.1.2.1 Normalised REE plot for G1 and G2 samples

Overall, all three types of elements (*i.e.* major, trace and REEs) follow the same trend during the Late Hauterivian and the Barremian, with some minor exceptions. The results are used in directly interpreted ratios in part ''6. Discussion'' to understand the paleoclimatic conditions of the Late Hauterivian to Late Barremian time interval in this central part of the Algarve Basin.

5.3.2 Organic Carbon $\delta^{13}C$ stable isotopes geochemistry

The geochemical analysis of δ^{13}Corg stable isotopes was carried out on the organic material (palynological residues) of twenty-nine samples distributed along the Arrifes succession (Figure 5.3.2.1).

One of the main objective of this task was to characterise the perturbations in local or global carbon cycle with the study of the shifts of $\delta^{13}C_{org}$ values in the Arrifes succession. This task was also performed to detect hitherto unrecognised Lower Cretaceous Oceanic Anoxic Events (OAEs), as they reflect significant changes in environmental, climatic and marine conditions (Keller, 2008). OAEs are characterised by a decrease in available dissolved oxygen (DO) in the water column, can severely disrupt aerobic organisms and thus disrupt trophic chains and entire ecosystems (Leckie et al., 2002). Organisms die and the decomposition of their bodies results in increased fluxes of organic carbon (C_{org}) to the seabed. As a result, an increase in C_{org} burial in sediments occurs which is expressed by positive excursions of $\delta^{13}C$ in inorganic carbonates and by negative excursions, if the study is carried out on organic residues, as it is the case in this work (Wang et al., 2014; Arthur et al., 1988).

In addition, other environmental phenomena can be detected through this analysis, as excursions can originate from increased volcanic activity. Indeed, if volcanoes release excessive ^{13}C-poor CO_2, this discharge will have the impact of increasing the values of $\delta^{13}C$ in the natural carbon reservoirs (Baudin and Riquier, 2014; Huck, 2013).

Table 5.3.2.1 Results for organic Carbon $\delta^{13}C_{org}$ stable isotopes geochemistry

Note: The green colour stands for positives excursions of $\delta^{13}C_{org}$, while red is for the negatives ones.

Layer n°	Sample code	Height (m)	$\delta^{13}C_{org}$	TOC (%*wt*)	Layer n°	Sample code	Height (m)	$\delta^{13}C_{org}$	TOC (%*wt*)	Layer n°	Sample code	Height (m)	$\delta^{13}C_{org}$	TOC (%*wt*)
4	**P003,1**	8	-23,598	1,101	89	**P089,1**	87,1	-21,534	0,287	152	**P152,2**	152,9	-21,525	1,093
6	**P005,1**	13,8	-21,275	4,126	95	**P095,1**	91,95	-22,402	2,073	154	**P154,1**	154	-20,378	0,907
8	**P008,1**	15,5	-20,54	1,365	108	**P108,1**	105,2	-20,625	0,224	158	**P168,1**	157,1	-23,267	0,257
17	**P017,1**	31,35	-21,173	3,266	114	**P114,1**	110,4	-20,462	0,765	162	**P162,1**	161,3	-21,699	5,533
20	**P020,1**	32,85	-18,097	0,060	124	**P124,1**	124,6	-20,846	0,054	172	**P173,2**	170,3	-22,157	2,647
32	**P032,1**	42,95	-20,596	1,261	126	**P126,1**	126,4	-20,889	7,776	173	**P173,3**	171,2	-24,779	0,372
53	**P066,1**	66,3	-18,585	0,288	130	**P130,1**	127,85	-20,789	5,743	175	**P175,2**	174,4	-23,039	1,586
59	**P071,1**	70,85	-20,028	0,251	143	**P153,1**	143,7	-22,391	1,043	178	**P178,1**	177,2	-22,195	0,395
71	**P081,1**	79,85	-21,265	0,590	145	**P155,1**	147,1	-24,277	24,565	193	**P190,5**	193,5	-22,965	0,363
76	**P085,1**	81,95	-21,086	20,455	148	**P158,1**	149	-23,195	0,257					

Note: Height is from the base of sequence.

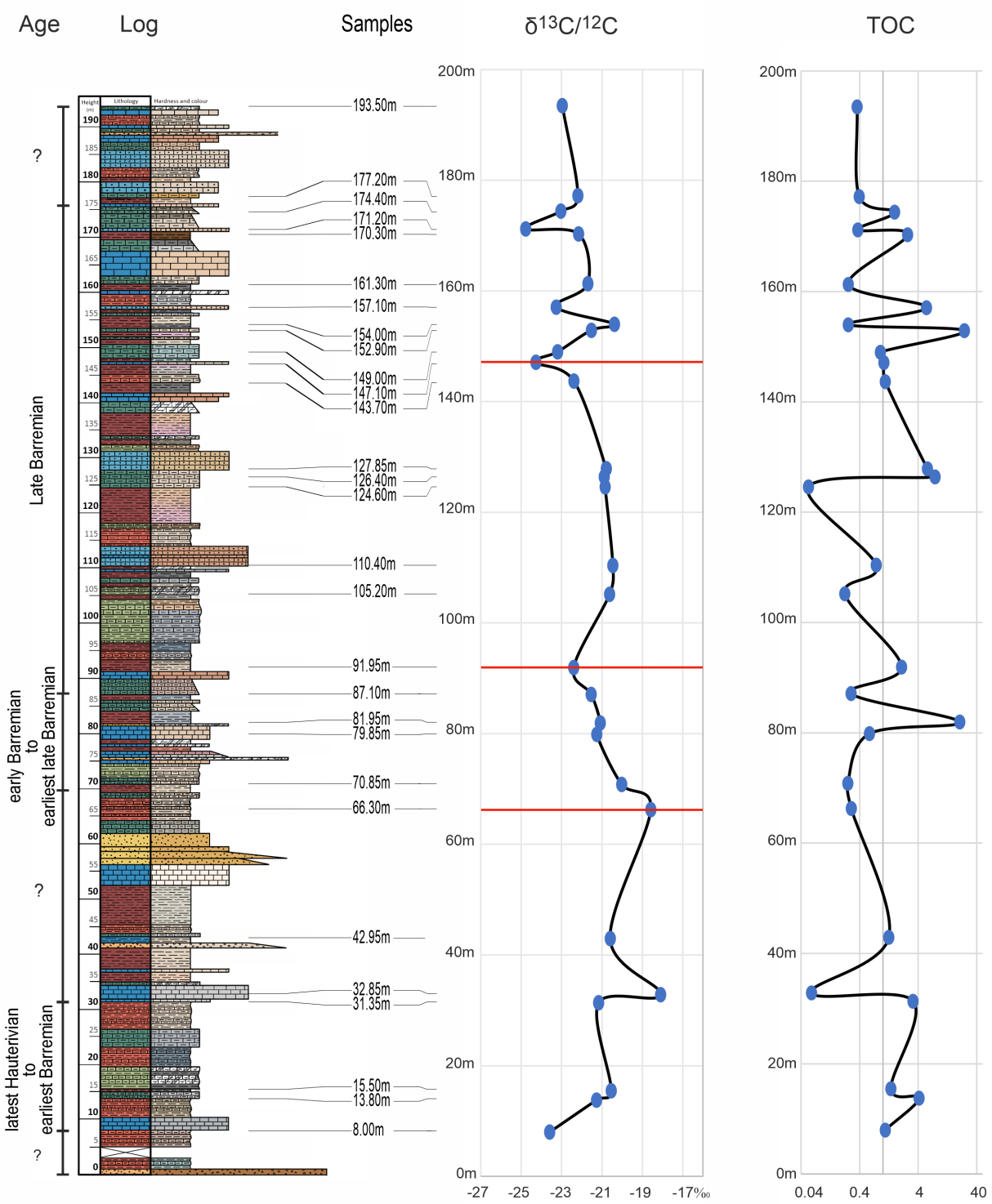


Figure 5.3.2.1 Plotted results for organic Carbon $\delta^{13}C$ stable isotopes geochemistry in ‰ and Total Organic Content (TOC) in %, the red bars delineate the four segments described below

Note: The TOC graph is projected with a 10 base logarithmic scale.

Table 5.3.2.1 and Figure 5.3.2.1 report the results obtained for the $\delta^{13}C_{org}$. $\delta^{13}C_{org}$ values range from -24.779‰ (P173.3) to -18.097‰ (P020.1). The $\delta^{13}C_{org}$ curve can be divided into four segments according to the general trend of the $\delta^{13}C_{org}$ values: (1) from samples

P003.1 to P066.1 where the values are increasing including a peak at -18.097‰ in P020.1; (2) samples P071.1 to P095.1 exhibit a decreasing trend, reaching a minimum value of -22.402‰ in sample P095.1; (3) samples P108.1 to P155.1 is a segment of the $\delta^{13}C_{org}$ curve where at first there is an increase to -20.625‰ (P108.1), then a continuous decrease to -24.277 ‰ (P155.1); (4) samples P158.1 to P190.5 where the $\delta^{13}C_{org}$ values fluctuate rapidly, although the general trend is to a decrease of the values. This trend continues and follow the decrease trend in $\delta^{13}C_{org}$ values observed in the previous segment of the $\delta^{13}C_{org}$ curve.

In summary, the interpreted segments of the $\delta^{13}C_{org}$ curve define two major trends, starting from the base a positive trend is observed, followed by a negative trend until the top of the succession. This general curve is punctuated with a modest negative δ^{13}Corg excursion that peak at 66.3m from the base of the succession. This negative punctuated excursion coincides with the limit between the earliest Late Barremian and the Late Barremian strata, and is correlated within a general transgressive trend.

Figure 5.3.2.1 also show the Total Organic Content (TOC) of the samples expressed in percentage of the weight of the rock sample (%*wt*). TOC's values show a huge variability, with a minimum of ≈0,04 and a maximum value of ≈38%. The more organic-rich samples are from marls and marly limestones associated with Lithofacies G and I, whereas the more organic lean samples are associated with Lithofacies E and F. Comparing TOC's values to the $\delta^{13}C_{org}$ general curve, there is no apparent trend.

6. Discussion

The main objective of this study is to reconstruct the climatic and oceanographic conditions (including the influence of eustatic sea-level fluctuations and periods of marine anoxia) in the Early Cretaceous Algarve Basin (Portugal) through the Arrifes stratigraphic sequence, southwest of Albufeira. To this goal, observations from all the techniques used (1) sedimentology, (2) palynology, (3) whole-rock geochemistry and (4) $\delta^{13}C_{org}$ isotopes geochemistry, have been correlated in this discussion.

6.1 The Age of the Arrifes stratigraphic succession

Rey and Ramalho (1974) assigned an Aptian age to the Arrifes succession, based on its stratigraphic position and facies observation, similar to the top of the Luz Formation located in the western Algarve Basin (Margas de Luz). However, following logging and more detailed observations of the different lithofacies, the lithologic correlation to the Luz (Aptian) sequence was unmatchable.

Based on the observations of the palynological organic residues content, by observing the first occurrence of three dinoflagellate species when correlated to the ammonite biozones of Leereveld (1997), the researchers Márcia Mendes and Zélia Pereira from LNEG (Porto) were able to assign three new ages to the Arrifes succession (Figure 6.1.1).

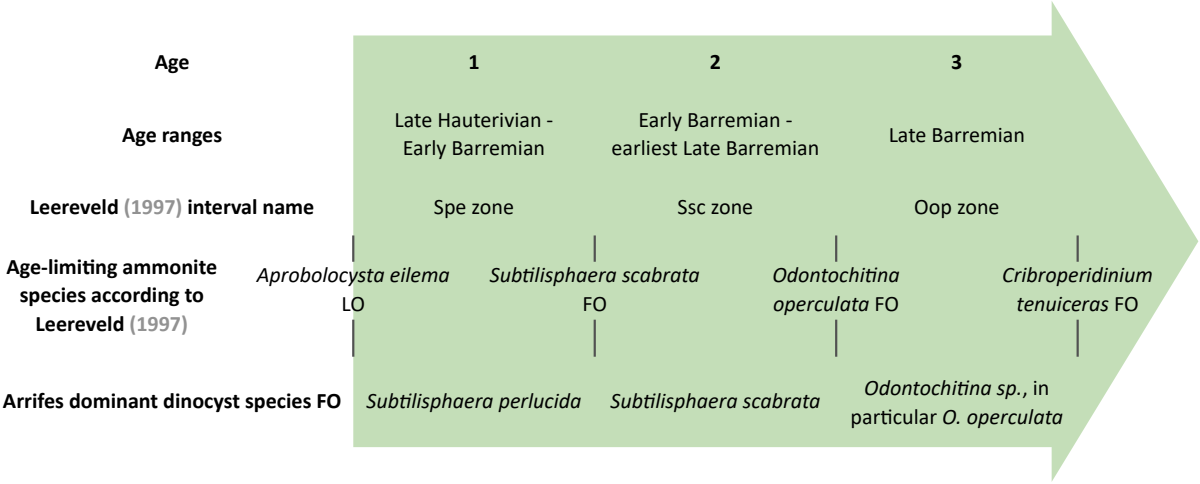


Figure 6.1.1 Age ranges attributed to Arrifes stratigraphic sequence; FO: First Occurence and LO: Last Occurrence; Leereveld (1997)

Thus, from the base until the sample P017.1 the succession is of latest Hauterivian to earliest Barremian age. The middle part of the succession from sample P081.1 to sample P085.1 is assigned to the Early Barremian to the earliest Late Barremian. Finally, the upper part of the succession above sample P095.1 is assigned a Late Barremian age. This is a new dating for the Arrifes stratigraphic sequence, meaning that it is no older than the Late Hauterivian and no younger than the Early Aptian. As described earlier, some authors considered the Arrifes succession of Aptian age, whereas other indicated an unconstrained age of Berriasian to Barremian. This also allow the recognition, for the first time, of Late Hauterivian to Late Barremian strata in the central Algarve Basin.

With this new age for the Arrifes sequence, it is now possible to correlate it with the stratigraphic scheme proposed by Rey (2006) for the Lower Cretaceous strata in western Algarve Basin. Accordingly, the Arrifes sequence age correlates to the Salema Formation and the Lower part of the Barrancão Formation (Figure 6.1.3). The intra-Barremian unconformity proposed by Rey (2006) for the western Algarve, was not identified or recognised in our work. We didn't detect any time related break in the sedimentary succession of Arrifes, neither the palynological ages support an hiatus.

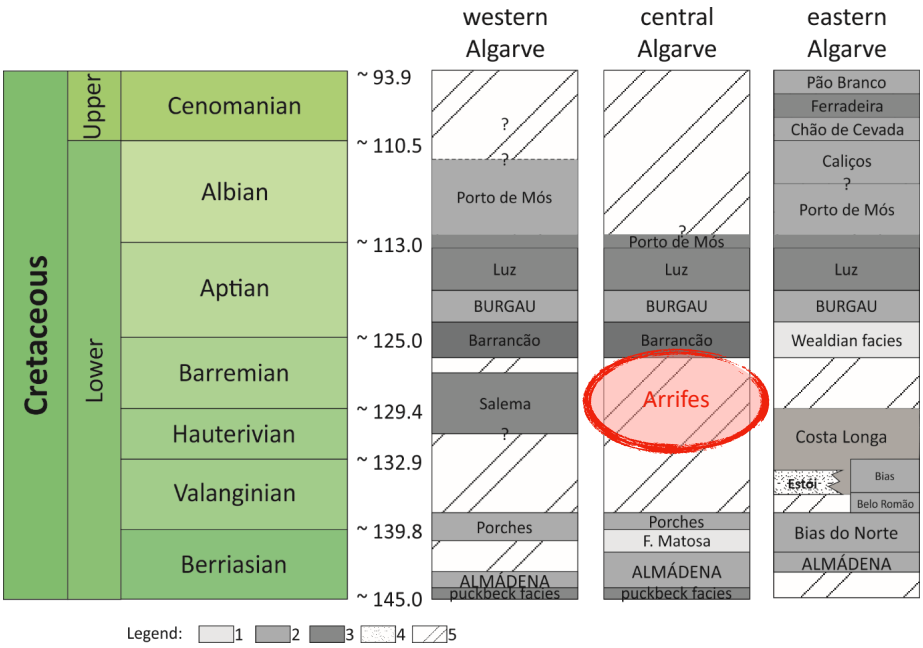


Figure 6.1.2 Lithostratigraphic scheme for the Lower Cretaceous Algarve Basin (Portugal) by Mendes et al. (in preparation), after Rey (2009)

6.2 Paleoweathering, recycling and sediment sources

Based on the stratigraphic position of the sample, the whole-rock geochemical data obtained for the Arrifes sequence was divided into two groups: G1, representing the Late Hauterivian to the Early Barremian layers, and G2 including the Mid to Late Barremian layers. At first glance, trace and major element results are almost superimposed, indicating similar depositional conditions for samples of both groups. The major and trace elements and Rare Earth Elements (REEs) ratios were used to produce graphs that help to reconstruct the source to sink history of the sediments. Our results are always compared and correlated to those of Dinis et al. (2020) work for the Lower Cretaceous formation in western Algarve, allowing the Arrifes succession to be geochemically compared at a regional scale.

6.2.1 Paleoweathering indices

Weathering intensity at the source area is one of the main factors that influence the mineralogy of sedimentary rocks. Elements such as Cs, Rb and Ba are preferentially fixed in weathering profiles through adsorption on clays, whereas Na, Ca and Sr are leached weathering profiles (Nesbitt et al., 1980). To asses weathering conditions Nesbitt and Young (1982) proposed the Chemical Index of Alteration (CIA), which reflects the intensity of chemical weathering in the source area. CIA varies from ≈50 for unweathered igneous rocks to near 100 for residual clays enriched in kaolinite and Al oxy-hydroxides. CIA is calculated using molar proportions of the following oxides: $CIA=[Al_2O(Al_2O_3\ CaO^*\ Na_2O+K_2O)]\times100$, where CaO* is the amount of CaO incorporated in the silicate fraction of the sample only, after correction for Ca contained in carbonate (Fedo et al., 1995; McLennan et al., 1993). The chemical weathering index (CIX) is calculated using molar proportions according to the following formula: $CIX=[Al_2O_3(Al_2O_3\ K_2O\ Na_2O)]\times100$. As CIA, the CIX index increases as the intensity of weathering also increases. Lastly, to minimise sorting effects, we also adopted the indices of element mobility (αAlE) of Garzanti et al. (2013).

Due to the fact that all the samples analysed were carbonate rich, indices CIX (Garzanti et al., 2014) and CPA (Chemical Proxy of Alteration) (Buggle et al., 2011) were used in order to avoid the bias introduced by the presence of non-silicate bound CaO (Dinis et al., 2020). The ratios Na_2O/Sm and K_2O/Th used by Dinis et al. (2020) for the Lower Cretaceous

formations in western Algarve Basin were also adopted. Thus, we will have the same geochemical indices so we can compare to it, and better evaluate our work.

The results of all paleoweathering indices calculated are illustrated in Figures 6.2.1.1, 6.2.1.2, 6.2.1.3 and 6.2.1.4, where the values for the same indices calculated by Dinis et al. (2020) for the Lower Cretaceous formations in western Algarve Basin are also plotted. The aim is to compare and refine the interpretations of the sedimentary and climatic conditions during the deposition of these strata, at the local scale of Arrifes, and at the regional scale of the Algarve Basin. For each of these figures, the colour legend is:

- **G1 of the Arrifes sequence:** blue diamond;
- **G2 of the Arrifes sequence:** red diamond;
- **Salema Formation:** orange circle;
- **Barrancão Formation:** grey circle;
- **Burgau Formation:** yellow circle;
- **Luz Formation:** green circle;
- **UCC standard:** purple triangle;
- **PAAS standard:** purple square.

The main results from the calculation of the different weathering are described with the following tables (and associated plots) where:

- **Med**: the value that separates the Lower half from the upper half of the data;
- **STD:** Standard Deviation;
- **Max:** the maximum value;
- **Min:** the minimum value;
- **X:** the average *i.e.* sum of all values divided by the number of the values.

- **CIX**: The CIX values (Table 5.3.1.1.4) vary from 73 to 80 for the samples of G1 group, and from 74 to 81 for G2. The low variability of the CIX values indicate moderate to high steady-state weathering in the source area. The values calculated to CIX are comparable to those of Salema, Barrancão and Luz Formations. For G2, the point exceeding 90 appears to be an outlier. The values for CIA and CPA are available in Appendix 6.

Table 6.2.1.1 Chemical weathering index (CIX), including data from Dinis et al. (2020)

	CIX — Chemical weathering index				
	Méd.	STD	Max.	Min.	X
Arrifes Formation: G1 from Late Hauterivian to Early Barremian (n=7)	74,91	2,44	79,75	72,83	73,91
Arrifes Formation: G2 from Mid to Late Barremian (n=15)	78,27	4,05	90,96	73,83	77,78
Salema Formation (n=13) (Dinis et al. 2020)	75,78	1,79	78,14	72,89	75,91
Barrancão Formation (n=4) (Dinis et al. 2020)	75,94	0,73	76,92	75,15	75,84
Burgau Formation (n=3) (Dinis et al. 2020)	81,27	1,32	82,76	80,24	80,81
Luz Formation (n=16) (Dinis et al. 2020)	77,54	2,69	83,76	73,90	76,87

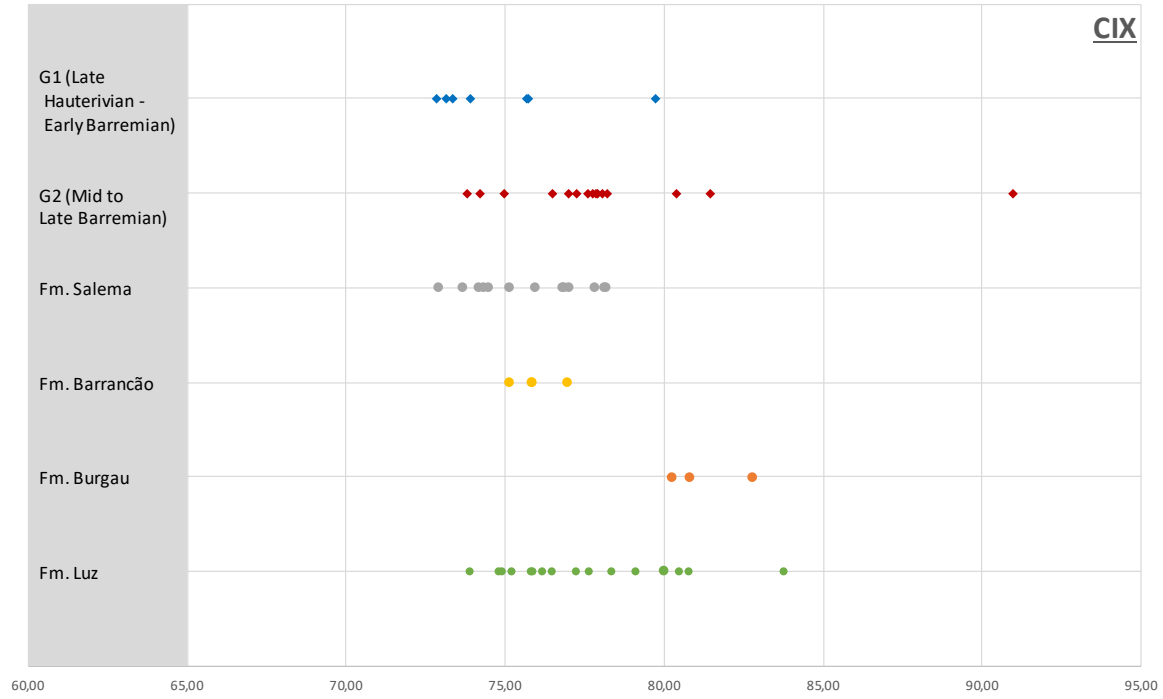


Figure 6.2.1.1 Plotted CIX data, including data from Dinis et al. (2020)

- **Na_2O/Sm**: G2 shows relatively scattered values ranging from ≈350 to ≈940 which are spread over G1, Salema and Luz Formations. G1 is only included in the high values of G2; however, it correlates well with the Salema Formation (≈590 to ≈850).

Table 6.2.1.2 Na_2O/Sm ratio data, including data from Dinis et al. (2020)

	Na2O/Sm				
	Méd.	STD	Max.	Min.	X
Arrifes Formation: G1 from Late Hauterivian to Early Barremian (n=7)	690,92	87,46	852,46	594,41	674,42
Arrifes Formation: G2 from Mid to Late Barremian (n=15)	614,28	171,33	938,51	352,42	637,81
Salema Formation (n=13) (Dinis et al. 2020)	710,03	81,25	837,44	584,96	674,85
Barrancão Formation (n=4) (Dinis et al. 2020)	292,18	75,23	383,75	220,44	282,26
Burgau Formation (n=3) (Dinis et al. 2020)	254,66	86,34	383,75	75,23	237,49
Luz Formation (n=16) (Dinis et al. 2020)	435,24	99,79	719,42	304,57	417,49

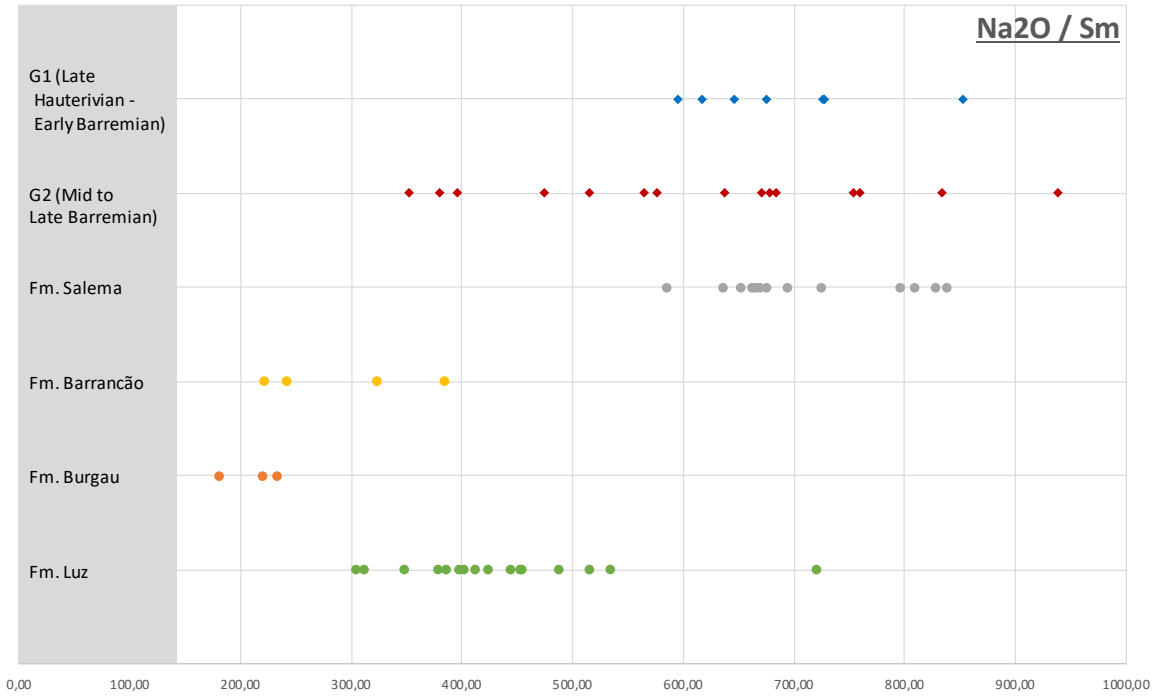


Figure 6.2.1.2 Plotted Na_2O/Sm data, including data from Dinis et al. (2020)

- **K_2O/Th*1000**: For this ratio, only the Salema Formation fits the G1 and G2 groups within a range of ≈5 to ≈10. The other Lower Cretaceous formations have Lower values being partially or completely below 4.

Table 6.2.1.3 K_2O/Th*1000, including data from Dinis et al. (2020)

	K2O/Th*1000				
	Méd.	STD	Max.	Min.	X
Arrifes Formation: G1 from Late Hauterivian to Early Barremian (n=7)	7,14	1,53	9,55	5,06	6,72
Arrifes Formation: G2 from Mid to Late Barremian (n=15)	7,11	4,53	22,18	1,69	6,57
Salema Formation (n=13) (Dinis et al. 2020)	6,73	1,00	9,32	5,64	6,49
Barrancão Formation (n=4) (Dinis et al. 2020)	3,51	0,39	3,81	2,94	3,65
Burgau Formation (n=3) (Dinis et al. 2020)	2,99	0,97	3,81	0,39	3,22
Luz Formation (n=16) (Dinis et al. 2020)	4,36	1,29	7,48	2,59	4,23

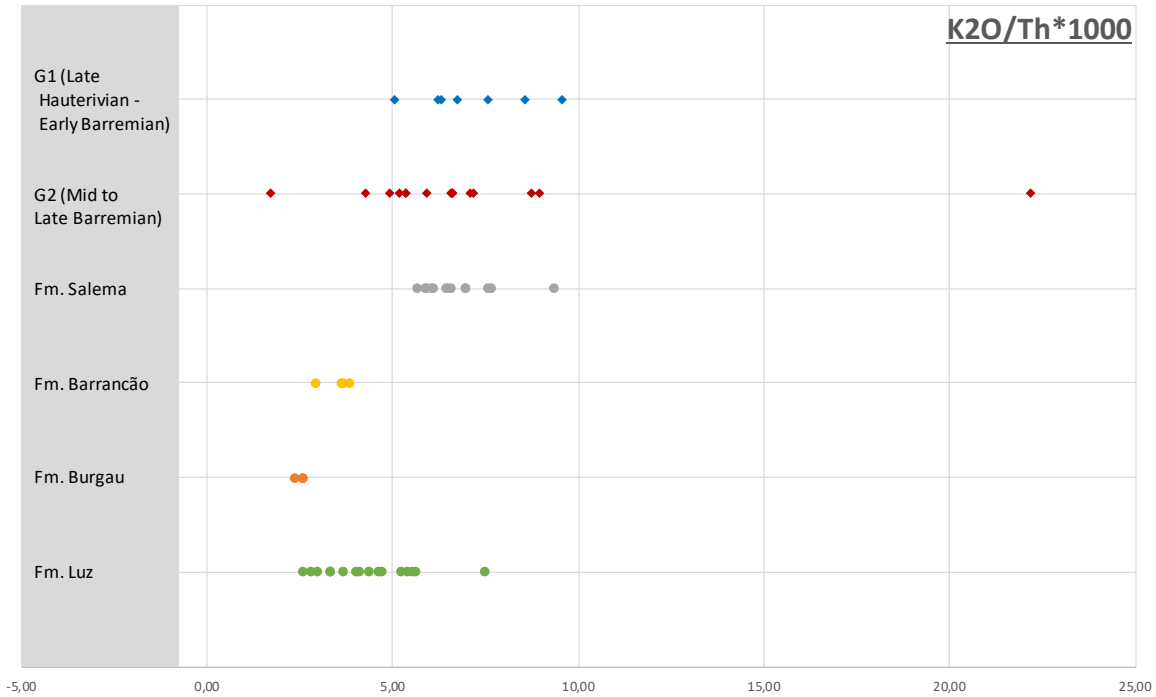
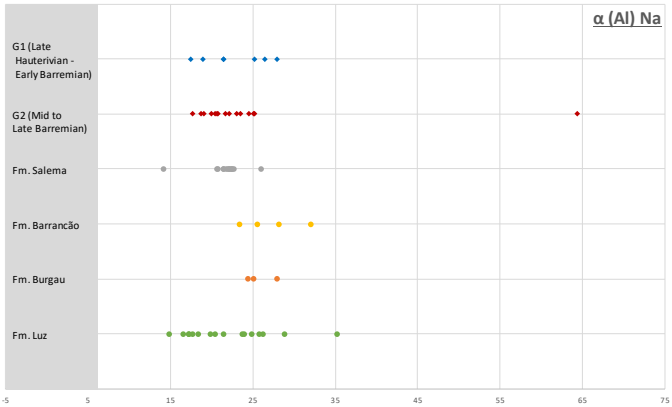
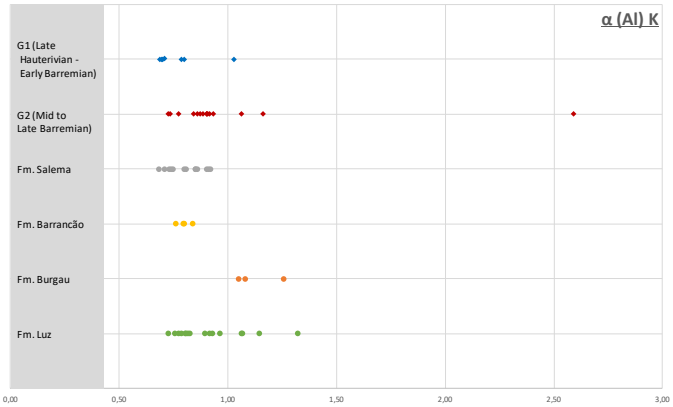


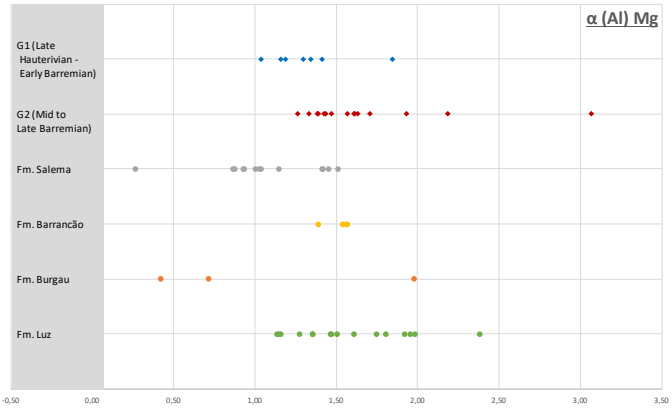
Figure 6.2.1.3 Plotted K_2O/Th*1000 data, including data from Dinis et al. (2020)



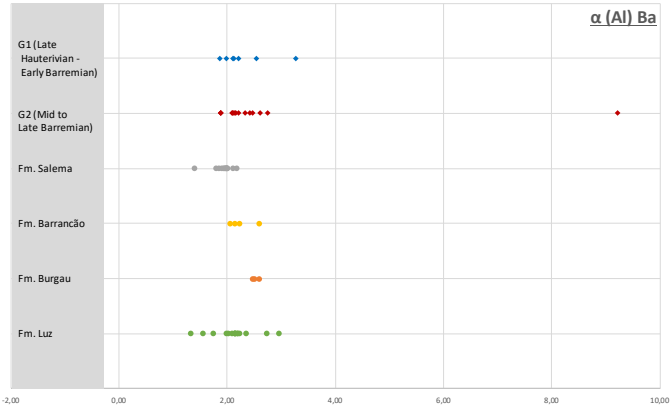
α(Al)Na: The values of G1 and G2 groups range from ≈16 to ≈26, and correlate well with range values of the Salema and Luz Formations. Again, for G2 group, the value ≈65 is interpreted as an outlier.



α(Al)K: For this ratio the patterns plot similar as the ratio previously described, *i.e.* all Lower Cretaceous Formations show the same trend with values between ≈0.4 and 1.4. For G2 group, the sample exceeding the value 2.5 is an outlier.



α(Al)Mg: The values calculated for this ratio, show for more scattered values of all indices. However, the values of G1 and G2 agree with those of the Salema, Barrancão and Luz Formations. For G2 group, the point around 3 is, again, an outlier.



α(Al)Ba: The values calculated for this paleoweathering index, show values plotting relatively tight and around the values ≈1.7 to ≈3 for G1 and G2 groups, and all the other Lower Cretaceous formations.

Figure 6.2.1.4 Plotted and description Indices of element mobility (αAlE), including data from Dinis et al. (2020); the detailed data are available in the Appendix 6

Overall, the paleoweathering discriminating indices calculated for G1 and G2 groups, are within the ranges of the same indices calculated by Dinis et al. (2020), for the Lower Cretaceous formations of western Algarve Basin. However, a more detail analysis suggest that the results of the G1 and G2 groups paleoweathering indices, correlated better to the Salema and Barrancão Formations. In conclusion, the paleoweathering indices demonstrates that the Algarve Basin was subjected to the same environmental and climatic conditions during Early Cretaceous times.

6.2.2 Paleoweathering conditions

The chemical weathering index (CIX) is a way of understanding the rate of alteration present on the continents, which can reflect past climatic conditions. More humid when chemical weathering is intense or more arid when chemical weathering is weak. Other indices that assess the degree of chemical alteration are: α(Al)Na, α(Al)K, α(Al)Mg and α(Al)Ba. Conversely for the ratios Na_2O/Sm and K_2O/Th, the climate is humid when they increase and drier when they decrease (Dinis et al., 2020; Jorge et al., 2013).

The CIX graph (Figure 6.2.2.1) shows that the sediments of G1 were moderately weathered exposing CIX values in the interval [73;80]. For G2, the degree of weathering is slightly higher with values oscillating between [74;82], the point above 90 appears to be an outlier. The results are slightly lower than the other formations of the Algarve Basin indicating that the local climatic conditions were less humid in the Late Hauterivian to Early Barremian. Nevertheless, G2 exhibits higher values than G1, indicating that conditions became more humid in the Late Barremian.

The G1 values for Na_2O/Sm and K_2O/Th ratios are concentrated in a range of high values in relation to the Barrancão, Burgau and Luz Formations, which can be correlated with the wet conditions of the Late Hauterivian (Fölmi, 2012; Masse and Fenerci-Masse, 2008). The G2 values for Na_2O/Sm and K_2O/Th are very scattered, ranging from [350;940] and [4;8] respectively, indicating that the layers were subjected to sometimes wet and sometimes dry climatic conditions. This can be correlated with the fact that the Late Barremian experienced a change from arid to humid climate (Weissert et al., 1979).

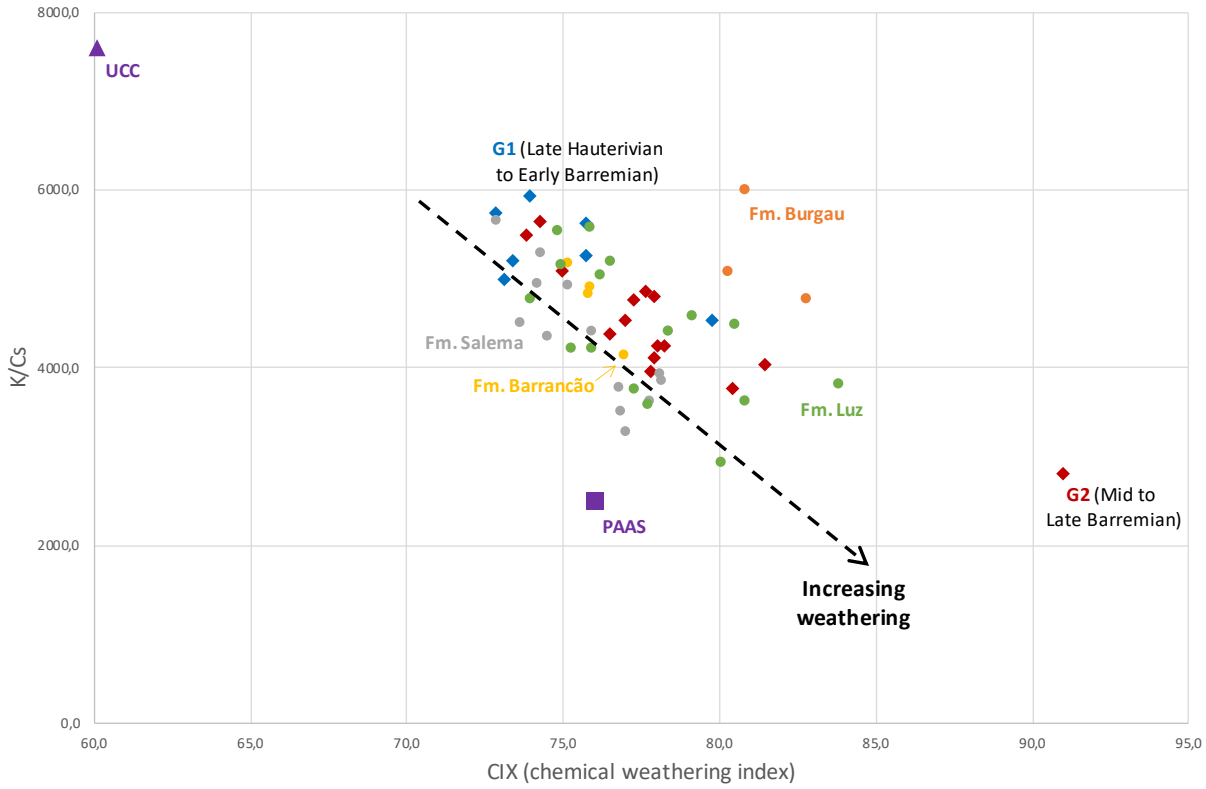


Figure 6.2.2.1 Paleoweathering plot, including data from Dinis et al. (2020)

CIX, Na_2O/Sm and K_2O/Th values for G1, G2 groups and those of the Salema Formation are of the same order of magnitude, emphasising that the sedimentary depositional conditions of these two rock units were subject to the same chemical weathering conditions and thus exposed to the same climatic conditions.

6.2.3 Recycling

The Th/Sc—Zr/Sc ratios (Figure 6.2.3.1) allow us to observe the degree of recycling of the sediments. For G1, G2, Luz Formation and Salema Formation samples, it can be observed that the values are relatively low compared to Barrancão and Burgau Formations. This indicates that (1) Arrifes, Luz and Salema Formations were subjected to the same recycling conditions, and (2) that the rate of alteration and transport was lower and therefore that the climatic conditions were relatively less humid and drier than Barrancão and Burgau Formations at the time of deposition.

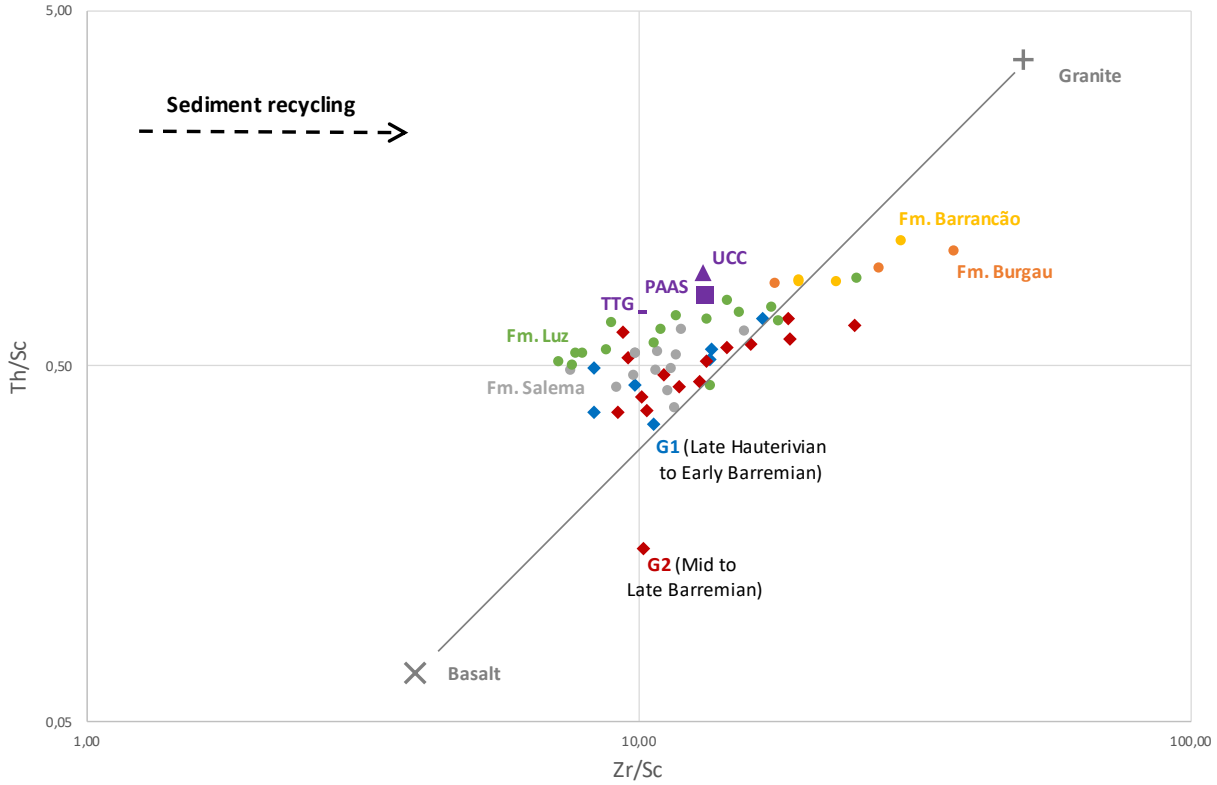


Figure 6.2.3.1 Sediment's recycling plot, including data from Dinis et al. (2020)

6.2.4 Source of sediments

The Cr/Th—Th/Sc and Th/Co—La/Sc ratios are sensitive in discriminating the overall constitution of the original rocks of the sediments, making it possible to characterise geologically the regions that acted as sources of the sediments. Normally the discrimination is achieved by assessing if the source areas were dominated by felsic or mafic magmatic rocks. In Figure 6.2.4.1, it can be observed that G1 and G2 do not show Cr/Th values above 25 (except for the outlier of G2) indicating a dominant felsic source for the sediments. This is not surprising since in the Algarve Basin, basic magmatic formations are restricted to the Late Triassic to Early Jurassic Central Atlantic Magmatic Province magmatism. Moreover during the Lower Cretaceous, there is no geological evidence of being exposed, as well as, meta-sedimentary rocks (Jorge et al., 2013). This is supported by Figure 6.2.4.2, which shows that the entire data set is located around siliceous rocks.

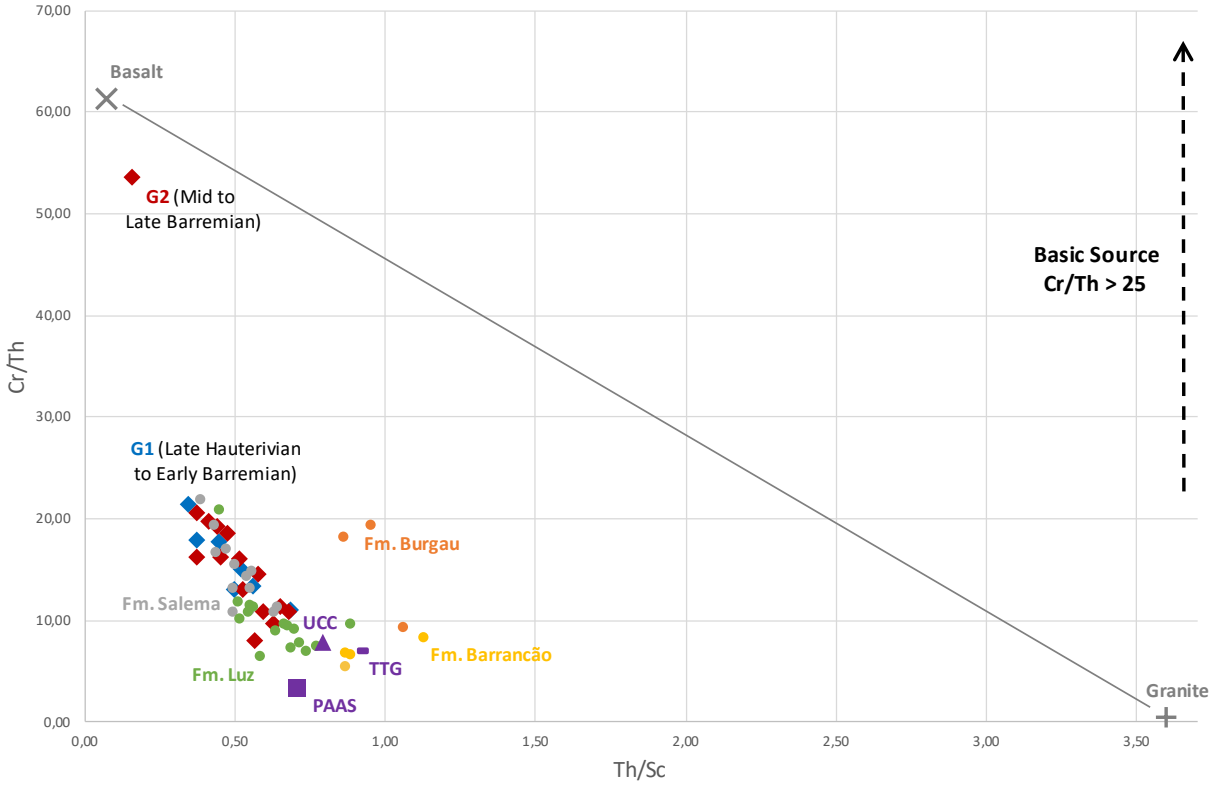


Figure 6.2.4.1 Sediments' source plot (1), including data from Dinis et al. (2020)

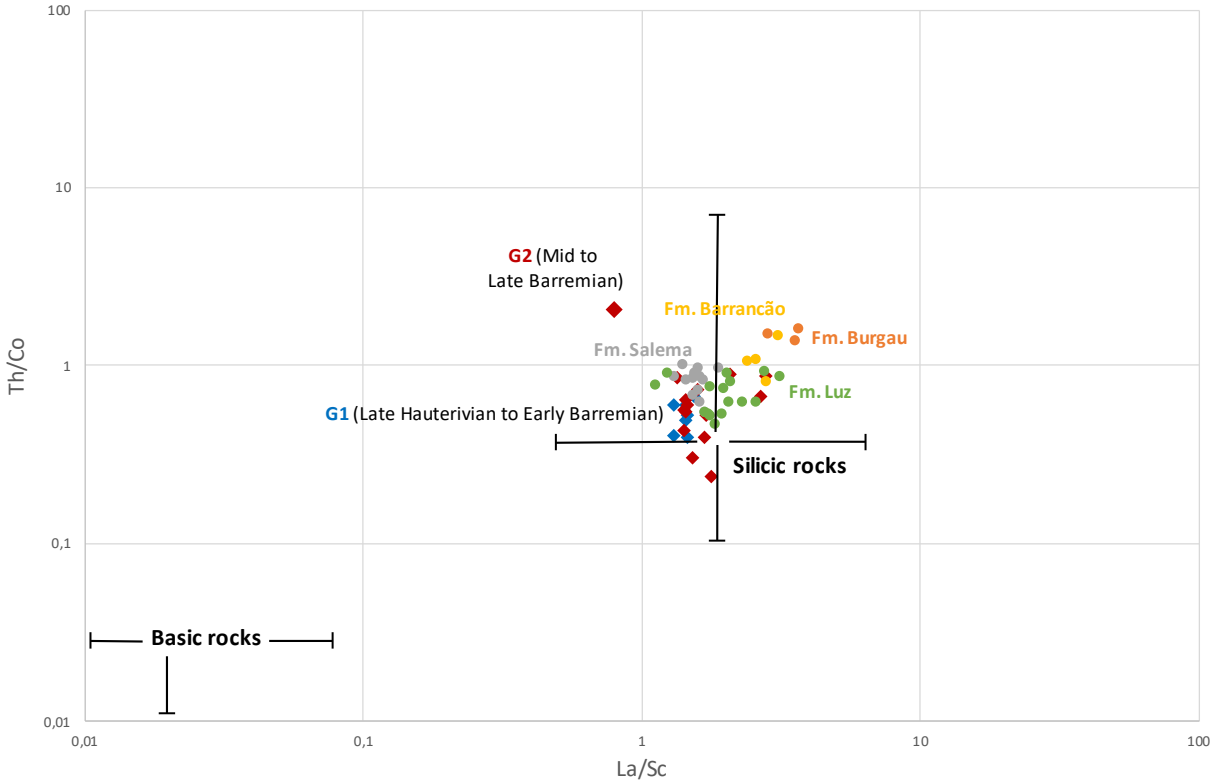


Figure 6.2.4.2 Sediments' source plot (2), including data from Dinis et al. (2020)

Furthermore, the scatter of points G1 and G2 is relatively concentrated, showing that the source of their sediments is similar. Furthermore, the rock formation that most closely resembles the Arrifes succession is once again the Salema Formation, where a source of felsic rock have been determined (Dinis et al., 2020). Therefore, the most likely source area of the sediments in the Arrifes succession, was the exposed Variscan basement of the South Portuguese Zone (SPZ), consisting of several siliciclastic units and the Volcano-Sedimentary Complex of the Iberian Pyrite Belt, which is dominated by felsic volcanic rocks (Oliveira, 1990).

Thus, the Arrifes stratigraphic sequence experienced a drier Late Hauterivian to Early Barremian period, with some short-lived wet conditions, probably concentrated in the latest Hauterivian when global environmental conditions were humid (Föllmi, 2012; Masse and Fenerci-Masse, 2008). Subsequently, conditions became wetter, thus more humid, during the Late Barremian times, as indicated by higher chemical weathering and recycling indices. This is consistent with Weissert et al. (1979) who asserted this climatic change through palynological studies of the *Classopolis* genus. Furthermore, the Arrifes succession shows similarities with the Salema Formation, which may be due to the fact that they were time coeval and belonging to the same depositional basin, which was subject to the same regional environmental and climatic conditions (Dinis et al., 2020).

6.3 Arrifes paleoenvironmental conditions

A general description of the environmental conditions is now possible through the interpretation and correlation of results obtained from (1) sedimentology; (2) palynology analysis, including dating and SP/D ratio; (3) whole-rock geochemistry; and (4) $\delta^{13}C_{org}$ stable isotope analysis. The environmental evolution of the Arrifes stratigraphic sequence during Late Hauterivian to Late Barremian times will be discussed, as well as, on the paleoclimatic and marine conditions, including eustatic sea-level fluctuations and anoxia events.

Figure 6.3.1 is a paleoreconstruction of the depositional environments in the Arrifes succession; and Figure 6.3.1 is a summary figure of simplified stratigraphic log associated with (1) the evolution of the depositional environments; (2) interpreted sea-level curve (transgression-regression); (3) global eustatic sea-level from Haq (2014); (4) SP/D ratios from Mendes et al. (in preparation); (5) $\delta^{13}C_{org}$ evolution and (6) Total Organic Content evolution.

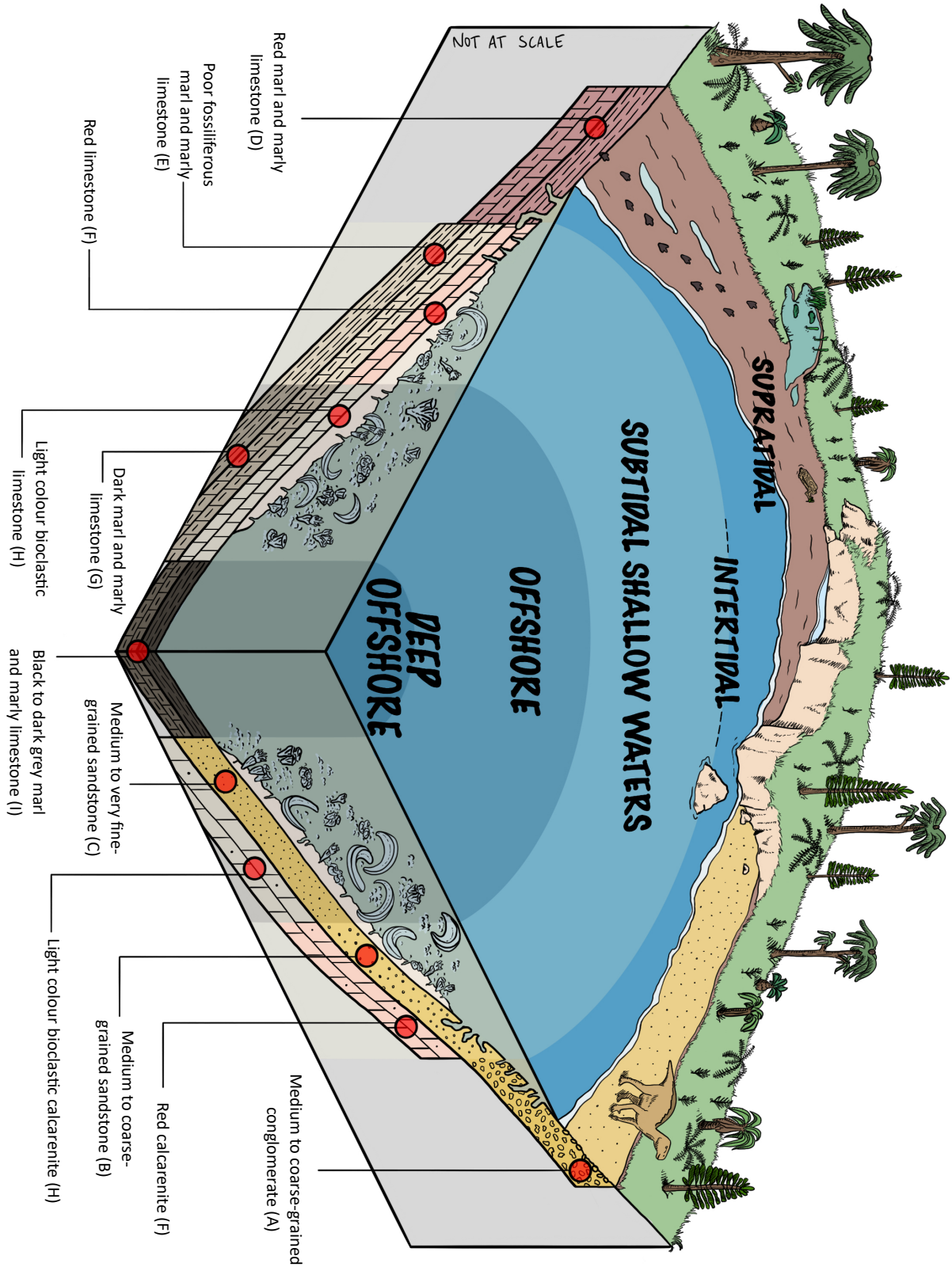


Figure 6.3.1 Paleoenvironmental reconstruction of the Arrifes stratigraphic sequence

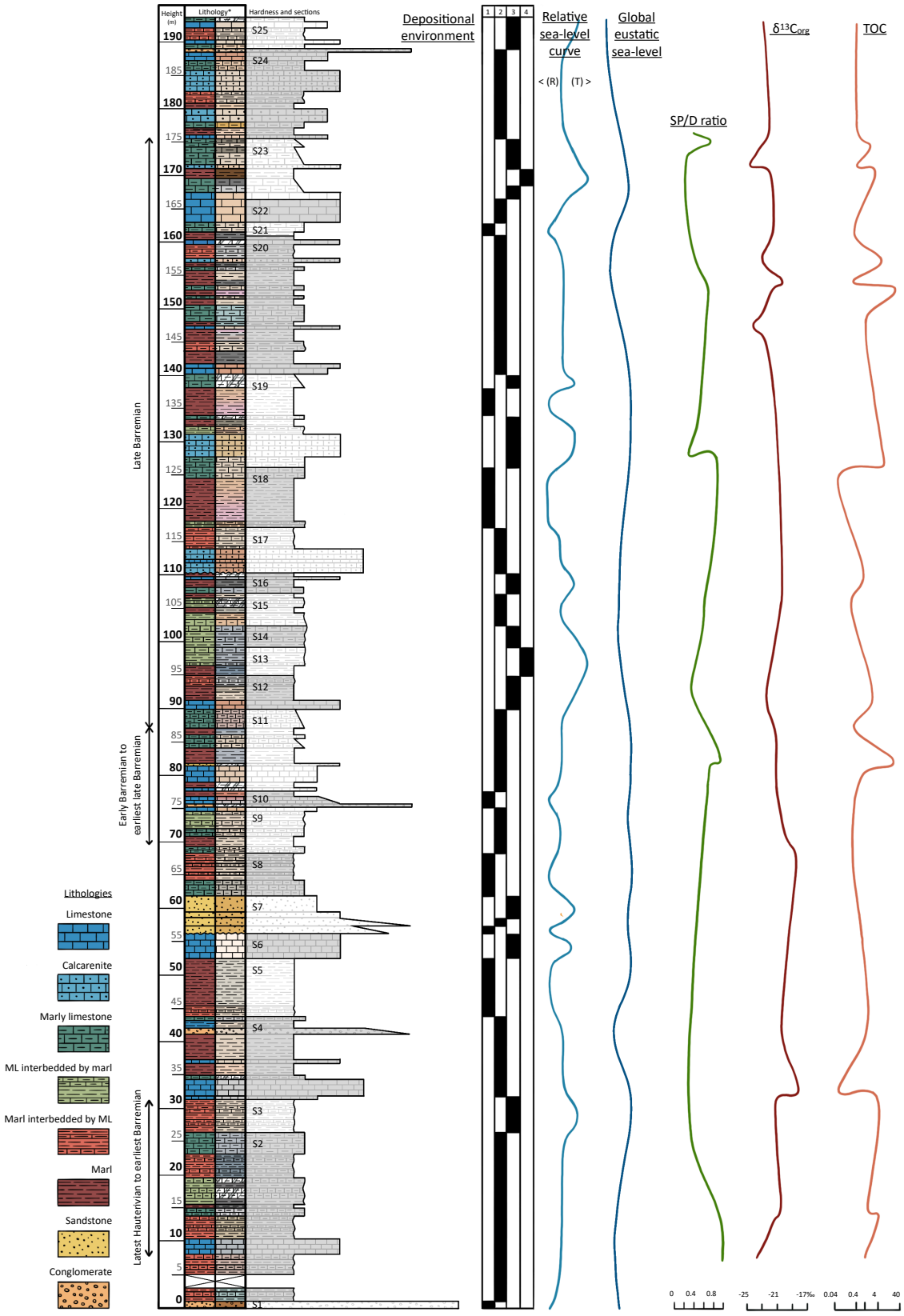


Figure 6.3.2 Summary figure coupling the log of Arrifes stratigraphic sequence; the four main depositional environments (1) supratidal, (2) subtidal, (3) offshore, (4) deep offshore; Arrifes relative sea-level curve (R) regression, (T) transgression; the global eustatic sea-level is from Haq (2014); the SP/D ratio curve is from Mendes et al. (in preparation); organic $\delta^{13}C$ and Total Organic Content curves from organic geochemistry

6.3.1 Age 1: Late Hauterivian to Early Barremian

This age takes into account layers starting at the base of the stratigraphic sequence up to sample P017.1. The sedimentary deposition of the Arrifes succession started by a coarse reddish conglomerate emplaced in proximal environments, a supratidal beach deposition with possible exposure phases.

Then (Section n°2), facies deposition show intertidal to subtidal environments, indicating therefore, a moderate sea-level rise trend. The sea-level rose slightly and a shallow water developed across a carbonate platform allowing the establishment of muddy carbonate deposits. Conditions became more marine but are still very proximal as evidenced by the SP/D ratios obtained in samples P003.1 and P005.1 which give values of 0.99 and 0.93 respectively, indicating continental influence, which largely prevailed over oceanic processes.

The Late Hauterivian climate was humid, favouring material and nutrient fluxes from the continents to the oceans (Föllmi, 2012; Weissert et al., 1998). This is indicated by the strong presence of plant debris, as well as the possible Oceanic Anoxic Event detected in the $\delta^{13}C_{org}$ depleted value (-23.598‰) recorded in sample P003.1, taken from a thin layer of dark marl. However, this is speculative since there is no $\delta^{13}C_{org}$ values for the stratigraphic succession older than sample P003.1. Thus, if this corresponds to a $\delta^{13}C_{org}$ negative excursion, it is correlated with Late Hauterivian times, and could indicate a manifestation of the Faraoni OAE (Baudin and Riquier, 2014; Haq, 2014; Föllmi, 2012; Masse and Fenerci-Masse, 2008; Baudin, 2005; Weissert et al., 1998).

Section n°3 indicates the continuation of sea-level rise until the last validated Late Hauterivian to earliest Barremian bed. Furthermore, SP/D of sample P017.1 is equal to 0.28, reinforcing the idea of fully marine environmental conditions. This may be correlated with the wet climate and associated marine transgression characteristic of this period (Haq, 2014; Baudin and Riquier, 2014).

The Late Hauterivian to earliest Barremian Arrifes succession indicates a transgressive phase, from a nearshore proximal environment to offshore conditions. However, most of this initial sedimentary depositional cycle occurred mainly in a shallow environment under intertidal influence, representing 82% of the total thickness of layers n°1 to 17. Moreover, in the Arrifes succession, this age may have been marked by the F-OAE.

6.3.2 Age 2: Early Barremian to earliest Late Barremian

Palynological dating is not precise for layers between n°18 and n°71, but lithofacies and palynofacies interpretations suggest that the climate changed to become less humid and more arid, as described for the Early Barremian times (Föllmi, 2012; Masse and Fenerci-Masse, 2008).

The stratigraphic sequence in Section n°4 indicates a regressive phase (sea-level fall), evolving towards shallow intertidal environments again. This drop in sea-level, could suggest a correlation with the global regression of the Early Barremian (Baudin and Riquier, 2014; Haq, 2014). Numerous carbonate platforms have developed during this geological period of time, marked by the strong building of carbonate rocks. Moreover, the results of the $\delta^{13}C_{org}$ isotopic analysis give for P020.1 indicates a positive excursion of the whole succession, with a value of -18.097‰, also corresponding to a strong decrease in the TOC's values. Hence, environmental conditions had become optimal for the development of life, possibly marking the end of the F-OAE anoxic episode. Furthermore, samples P020.1, P028.1, P030.1 and P032.1 are all dominated by opaque phytoclasts (75%, 74%, 44% and 52%). It can suggest the presence of nearby forests frequently affected by seasonal forest fires. Indeed, these microscopic plant debris are carried away by the smoke and some of them can be transported to the ocean basins (Rehn, 2021). The presence of these fires could be the consequence of the return to a warm and dry climate, as it was the case at the beginning of the Barremian (Föllmi, 2012; Bond et al., 2010; Masse and Fenerci-Masse, 2008). The regression phase initiated in Section n°4, continued through Section n°5 until it reached the most proximal environment observable in the Arrifes succession.

Then (Section n°6), the 3.9m thick bioclastic limestone indicates a return to marine carbonate deposition. Its deposition occurred after major and abrupt flood event as conditions rapidly became offshore, marking a transgressive phase with rapid sea-level rise allowing the deposition of shallow water carbonates. However, this phase was short-lived, as supratidal environments re-establishes in the overlying section.

Analysing the detrital succession of Section n°7, it indicates an overall deepening trend of the depositional environment, possibly linked to a transgressive phase. The erosive conglomerate at the base of the section, could have been a tidal channel that was abandoned and then filled with finer sediments. Secondly, the fining upward trend observed in the beds of this interval, as well as the observed succession of sedimentary structures (*e.g.*

parallel current lamination, then herringbone-cross-stratification, and finally Hummocky Cross-Stratification), suggest that the velocity of the currents decreased over time reinforcing the idea of a sea-level rise, changing toward deeper environment (Nichols, 2009, Boggs, 2006), although the sea floor was oxygenated as shown by the burrows. This section interval indicates, also, the momentary interruption of the carbonate deposition across the platform, indicating proximity to the shoreline and its influence on the sedimentary environments.

After the transgressive phase attributed to the clastic section interval n°7, a new phase of regression occurred until the establishment of the most proximal depositional conditions (supratidal). Furthermore, the unprecedented 87% dominance of opaque debris in sample P066.1 (layer n°53) may suggest more frequent episodes forest fires as regularly experienced in the arid Barremian climate (Rehn, 2021; Bond et al., 2010). Furthermore, this sample represents the second largest positive excursion $\delta^{13}C_{org}$ correlated with a slight decrease in TOC's, suggesting global lower sequestration of organic carbon in the sediments. Then, the sedimentary environment deepened slightly, giving way to a shallow water environment where muddy carbonate platforms developed.

The earliest Mid Barremian is represented by Section n°8, 9, 10 and 11. From Section n°8 to n°10, this period was characterised by minor fluctuations in sea-level, oscillating between supratidal and subtidal environments. In Section n°11 two samples were taken, P081.1 and P085.1, giving SP/D ratios of 0.69 and 0.96 respectively indicating that conditions were still dominated by continental processes. However, this same section interval marks the beginning of a long phase of transgression (sea-level rise).

The Early Barremian sediments were predominantly deposited in a warm, tidally influenced shallow water carbonate environment with some proximal (supratidal) or deeper (offshore) phases. The climate was arid as suggested by the large number of opaque phytoclasts observed in the palynofacies analysis (Rehn, 2021; Bond et al., 2010). This correlates with the overall Cretaceous environmental conditions that postulate a warm and arid climate for the Early Barremian (Föllmi, 2012; Masse and Fenerci-Masse, 2008). However, in the Arrifes stratigraphic succession, the last section of this age seems to mark the beginning of an oceanic transgressive phase.

6.3.3 Age 3: Late Barremian

From Section n°12 up to Section n°13, the Arrifes stratigraphic sequence experienced a sea-level rise recorded in a 23.75m thick sedimentary pile. This longer-term oceanographic change may be related to the global eustatic deepening that occurred during the Mid Barremian (Baudin and Riquier, 2014; Haq, 2014). These fully marine conditions are highlighted by the SP/D ratios of sample P095.1 and P097.1 which show a high proportion of dinocysts with values of 0.35 and 0.33 respectively. Furthermore, transgression phases can be accompanied by spectacular growth of carbonate platforms, as presented in Section n°12 interval, increasing the demand for dissolved oxygen that can lead to oxygen depletion and increase the accumulation of organic-rich sediments (Baudin and Riquier, 2014; Baudin, 2005; Weissert, 1998). So, it is possible to correlate the occurrences of very dark laminated marls and marly limestones beds without bioturbation, to these events as sample P095.1 shows a strong negative excursion of -22.402‰ for $\delta^{13}C_{org}$ corresponding to a small peak in TOC's. In the arid Mid Barremian climate, this C_{org} accumulation can be explained by a phase of density stratification in an environment where the thermohaline circulation was slowed or even stopped (Baudin and Riquier, 2014; Wang et al., 2014; Weissert et al., 1979).

Sections n°14, 15, 16 and 17 as a whole constitute a regressive sequence, punctuated by minor fluctuations in sea-level that changed depositional conditions between the offshore transitional zone and the intertidal zone. This is supported by the palynological studies showing a stronger continental influence with SP/D=0.58 for sample P106.1. This 18.25m thick sedimentary pile is composed of carbonates rich in shell debris, showing the establishment of flourishing carbonate platforms, as may have been present in large numbers in the Early Cretaceous (Föllmi, 2012). The $\delta^{13}C_{org}$ isotopic data do not fluctuate much, indicating an episode of relatively stable climatic and oceanographic conditions.

Finally, an eustatic drop in sea-level is suggested by the following section interval (Section n°18), that allowed the establishment of a regularly exposed carbonated tidal flats in a supratidal landscape. This scenario is reinforced by the SP/D ratio observed in sample P126.1 with a value of 0.88, indicating a predominance of terrestrial derived palynomorphs over marine palynomorphs.

In Section n°19, the results of the SP/D ratios give values of 0.30 and 0.46 for samples P130.1 and P134.1 respectively, indicating the dominance of marine processes over continental. A rapid deepening trend may have allowed a muddy carbonate platforms to

form. In this offshore environment, the regular presence of marl and the good preservation of fossils indicate that the general depositional conditions were relatively calm. However, the presence of broken shells at the end of the section may suggest storm events (Nichols, 2009; Boggs, 2006). In addition, the supratidal episode marked by layer n°138, may indicate an abrupt sea-level fall during the time of its deposition.

Section n°20 represents again, a phase of sea-level fall, with the establishment of subtidal dominated environments. Indeed, the ratio of sporomorphs to dinocysts gives values of 0.66 for P153.1 and 0.69 for P155.1 indicating a dominant continental influence. In these warm shallow waters, few muddy carbonate platforms were able to establish themselves and the sediment was relatively well-oxygenated, as indicated by the numerous *Thalassinoids*. In addition, samples P160.1 and P168.1 are dominated by more than 70% opaque phytoclasts indicating the possible presence of nearby forest fires and the proximity of vegetated continental areas. In terms of Lower Cretaceous climatic conditions, it could be correlated to the hot and arid climatic conditions of the time (Rehn, 2021; Fölmi, 2012; Bond et al., 2010; Masse and Fenerci-Masse, 2008).

Furthermore, in Section n°20, many samples show interesting values for the study of organic carbon stable isotopes. Firstly, the thin layer of very dark marl, especially mentioned for bed n°145 (P155.1), is determined by the second largest negative excursion of $\delta^{13}C_{org}$ recorded in the stratigraphic sequence. The latter reaches -24.277‰ and also corresponds to a distinct increase in TOC's in the sediments. Thus, it is likely that the thin dark marl layers of this section were deposited not during an OAE, but on the distal offshore part of the carbonate platform. Because, hitherto no major OAE has been recorded for the Barremian period (Baudin and Riquier, 2015; Haq, 2014; Baudin, 2005).

This section is also marked by other negative $\delta^{13}C_{org}$ excursions, including P153.1, P158.1 and P168.1 samples. However, these increases in C_{org} could have different origins. Sample P158.1 was collected in a highly bioturbated marl indicating that the environment was therefore oxygenated. Thus, this accumulation of C_{org} could rather come from an increased flow of sediments towards the ocean basins preventing the decomposition of organic matter. Concerning P153.1 and P168.1 samples, they were collected in dark marls devoid of biological activity, and could, therefore, be due to an episode of oxygen depletion induced by density stratification or by the consumption of available dissolved oxygen by other organisms (Baudin and Riquier, 2014; Wang et al. 2014; Föllmi, 2012; Leckie et al., 2002; Weissert et al. 1979; Weissert et al. 1998). Regardless of the origin of the negative

excursion of P158.1, the other samples described could suggest that the environment has changing cyclically from anoxic to oxygenated to anoxic, and so on. Finally, the oceanic regression phase finally reached its maximum by reaching an exposed tidal flat environment suggested by the presence of terrestrial dinosaur footprints in Section n°21.

Then (Section n°22), a short cycle of sea-level rise, correlated with global eustatism (Haq, 2014) allowed the return of carbonate platform deposition. This transgressive phase continued until it reached offshore conditions as shown in Section n°23. The latter is marked by a deep environment, although depth was probably less than fifty meters, including also, a short deepening phase (offshore more than fifty meters deep for layers n°172 and 173) which allowed the accumulation of 2.8m thick of dark grey and dark brown marls. Palynological study underlines these fully marine conditions as it provides the lowest SP/D ratio of the entire succession (0.21 for P173.2). However, what allows us to affirm that the conditions were shallower in Section n°23 than in layers n°172 and 173, are the values of the SP/D ratio obtained in samples P175.1, P175.2, P176.a, P176.b, which oscillate between 0.38 and 0.77. Despite relatively deep environmental conditions, the numbers of sporomorphs increased, indicating a stronger continental influence, thus, a clearer coastline proximity.

Furthermore, the results of the stable isotope analysis provide interesting values to interpret for the detection of OAEs. Indeed, this section of seven strata is marked by three negative excursions, including the most notable of the entire Arrifes succession reaching -24.779‰ for P173.3. The other negative excursions are detected in P173.2 and P175.2 which give values of -22.157 and -23.039‰, respectively. Weissert et al. (1979) characterised the Late Barremian as a return to a wetter climate. Increased precipitation favours continental weathering and thus, nutrient fluxes to the oceans, which can lead to increased primary biologic activity and trigger climate-induced eutrophication in marine ecosystems, specially in restricted shallow marine environments prone to water stratification. In addition, transgression phases can be linked to exceptional growths of carbonate platforms by creating relatively deep warm environments. Both factors imply an increasing demand for dissolved oxygen, reinforcing the idea of an oxygen depletion episode during the deposition of Section n°23 (Baudin and Riquier, 2014; Hu et al., 2012; Baudin, 2005; Weissert, 1998).

Section n°24 indicates a sea-level fall in relation to the previous sections. The environment became shallower allowing the establishment of a muddy carbonate intertidal zone across the platform. Shelly fauna flourished in these environments, as did benthic organisms as indicated by the dense concentration of *Thalassinoids* burrows. These life-

supporting conditions were maintained for a relatively long time, resulting in a sedimentary succession of 13.3m thick.

The final section (Section n°25) marked a final phase of transgression, were an offshore environment, below storm-wave base, established in the carbonate platform. However, the desiccated cracks in a marl bed (layer n°193) suggest a phase of exposure, and thus, rapid and abrupt sea-level changes. Moreover, isotopic data of sample P193.1 is characterised by a negative excursion of -22.965‰ for $\delta^{13}C_{org}$. This increase in C_{org} could have originated from an enhanced flux of continental material to the oceans, accentuated by the wet climate of Late Barremian times. In fact, if the sedimentation rates are high enough and biological primary productivity is also high, the decomposition of organic matter can be slowed and minimised by being rapidly buried with sediments. Indeed under these conditions, although dissolved in the sediments due to high sedimentation rates, the organic matter can accumulate and become preserved in the sediments in considerable quantities (Baudin and Riquier, 2014; Föllmi, 2012; Leckie et al., 2002; Weissert et al. 1979).

The Late Barremian is the thickest deposit in the Arrifes stratigraphic sequence. In this time interval, the four depositional environments (from supratidal to deep offshore) alternated, showing numerous fluctuations in sea-level. The general trend was towards transgression, which is consistent with existing scientific knowledge (Baudin and Riquier, 2014; Haq, 2014). This idea is supported by some low SP/D ratios with respect to the whole stratigraphic sequence. Initially the climate was arid as shown by the large proportions of opaque debris (Rehn, 2021; Fölmi, 2012; Bond et al., 2010; Masse and Fenerci-Masse, 2008), or by the density stratifications probably detected (Baudin and Riquier, 2014; Wang et al., 2014; Weissert et al., 1979). It then switched to a wet regime, implied by increases in nutrient fluxes from continents toward oceans. Overall, temperatures were high (Föllmi, 2012; Hu et al., 2012; Litter et al., 2011). These warm climatic conditions were conducive to marine life as Late Barremian saw the development of extensive carbonate platforms as evidenced by the numerous bivalve fossils observed in the sedimentary layers. Furthermore, the *Thalassinoids* burrows indicate that the sediments were relatively well-oxygenated. However, the organic-rich sediments show that some oxygen depletion episodes took place, of various origins, although not linked to the large scale oxygen depletion events that are OAEs (Baudin and Riquier, 2015; Haq, 2014; Baudin, 2005). Indeed, they were mainly induced by climatic consequences such as density stratification or increased continental flows to the ocean (Baudin and Riquier, 2014; Wang et al., 2014; Weissert et al., 1979).

7. Conclusions

The objectives set at the beginning of the project were accomplished. Firstly, the palynological dating of Mendes et al. (in preparation) was necessary to place the succession in the correct geological frame time to make more precise correlations with the knowledge already established for the Early Cretaceous geology of the Algarve Basin and of global scale. Thus, the sequence could be divided into three different ages, from the oldest to the youngest: (1) Late Hauterivian to earliest Barremian; (2) Early Barremian to earliest Late Barremian; and (3) Late Barremian. All analytical techniques were complementary and allowed general conclusions about the environmental, paleoclimatic and paleoceanographic conditions that controlled the deposition of the Arrifes stratigraphic sequence.

7.1 Past environments of deposition

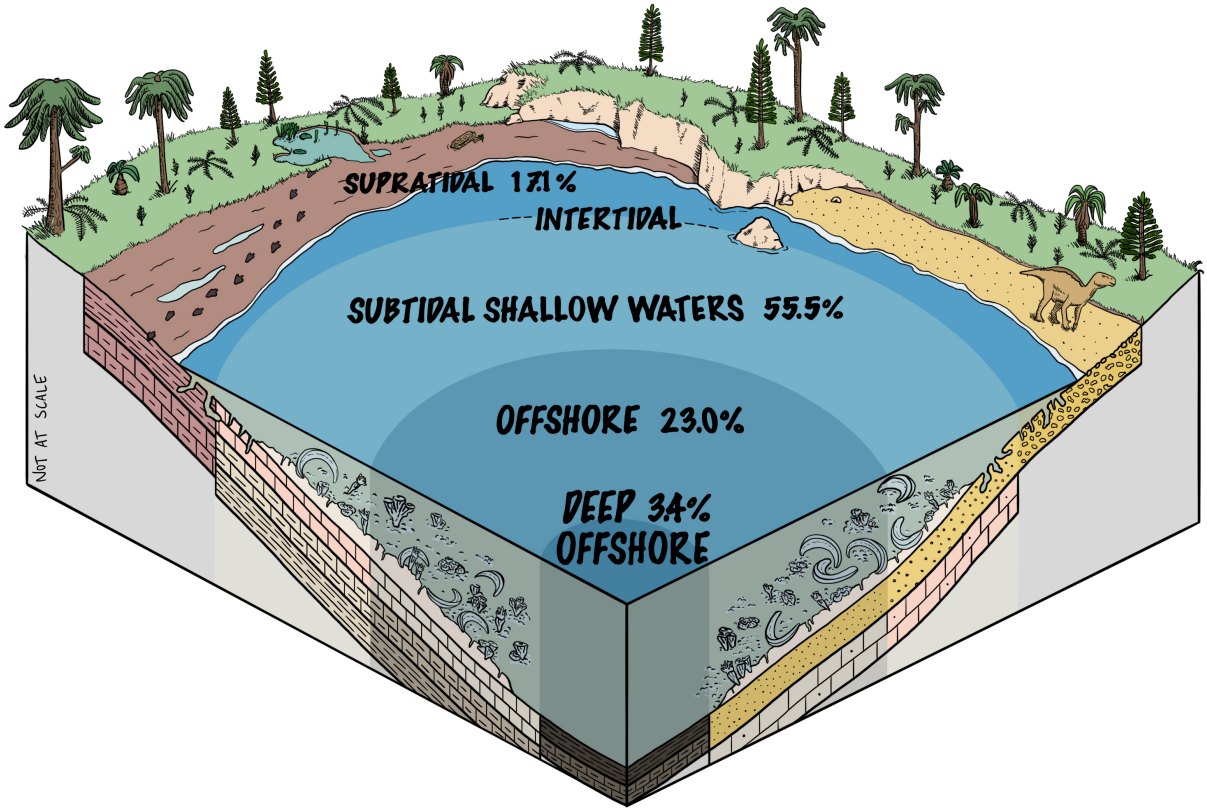


Figure 7.1.1 Proportion of the depositional environments in the Arrifes succession

Note: 1% is missing due to a fault induced break of 2m near the beginning of the sequence.

The detailed analysis of the lithofacies allowed the recognition of the main depositional environments, and how they evolved through the time of deposition. The main depositional environments are represented by shallow water intertidal sediments, representing 107.5m thickness or 55.5% of the total thickness of the Arrifes stratigraphic succession. Moderately deep offshore conditions are the second most dominant (23%), followed by supratidal (17.1%), and finally, the deep offshore domain represents only 3.4% (Figure 7.1.1). Thus, it can be stated that the Arrifes landscape, from the Late Hauterivian to the Late Barremian was a generally tidally influenced shallow coastal environment, including some relatively offshore deep water sediments associated to the peak of transgressive phases (sea-level rise).

7.2 Paleoclimatic conditions

The whole-rock geochemistry data in combination with the work of Dinis et al. (2020) indicated that the climate was relatively warm but experienced changes. It went from relatively wet to arid at the Hauterivian-Barremian boundary (132.9 My) marked by the occurrence and dominance in opaque phytoclasts in the palynofacies, and then changed to more humid conditions during the Late Barremian. These can be correlated with regional and worldwide geological events described for this geological time period (Föllmi, 2012; Bond et al., 2010; Masse and Fenerci-Masse, 2008; Weissert et al., 1979).

7.3 Paleoceanographic conditions and associated sea-level changes

The sea-level has undergone numerous fluctuations that had a profound effect on the sedimentation sequence. Depositional environments have mainly oscillated between intertidal-subtidal to offshore, or intertidal-subtidal to supratidal-intertidal environments. The Late Hauterivian is marked by a transgressive phase, whereas the geological record from the Early Barremian indicate a regressive trend as described by Baudin and Riquier (2014) and Haq (2014). However, the Late Barremian was the time interval most marked by offshore conditions including deep offshore phases (above fifty meters of water column), indicating a deepening trend and a prolonged periods where subtidal environments dominated. Overall, we can see that the sea-level fluctuations of Arrifes environment a relatively well correlated with the global eustatic trend (Haq, 2014), which confirms that the Early Cretaceous sedimentation was mainly controlled by these global changes in central Algarve (Rey, 1986).

7.4 Oceanic Anoxia Events (OAEs)

Few oxygen depletion periods could be detected in the Arrifes sequence, and their origins differ from each other. The Late Hauterivian OAE (*cf.* Section n°2, sample P003.1) is probably related to the major global Faraoni OAE (F-OAE) that disrupted many ecosystems on a global scale (Baudin and Riquier, 2014; Haq, 2014; Föllmi, 2012; Masse and Fenerci-Masse, 2008; Baudin, 2005; Weissert et al., 1998). In the Mid Barremian (*cf.* Section n°12, sample P095.1), arid climate and low precipitation strongly slowed down the thermohaline circulation, causing density stratification of the water column and depletion of dissolved oxygen (DO) in the seabed (Baudin and Riquier, 2014; Wang et al., 2014; Weissert et al., 1979). As for Late Barremian wet period, C_{org} accumulations were not induced by the same forcing mechanisms, with (1) offshore depositional conditions (*cf.* Section n°20, sample P155.1); (2) an exceptional high sedimentation rate allowing the preservation of organic matter (*cf.* Section n°20, sample 158.1; Section n°25, sample 193.1); (3) high rates of continental weathering increasing nutrient fluxes that caused climate-induced eutrophication strongly increasing the demand for DO, and thus its depletion (*cf.* Section n°23, samples P173.2, P173.3 and P175.2); or (4) transgression phases created shallow epicontinental basins causing exceptional growth of carbonate platforms that also increased the demand for DO in water (Baudin and Riquier, 2014; Wang et al. 2014; Föllmi, 2012; Hu et al, 2012; Baudin, 2005; Leckie et al., 2002; Weissert, 1998; Weissert et al. 1998; Weissert et al. 1979).

7.5 Biodiversity

The shallow marine and relatively deep warm water carbonate environments, have allowed many mud-rich carbonate platforms to become established, shown by the numerous bivalves and gastropods shells. This is particularly true during transgression phases when rising sea-levels flooded the continent creating relatively deep warm environments (Baudin and Riquier, 2014; Baudin, 2005; Weissert, 1998). Furthermore, the recurrent presence of bioturbations and *Thalassinoids* burrows indicates that the substrate was regularly oxygenated allowing benthic organisms to flourish.

7.6 Arrifes succession in the context of the Algarve Basin

Whole-rock geochemistry indicated similar paleoweathering and recycling conditions between Arrifes and the Salema and Barrancão successions, especially with Salema. It is

suggested with the contemporaneity between the two rock successions, aspect that is confirmed by the new palynological ages. This correlation is further supported by the fact that the Salema Formation is also characterised by tidally influenced shallow water carbonates (Dinis et al., 2020; Rey, 2006; Rey and Ramalho, 1974).

7.7 Possible future works on the Arrifes sequence

Below are a few ideas for future works in the Arrifes stratigraphic section, which are either a follow-up of the present work, or works that are a consequence of the results achieved in this work. These ideas are:

- Make a detailed sampling in stratigraphic intervals where a precise age could not be assigned by palynological studies, more specifically between samples P017.1 and P081.1.
- Make detailed paleontological and palecological studies of the invertebrate fauna present in the succession (bivalves, gastropods, *etc.*) to refine their stratigraphic distribution in the Tethyan realm, and constrain more accurately the depositional environments.
- Carry out geochemical analyses of stable oxygen and carbon isotopes on shell of marine invertebrates to get information on the sea temperatures, and therefore on the paleoceanographic and paleoclimatic conditions, during the Late Hauterivian to Late Barremian time interval in the Algarve Basin. Also to test these techniques to confirm the presence of OAE in the shallow environments of the carbonate platforms.
- Carry out a detailed reconnaissance of the opaque phytoclasts to determine whether their origin is really due to forest fires using various techniques as electron scanning microscopy and biomarkers.

References

- **Atta-Peters, D. and Kyorku, N.A. (2013)** Palynofacies analysis and sedimentary environment of Early Cretaceous sediments from Dixcove 4-2x well, Cape Three Points, offshore Tano Basin, western Ghana International - Research Journal of Geology and Mining (IRJGM), Vol 3 (7), p 2275 - 6618, pp. 270 - 281. http:/dx.doi.org/10.14303/irjgm.2013.027
- **Alvarez, L.W, Alvarez, W., Asaro, F. and Michel, H.V (1980)** Extraterrestrial Cause for the Cretaceous-Tertiary Extinction - Sciences Vol 208, p 1095 - 1108, Issue 4448 https://doi.org/10.1126/science.208.4448.1095
- **Alves, T.M., Moita, C., Cunha, T., Ullnaess, M., Myklebust, R., Monteiro, J. H., and Manuppella, G. (2009)** Diachronous evolution of Late Jurassic–Cretaceous continental rifting in the northeast Atlantic (west Iberian margin) - Tectonics, vol 28, TC4003. https://doi.org/10.1029/2008TC002337
- **Badiola, A., Canudo, J.I, and Cuenca-Bescós, G. (2008)** New Multituberculate mammals from the Hauterivian/Barremian transition of Europe (Iberian Peninsula) - Palaeontology, Vol 51, p 1455-1469. https://doi.org/10.1111/J.1475-4983.2008.00822.X
- **Baudin, F. (2005)** A Late Hauterivian short-lived anoxic event in the Mediterranean Tethys: the 'Faraoni Event' - Comptes Rendus Geoscience, Vol 337 (16), p 1532-1540, ISSN 1631-0713. https://doi.org/10.1016/j.crte.2005.08.012
- **Baudin, F. and Riquier, L. (2014)** The Late Hauterivian Faraoni 'Oceanic Anoxic Event': an update - Bulletin de la Société Géologique de France, Vol 185, p 359-377. https://doi.org/10.2113/gssgfbull.185.6.359
- **Benton, M.J. (2016)** Origins of Biodiversity - PLoS Biol, Vol 14 (11) : e2000724. https://doi.org/10.1371/journal.pbio.2000724
- **Berthou, P.Y, Correia, F., Prates, S. and Taugourdeau, J. (1983)** Essai de synthèse du Crétacé de l'Algarve: biostratigraphie, paléogéographie et sédimentation argileuse - Bulletin d'information des géologues du Bassin de Paris, Vol 20 (2); p 3 - 18, ISSN 0374-1346
- **Boggs Jr., S. (2006)** Principles of Sedimentology and Stratigraphy - 4th Edition, University of Oregon
- **Bombardiere, L and Gorin, G.E (2000)** Stratigraphical and lateral distribution of sedimentary organic matter in Upper Jurassic carbonates of SE France — Sedimentary Geology, Vol 132 (3 - 4), p 177 - 203, ISSN 0037-0738. https://doi.org/10.1016/S0037-0738(00)00006-3
- **Bond, W.J and Scott, A.C (2010)** Fire and the spread of flowering plants in the Cretaceous - New Phytologist, Vol 188, p 1137-1150. https://doi.org/10.1111/j.1469-8137.2010.03418.x
- **Bouysse., P. et al. (2014)** Geological Map of the World at 1:35 M - revised issue, 3rd edition, Commision for the Geological map of the World - Commission de la Carte Géologie du Monde
- **Brenner G.J (1996)** Evidence for the Earliest Stage of Angiosperm Pollen Evolution: A Paleoequatorial Section from Israel - Taylor D.W., Hickey L.J. (eds) Flowering Plant Origin, Evolution and Phylogeny, Springer, Boston, MA. https://doi.org/10.1007/978-0-585-23095-5_5
- **Buggle, B., Glaser, B., Hambach, U., Gerasimenko, N. and Marković, S. (2011)** An evaluation of geochemical weathering indices in loess–paleosol studies -

Quaternary International, Vol 240 (1-2), p 12-21, ISSN 1040-6182. https://doi.org/10.1016/j.quaint.2010.07.019

- **Church, J.A., Godfrey, S., Jackett, D.R. and McDougall, T.J. (1991)** A Model of Sea-level Rise Caused by Ocean Thermal Expansion - Journal of Climate, Vol 4 (4), p 438 - 456. https://doi.org/10.1175/1520-0442(1991)004<0438:AMOSLR>2.0.CO;2
- **Coccioni, R., Luciani, V. and Marsili, A. (2006)** Cretaceous Oceanic Anoxic Events and radially elongated chambered planktonic foraminifera: Paleoecological and paleoceanographic implications - Palaeogeography, Palaeoclimatology, Palaeoecology, Vol 235 (1-3), p 66-92, ISSN 0031-0182. https://doi.org/10.1016/j.palaeo.2005.09.024
- **Cohen, K.M., Finney, S.C., Gibbard, P.L. and Fan, J.X. (2013; updated)** The ICS International Chronostratigraphic Chart - Episodes 36: 199 - 204. https://stratigraphy.org/ICSchart/ChronostratChart2020-03.pdf
- **Coiffard, C., Gomez, B., and Thevenard, F. (2007)** Early Cretaceous angiosperm invasion of Western Europe and major environmental changes - Annals of botany, Vol 100 (3), p 545–553. https://doi.org/10.1093/aob/mcm160
- **Company, M., Aguado,R., Sandoval, J., Tavera, J.M, Jiménez de Cisneros, C. and Vera, J.A (2005)** Biotic changes linked to a minor anoxic event (Faraoni Level, latest Hauterivian, Early Cretaceous) - Palaeogeography, Palaeoclimatology, Palaeoecology, Vol 224 (1-3), p 186-199, ISSN 0031-0182. https://doi.org/10.1016/j.palaeo.2005.03.034
- **Correia, F.M.C. (1989)** Estudo bioestratigráfico e microfacies do Cretácico carbonatado da bacia sedimentar meridional Portuguesa (Algarve) - Dissertation presented for obtaining a PhD degree in Geology, Department of Geology, FCUL, Lisbon, 377 p. https://sapientia.ualg.pt/bitstream/10400.1/511/2/Dissertação.pdf
- **Dickson, J.A. (1965)** Modified Staining Technique for Carbonates in Thin Section - Nature, Vol 205**,** 587. https://doi.org/10.1038/205587a0
- **Diedrich, C. (2011)** Upper Jurassic tidal flat megatracksites of Germany : coastal dinosaur migration highways between European islands, and a review of the dinosaur footprints - Palaeobiodiversity and Palaeoenvironments, Vol 91, p 129 - 155. https://doi.org/10.1007/s12549-010-0044-y
- **Dinis, P.A., Carvalho, J., Callapez, P.M., Mendes, M.M., Santos, V.F. and Fernandes, P. (2020)** Composition of Lower Cretaceous mudstones of the Algarve Basin and implications for Iberian palaeoclimates - Cretaceous Research, Vol 110, 104404, ISSN 0195-6671. https://doi.org/10.1016/j.cretres.2020.104404
- **Dinis, J., Oliveira, F., Rey, J. and Duarte, I. (2010)** Finding Geological Heritage: Legal Issues on Private Property and Fieldwork. The Case of Outstanding Early Angiosperms (Barremian to Albian, Portugal) - Geoheritage, Vol 2, p 77 - 90. https://doi.org/10.1007/s12371-010-0013-x
- **El Hajjar, A., Eid, J., Bouchemella, S., Ouahbi, T. and Taibi, S. (2019)** Retrait et fissuration des sols argileux par dessiccation - *Academic Journal of Civil Engineering*, Vol *36* (1), p 624-628. https://doi.org/10.26168/ajce.36.1.135
- **Estwing France website (09/2021)** Geological hammer Figure 4.1.2. https://www.estwing-france.com/marteau-pioche-de-geologie-estwing
- **Fan, D (2013)** Classifications, sedimentary features and facies associations of tidal flats — Journal of Palaeogeography, Vol 2,

p 66-80. https://doi.org/10.3724/SP.J.1261.2013.00018

- **Fedo, C.M., Nesbitt, H.N., and Young G.M. (1995)** Unraveling the effects of potassium metasomatism in sedimentary rocks and paleosols, with implications for paleoweathering conditions and provenance - Geology, Vol 23 (10), p 921 - 924. https://doi.org/10.1130/0091-7613(1995)023<0921:UTEOPM>2.3.CO;2
- **Fernandes, P., Rodrigues, B., Borges, M., Matos, V. and Clayton, G. (2013)** Organic maturation of the Algarve Basin (southern Portugal) and its bearing on thermal history and hydrocarbon exploration - Marine and Petroleum Geology, Vol 46, p 210 - 233, ISSN 0264-8172. https://doi.org/10.1016/j.marpetgeo.2013.06.015
- **Föllmi, K.B. (2012)** Early Cretaceous life, climate and anoxia - Cretaceous Research, Vol 35, p 230 - 257, ISSN 0195-6671. https://doi.org/10.1016/j.cretres.2011.12.005
- **Friis, E.M., Pedersen, K.R. and Crane, P.R. (2010)** Cretaceous diversification of angiosperms in the western part of the Iberian Peninsula - Review of Palaeobotany and Palynology, Vol 162 (3), p 341 - 361, ISSN 0034-6667. https://doi.org/10.1016/j.revpalbo.2009.11.009
- **Garzanti, E., Padoan, M., Setti, M., López-Galindo, A. and Villa, I.M (2014)** Provenance versus weathering control on the composition of tropical river mud (southern Africa) - Chemical Geology, Vol 366, p 61-74, ISSN 0009-2541. https://doi.org/10.1016/j.chemgeo.2013.12.016
- **Garzanti, E., Padoan, M., Setti, M., Najman, Y., Peruta, L., and Villa, I.M (2013)** Weathering geochemistry and Sr-Nd fingerprints of equatorial upper Nile and Congo muds - Geochemistry Geophysics Geosystems, Vol 14, p 292– 316. https://doi.org/10.1002/ggge.20060
- **Godet, A., Bodin, S., Föllmi, K.B, Vermeulen, J., Gardin, S., Fiet, N., Adatte, T., Berner, Z., Stüben, S. And Schootbrugge, B.V (2006)** Evolution of the marine stable carbon-isotope record during the Early Cretaceous: A focus on the Late Hauterivian and Barremian in the Tethyan realm - Earth and Planetary Science Letters, Vol 242 (3 - 4), p 254 - 271, ISSN 0012-821X. https://doi.org/10.1016/j.epsl.2005.12.011
- **Hallam, A. (1985)** A review of Mesozoic climate - Journal of the Geological Society, Vol 142, p 433-445. https://doi.org/10.1144/gsjgs.142.3.0433
- **Haq, B.U. (2014)** Cretaceous eustasy revisited - Global and Planetary Change, Vol 113, p 44 - 58, ISSN 0921-8181. https://doi.org/10.1016/j.gloplacha.2013.12.007
- **Hay, W.W. (2017)** Toward understanding Cretaceous climate : an updated review - Science China Earth Sciences, Vol 60, p 5 - 19. https://doi.org/10.1007/s11430-016-0095-9
- **Hay, W.W. and Floegel, S. (2012)** New thoughts about the Cretaceous climate and oceans - Earth-Science Reviews, Vol 115 (4), p 262 - 272, ISSN 0012-8252. https://doi.org/10.1016/j.earscirev.2012.09.008
- **Heimhofer, U., Hochuli, P.A., Burla, S., and Weissert, H. (2007)** New records of Early Cretaceous angiosperm pollen from Portuguese coastal deposits: Implications for the timing of the Early angiosperm radiation - Review of Palaeobotany and Palynology, Vol 144 (1 - 2), p 39 - 76, ISSN 0034-6667. https://doi.org/10.1016/j.revpalbo.2005.09.00
- **Hu, X., Wagreich, M. and Yilmaz, I.O. (2012)** Marine rapid environmental/climatic change in the Cretaceous greenhouse world - Cretaceous Research, Vol 38, p 1 - 6, ISSN 0195-6671. https://doi.org/10.1016/j.cretres.2012.04.012

- **Huck, S., Heimhofer, U., Immenhauser, A. and Weissert, H. (2013)** Carbon-isotope stratigraphy of Early Cretaceous (Urgonian) shoal-water deposits: Diachronous changes in carbonate-platform production in the north-western Tethys - Sedimentary Geology, Vol 290, p 157 - 174, ISSN 0037-0738. https://doi.org/10.1016/j.sedgeo.2013.03.016
- **Huber, B.T., Norris, R.D. and MacLeod K.G. (2002)** Deep-sea paleotemperature record of extreme warmth during the Cretaceous - Geology, Vol 30 (2), p 123 - 126. https://doi.org/10.1130/0091-7613(2002)030<0123:DSPROE>2.0.CO;2
- **Jorge, R.C.G.S., Fernandes, P., Rodrigues, B., Pereira, Z. and Oliveira, J.T. (2013)** Geochemistry and provenance of the Carboniferous Baixo Alentejo Flysch Group, South Portuguese Zone - Sedimentary Geology, Vol 284 - 285, p 133 - 148, ISSN 0037-0738. https://doi.org/10.1016/j.sedgeo.2012.12.005
- **Kahle, M., Kleber M. and Jahn, R. (2002)** Review of XRD-based quantitative analyses of clay minerals in soils: the suitability of mineral intensity factors - Geoderma, Vol 109 (3 - 4), p 191 - 205, ISSN 0016-7061. https://doi.org/10.1016/S0016-7061(02)00175-1
- **Keller, G. (2008)** Cretaceous climate, volcanism, impacts, and biotic effects - Cretaceous Research, Vol 29, Issues 5 - 6, p 754 - 771, ISSN 0195-6671. https://doi.org/10.1016/j.cretres.2008.05.030
- **Kullberg, J.C., Pais, J. and Manuella, G. (1992)** Aspectos gerais da tectónica alpina no Algarve - Ciências da Terra, Vol 11, pp. 293 - 302, ISSN 2183-4431. https://cienciasdaterra.novaidfct.pt/index.php/ct-esj/article/view/142
- **Larousse online** - Encyclopedic dictionary. https://www.larousse.fr/ (visited in 01/2021)
- **Leckie, R.M., Bralower, T.J. and Cashman, R. (2002)** Oceanic Anoxic Events and plankton evolution : Biotic response to tectonic forcing during the mid-Cretaceous - Paleoceanography, Vol 17 (3). https://doi.org/10.1029/2001PA000623
- **Le Pichon, X. and Huchon, P. (1984)** Geoid, Pangea and convection - Earth and Planetary Science Letters, Vol 67 (1), p 123 - 135, ISSN 0012-821X. https://doi.org/10.1016/0012-821X(84)90044-X
- **Leereveld, H. (1997)** Hauterivian-Barremian (Lower Cretaceous) dinoflagellate cyst stratigraphy of the western Mediterranean - Cretaceous Research, Vol 18, p 421 - 456
- **Mahoney, J.J., Duncan, R.A., Tejada, M.L.G., Sager, W.W. and Bralower, T.J. (2005)** Jurassic - Cretaceous boundary age and mid - ocean - ridge - type mantle source for Shatsky Rise - Geology, Vol 33 (3), p 185 - 188. https://doi.org/10.1130/G21378.1
- **Masse, J., and Fenerci-Masse, M. (2008)** Time contrasting palaeobiogeographies among Hauterivian–Lower Aptian rudist bivalves from the Mediterranean Tethys, their climatic control and palaeoecological implications - Palaeogeography, Palaeoclimatology, Palaeoecology, Vol 269, p 54-65. https://doi.org/10.1016/j.palaeo.2008.07.024
- **Maru, K., Aizawa, M., Kai, K.M and Sawa, A.F (2007)** Note of Orbitolinid foraminifera from the Lower Aptian (Cretaceous) Shimanoshita Mudstoner, Lower Yezo Group, Hokkaido, Japan.
- **McDonough, W.F. and Sun, S.S. (1995)** The composition of the Earth - Chemical Geology, Vol 120 (3 - 4), p 223 - 253, ISSN 0009-2541. https://doi.org/10.1016/0009-2541(94)00140-4
- **McLennan, S. (2001)** Relationships between the trace element composition of sedimentary rocks and upper continental

crust - Geochemistry Geophysics Geosystems, Vol 2. https://doi.org/10.1029/2000GC000109

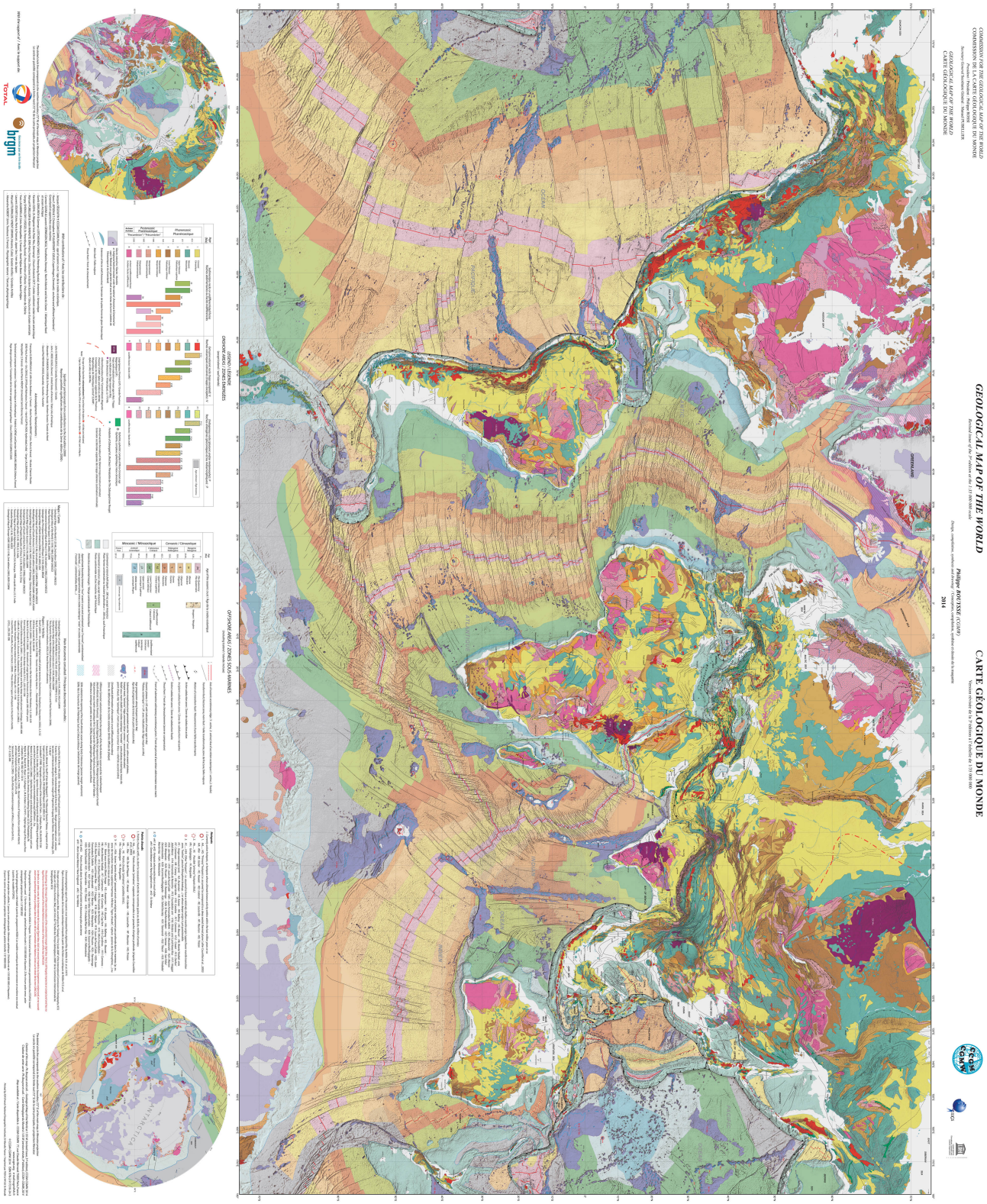
- **McLennan, S.M, Hemming, S.R, McDaniel, D.K, and Hanson, G.N (1993)** Geochemical approaches to sedimentation, provenance, and tectonics - Geological Society of America, Special Papers, Vol 285, p 21-40. https://doi.org/10.1130/SPE284-p21
- **Mendes, M., Descamps, G.S., Fernandes, P., Lopes, G. and Pereira, Z (2021)** The new Barremian (Lower Cretaceous) record of the Arrifes section (Algarve Basin, Portugal): a palynostratigraphic and paleoenvironment approach — Not finish
- **Meyers, P.A. (1997)** Organic geochemical proxies of paleoceanographic, paleolimnologic, and paleoclimatic processes - Organic Geochemistry, Vol 27 (5 - 6), p 213 - 250, ISSN 0146-6380. https://doi.org/10.1016/S0146-6380(97)00049-1
- **Moore, D. and Reynolds, R. (1997)** X-Ray-Diffraction and the identification and analysis of clay minerals - Oxford University Press, New York
- **Nesbitt, H. and Young, G. (1982)** Early Proterozoic climates and plate motions inferred from major element chemistry of lutites - Nature, Vol 299, p 715-717. https://doi.org/10.1038/299715a0
- **Nesbitt, H.W, Markovics, G. and Price, R.C (1980)** Chemical processes affecting alkalis and alkaline earths during continental weathering - Geochimica et Cosmochimica Acta, Vol 44 (11), p 1659-1666, ISSN 0016-7037. https://doi.org/10.1016/0016-7037(80)90218-5
- **Nichols, G. (2009)** Sedimentology and Stratigraphy - 2nd Edition, John Wiley and Sons Ltd. Publication
- **Oggs, J.G., Oggs, G., and Gradstein, F.M. (2008)** The concise geologic time scale - Cambridge University press, Chap 12, p 117 - 127
- **Oliveira J.T. (1990)** Stratigraphy and Synsedimentary Tectonism. In : Dallmeyer R.D., Garcia E.M. (eds) Pre-Mesozoic Geology of Iberia. IGCP-Project 233 (Terranes in the Circum-Atlantic Paleozoic Orogens). Springer, Berlin, Heidelberg. https://doi.org/10.1007/978-3-642-83980-1_23
- **Piasecki S. (1986)** Palynological analysis of the organic debris in the Lower Cretaceous Jydegård Formation, Bornholm, Denmark, Grana, Vol 25 (2), p 119 - 129. https://doi.org/10.1080/00173138609428891
- **Priyanka, M., Madhav, K., Vandana, P., and Yogesh, J. (2015)** Palynostratigraphy, palynofacies and depositional environment of a lignite-bearing succession at Surkha Mine, Cambay Basin, north-western India - Acta Palaeobotanica, Vol 55 (2). https://doi.org/10.1515/acpa-2015-0010
- **Ramos, A., Fernández, O., Muñoz, J.A. and Terrinha, P. (2017)** Impact of basin structure and evaporite distribution on salt tectonics in the Algarve Basin, Southwest Iberian margin - Marine and Petroleum Geology, Vol 88, p 961 - 984, ISSN 0264-8172. https://doi.org/10.1016/j.marpetgeo.2017.09.028
- **Ramos, A., Fernández, O., Terrinha, P. et al. (2016)** Extension and inversion structures in the Tethys–Atlantic linkage zone, Algarve Basin, Portugal - Internal Journal of Earth Sciences (Geol Rundsch), Vol 105, p 1663 - 1679. https://doi.org/10.1007/s00531-015-1280-1 285384095
- **Rauscher, R., Hilly, J., Hanzo, M. and Marchal C. (1995)** Palynologie des couches de passage du Trias supérieur au Lias dans l'Est du Bassin Parisien. Problèmes de datation du «Rhétien» de Lorraine - Sciences Géologiques, bulletins et mémoires, Vol 48 (1-3), p 159-185, ISSN 0302-2692. https://www.persee.fr/doc/sgeol_0302-2692_1995_num_48_1_1927

- **Rehn, E. (2021)** HOW TO: Record fires that burned thousands of years ago - Pages horizons, Vol 1, p 41-43. https://doi.org/doi.org/10.22498/pages.horiz.1.41
- **Rey, J (2009)** Les Formations Crétacées de l'Algarve Oriental - Comunicações Geológicas, Vol 96, p 19-38.
- **Rey, J (2006)** Les Formations Crétacées de l'Algarve Occidental et Central - Comunicações Geológicas, Vol 93, p 39-80.
- **Rey, J. (1986)** Micropaleontological assemblages, paleoenvironments and sedimentary evolution of Cretaceous deposits in the Algarve (Southern Portugal) - Palaeogeography, Palaeoclimatology, Palaeoecology, Vol 55 (2-4), p 233-246. https://doi.org/10.1016/0031-0182(86)90152-5
- **Rey, J. (1983)** Le Crétacé de l'Algarve : Essai de Synthèse - Comunicações dos Serviços Geológicos de Portugal, Vol 69, p 19 - 38, ISSN 1647-581X. http://www.scielo.mec.pt/scielo.php?pid=S1647-581X2009000100002andscript=sci_arttextandtlng=en
- **Rey, J. and Ramalho, M. (1974)** Le Crétacé inférieur de l'Algarve occidental (Portugal) - Serviços Geológicos de Portugal, Vol 5, p 155–181.
- **Santos, V.F, Agostinho, M., Barroso-Barcenilla, F., Callapez, P.M, Castanera, D., Fernandes, P., Oliveira, B.T., Rodrigues, L.A and Segura, M (2016)** First evidence of sauropod tracks in the Lower Cretaceous of the Algarve Basin (Portugal) - Poster presentation of Palaeobiology of trace fossils, p 216-217.
- **Santos, V.F., Callapez, P.M. and Rodrigues, N.P.C. (2013)** Dinosaur footprints from the Lower Cretaceous of the Algarve Basin (Portugal): New data on the ornithopod palaeoecology and palaeobiogeography of the Iberian Peninsula - Cretaceous Research, Vol 40, p 158 - 169, ISSN 0195-6671. https://doi.org/10.1016/j.cretres.2012.07.001 Uptake of CO2, SO2, HNO3 and HCl on Calcite (CaCO3) at 300 K: Mechanism and the Role of Adsorbed Water
- **Santschi, C. and Rossi, M.J (2006)** Uptake of CO2, SO2, HNO3 and HCl on Calcite (CaCO3) at 300 K: Mechanism and the Role of Adsorbed Water - The Journal of Physical Chemistry A, Vol 10 (21), p 6789-6802. https://doi.org/10.1021/jp056312b
- **Scotese, C.R. (2014)** Atlas of Early Cretaceous Paleogeographic Maps, PALEOMAP Atlas for ArcGIS - The Cretaceous, vol 2, Maps 23-31, Mollweide Projection, PALEOMAP Project, Evanston, IL.
- **Sephton, S., Looy, C.V, Veefkind, R.J, Brinkhuis, H. De Leeuw, J.W and Visscher, H. (2002)** Synchronous record of d13C shifts in the oceans and atmosphere at the end of the Permian - Geological Society of America, Special paper 356, p 455-462 (no DOI but, https://repository.geologyscience.ru/bitstream/handle/123456789/29192/Seph_02.pdf?sequence=1&isAllowed=y)
- **Sheldon, P., Coe, A. And Hyden, F. (2011)** Book 3 Fossils and Sedimentary Rocks, based in part on earlier contributions by Brown, E., Skelton, P. And Wilson, C. - 2nd Edition, The Open University, S276 Geology Science: level 2
- **Shinn, E.A (1968)** Practical Significance of Birdseye Structures in Carbonate Rocks — Journal of Sedimentary Petrology, Vol 38 (1), p 215-223. https://doi.org/10.1306/74D7191F-2B21-11D7-8648000102C1865D
- **Skelton, P.W., Spicer, R.A., Kelley, S.P. and Gilmour, I. (2003)** The Cretaceous World - Cambridge University press
- **Strickson, E., Prieto-Márquez, A., Benton, M. et al. (2016)** Dynamics of dental evolution in ornithopod dinosaurs -

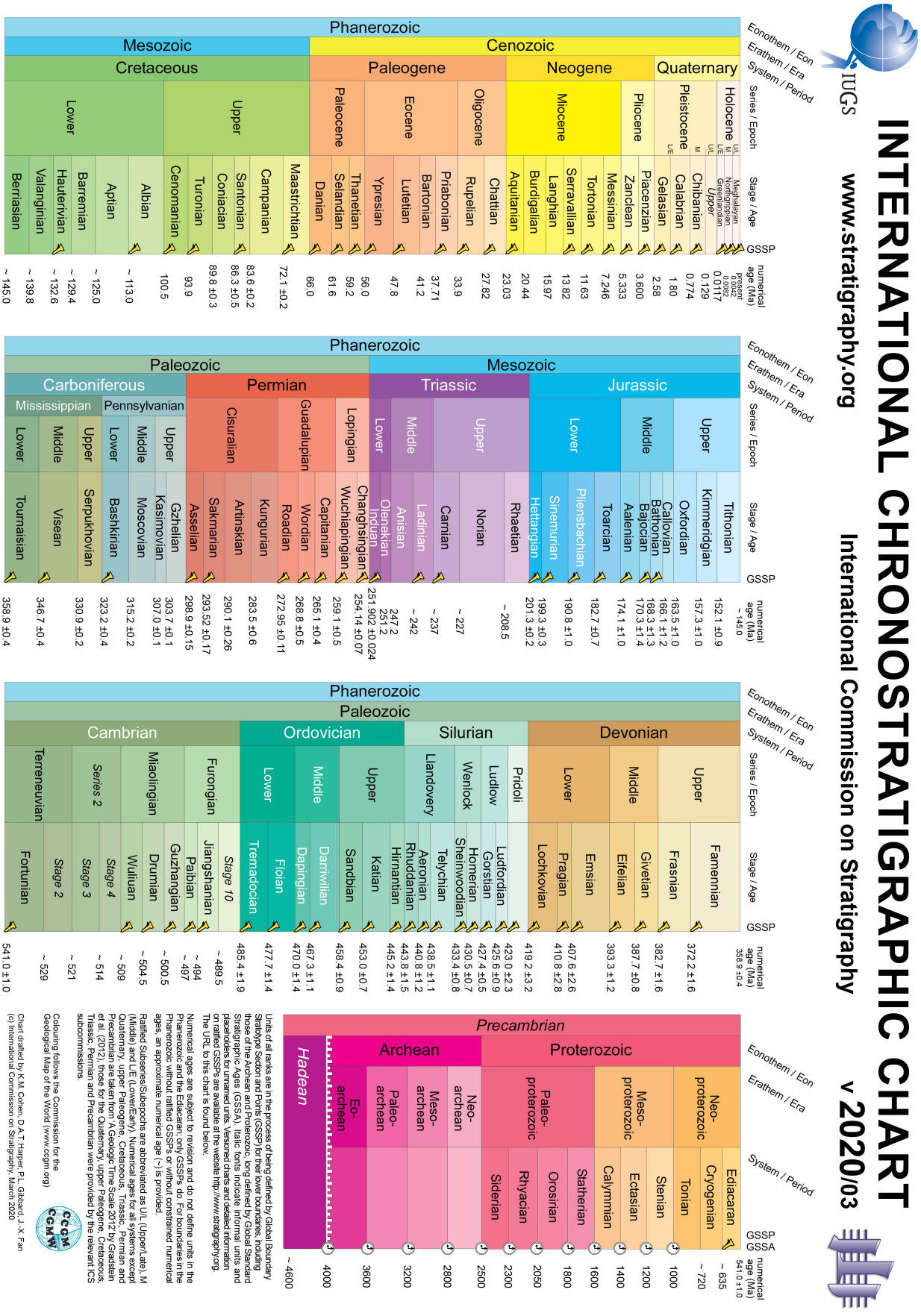
Scientific Report, Vol 6, article 28904. https://doi.org/10.1038/srep28904

- **Taylor S.R and McLennan, S.M (1985)** The chemical composition of the Archaean crust - Geological Society, London, Special Publications, Vol 24, p 173-178. https://doi.org/10.1144/GSL.SP.1986.024.01.16
- **Terrinha, P. (1998)** Structural geology and tectonic evolution of the Algarve Basin, South Portugal - PhD thesis, Imperial College, London.
- **Terrinha, P., Rocha, R.B, Rey, J., Cachão, M., Moura, D., Roque, C., Martins, I., Valadares, V., Cabral, J., Azevedo, M.R, Barbero, I., Clavijo, E., Dias, R.P, Matias, H., Madeira, J., Silva, C.M, Munhá, J., Rebelo, J., Ribeiro, I., Vicente, J., Noiva, J., Youbi, N. and Bensalah, M.K (2013)** A Bacia do Algarve: Estratigrafia, Paleogeografia e Tectónica - A Geologia de Portugal from Dias, R. Araújo, A, Terrinha, P. and Kullberg, J. C., Escolar Editora, Vol 2, p 195 - 350.
- **Trindade, M.J., Rocha, F. and Dias, M.I. (2006)** Geochemical and mineralogical characterization of a Lower Cretaceous sedimentary profile from central Algarve (Portugal) - Journal of Geochemical Exploration, Vol 88 (1 - 3), p 450 - 453, ISSN 0375-6742. https://doi.org/10.1016/j.gexplo.2005.08.095
- **Trindade, M.J., Dias, M.I., Coroado, J. et al. (2010)** Firing Tests on Clay-Rich Raw Materials from the Algarve Basin (Southern Portugal) : Study of Mineral Transformations with Temperature. Clays and Clay Minerals, Vol 58 (2), 1p 88 - 204. https://doi.org/10.1346/CCMN.2010.0580205
- **Trindade, M.J., Rocha, F., Dias, M.I., Prudêncio, M. I. (2013)** Mineralogy and grain-size distribution of clay-rich rock units of the Algarve Basin (South Portugal). Clay Minerals, Vol 48 (1), p 59 - 83. https://doi.org/10.1180/claymin.2013.048.1.04
- **Wang, Y., Huang, C., Sun, B., Quan, C., Wu, J. and Lin, Z. (2014)** Paleo-CO_2 variation trends and the Cretaceous greenhouse climate - Earth-Science Reviews, Vol 129, p 136 - 147, ISSN 0012-8252. https://doi.org/10.1016/j.earscirev.2013.11.001
- **Wardana, S. (2016)** Problem encountered when producing carbonate sand reservoir. https://www.researchgate.net/publication/303702743
- **Weissert, H. (1989)** C-Isotope stratigraphy, a monitor of paleoenvironmental change: A case study from the Early cretaceous. Surveys in Geophysics, Vol 10, p 1 - 61. https://doi.org/10.1007/BF01901664
- **Weissert, H., Lini, A., Föllmi K.B., and Kuhn, O. (1998)** Correlation of Early Cretaceous carbon isotope stratigraphy and platform drowning events : a possible link? - Palaeogeography, Palaeoclimatology, Palaeoecology, Vol 137 (3 - 4), p 189 - 203, ISSN 0031-0182. https://doi.org/10.1016/S0031-0182(97)00109-0
- **Weissert, H., McKenzie, J. and Hochuli, P. (1979)** Cyclic anoxic events in the Early Cretaceous Tethys Ocean - Geology, Vol 7, p 147-151. https://doi.org/10.1130/0091-7613(1979)7%3C147:CAEITE%3E2.0.CO;2
- **Wentworth, C.K. (1922)** A scale of grade and class terms for clastic sediments - Journal of Geology, Vol 30, p 377 - 394. https://www.jstor.org/stable/30063207
- **Wilson, R.C.L. (1975)** Atlantic opening and Mesozoic continental margin basins of Iberia - Earth and Planetary Science Letters, Vol 25 (1), p 33 - 43, ISSN 0012-821X. https://doi.org/10.1016/0012-821X(75)90207-1
- **Wing, S.L and Boucher L.D (1998)** Ecological aspects of the Cretaceous flowering plant radiation - Annual Review of Earth and Planetary Sciences, Vol 26, p 379-421. https://doi.org/10.1146/annurev.earth.26.1.379

Appendix 1. The Geological Map of the World (Bouysse et al., 2014)



Appendix 2. International Chronostratigraphic Chart (Cohen et al., 2013; updated)



Appendix 3. Whole-rock geochemistry

Quality Analysis ... **Actlabs** *Innovative Technologies*

Report No.: **A21-12311**
Report Date: **20-Jul-21**
Date Submitted: **30-Jun-21**
Your Reference:

Universidade do Algarve
8005-139 FARO
FARO
Portugal

ATTN: PAULO FERNANDES

CERTIFICATE OF ANALYSIS

22 Pulp samples were submitted for analysis.

The following analytical package(s) were requested:		Testing Date:
4B-INAA(Lithores)	QOP INAAGEO (INAA)	2021-07-13 11:41:35
4LITHORES + 4B1 (11+)	QOP WRA/ QOP WRA 4B2/QOP Total (/Major/Trace Elements Fusion ICPOES/ICPMS/Total Digestion ICPOES)	2021-07-08 09:44:16

REPORT **A21-12311**

This report may be reproduced without our consent. If only selected portions of the report are reproduced, permission must be obtained. If no instructions were given at time of sample submittal regarding excess material, it will be discarded within 90 days of this report. Our liability is limited solely to the analytical cost of these analyses. Test results are representative only of material submitted for analysis.

Notes:

Values which exceed the upper limit should be assayed for most accurate values.

We recommend using option 4B1 for accurate levels of the base metals Cu, Pb, Zn, Ni and Ag. Option 4B-INAA for As, Sb, high W >100ppm, Cr >1000ppm and Sn >50ppm by Code 5D. Values for these elements provided by Fusion ICP/MS, are order of magnitude only and are provided for general information. Mineralized samples should have the Quant option selected or request assays for values which exceed the range of option 4B1. Total includes all elements in % oxide to the left of total. Zr is now being reported from FUS-ICP instead of FUS-MS.

SCC Accredited LAB LAB Accrédité CCN TM

LabID: 266

CERTIFIED BY:

Emmanuel Eseme , Ph.D.
Quality Control Coordinator

ACTIVATION LABORATORIES LTD.
41 Bittern Street, Ancaster, Ontario, Canada, L9G 4V5
TELEPHONE +905 648-9611 or +1.888.228.5227 FAX +1.905.648.9613
E-MAIL Ancaster@actlabs.com ACTLABS GROUP WEBSITE www.actlabs.com

Analyte Symbol	Au	As	Br	Cr	Ir	Sc	Se	Sb	Mass	SiO2	Al2O3	Fe2O3(T)	MnO	MgO	CaO	Na2O	K2O	TiO2	P2O5	LOI	Total	Sc	Be
Unit Symbol	ppb	ppm	ppm	ppm	ppb	ppm	ppm	ppm	g	%	%	%	%	%	%	%	%	%	%	%	%	ppm	ppm
Lower Limit	2	0.5	0.5	5	5	0.1	3	0.2		0.01	0.01	0.01	0.001	0.01	0.01	0.01	0.01	0.001	0.01		0.01	1	1
Method Code	INAA	INAA	INAA	INAA	INAA	INAA	INAA	INAA	INAA	FUS-ICP	FUS-ICP	FUS-ICP	FUS-ICP	FUS-ICP	FUS-ICP	FUS-ICP	FUS-ICP	FUS-ICP	FUS-ICP	GRAV	FUS-ICP	FUS-ICP	FUS-ICP
P002.1	< 2	12.1	< 0.5	130	< 5	20.1	< 3	1.7	1.25	52.10	19.74	9.04	0.032	2.13	0.14	0.29	6.26	1.052	0.05	8.11	98.95	20	3
P003.1	< 2	25.9	< 0.5	125	< 5	16.9	< 3	1.6	1.27	53.59	20.03	6.28	0.021	2.06	0.41	0.24	5.57	1.032	0.04	10.00	99.27	17	3
P017.1	4	25.7	21.5	108	< 5	14.3	< 3	1.2	1.06	54.66	17.53	5.88	0.020	1.96	1.26	0.17	4.94	0.988	0.04	11.25	98.70	14	3
P020.1	2	10.5	10.0	112	< 5	15.1	< 3	1.1	1.05	55.49	17.67	6.53	0.022	2.47	0.31	0.18	5.65	1.042	0.04	9.12	98.52	15	3
P032.1	< 2	3.5	10.7	108	< 5	13.8	< 3	1.2	1.44	55.49	17.40	6.62	0.015	2.18	0.33	0.16	5.43	1.032	0.04	9.73	98.42	14	3
P085.1	< 2	50.3	3.4	134	< 5	17.0	< 3	2.6	1.08	51.98	21.73	6.21	0.052	1.71	0.26	0.26	4.70	1.065	0.04	11.03	99.03	17	3
P089.1	< 2	5.3	1.7	130	< 5	19.6	< 3	1.4	1.07	54.34	19.20	7.34	0.029	2.35	0.10	0.26	6.22	1.095	0.06	8.47	99.48	20	4
P106.1	< 2	42.0	8.2	130	< 5	16.0	< 3	1.4	1.12	52.58	22.60	6.11	0.024	1.50	0.28	0.29	4.32	1.014	0.05	10.34	99.10	16	3
P108.1	< 2	33.2	3.0	129	< 5	15.3	< 3	1.7	1.02	54.83	18.91	7.28	0.021	1.75	0.32	0.21	4.82	0.954	0.04	10.22	99.37	15	3
P124.1	< 2	0.8	< 0.5	82	< 5	18.0	< 3	0.8	1.08	59.94	20.07	3.55	0.009	0.95	0.47	0.08	1.72	0.813	< 0.01	11.44	99.04	18	3
P126.1	< 2	32.7	6.4	105	< 5	16.2	< 3	1.8	1.23	58.25	16.69	6.19	0.022	1.69	0.25	0.17	4.11	1.137	0.04	10.08	98.62	16	3
P152.1	< 2	5.8	8.5	102	< 5	13.9	< 3	0.9	1.03	62.58	16.23	5.95	0.022	1.70	0.19	0.20	4.90	1.063	0.06	7.73	100.6	15	3
P152.2	< 2	13.2	< 0.5	105	< 5	17.4	< 3	1.6	1.15	53.69	20.02	8.71	0.028	2.09	0.18	0.27	5.76	0.957	0.05	8.43	100.2	18	3
P153.1	5	32.8	9.0	125	< 5	18.3	< 3	1.5	1.01	55.23	20.58	6.06	0.019	1.86	0.25	0.21	5.16	1.067	0.03	10.07	100.5	19	3
P154.1	< 2	9.2	< 0.5	106	< 5	17.6	< 3	1.4	1.20	55.78	19.29	7.47	0.026	2.22	0.16	0.28	5.89	1.065	0.08	7.61	99.87	19	3
P162.1	< 2	68.6	18.5	114	< 5	13.8	3	2.6	1.08	53.10	19.08	6.66	0.028	1.70	0.33	0.24	4.67	1.022	< 0.01	12.11	98.93	14	3
P173.1	< 2	5.2	9.8	118	< 5	14.1	3	1.2	1.09	57.47	18.59	5.56	0.021	2.03	0.76	0.22	4.80	1.039	0.03	8.96	99.49	15	3
P173.2	< 2	41.3	15.5	89	< 5	12.0	< 3	1.4	1.10	61.31	16.08	5.47	0.021	1.37	0.28	0.20	3.83	1.116	0.02	8.95	98.66	13	2
P173.3	10	36.4	12.6	124	< 5	14.1	< 3	1.4	1.04	51.90	21.03	7.00	0.017	1.58	0.38	0.22	4.40	1.019	0.03	11.71	99.29	15	3
P175.2	< 2	19.9	11.7	103	< 5	14.1	< 3	1.8	1.12	56.07	18.35	5.66	0.034	1.87	0.38	0.20	4.51	0.985	0.03	10.98	99.08	14	3
P181.1	< 2	16.9	6.3	123	< 5	16.0	< 3	1.7	1.12	54.70	21.58	6.11	0.019	1.94	0.25	0.25	5.23	1.004	0.03	9.75	100.9	17	3
P193.1	< 2	24.1	14.2	130	< 5	15.8	< 3	1.3	1.02	55.18	20.46	6.80	0.021	2.02	0.21	0.28	5.39	0.968	0.05	8.70	100.1	17	3

Analyte Symbol	V	Cr	Co	Ni	Cu	Zn	Cd	S	Ga	Ge	As	Rb	Sr	Y	Zr	Nb	Mo	Ag	In	Sn	Sb	Cs	Ba
Unit Symbol	ppm	ppm	ppm	ppm	ppm	ppm	ppm	%	ppm	ppm	ppm	ppm	ppm	ppm	ppm	ppm	ppm	ppm	ppm	ppm	ppm	ppm	ppm
Lower Limit	5	20	1	1	1	1	0.5	0.001	1	0.5	5	1	2	0.5	1	0.2	2	0.3	0.1	1	0.2	0.1	2
Method Code	FUS-ICP	FUS-MS	FUS-MS	TD-ICP	TD-ICP	TD-ICP	TD-ICP	TD-ICP	FUS-MS	FUS-MS	FUS-MS	FUS-MS	FUS-ICP	FUS-MS	FUS-ICP	FUS-MS	FUS-MS	TD-ICP	FUS-MS	FUS-MS	FUS-MS	FUS-MS	FUS-ICP
P002.1	144	110	15	43	12	110	< 0.5	0.006	27	1.6	11	268	66	21.0	167	17.3	< 2	< 0.3	0.1	4	1.4	10.4	386
P003.1	149	100	11	39	17	92	< 0.5	0.503	25	0.9	6	212	57	17.2	179	16.3	< 2	< 0.3	0.1	3	1.0	8.2	342
P017.1	112	90	20	33	20	77	< 0.5	0.580	24	1.2	16	206	53	17.6	240	21.6	3	< 0.3	0.1	3	0.9	7.8	288
P020.1	119	100	14	42	21	110	< 0.5	0.148	23	1.6	10	252	49	16.7	205	18.3	< 2	< 0.3	0.1	3	1.1	9.0	252
P032.1	97	100	12	35	18	87	< 0.5	0.007	23	1.8	< 5	200	37	17.7	185	18.0	< 2	< 0.3	0.1	3	1.1	7.6	193
P085.1	150	120	19	57	103	79	< 0.5	1.75	25	1.0	14	194	60	16.0	167	16.9	5	1.9	0.1	3	1.9	8.6	375
P089.1	134	140	18	38	26	100	< 0.5	0.018	23	2.1	< 5	253	56	16.9	162	15.8	3	< 0.3	0.1	3	1.3	9.0	351
P106.1	143	120	12	34	39	63	< 0.5	2.09	26	1.9	26	186	62	14.9	162	16.9	< 2	0.4	0.1	3	1.3	8.9	383
P108.1	135	110	12	34	23	65	< 0.5	2.09	24	1.3	17	199	49	16.1	181	16.1	< 2	0.6	0.1	3	1.1	8.4	310
P124.1	48	70	5	26	4	17	< 0.5	0.005	15	1.2	< 5	87	20	16.4	259	14.4	< 2	< 0.3	0.1	2	0.8	5.1	79
P126.1	134	90	15	36	39	36	< 0.5	2.13	20	1.1	9	166	42	19.4	304	16.5	3	0.4	0.1	2	1.2	7.1	232
P152.1	162	120	14	29	12	57	< 0.5	0.008	20	1.9	6	183	45	22.5	259	17.3	3	< 0.3	0.1	3	1.3	7.2	312
P152.2	142	90	15	45	10	79	< 0.5	0.009	25	1.9	11	241	55	18.1	159	15.7	< 2	0.3	0.1	4	1.4	9.4	349
P153.1	155	110	16	46	27	55	< 0.5	1.11	24	1.6	17	185	51	18.2	175	15.9	2	0.4	0.1	3	1.3	8.8	272
P154.1	119	100	15	41	14	85	< 0.5	0.007	24	2.2	6	237	60	21.6	165	17.4	< 2	< 0.3	0.1	4	1.0	8.9	332
P162.1	148	100	30	60	31	54	< 0.5	3.49	23	1.0	11	205	47	18.0	183	16.4	10	0.4	< 0.1	3	1.7	9.8	296
P173.1	140	100	9	38	57	57	< 0.5	0.008	23	1.5	5	198	50	21.5	225	17.0	< 2	< 0.3	0.1	4	0.9	8.8	320
P173.2	112	90	9	32	19	43	< 0.5	2.56	20	1.5	21	157	44	25.2	295	17.4	2	0.5	< 0.1	3	1.2	7.5	309
P173.3	164	120	17	44	29	43	< 0.5	3.74	24	1.3	16	189	52	15.8	156	16.2	2	0.4	< 0.1	3	1.0	9.7	315
P175.2	145	100	12	37	25	50	< 0.5	2.24	23	0.8	10	198	46	18.3	182	15.2	4	0.4	0.1	3	1.3	9.1	270
P181.1	155	110	7	32	28	65	< 0.5	0.007	26	1.8	11	233	51	15.6	165	16.0	< 2	< 0.3	0.1	4	1.1	10.2	364
P193.1	159	110	8	39	28	68	< 0.5	0.009	26	1.7	21	228	55	16.3	161	15.5	< 2	< 0.3	0.1	4	1.5	10.2	394

Analyte Symbol	La	Ce	Pr	Nd	Sm	Eu	Gd	Tb	Dy	Ho	Er	Tm	Yb	Lu	Hf	Ta	W	Tl	Pb	Bi	Th	U
Unit Symbol	ppm	ppm	ppm	ppm	ppm	ppm	ppm	ppm	ppm	ppm	ppm	ppm	ppm	ppm	ppm	ppm	ppm	ppm	ppm	ppm	ppm	ppm
Lower Limit	0.05	0.05	0.01	0.05	0.01	0.005	0.01	0.01	0.01	0.01	0.01	0.005	0.01	0.002	0.1	0.01	0.5	0.05	5	0.1	0.05	0.01
Method Code	FUS-MS	FUS-MS	FUS-MS	FUS-MS	FUS-MS	FUS-MS	FUS-MS	FUS-MS	FUS-MS	FUS-MS	FUS-MS	FUS-MS	FUS-MS	FUS-MS	FUS-MS	FUS-MS	FUS-MS	FUS-MS	TD-ICP	FUS-MS	FUS-MS	FUS-MS
P002.1	31.1	57.8	6.45	22.9	4.30	0.860	3.33	0.56	3.81	0.77	2.37	0.370	2.64	0.419	4.3	1.19	2.0	0.67	13	0.3	9.96	1.69
P003.1	24.5	44.5	4.94	18.1	3.30	0.722	2.66	0.47	3.05	0.64	1.97	0.307	2.15	0.356	4.3	1.23	2.0	0.83	13	< 0.1	5.83	2.82
P017.1	20.4	37.7	4.20	15.5	2.86	0.556	2.26	0.43	3.03	0.65	1.92	0.298	2.04	0.317	6.1	1.50	41.8	0.57	14	< 0.1	9.77	4.88
P020.1	21.6	39.6	4.45	15.6	2.92	0.543	2.40	0.42	2.89	0.62	1.82	0.287	2.00	0.299	5.3	1.30	2.1	0.67	18	0.1	8.41	3.92
P032.1	18.0	32.9	3.62	13.1	2.48	0.524	2.35	0.41	2.83	0.61	1.88	0.291	1.90	0.296	4.9	1.46	2.4	0.48	7	0.2	7.17	1.71
P085.1	24.9	43.8	4.83	17.4	3.05	0.639	2.28	0.41	2.74	0.59	1.79	0.281	1.98	0.310	4.3	1.48	2.5	1.89	86	< 0.1	7.54	3.93
P089.1	25.4	46.9	5.40	19.8	3.58	0.745	2.70	0.50	3.23	0.69	2.09	0.309	2.28	0.363	4.5	1.27	6.9	0.52	9	< 0.1	7.27	2.59
P106.1	23.1	41.1	4.72	16.2	3.09	0.615	2.47	0.40	2.62	0.55	1.76	0.274	1.98	0.320	4.4	1.76	2.3	0.73	18	0.1	6.58	1.98
P108.1	21.8	39.8	4.45	16.9	3.13	0.648	2.58	0.45	2.81	0.63	1.92	0.298	2.00	0.315	4.7	1.41	1.2	1.06	17	< 0.1	6.71	4.08
P124.1	14.5	27.5	3.09	11.6	2.27	0.431	2.09	0.42	2.87	0.66	2.14	0.348	2.44	0.395	6.2	1.02	1.7	0.44	9	0.1	10.2	1.50
P126.1	23.2	44.5	5.06	19.2	3.58	0.702	2.81	0.51	3.44	0.70	2.20	0.355	2.48	0.381	7.0	1.06	1.5	1.03	22	< 0.1	9.64	3.38
P152.1	37.1	71.7	8.34	32.3	5.27	1.00	3.97	0.69	4.24	0.84	2.66	0.401	2.83	0.448	6.8	1.30	6.7	0.43	9	< 0.1	9.44	3.74
P152.2	24.7	45.5	5.11	18.2	3.58	0.694	2.98	0.50	3.21	0.67	2.10	0.327	2.21	0.335	4.1	1.13	1.4	0.59	9	0.2	6.45	1.84
P153.1	26.5	48.3	5.53	19.4	3.65	0.754	2.78	0.53	3.32	0.70	2.16	0.341	2.32	0.358	4.4	1.04	1.9	0.94	14	< 0.1	9.61	3.05
P154.1	28.1	52.4	6.05	22.6	4.39	0.833	3.21	0.63	3.88	0.83	2.47	0.371	2.47	0.387	4.5	1.32	2.9	0.61	11	< 0.1	11.0	2.42
P162.1	24.5	46.7	5.41	19.1	3.54	0.718	2.91	0.51	3.12	0.69	2.12	0.309	2.16	0.331	4.7	1.49	2.2	1.75	36	< 0.1	7.09	6.01
P173.1	29.3	55.5	6.24	23.1	4.27	0.813	3.56	0.64	3.97	0.82	2.48	0.376	2.50	0.380	5.5	1.42	1.5	0.70	9	0.3	8.12	2.23
P173.2	33.6	65.0	7.42	27.6	5.05	0.941	4.05	0.71	4.39	0.91	2.82	0.411	2.77	0.422	6.9	1.47	1.9	1.01	11	< 0.1	7.79	3.96
P173.3	23.6	43.5	4.93	17.9	3.22	0.645	2.47	0.44	2.92	0.60	1.90	0.281	1.91	0.323	4.0	1.15	1.5	0.93	19	< 0.1	6.66	2.48
P175.2	24.1	45.5	5.25	19.0	3.54	0.710	2.84	0.52	3.22	0.68	2.18	0.304	2.15	0.343	4.8	1.05	2.4	1.56	11	< 0.1	6.35	4.24
P181.1	21.3	41.0	4.65	17.1	3.29	0.605	2.58	0.45	2.85	0.62	1.87	0.309	2.08	0.330	4.1	1.20	1.9	0.81	12	0.2	5.99	2.20
P193.1	23.9	45.7	5.14	18.9	3.36	0.697	2.72	0.47	2.92	0.62	1.93	0.298	2.10	0.322	4.1	1.13	1.3	0.84	17	0.3	7.48	2.43

Analyte Symbol	Au	As	Sb	SiO2	Al2O3	Fe2O3(T)	MnO	MgO	CaO	Na2O	K2O	TiO2	P2O5	Total	Sc	Be	V	V	Cr	Co	Ni	Ni	Cu
Unit Symbol	ppb	ppm	ppm	%	%	%	%	%	%	%	%	%	%	%	ppm	ppm	ppm	ppm	ppm	ppm	ppm	ppm	ppm
Lower Limit	2	0.5	0.2	0.01	0.01	0.01	0.001	0.01	0.01	0.01	0.01	0.001	0.01	0.01	1	1	5	5	20	1	20	1	1
Method Code	INAA	INAA	INAA	FUS-ICP	FUS-ICP	FUS-ICP	FUS-ICP	FUS-ICP	FUS-ICP	FUS-ICP	FUS-ICP	FUS-ICP	FUS-ICP	FUS-ICP	FUS-ICP	FUS-ICP	FUS-MS	FUS-ICP	FUS-MS	FUS-MS	FUS-MS	TD-ICP	TD-ICP
NIST 694 Meas				11.08	1.88	0.75	0.014	0.34	43.27	0.87	0.53	0.117	30.21					1663					
NIST 694 Cert				11.2	1.80	0.790	0.0116	0.330	43.6	0.860	0.510	0.110	30.2					1740					
DNC-1 Meas				47.34	18.87	9.91	0.147	10.06	11.38	1.94	0.22	0.493	0.06		31			157					
DNC-1 Cert				47.15	18.34	9.97	0.150	10.13	11.49	1.890	0.234	0.480	0.070		31			148					
GBW 07113 Meas				71.25	12.76	3.19	0.143	0.14	0.58	2.53	5.46	0.285	0.05		5	4		< 5					
GBW 07113 Cert				72.8	13.0	3.21	0.140	0.160	0.590	2.57	5.43	0.300	0.0500		5.00	4.00		5.00					
SY-4 Meas				50.00	20.27	6.28	0.108	0.50	8.13	6.85	1.62	0.291	0.13		< 1	3	5	6		1			
SY-4 Cert				49.9	20.69	6.21	0.108	0.54	8.05	7.10	1.66	0.287	0.131		1.1	2.6	8.0	8.0		2.8			
Oreas 72a (4 Acid) Meas																						6200	313
Oreas 72a (4 Acid) Cert																						6930.000	316
BIR-1a Meas				48.09	15.42	11.37	0.172	9.55	13.46	1.83	0.01	0.962	0.02		43	< 1	327	338		52	180		
BIR-1a Cert				47.96	15.50	11.30	0.175	9.700	13.30	1.82	0.030	0.96	0.021		44	0.58	310	310		52	170		
ZW-C Meas																			60				
ZW-C Cert																			56.0				
OREAS 101b (Fusion) Meas																	80			46			
OREAS 101b (Fusion) Cert																	80			47			
OREAS 101b (4 Acid) Meas																						9	419
OREAS 101b (4 Acid) Cert																						8.2	412
OREAS 98 (4 Acid) Meas																							> 10000
OREAS 98 (4 Acid) Cert																							148000
NCS DC86318 Meas																							
NCS DC86318 Cert																							
SARM 3 Meas																							
SARM 3 Cert																							
USZ 42-2006 Meas																	126			3	< 20		
USZ 42-2006 Cert																	115.00			7.89	13.18		
OREAS 904 (4 Acid) Meas																						45	6150
OREAS 904 (4 Acid) Cert																						40.1	6120
OREAS 45d (4-Acid) Meas																						243	375
OREAS 45d (4-Acid) Cert																						231.0	371
REE-1 Meas																			290	1			
REE-1 Cert																			277	1.58			
OREAS 905 (INAA) Meas	373	37.8	2.2																				
OREAS 905 (INAA) Cert	391	36.2	1.96																				
OREAS 96 (4 Acid) Meas																							> 10000
OREAS 96 (4																							39300

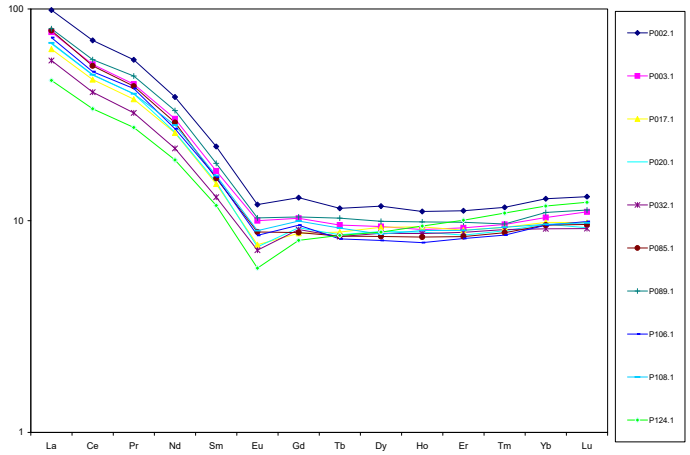
Analyte Symbol	Au	As	Sb	SiO2	Al2O3	Fe2O3(T)	MnO	MgO	CaO	Na2O	K2O	TiO2	P2O5	Total	Sc	Be	V	V	Cr	Co	Ni	Ni	Cu
Unit Symbol	ppb	ppm	ppm	%	%	%	%	%	%	%	%	%	%	%	ppm	ppm	ppm	ppm	ppm	ppm	ppm	ppm	ppm
Lower Limit	2	0.5	0.2	0.01	0.01	0.01	0.001	0.01	0.01	0.01	0.01	0.001	0.01	0.01	1	1	5	5	20	1	20	1	1
Method Code	INAA	INAA	INAA	FUS-ICP	FUS-ICP	FUS-ICP	FUS-ICP	FUS-ICP	FUS-ICP	FUS-ICP	FUS-ICP	FUS-ICP	FUS-ICP	FUS-ICP	FUS-ICP	FUS-ICP	FUS-MS	FUS-ICP	FUS-MS	FUS-MS	FUS-MS	TD-ICP	TD-ICP
Acid) Cert																							
OREAS 923 (4 Acid) Meas																						38	4440
OREAS 923 (4 Acid) Cert																						35.8	4230
OREAS 621 (4 Acid) Meas																						29	3600
OREAS 621 (4 Acid) Cert																						26.2	3630
Oreas 77b (4 Acid) Meas																						> 10000	3250
Oreas 77b (4 Acid) Cert																						113000	3430
OREAS 681 (4 Acid) Meas																						460	262
OREAS 681 (4 Acid) Cert																						503	264
OREAS 147 (4 Acid) Meas																						23	299
OREAS 147 (4 Acid) Cert																						21.2	298
Oreas 521 (4 Acid) Meas																						67	5850
Oreas 521 (4 Acid) Cert																						73	6070
OREAS 70b (4 Acid) Meas																						1950	47
OREAS 70b (4 Acid) Cert																						2180	52
P126.1 Orig																						36	39
P126.1 Dup																						36	39
P154.1 Orig				55.38	19.14	7.40	0.026	2.20	0.17	0.27	5.84	1.060	0.07	99.15	19	3	109	119	90	15	< 20		
P154.1 Dup				56.19	19.44	7.54	0.026	2.24	0.16	0.29	5.93	1.070	0.09	100.6	19	4	107	119	100	15	< 20		
P193.1 Orig				55.51	20.61	6.81	0.022	2.04	0.21	0.28	5.42	0.975	0.06	100.6	17	3	151	161	110	8	40		
P193.1 Dup				54.85	20.32	6.78	0.021	2.00	0.21	0.27	5.36	0.961	0.04	99.52	17	3	149	156	120	8	40		
Method Blank				< 0.01	< 0.01	0.01	0.003	< 0.01	< 0.01	< 0.01	< 0.01	< 0.001	0.01		< 1	< 1	< 5	< 5	< 20	< 1	< 20		
Method Blank																						< 1	< 1
Method Blank																						< 1	< 1
Method Blank				0.01	0.01	0.01	0.003	0.02	0.01	< 0.01	< 0.01	0.001	< 0.01		< 1	< 1		< 5					
Method Blank				0.01	< 0.01	0.01	0.003	< 0.01	< 0.01	< 0.01	< 0.01	0.001	< 0.01		< 1	< 1		< 5					

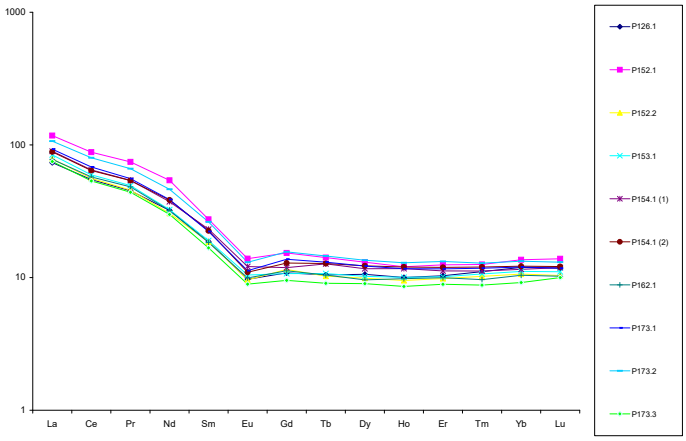
Analyte Symbol	Cu	Zn	Zn	Cd	S	Ga	Ge	As	Rb	Sr	Sr	Y	Y	Zr	Nb	Mo	Ag	In	Sn	Sb	Cs	Ba	Ba
Unit Symbol	ppm	ppm	ppm	ppm	%	ppm	ppm	ppm	ppm	ppm	ppm	ppm	ppm	ppm	ppm	ppm	ppm	ppm	ppm	ppm	ppm	ppm	ppm
Lower Limit	10	1	30	0.5	0.001	1	0.5	5	1	2	2	0.5	1	1	0.2	2	0.3	0.1	1	0.2	0.1	3	2
Method Code	FUS-MS	TD-ICP	FUS-MS	TD-ICP	TD-ICP	FUS-MS	FUS-MS	FUS-MS	FUS-MS	FUS-MS	FUS-ICP	FUS-MS	FUS-ICP	FUS-ICP	FUS-MS	FUS-MS	TD-ICP	FUS-MS	FUS-MS	FUS-MS	FUS-MS	FUS-MS	FUS-ICP
NIST 694 Meas																							
NIST 694 Cert																							
DNC-1 Meas											145		15	37									107
DNC-1 Cert											144.0		18.0	38									118
GBW 07113 Meas											42		44	400									501
GBW 07113 Cert											43.0		43.0	403									506
SY-4 Meas			90			33			54	1170	1192	117	112	528	13.3						1.4	341	339
SY-4 Cert			93			35			55.0	1191	1191	119	119	517	13						1.5	340	340
Oreas 72a (4 Acid) Meas					1.67																		
Oreas 72a (4 Acid) Cert					1.74																		
BIR-1a Meas	130		70							107	109	14.7	13	16	0.4					0.6			9
BIR-1a Cert	125		70							110	110	16	16	18	0.6					0.58			6
ZW-C Meas			1010			92			> 1000						209				> 1000	4.5	266		
ZW-C Cert			1050			99			8500						198				1300	4.2	260		
OREAS 101b (Fusion) Meas	420											176				20							
OREAS 101b (Fusion) Cert	420											178				21							
OREAS 101b (4 Acid) Meas																							
OREAS 101b (4 Acid) Cert																							
OREAS 98 (4 Acid) Meas		1340			16.3												43.0						
OREAS 98 (4 Acid) Cert		1360			15.5												45.1						
NCS DC86318 Meas									390			> 10000									11.2		
NCS DC86318 Cert									369.42			17008									11.88		
SARM 3 Meas															> 1000								
SARM 3 Cert															978								
USZ 42-2006 Meas	20		460							5020		164			34.0	36						307	
USZ 42-2006 Cert	27.37		469							4900		167			31.00	34.40						307	
OREAS 904 (4 Acid) Meas		29			0.066												0.6						
OREAS 904 (4 Acid) Cert		26.3			0.0630												0.551						
OREAS 45d (4-Acid) Meas		45			0.045																		
OREAS 45d (4-Acid) Cert		45.7			0.049																		
REE-1 Meas	80							121	> 1000	128		5590							507		1.1	101	
REE-1 Cert	79.7							124	1050	129		5480							498		1.07	100.1	
OREAS 905 (INAA) Meas																							
OREAS 905 (INAA) Cert																							
OREAS 96 (4 Acid) Meas		461			4.23												11.5						
OREAS 96 (4 Acid) Cert		457			4.19												11.5						

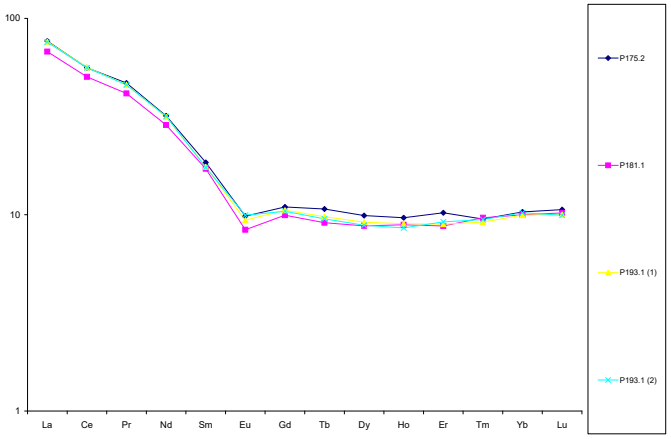
Analyte Symbol	Cu	Zn	Zn	Cd	S	Ga	Ge	As	Rb	Sr	Sr	Y	Y	Zr	Nb	Mo	Ag	In	Sn	Sb	Cs	Ba	Ba
Unit Symbol	ppm	ppm	ppm	ppm	%	ppm	ppm	ppm	ppm	ppm	ppm	ppm	ppm	ppm	ppm	ppm	ppm	ppm	ppm	ppm	ppm	ppm	ppm
Lower Limit	10	1	30	0.5	0.001	1	0.5	5	1	2	2	0.5	1	1	0.2	2	0.3	0.1	1	0.2	0.1	3	2
Method Code	FUS-MS	TD-ICP	FUS-MS	TD-ICP	TD-ICP	FUS-MS	FUS-MS	FUS-MS	FUS-MS	FUS-MS	FUS-ICP	FUS-MS	FUS-ICP	FUS-ICP	FUS-MS	FUS-MS	TD-ICP	FUS-MS	FUS-MS	FUS-MS	FUS-MS	FUS-MS	FUS-ICP
OREAS 923 (4 Acid) Meas		373		< 0.5	0.724												2.0						
OREAS 923 (4 Acid) Cert		345		0.420	0.691												1.60						
OREAS 621 (4 Acid) Meas		> 10000		293	4.64												71.6						
OREAS 621 (4 Acid) Cert		52200		284	4.48												69.0						
Oreas 77b (4 Acid) Meas		180		1.3													1.5						
Oreas 77b (4 Acid) Cert		205		1.20													1.62						
OREAS 681 (4 Acid) Meas		78			0.102												< 0.3						
OREAS 681 (4 Acid) Cert		88.0			0.109												0.118						
OREAS 147 (4 Acid) Meas		151			0.016																		
OREAS 147 (4 Acid) Cert		138			0.0300																		
Oreas 521 (4 Acid) Meas		22			1.73												1.2						
Oreas 521 (4 Acid) Cert		24			1.80												0.89						
OREAS 70b (4 Acid) Meas		99		< 0.5	0.288												< 0.3						
OREAS 70b (4 Acid) Cert		110		0.4	0.309												0.2						
P126.1 Orig		36		< 0.5	2.13												0.5						
P126.1 Dup		36		< 0.5	2.12												0.4						
P154.1 Orig	10		60			23	2.2	6	237	58	60	21.8	21	165	17.1	< 2		0.1	3	1.1	8.9	309	328
P154.1 Dup	20		60			24	2.2	6	236	57	60	21.5	21	164	17.7	< 2		0.1	4	0.9	9.0	307	336
P193.1 Orig	30		60			26	1.7	22	228	53	56	16.4	16	161	15.4	< 2		0.1	4	1.5	10.2	387	396
P193.1 Dup	30		60			26	1.7	20	227	53	54	16.2	15	160	15.7	2		0.1	4	1.5	10.2	384	392
Method Blank	< 10		< 30			< 1	< 0.5	< 5	< 1	< 2	< 2	< 0.5	< 1	3	< 0.2	< 2		< 0.1	< 1	< 0.2	< 0.1	< 3	2
Method Blank		< 1		< 0.5	0.002												< 0.3						
Method Blank		< 1		< 0.5	0.002												< 0.3						
Method Blank											< 2		< 1	2									3
Method Blank											< 2		< 1	2									2

Analyte Symbol	La	Ce	Pr	Nd	Sm	Eu	Gd	Tb	Dy	Ho	Er	Tm	Pb	Yb	Lu	Hf	Ta	W	Tl	Bi	Th	U
Unit Symbol	ppm	ppm	ppm	ppm	ppm	ppm	ppm	ppm	ppm	ppm	ppm	ppm	ppm	ppm	ppm	ppm	ppm	ppm	ppm	ppm	ppm	ppm
Lower Limit	0.05	0.05	0.01	0.05	0.01	0.005	0.01	0.01	0.01	0.01	0.01	0.005	5	0.01	0.002	0.1	0.01	0.5	0.05	0.1	0.05	0.01
Method Code	FUS-MS	FUS-MS	FUS-MS	FUS-MS	FUS-MS	FUS-MS	FUS-MS	FUS-MS	FUS-MS	FUS-MS	FUS-MS	FUS-MS	TD-ICP	FUS-MS	FUS-MS	FUS-MS	FUS-MS	FUS-MS	FUS-MS	FUS-MS	FUS-MS	FUS-MS
NIST 694 Meas																						
NIST 694 Cert																						
DNC-1 Meas																						
DNC-1 Cert																						
GBW 07113 Meas																						
GBW 07113 Cert																						
SY-4 Meas	61.5	127	15.3	58.9	13.3	1.94	13.3	2.63	18.3	4.22	14.0	2.16		14.6	2.13	10.2	0.84					0.70
SY-4 Cert	58	122	15.0	57	12.7	2.00	14.0	2.6	18.2	4.3	14.2	2.3		14.8	2.1	10.6	0.9					0.8
Oreas 72a (4 Acid) Meas																						
Oreas 72a (4 Acid) Cert																						
BIR-1a Meas	0.60	2.00		2.50	1.20	0.590								1.60								
BIR-1a Cert	0.63	1.9		2.5	1.1	0.55								1.7								
ZW-C Meas	30.7	104	9.70	25.6	6.90		4.30										81.5	324	32.9			19.4
ZW-C Cert	30.0	97	9.5	25.0	6.6		4.70										82	320	34			20.0
OREAS 101b (Fusion) Meas	825	1370	130	394	51.0	7.98		5.34	32.0	6.39	18.8	2.73		17.9	2.64						37.2	405
OREAS 101b (Fusion) Cert	789	1331	127	378	48	7.77		5.37	32.1	6.34	18.7	2.66		17.6	2.58						37.1	396
OREAS 101b (4 Acid) Meas													24									
OREAS 101b (4 Acid) Cert													23									
OREAS 98 (4 Acid) Meas													312									
OREAS 98 (4 Acid) Cert													345									
NCS DC86318 Meas	> 2000	438	759	> 2000	> 1000	19.5	> 1000	497	> 1000	597	> 1000	269		> 1000	258						70.5	
NCS DC86318 Cert	1960	432	737	3429	1725	18.91	2168	468	3224	560	1750	271		1844	264						67.0	
SARM 3 Meas																						
SARM 3 Cert																						
USZ 42-2006 Meas	> 2000	> 3000	> 1000	> 2000	519	87.0				7.65				17.7							979	
USZ 42-2006 Cert	21100	27600	2300	6500	539	87.22				7.86				17.85							946	
OREAS 904 (4 Acid) Meas													10									
OREAS 904 (4 Acid) Cert													10.6									
OREAS 45d (4-Acid) Meas													23									
OREAS 45d (4-Acid) Cert													21.8									
REE-1 Meas	1660	> 3000	446	1480	398	24.4	411	112	889	212	719	110		707		494					784	148
REE-1 Cert	1661	3960	435	1456	381	23.5	433	106	847	208	701	106		678		479					719	137
OREAS 905 (INAA) Meas																						
OREAS 905 (INAA) Cert																						
OREAS 96 (4 Acid) Meas													95									
OREAS 96 (4 Acid) Cert													101									

Analyte Symbol	La	Ce	Pr	Nd	Sm	Eu	Gd	Tb	Dy	Ho	Er	Tm	Pb	Yb	Lu	Hf	Ta	W	Tl	Bi	Th	U
Unit Symbol	ppm	ppm	ppm	ppm	ppm	ppm	ppm	ppm	ppm	ppm	ppm	ppm	ppm	ppm	ppm	ppm	ppm	ppm	ppm	ppm	ppm	ppm
Lower Limit	0.05	0.05	0.01	0.05	0.01	0.005	0.01	0.01	0.01	0.01	0.01	0.005	5	0.01	0.002	0.1	0.01	0.5	0.05	0.1	0.05	0.01
Method Code	FUS-MS	FUS-MS	FUS-MS	FUS-MS	FUS-MS	FUS-MS	FUS-MS	FUS-MS	FUS-MS	FUS-MS	FUS-MS	FUS-MS	TD-ICP	FUS-MS	FUS-MS	FUS-MS	FUS-MS	FUS-MS	FUS-MS	FUS-MS	FUS-MS	FUS-MS
OREAS 923 (4 Acid) Meas													78									
OREAS 923 (4 Acid) Cert													83.0									
OREAS 621 (4 Acid) Meas													> 5000									
OREAS 621 (4 Acid) Cert													13600									
Oreas 77b (4 Acid) Meas													61									
Oreas 77b (4 Acid) Cert													61.0									
OREAS 681 (4 Acid) Meas													7									
OREAS 681 (4 Acid) Cert													10.2									
OREAS 147 (4 Acid) Meas													30									
OREAS 147 (4 Acid) Cert													27.8									
Oreas 521 (4 Acid) Meas													10									
Oreas 521 (4 Acid) Cert													9.3									
OREAS 70b (4 Acid) Meas													11									
OREAS 70b (4 Acid) Cert													14									
P126.1 Orig													23									
P126.1 Dup													21									
P154.1 Orig	28.3	52.7	6.06	22.3	4.45	0.874	3.08	0.62	3.79	0.82	2.39	0.358		2.40	0.384	4.4	1.22	2.4	0.57	0.2	11.0	2.45
P154.1 Dup	27.9	52.1	6.04	23.0	4.33	0.792	3.34	0.63	3.98	0.84	2.54	0.384		2.54	0.391	4.6	1.41	3.4	0.64	< 0.1	10.9	2.39
P193.1 Orig	24.0	45.8	5.15	18.8	3.37	0.677	2.73	0.48	2.98	0.63	1.91	0.294		2.07	0.324	4.2	1.12	1.6	0.85	0.3	7.45	2.46
P193.1 Dup	23.8	45.6	5.14	18.9	3.35	0.718	2.70	0.47	2.87	0.60	1.96	0.302		2.13	0.321	4.0	1.15	1.0	0.83	0.3	7.51	2.39
Method Blank	< 0.05	< 0.05	< 0.01	< 0.05	< 0.01	< 0.005	< 0.01	< 0.01	< 0.01	< 0.01	< 0.01	< 0.005		< 0.01	< 0.002	< 0.1	< 0.01	< 0.5	< 0.05	< 0.1	< 0.05	< 0.01
Method Blank													< 5									
Method Blank													< 5									
Method Blank																						
Method Blank																						


100
10
1
La
Ce
Pr
Nd
Sm
Eu
Gd
Tb
Dy
Ho
Er
Tm
Yb
Lu
P002.1
P003.1
P017.1
P020.1
P032.1
P085.1
P089.1
P106.1
P108.1
P124.1


1000
100
10
1
La
Ce
Pr
Nd
Sm
Eu
Gd
Tb
Dy
Ho
Er
Tm
Yb
Lu
P126.1
P152.1
P152.2
P153.1
P154.1 (1)
P154.1 (2)
P162.1
P173.1
P173.2
P173.3


100
10
1
La
Ce
Pr
Nd
Sm
Eu
Gd
Tb
Dy
Ho
Er
Tm
Yb
Lu
P175.2
P181.1
P193.1 (1)
P193.1 (2)

Appendix 4. Arrifes stratigraphic log — Details of the layers

- **Height:** from the base of the sequence
- **Hardness:** somethingStone (grainstone, mudstone, packstone, *etc.*)
- **Color code:** L. Light; D. Dark; Gr. Grey; Bei. Beige; Or. orange; Yel. Yellow; Pur. Purple; Bro. brown
- **Description color code:** Black: general information; Blue: lithology information; Green: first environnemental conditions
- **Sample code:** P are samples used for palynological analysis; G are for geochemical analysis
- **Palynofacies:** Use SP/D ratio from Mendes et al. (in preparation) for continental vs. marine influence or just write Pal. when they are dominant; the others stand for when phytoclasts (phytoc.) or Amorphous Organic Matter (AOM) are dominant in counting process
- **Env:** (1) from supratidal to intertidal; (2) from intertidal to subtidal shallow waters; (3) offshore below 50m with life evidences; (4) offshore above 50m without life evidences
- **Note:** Some sample code don't correspond to its layer's number, *e.g.* P066.1 stands for layer n°53

N°	Height (m)	Thickness (m)	Hardness	Color	Lithology and specificities	Sample	SP/D Phytoc. AOM	Env.
Base of sequence			Sand	Bei.	The Arrifes sequence starts with a **beach** deposit dated from the Miocene (unconformity) which is erosive regarding the Cretaceous formation below (eroded by Miocene deposit)			
Section n°1: Facies A (1m)								
1	1	1	Grain	Red-bro.-or. (clasts = same)	**CONGLOMERATE very coarse**; LIMESTONE and dolomite clasts (mm-10cm rounded-angular); *HCL:* a little fuzzy; *Dolomite:* very little; (1) Debris/ mudflow? Erosion event? High energy?; «Looks like a carbonate breccia, not organised. It is thick, maybe transported by an event? Tectonics?»; (2) limestone ➜ deposition ➜ exposed ➜ karstification (crack) ➜ filled with the CONGLOMERATE ➜ ➜ Marine proximal - shallow waters			1
Section n°2: Facies E - F (25.85m)								
2	3	2	Mud	Green-gr.	**MARL interbedded by MARLY LIMESTONE layers (ML)** (0.25-0.3m thick; gr.-yel.-bei.-creamy color)	P/G002.1		2
3	5	2	BREAK	BREAK	**BREAK** fault contact ➜ drag fold; «early lithification of the LIMESTONE in a very shallow env., exposing the carbonate platform (bei.-gr.)»			
4	8	3	Mud	Gr.-yel.-blueish-bei.-red-pur.	**MARL interbedded by ML layers** (<0.3m thick; gr.-blue color); dark layer (top); coal, plant material in MARL-CONGLOMERATE (small red bei. pebbles) ➜ Debris flow? Landslide? ; «I don't think it was exposed» ➜ ➜ Shallow waters	P/G003.1	SP/D: 0.99	2
5	10.4	2.4	Pack	Bei.-gr.-blue	**LIMESTONE**; base is homogeneous, fine grained, few bioturbation (biot.); top is mixed biot., more biot. upwards ➜ ➜ Coastal lagoon?			2
6	13.8	3.4	Mud	Yel.-gr.-blue	**MARL interbedded by ML layers**; dark layer (top)	P005.1	SP/D: 0.93	2
7	15.1	1.3	Mud-wack	Gr.	**MARLY LIMESTONE**; coal			2
8	15.5	0.4	Mud	D. gr.	**MARL**	P008.1	Phytoc.	2
9	19.5	4	Mud-wack	X	**MARLY LIMESTONE interbedded by MARL layers** (<0.05m; dark)			2

10	21.3	1.8	Mud	Gr.-bei.-D. gr.-blueish	**MARL interbedded by MARLY LIMESTONE layers**; some coal; last layer is a LIMESTONE with broken oysters: storm? ➜ ➜ Major change since the beginning: same env. But more marine; from now, more blueish			2
11	23.1	1.8	Mud	X	**MARL interbedded by MARLY LIMESTONE layers**; wood debris			2
12	24.4	1.3	Mud-wack	Gr.-green-blue	**MARLY LIMESTONE** with intra-clasts that are small piece of plant material (organic matter, OM); wood debris			2
13	24.55	0.15	Mud	D. gr.	**MARL**			2
14	26.35	1.8	Mud-wack	Gr.-bei.	**MARLY LIMESTONE**			2
15	26.75	0.4	Mud	Gr.-bei.-D. gr.	**MARL**			2
16	26.85	0.1	Grain	Gr.-pink	**LIMESTONE shallow water**; birdseye; ciment ➜ ➜ intertidal?			2
Section n°3: Facies G (4.95m)								
17	31.35	4.5	Mud	Bei.-gr.	**MARL interbedded by ML layers**; dark layer (top)	P/G017.1	SP/D: 0.28	3
18	31.8	0.45	Mud and Mud-wack	L. & D. gr.	**LIMESTONE** (2 layers; light gr.) **interbedded with MARL** (dark gr.)			3
Section n°4: B - E - F (10.05m)								
19	32.4	0.6	Pack-grain	L. gr.	**LIMESTONE** hard; grain size is fining-up; may have some wave controlled deposition ➜ ➜ nearshore			2
20	32.85	0.45	Mud and Mud-wack	L. & D. gr.	**LIMESTONE** (light gr.); **then a MARL layer** (dark gr.)	P/G020.1	Phytoc.	2
21	33.2	0.35	Pack-grain	L. gr.-bei.(-pink)	**LIMESTONE hard and compact**; fine grained (quite homogeneous); *Dolomite*: No, 100% calcite (pink coloration); must be calcarenite «a bit gritty»; parallel lamination ➜ ➜ really nearshore or close to the beach			2
22	33.75	0.55	Mud and Mud-wack	L. & D. gr.	**MARL** (dark gr.); **then a LIMESTONE layer** (light gr.)			2
23	33.95	0.2	Pack-grain	L. gr.-bei.(-pink)	**LIMESTONE hard and compact**; fine grained (quite homogeneous)			2
24	34.65	0.7	Mud and Mud-wack	X	**LIMESTONE**; then a MARL layer			2
25	34.95	0.3	Mud-wack	X	**MARLY LIMESTONE**			2
26	36.75	1.8	Mud	Bei.-pinkish	**MARL**			2
27	37.25	0.5	Pack	Gr.-bei.	**LIMESTONE**			2
28	41.05	3.8	Mud	Gr.-bei.	**MARL**; calcite mineral; geode	P028.1		2
29	41.85	0.8	Gravel to Sand	L. gr.-pinkish	**CONGLOMERATE**; grain size is fining-up; first 0.2m: CONGLOMERATE with gravels; then 0.45m: parallel laminations; last 0.15m wavy lamination ➜ ➜ decreasing energy?			2
30	42.05	0.2	Mud	D. gr.	**MARL**; color is becoming light bei. towards the top	P/G030.1	Phytoc.	2
31	42.35	0.3	Pack-grain	L. gr.-pink	**LIMESTONE**			2
32	42.95	0.6	Mud-wack	Gr.-bei.	**MARL** (dark gr.) **and ML** (pinkish)	P/G032.1	Phytoc.	2
33	43.2	0.25	Pack-grain	L. gr.-pink	**LIMESTONE**			2
34	43.45	0.25	Mud	D. gr.	**MARL**			2
35	43.65	0.2	Mud-wack	Gr.	**MARLY LIMESTONE**			2
Section n°5: Facies D (8.7m)								
36	45.35	1.7	Mud	Gr.-pinkish	**MARL interbedded by few ML**			1
37	52.35	7	Mud	Gr.-pinkish-green-bei.	**MARL**; top looks bioturbated; spotted with gr.-pinkish-green-bei. colors			1
Section n°6: Facies H (3.9m)								
38	56.25	3.9	Pack	L. bei.	**LIMESTONE**; iron oxyde and calcite nodules (kaki color)			3
Section n°7: A - B - C (5.7m)								
39	56.45	0.2	Sand	Yel.-or.-bei.	**CONGLOMERATE** with granule to coarse angular sand (quartz); fining-upwards			1
40	56.65	0.2	Sand	Yel.-or.-bei.	**SANDSTONE coarse**; parallel laminations			2

41	57.35	0.7	Sand	Yel.-or.-bei.	**SANDSTONE medium to coarse**; calcite ciment; herringbone cross-stratification ➜ ➜ tidal?			2
42	58.25	0.9	Sand	Yel.-or.-bei.	**EROSIVE CONGLOMERATE** with large clastic quartz and pebbles; clast support; fining-up, sand fining upwards; biot. (0.3m top)			2
43	58.55	0.3	Sand	Yel.-or.-bei.	**SANDSTONE medium-fine**; more homogeneous; clastic with carbonated ciment; few biot.			3
44	58.9	0.35	Sand	Yel.-or.-bei.	**SANDSTONE medium**; HCS ➜ storm?; biot. (top)			3
45	59.4	0.5	Sand	Yel.-or.-bei.	**SANDSTONE medium**; HCS ➜ storm?			3
46	60.65	1.25	Sand	Yel.-or.-bei.	**SANDSTONE very fine**; carbonated matrix; *HCL:* low; biot. (0.2m top)			3
47	61.95	1.3	Sand	Yel.-or.-bei.	**SANDSTONE very fine**; carbonated matrix; *HCL:* low; biot. (0.3m top)			3
Section n°8: Facies D (6.35m)								
48	62.35	0.4	Mud-wack	X	**MARLY LIMESTONE**; «more calcitic»			1
49	63.75	1.4	Mud and Mud-wack	Gr.-bro.-blueish-bei.-D. gr.	**MARLY LIMESTONE broken beds** (blueish-bei.) **supported by MARL** ➜ faulting; very dark MARL layer (few cm); rust level (top) ➜ oxygenation			1
50	64.25	0.5	Mud-wack	X	**MARLY LIMESTONE**			1
51	64.95	0.7	Mud	Blue-bei.-red-bro.	**MARL**; color spotted			1
52	65.45	0.5	Mud-wack	X	**MARLY LIMESTONE**			1
53	66.3	0.85	Mud	X	**MARL**	P066.1	Phytoc.	1
54	66.7	0.4	Mud-wack	Gr.-bei.-red	**MARLY LIMESTONE**: biot.			1
55	68.3	1.6	Mud and Mud-wack	X	**MARL** (2 layers: 0.35, 0.9m) **interbedded by a MARLY LIMESTONE bed** (0.35m); rust level (top)			1
Section n°9: Facies E - F (7m)								
56	68.7	0.4	Mud-wack	X	**MARLY LIMESTONE**; little calcite pebbles			2
57	68.8	0.1	Mud	X	**MARL**			2
58	69.35	0.55	Mud-wack	X	**MARLY LIMESTONE**			2
59	70.85	1.5	Mud	X	**MARL**	P071.1		2
60	71.95	1.1	Mud-wack	X	**MARLY LIMESTONE**			2
61	74.6	2.65	Mud and Mud-wack	X	**MARL** (4 layers: 0.3, 0.5, 0.2, 0.25m) **and 3 ML interbedded** (0.55, 0.45, 0.4m) ➜ ➜ Since n°48: shallow env. with very few biot. ➜ conditions not so good for life			2
62	75.3	0.7	Wack	X? More red	**LIMESTONE**; less mud ➜ there has been a change in sedimentation ➜ ➜ in conditions; honey comb sedimentary structure			2
Section n°10: Facies A - D (2.15m)								
63	75.5	0.2	Gravel	X	**CONGLOMERATE** with shells and clasts; lot of small broken shells; erosion surface; carbonated ciment ➜ ➜ very shallow water with high energy ➜ tidal channel? platform floor? high turbidity current?			1
64	75.75	0.25	Mud	Red	**MARL** ➜ quick depth variation ➜ ➜ tidal flat? flood?			1
65	76.9	1.15	Pack to wack	Gr. to red	**LIMESTONE**; layer thickening upwards; red shading from gr. to red			1
66	77.45	0.55	Mud	Reddish	**MARL** ➜ oxydation, tidal flat?	P077.1	Phytoc.	1
Section n°11: B - E - F (13.2m)								
67	77.7	0.25	Mud-wack	X	**MARLY LIMESTONE**			2
68	78.1	0.4	Wack	Spotted ?	**LIMESTONE**; color spotted			2
69	78.85	0.75	Mud	X	**MARL**			2
70	79.45	0.6	Wack	X	**LIMESTONE**			2
71	79.85	0.4	Mud	Black	**MARL**; dark color ➜ full of OM	P081.1	SP/D: 0.69	2
72	80.65	0.8	Wack	Bei.	**LIMESTONE**; biot. (burrow)			2

73	80.75	0.1	Mud	X	**MARL**; plant material			2
74	81.5	0.75	Wack	Reddish	**LIMESTONE**; biot. everywhere			2
75	81.65	0.15	Sand	X	**SANDSTONE**; carbonated ciment; ➜ high energy			2
76	81.95	0.3	Mud	Gr.-blue	**MARL**	P/G085.1	SP/D: 0.96	2
77	82.85	0.9	Wack then mud	Limestone then marl	**LIMESTONE** (0.4m): bei.-or.-red; micrite; (smooth) **transition to marl** (0.5m): light gr.-blueish			2
78	84.1	1.25	Mud	Gr.-red-or.	**MARL**; color spotted			2
79	84.6	0.5	Mud-wack then mud	X	**MARLY LIMESTONE** (0.2m); **transition to marl** (0.3m)			2
80	85.6	1	Mud-wack then mud	Gr.-bei.	**MARLY LIMESTONE** (0.3m); **transition to marl** (0.7m; more reddish)			2
88	86.1	0.5	Mud-wack	Gr.-bei.	**MARLY LIMESTONE**			2
89	87.1	1	Mud	Gr.-bei.-blue	**MARL**; dark layer (top)	P/G089.1		2
90	87.95	0.85	Mud-wack then mud	Reddish-pinkish	**MARLY LIMESTONE**; **transition to a marl**; biot.			2
91	89.95	2	Mud-wack then mud	L. gr.-bei.-reddish	**MARLY LIMESTONE** (1.3m); **transition to marl** (0.7m); biot. horizontal burrows (*i.e.* galeries) filled with carbonate			2
92	90.55	0.6	Wack	Bei.-red	**LIMESTONE** mix calcite - very fine dolomite (origin?); «bro. sugar»; second porosity; sparite; calcite geodes; tiny spot of rust			2
93	90.65	0.1	Mud	Bei.	**MARL**; biot. *Thalassinoids* ➜ ➜ shallow; shelf			2
Section n°12: Facies G - H (4.45m)								
94	91.35	0.7	Pack	Bei.-or.-red	**LIMESTONE** made of foraminifers (orbitulina); other broken shells (oyster); calcite geodes			3
95	91.95	0.6	Mud	Gr.-bei.	**MARL**	P095.1	SP/D: 0.35	3
96	92.3	0.35	Mud-wack	Gr.	**MARLY LIMESTONE**; full of small broken shells (bivalves); biot.			3
97	93	0.7	Mud	Gr.-D. gr.	**MARL**; dark laminations ➜ anoxic event?	P097.1	SP/D: 0.33	3
98	93.4	0.4	Mud-wack	Gr.-bei.	**MARLY LIMESTONE**; a lot of broken shells (oysters); biot.; broken oyster shells - marl cycles ➜ looks like debris flow			3
99	93.7	0.3	Mud	Gr.-D. gr.	**MARL**; dark laminations ➜ anoxic event?			3
100	95.1	1.4	Mud	L. gr.	**MARL interbedded by more competent limestone layers**; shells (oysters); biot.; broken oyster shells - marl cycles ➜ looks like debris flow			3
Section n°13: Facies I (3.95m)								
101	96.4	1.3	Mud	D. gr.-blueish	**MARL**; «pure mud, nothing inside»			4
102	98.8	2.4	Mud-wack	Gr.-blueish	**MARLY LIMESTONE interbedded by few mar beds** (<0.2m); biot.; much less shell (oyster) «less evidence of life»; dark layer (top) bitume?			4
103	99.05	0.25	Mud	D. gr.	**MARL** «pure dark marl»			4
Section n°14: Facies G (3.9m)								
104	101.55	2.5	Mud-wack	Gr.-blueish	**MARLY LIMESTONE interbedded by few marl beds** (<0.2m); biot.; shells (oysters); biot.; broken oyster shells - marl cycles ➜ looks like debris flow			3
105	102.95	1.4	Mud-wack	Gr.-bei.	**MARLY LIMESTONE interbedded by few marl beds** (< 0.1m); biot.; few big shells (oysters and clams) ➜ ➜ typical of muddy platform; carbonated balls «lumpy limestone»			3
Section n°15: Facies E (4.35m)								
106	103.15	0.2	Mud	X	**MARL**; full of plant material	P/G106.1	SP/D: 0.58	2
107	104.45	1.3	Mud-wack	Bei.-or.-red	**MARLY LIMESTONE interbedded by few marl beds**; biot.; carbonated balls «lumpy LIMESTONE»; geode			2
108	105.2	0.75	Mud	Gr.-bro.	**MARL**; few biot.; plant material and coal (continent); wood debris	P/G108.1		2
109	106.8	1.6	Mud-wack	X	**MARLY LIMESTONE interbedded by few marl beds**			2

110	107.3	0.5	Mud	Bei.	**MARL**			2
Section n°16: Facies G - H (3.1m)								
111	108.3	1	Mud-wack	Gr.-bei.-blue	**MARLY LIMESTONE**; biot.; full (>50%) of tiny fragments of shell (mix)			3
112	109.5	1.2	Mud	D. gr.-gr.	**MARL**			3
113	109.85	0.35	Pack	Bei.-blue	**LIMESTONE hard and competent** full of fossils; carbonated balls «lumpy limestone»			3
114	110.4	0.55	Mud	X	**MARL**; dark (top); «still in platform»	P114.1	Phytoc.	3
Section n°17: Facies E - F (6.9m)								
115	110.95	0.55	Grain	Reddish	**EROSIVE CALCARENITE**; fine grained; full of bioclasts (well preserved oyster); fining-up; broken gastropods at base ➜ ➜ shallow water and high energy ➜ tidal channel? beach deposit?			2
116	111.65	0.7	Grain	Reddish	**CALCARENITE very hard**; coarser than n°115; broken shells; full of fossils; grains fining-up; a very fine lamination appears on the way up ➜ water movement			2
117	111.95	0.3	Grain	Reddish	**LIMESTONE medium to coarse**; no lamination; broken shells			2
118	112.35	0.4	Mud	Gr.	**MARL**	P120.1	50/50	2
119	113.8	1.45	Grain	Reddish	**CALCARENITE**; coarse grained; broken shells			2
120	114.15	0.35	Mud	D. gr.	**MARL**			2
121	114.4	0.25	Mud-wack	L. gr.	**MARLY LIMESTONE**			2
122	117.3	2.9	Mud	L. gr.-bei.	**MARL interbedded by thin ML layers** (<0.1m thick)			2
Section n°18: Facies D (9.1m)								
123	118.1	0.8	Mud-wack	Gr.-bei.-or.	**MARLY LIMESTONE interbedded by few thin MARL layers** (bei.-or. color)			1
124	124.6	6.5	Mud	Pur.-reddish to bei. shading	**MARL**; dark gr. layer (last 0.05m); clast of jet (coal); mix of calcite and dolomite white balls; HYPOTHESIS: Soil? Storm lagune? Exposed soil? Calcarenite nodules? Carbonate-laden water (gypsum? halite? calcite? dolomite?) rises in the soil and the minerals precipitate directly into it	P/G124.1	Phytoc.	1
125	126.2	1.6	Mud-wack	L. gr.-bei.	**MARLY LIMESTONE**; huge wood print			1
126	126.4	0.2	Mud	D. gr.-black	**MARL**; dark color, full of OM	P/G126.1	SP/D: 0.88	1
Section n°19: Facies G - H (13.85m) *Including n°138 (Facies B)*								
127	127	0.6	Mud-wack	L. gr.-bei.	**MARLY LIMESTONE**			3
128	127.15	0.15	Mud	D. gr.-black	**MARL**; dark color, full of OM			3
129	127.65	0.5	Mud-wack	L. gr.-bei.	**MARLY LIMESTONE**; some biot. (vertical *Thalassinoids*)			3
130	127.85	0.2	Mud	D. gr.-black	**MARL**; dark color, full of OM	P130.1	SP/D: 0.30	3
131	131.25	3.4	Pack	L. gr.-yellowish	**CALCARENITE very hard**; very biot. (last 0.4m)			3
132	131.45	0.2	Mud	Red	**MARL**			3
133	131.65	0.2	Mud-wack	Bei.	**MARLY LIMESTONE**			3
134	132.05	0.4	Mud	D.	**MARL**	P134.1	SP/D: 0.46	3
135	132.55	0.5	Mud-wack	Gr.-bei.	**MARLY LIMESTONE**			3
136	133.55	1	Mud	Gr.-bei.-black	**MARL**			3
137	134.05	0.5	Mud-wack	X	**MARLY LIMESTONE**; many biot.; «limestone balls» ➜ debris flow that had mixed muds and limestones?			3
138	138.25	4.2	Mud	Pur.-reddish to bei. shading	**MARL**; looks like n°124	P138.1	Phytoc.	1
139	138.75	0.5	Mud-wack then mud	X	**MARLY LIMESTONE** (0.3m), well preserved gastropods shells (calm); **transition to a marl** (0.2m)			3
140	140.25	1.5	Mud-wack then mud	X	**MARLY LIMESTONE** (0.8m), broken shells (mussels and oysters), biot.; **transition to a MARL** (0.7m)	P140.1	AOM	3
Section n°20: Facies E - F (19.65m)								

141	141.15	0.9	Wack-pack	Bei.-or.	**LIMESTONE**; biot. (horizontal *Thalassinoids* and tunnels); huge plant material in burrows			2
142	141.8	0.65	Pack	Bei.-or.	**LIMESTONE**; same than n°141 but more competent; biot. (vertical *Thalassinoids*)			2
143	143.7	1.9	Mud	D.	**MARL**; very dark color, full of OM	P/G153.1	SP/D: 0.66	2
144	145.2	1.5	Mud-wack	Gr.-bei.	**MARLY LIMESTONE**; a thin marl layer (gr.)			2
145	147.1	1.9	Mud	Changing color	**MARL**; 4 different colors: 0.4m light gr., 0.4m pinkish-reddish, 0.5m light gr., 0.6m pur.; a thin very dark layer (sampling)	P155.1	SP/D: 0.69	2
146	147.4	0.3	Pack	Gr.-bei.	**LIMESTONE**; wave sedimentary feature ➜ ➜ very shallow conditions			2
147	148.2	0.8	Mud	Gr.-greenish	**MARL**			2
148	149	0.8	Mud-wack then mud	Gr.	**MARLY LIMESTONE** (0.4m), gastropods broken shells, biot. at the base (crab and lobsters huge horizontal *Thalassinoids*); **transition to a marl** (0.4m)	P158.1		2
149	150.6	1.6	Mud-wack	Gr.-green-blue	**MARLY LIMESTONE**			2
150	151.6	1	Mud	Gr.-bei.	**MARL**			2
151	151.9	0.3	Mud-wack	L. gr.-bei.	**MARLY LIMESTONE**; broken shells; some biot. like huge horizontal *Thalassinoids*			2
152	152.9	1	Mud	Pur.-red-gr.	**MARL**	P/G152.1 P/G152.2	AOM AOM	2
153	153.5	0.6	Mud-wack	L. gr.-bei.	**MARLY LIMESTONE** ➜ ➜ around this layer: middle intertidal part of the platform			2
154	154	0.5	Mud	D. gr.	**MARL**	P/G154.1	Phytoc. /AOM	2
155	155.4	1.4	Mud	Gr.-bei.	**MARL interbedded by 4 more competent limestone layers** (<0.2m thick; broken shells; some biot.			2
156	155.9	0.5	Mud	Gr.-bei.	**MARL**	P166.1	AOM	2
157	156.4	0.5	Mud-wack	L. gr.	**MARLY LIMESTONE**			2
158	157.1	0.7	Mud	D. gr.	**MARL**; reddish color (last 0.1m)	P168.1	Phytoc.	2
159	157.5	0.4	Pack	Bei.-pink	**CALCARENITE**; broken shells; biot.			2
160	159.9	2.4	Mud	Gr.	**MARL interbedded by ML layers** (which are < 0.1m thick and gr.-blue color); biot.	P160.1	Phytoc.	2
161	160.5	0.6	Pack	X	**LIMESTONE**; biot. (vertical burrows) ➜ vertical = energetic conditions			2
162	161.3	0.8	Mud	D.	**MARL**	P/G162.1	SP/D: 0.41	2
163	161.9	0.6	Mud-wack	Gr.-bei.	**MARLY LIMESTONE**; calcitic geode; many biot. (vertical burrows) at the base ➜ lack of oxygen (?) in first few cm of soil, causing the animals to dig deeper			2
Section n°21: Facies D (1.1m)								
164	162.4	0.5	Mud	Gr.-bei.	**MARL** ➜ ➜ not offshore but intertidal? tidal flat?	P164.1	Phytoc.	1
165	163	0.6	Mud-wack	Gr.-bei.	**MARLY LIMESTONE**; biot.; dinosaur footprints, two different species ➜ ➜ shallow env.			1
Section n°22: Facies E - F (3.6m)								
166	164.6	1.6	Pack	Bei.	**LIMESTONE**; bioclastic; biot.			2
167	165.2	0.6	Mud	Pinkish	**MARL**			2
168	165.8	0.6	Pack	Bei.	**LIMESTONE**; bioclastic; biot. (vertical burrows); same than n°166; current lamination ➜ due to tide? wave? ➜ ➜ shallow env.			2
169	166.6	0.8	Mud-wack then mud	Gr.-bei.	**MARLY LIMESTONE** (0.5m; bei.); **transition to a marl** (0.3m; dark gr.)			2
Section n°23: Facies G - H (9.1m) *Including n°172 and 173 (Facies I)*								
170	167.6	1	Pack	L. gr.	**LIMESTONE**; biot.; ➜ ➜ «trend is going deeper»			3

171	168.6	1	Mud-wack then mud	L. & D. gr. - reddish	**MARLY LIMESTONE**; **transition to marl;** from very dark to lighter gr.-red	P/G173.1	Phytoc.	3
172	170.3	1.7	Mud-wack then mud	D. gr.	**MARLY LIMESTONE** (1.1m); **transition to marl** (0.6m); biot.; ➜ transgression? oxygenation?	P/G173.2	SP/D: 0.21	4
173	171.2	0.9	Mud	D. bro.	**MARL** ➜ ➜ a lot of dark means maximum depth?	P/G173.3		4
174	171.6	0.4	Pack	Bei.	**CALCARENITE**; very bioturbated (*Thalassinoids*)			3
175	174.4	2.8	Mud-wack then mud	D. & gr.-bei.	**MARLY LIMESTONE** (gr.-bei.); **transition to marl** (gr. and soft)	P175.1 P/G175.2	SP/D: 0.38 SP/D: 0.77	3
176	175.7	1.3	Mud-wack then mud	D. & gr.-bei.	**MARLY LIMESTONE** (gr.-bei.); **transition to a marl** (dark gr. and soft); (same as n°175)	P176.1a P176.1b	SP/D: 0.66 SP/D: 0.39	3
Section n°24: Facies B - E - F (13.3m)								
177	176.1	0.4	Wack-pack	Bei.-pink	**LIMESTONE**; base: a lot of horizontal biot. (small and big for lobsters); top: fewer (➜ ➜ change in env.); some vertical burrows filled with sand; ➜ ➜ very shallow but <wave base; from now to end: color will be creamy-yellowish-bei.-or., while older layers are gr. and black			2
178	177.2	1.1	Mud	Pink then bei.	**MARL**; biot. in the pink part	P178.1	Phytoc.	2
179	178.2	1	Mud-wack	Or.	**MARLY LIMESTONE**; biot.			2
180	180.2	2	Wack-pack	L. gr.-bei.	**CALCARENITE**; biot.			2
181	180.9	0.7	Mud	Bei.	**MARL**	P/G181.1	Phytoc.	2
182	182.7	1.8	Mud-wack	L. gr.-bei.	**MARLY LIMESTONE interbedded by some small marl layers**; horizontal *Thalassinoids*; Base bed is a really clean ML, showing no biot. ➜ ➜ shallow water, can be <wave base in the platform			2
183	183.4	0.7	Pack then wack	L. gr.-bei.	**CALCARENITE**; biot. (*Thalassinoids*) (base); lamination (top); change in hardness; tiny black spots: probably small clast of silt/quartz; carbonated ciment; *HCL*: normal, a little bit of sand in this carbonated platform; ➜ ➜ shallow water			2
184	185.9	2.5	X	L. gr.-bei.	**CALCARENITE**; biot.; some bioclasts; tiny black spots: probably small clast of silt/quartz; carbonated ciment; *HCL*: normal, a little bit of sand in this carbonated platform; ➜ ➜ shallow water			2
185	187.4	1.5	Mud-Wack	Bei.	**MARLY LIMESTONE**; biot., most are horizontal ➜ the env. was quite			2
186	188.1	0.7	Wack-pack	Bei.-red	**LIMESTONE**; fine grained; biot.			2
187	188.8	0.7	Wack-pack	Bei.	**LIMESTONE hard**; base clean and biot. at top (horizontal *Thalassinoids*) ➜ ➜ shallow/subtidal			2
188	189	0.2	Gravel	Bei.	**CONGLOMERATE** with broken limestone; rip-up clasts; teepee; debris flow? ➜ ➜ tidal flat? shallow water - intertidal zone (rip-up)?			2
Section n°25: Facies G - H (4.8m) *Including n°193 (Facies A)*								
189	189.6	0.6	Mud-wack	Bei.	**MARLY LIMESTONE** ➜ ➜ from now to end: deepening trend			3
190	190.4	0.8	Pack	L. gr.-bei.	**LIMESTONE**; *HCL*: yes; very few broken shells; biot. (vertical burrows)			3
191	192.4	2	Mud-wack	L. gr.-bei.	**MARLY LIMESTONE interbedded by few marl beds**			3
192	193.2	0.8	Wack-pack	Gr.-bei.	**LIMESTONE** bioclastic; many broken oysters			3
193	193.5	0.3	Mud	D.	**MARL**; sandy desiccation cracks; mud — clay	P/G193.1	Phytoc.	1
194	193.8	0.3	Mud-wack	X	**MARLY LIMESTONE**; very few biot. (horizontal *Thalassinoids*) ➜ ➜ since n°189: deepening trend but still in platform (shells presence)			3

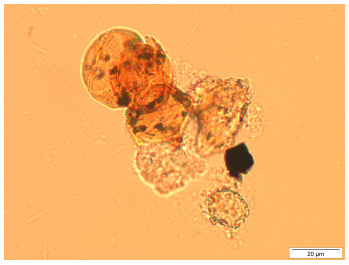
Appendix 5.1 Palynology including palynofacies analysis — P002.1

- **Height:** from the base of the sequence
- **Counts:** 250 particles were counted per sample (in %)
- **Pie Chart:** is based on each organic residue abundance

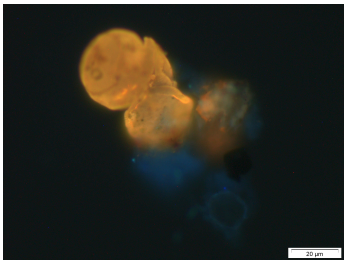
Layer n°	Height (m)	Sample code	Palynomorphe					Phytoclast		AOM
			Spore	Pollen	Dinocyst	Other marine	Unidentified	Opaque	Translucid	
2	3	**P002.1**	0,0	7,4	1,6	9,0	21,2	29,0	3,9	27,9
		Total %			39,2			32,9		27,9

Extra note:

- Some AOM show fluorescence
- Some AOM show pyrite
- Very few dinocysts
- Some bisacate pollen
- Some algae

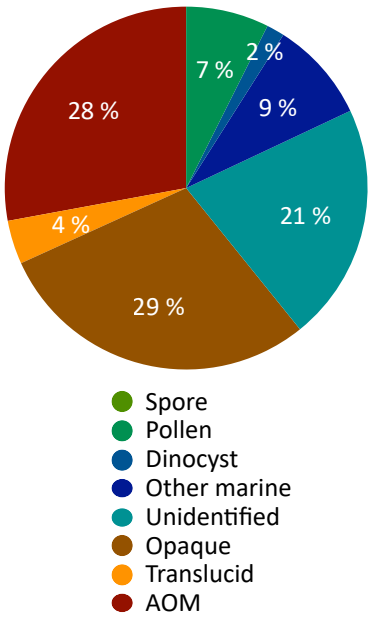


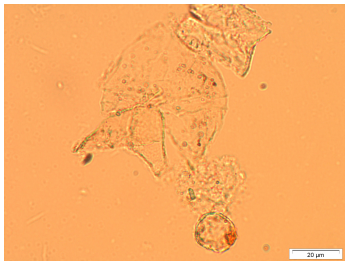
Classopolis pollen



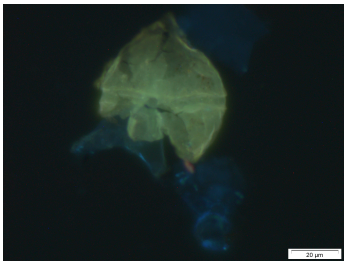
Classopolis pollen (UV fluorescence)

Detailed Pi Chart





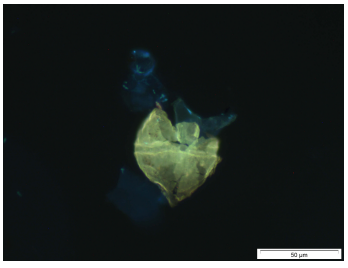
Dinocyst



Dinocyst (UV fluorescence)



Dinocyst



Dinocyst (UV fluorescence)

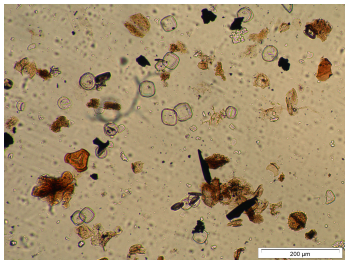
Appendix 5.2 Palynology including palynofacies analysis — P003.1

- **Height:** from the base of the sequence
- **Counts:** 250 particles were counted per sample (in %)
- **Pie Chart:** is based on each organic residue abundance

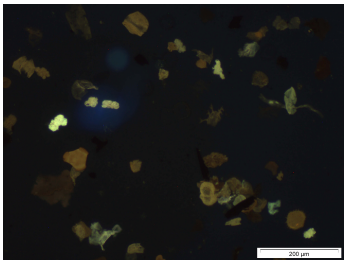
Layer n°	Height (m)	Sample code	Palynomorphe					Phytoclast		AOM
			Spore	Pollen	Dinocyst	Other marine	Unidentified	Opaque	Translucid	
4	8	**P003.1**	0,8	18,4	7,7	2,3	27,2	26,8	6,5	10,4
		Total %			56,4			33,3		10,4

Extra note:

- A lot of minerals
- Some AOM show fluorescence
- Some AOM are degraded
- Some algae

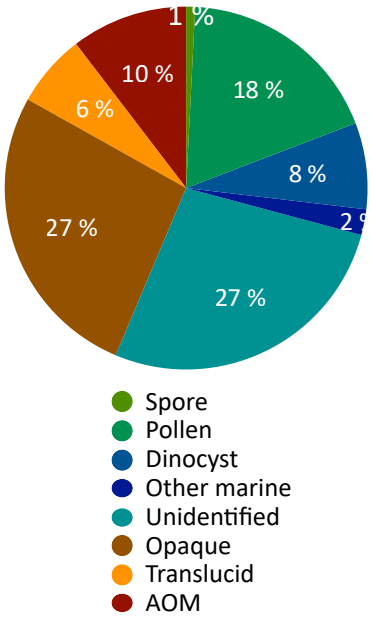


Overview



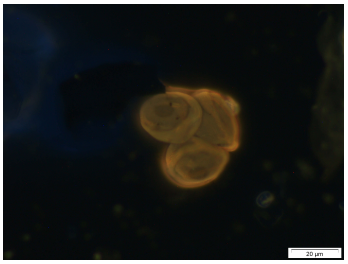
Overview (UV fluorescence)

Detailed Pi Chart

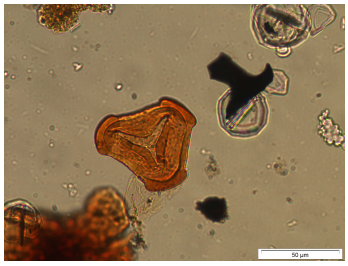




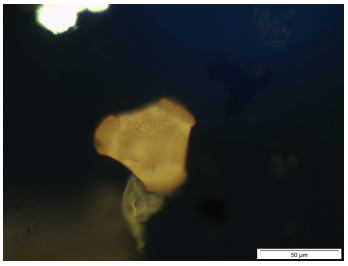
Classopolis pollen



Classopolis pollen (UV fluorescence)



Spore



Spore (UV fluorescence)

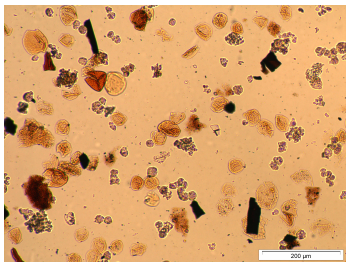
Appendix 5.3 Palynology including palynofacies analysis — P005.1

- **Height:** from the base of the sequence
- **Counts:** 250 particles were counted per sample (in %)
- **Pie Chart:** is based on each organic residue abundance

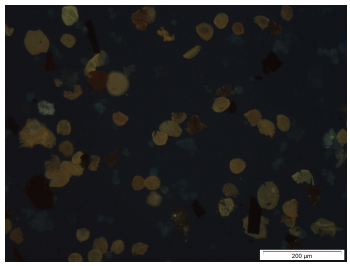
Layer n°	Height (m)	Sample code	Palynomorphe					Phytoclast		AOM
			Spore	Pollen	Dinocyst	Other marine	Unidentified	Opaque	Translucid	
6	13.8	**P005.1**	1,5	6,0	7,1	35,1	19,1	7,5	9,0	14,9
		Total %			68,8			16,5		14,9

Extra note:

- Abundant in palynomorphs
- Many of the pollen show pyrite
- Some algae

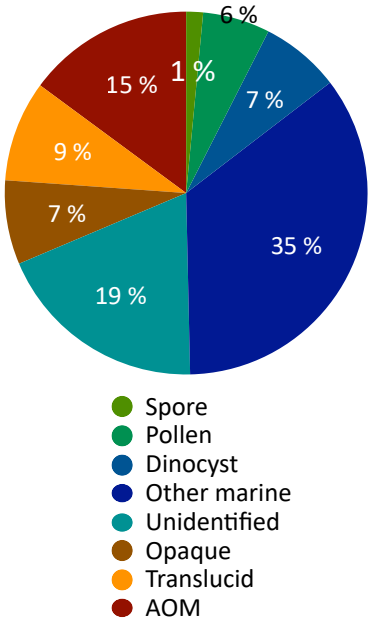


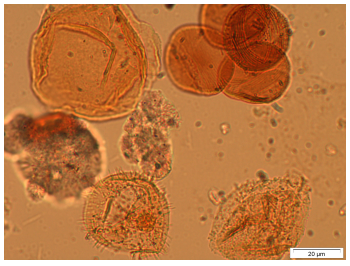
Overview



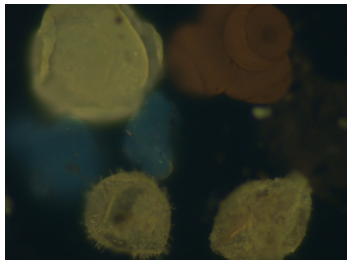
Overview (UV fluorescence)

Detailed Pi Chart

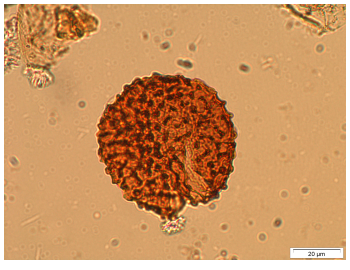




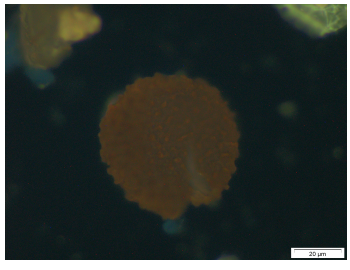
Classopolis pollen; dinocyst; algae



Classopolis pollen; dinocyst; algae (UV fluorescence)



Spore



Spore (UV fluorescence)

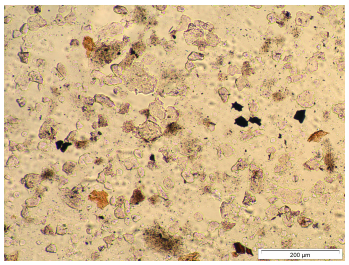
Appendix 5.4 Palynology including palynofacies analysis — P008.1

- **Height:** from the base of the sequence
- **Counts:** 250 particles were counted per sample (in %)
- **Pie Chart:** is based on each organic residue abundance

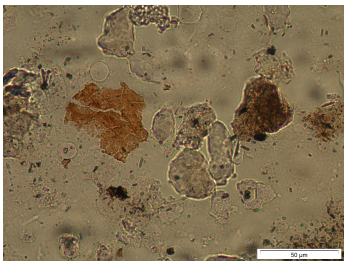
Layer n°	Height (m)	Sample code	Palynomorphe					Phytoclast		AOM
			Spore	Pollen	Dinocyst	Other marine	Unidentified	Opaque	Translucid	
8	15.5	**P008.1**	0,0	0,0	0,0	0,0	0,0	77,1	23,0	0,0
		Total %			0,0			100,1		0,0

Extra note:

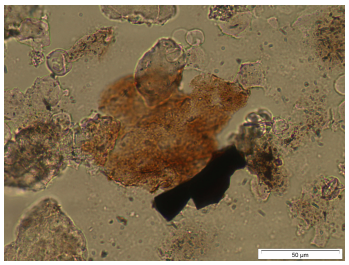
- Sample barren of palynomorphs



Overview

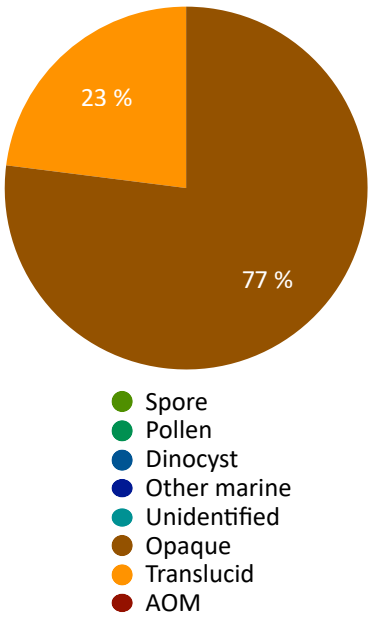


Phytoclasts



Phytoclasts

Detailed Pi Chart



Appendix 5.5 Palynology including palynofacies analysis — P017.1

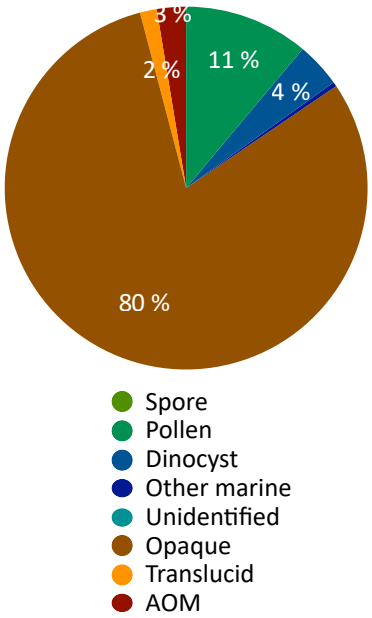
- **Height:** from the base of the sequence
- **Counts:** 250 particles were counted per sample (in %)
- **Pie Chart:** is based on each organic residue abundance

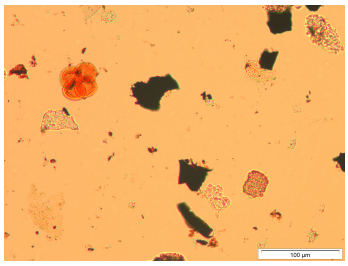
Layer n°	Height (m)	Sample code	Palynomorphe					Phytoclast		AOM
			Spore	Pollen	Dinocyst	Other marine	Unidentified	Opaque	Translucid	
17	31.35	**P017.1**	0,0	11,1	4,0	0,4	0,0	80,5	1,5	2,6
		Total %			15,5			82,0		2,6

Extra note:

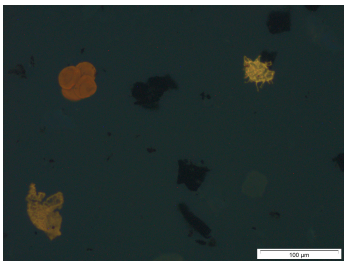
- Black phytoclasts are abundant
- Very few palynomorphs
- Very very few with pyrite
- Foraminifers
- Some chorate dinocysts (more distal)

Detailed Pi Chart





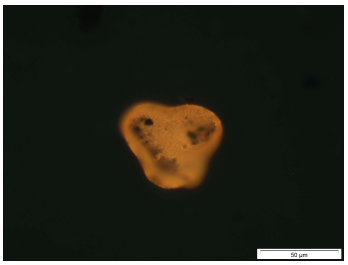
Overview



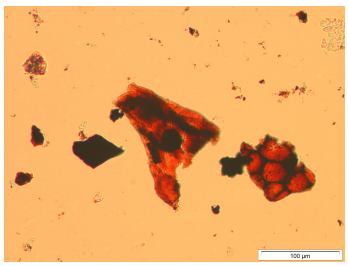
Overview (UV fluorescence)



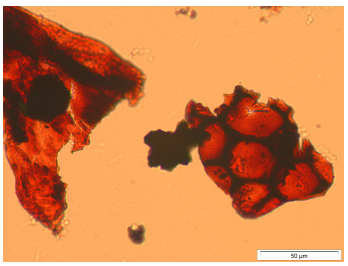
Spore



Spore (UV fluorescence)



Phytoclasts; foraminifer innerlining



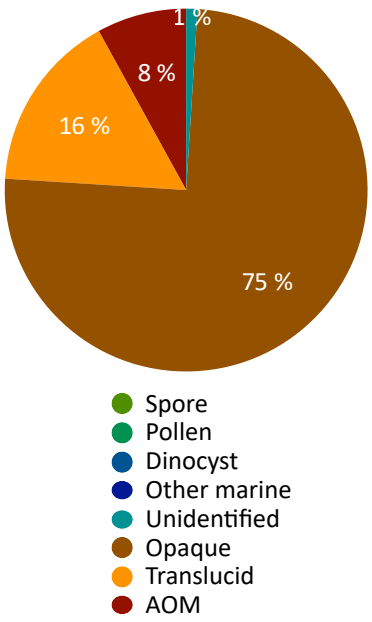
Phytoclasts; foraminifer innerlining (UV fluorescence)

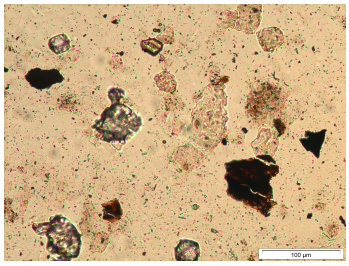
Appendix 5.6 Palynology including palynofacies analysis — P020.1

- **Height:** from the base of the sequence
- **Counts:** 250 particles were counted per sample (in %)
- **Pie Chart:** is based on each organic residue abundance

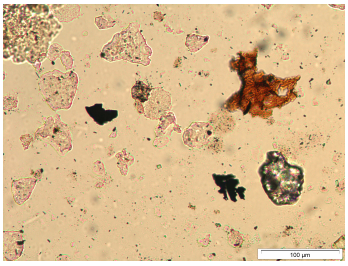
Layer n°	Height (m)	Sample code	Palynomorphe					Phytoclast		AOM
			Spore	Pollen	Dinocyst	Other marine	Unidentified	Opaque	Translucid	
20	32.85	**P020.1**	0,0	0,0	0,0	0,0	1,0	75,1	16,0	8,0
		Total %			1,0			91,1		8,0

Extra note:

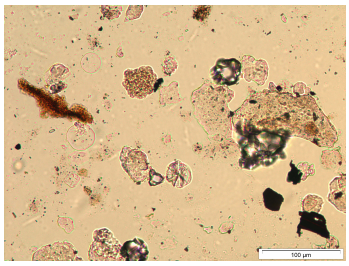




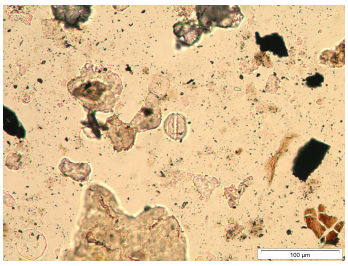
Phytoclasts opaque and translucid



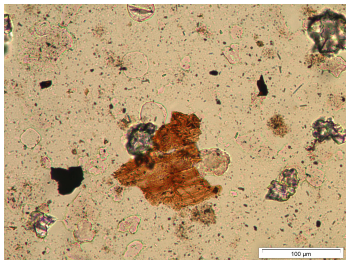
Phytoclasts opaque and translucid



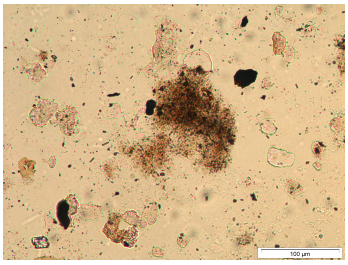
Phytoclasts opaque and translucid



Phytoclasts opaque and translucid



Phytoclasts opaque and translucid



AOM; Phytoclasts opaque

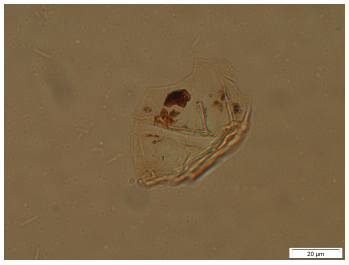
Appendix 5.7 Palynology including palynofacies analysis — P028.1

- **Height:** from the base of the sequence
- **Counts:** 250 particles were counted per sample (in %)
- **Pie Chart:** is based on each organic residue abundance

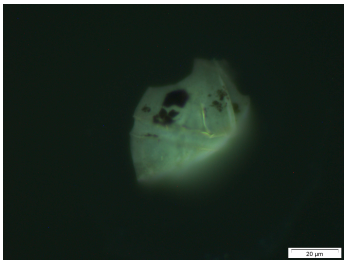
Layer n°	Height (m)	Sample code	Palynomorphe					Phytoclast		AOM
			Spore	Pollen	Dinocyst	Other marine	Unidentified	Opaque	Translucid	
28	41.05	**P028.1**	0,8	5,9	4,3	0,0	3,5	73,8	3,9	7,8
		Total %			14,5			77,7		7,8

Extra note:

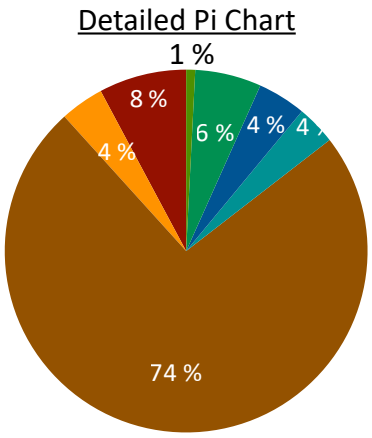
- Some dinocysts with pyrite



Armored dinocyst



Armored dinocyst (UV fluorescence)

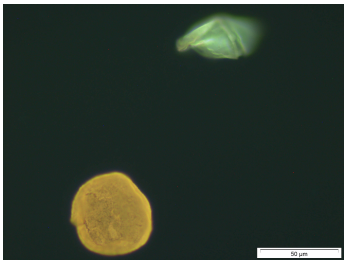




Phytoclasts opaque and translucid



Dinocyst; unidentified



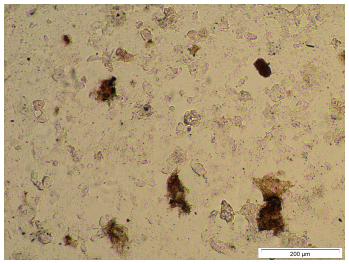
Dinocyst; unidentified (UV fluorescence)

Appendix 5.8 Palynology including palynofacies analysis — P030.1

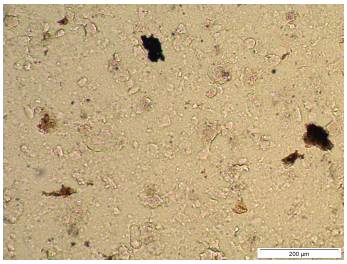
- **Height:** from the base of the sequence
- **Counts:** 250 particles were counted per sample (in %)
- **Pie Chart:** is based on each organic residue abundance

Layer n°	Height (m)	Sample code	Palynomorphe					Phytoclast		AOM
			Spore	Pollen	Dinocyst	Other marine	Unidentified	Opaque	Translucid	
30	42.05	**P030.1**	0,0	0,0	0,0	0,0	0,0	44,4	17,9	37,8
		Total %			0,0			62,3		37,8

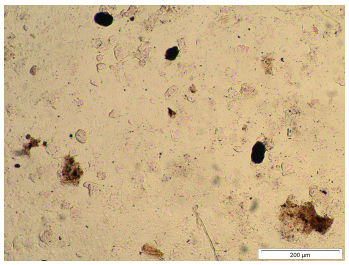
Extra note:



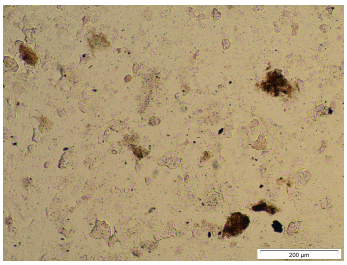
Phytoclasts opaque and translucid; AOM



Phytoclasts opaque and translucid; AOM

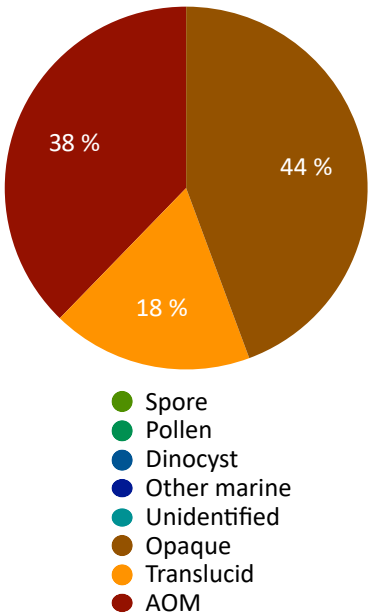


Phytoclasts opaque and translucid; AOM



Phytoclasts opaque and translucid; AOM

Detailed Pi Chart

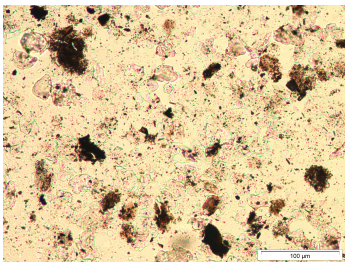


Appendix 5.9 Palynology including palynofacies analysis — P032.1

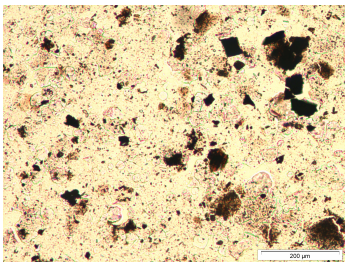
- **Height:** from the base of the sequence
- **Counts:** 250 particles were counted per sample (in %)
- **Pie Chart:** is based on each organic residue abundance

Layer n°	Height (m)	Sample code	Palynomorphe					Phytoclast		AOM
			Spore	Pollen	Dinocyst	Other marine	Unidentified	Opaque	Translucid	
32	42.95	**P032.1**	0,0	0,0	0,0	0,0	0,0	52,4	28,3	19,4
		Total %			0,0			80,7		19,4

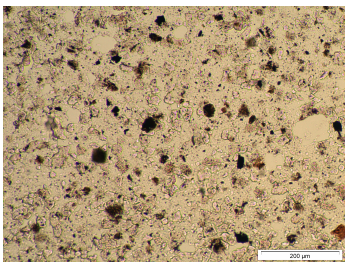
Extra note:
- Dirty sample



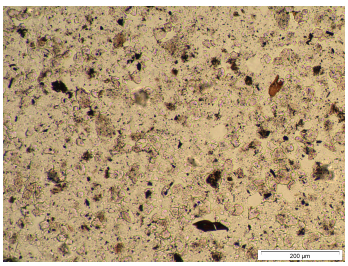
Overview



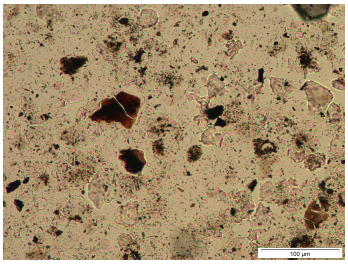
Overview



Overview

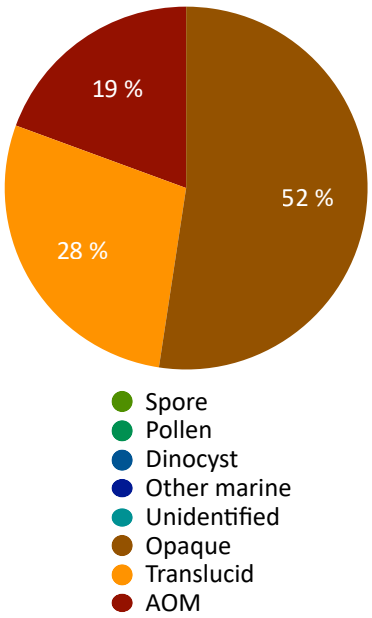


Overview



Overview

Detailed Pi Chart



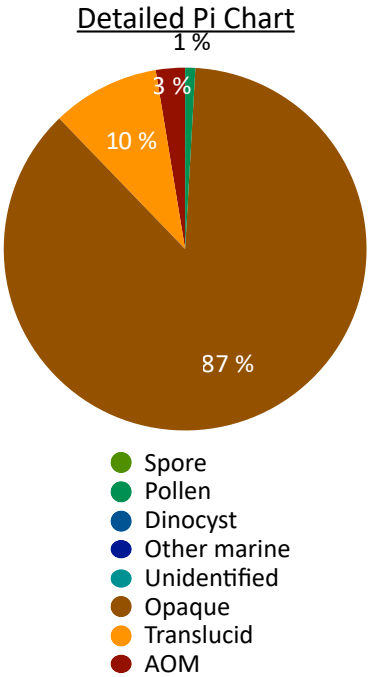
Appendix 5.10 Palynology including palynofacies analysis — P066.1

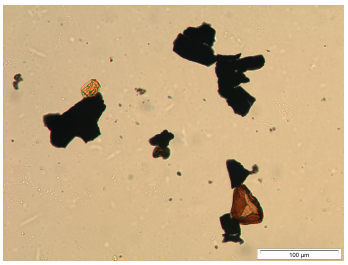
- **Height:** from the base of the sequence
- **Counts:** 250 particles were counted per sample (in %)
- **Pie Chart:** is based on each organic residue abundance

Layer n°	Height (m)	Sample code	Palynomorphe					Phytoclast		AOM
			Spore	Pollen	Dinocyst	Other marine	Unidentified	Opaque	Translucid	
53	66.3	**P066.1**	0,0	0,9	0,0	0,0	0,0	86,9	9,6	2,6
		Total %			0,9			96,5		2,6

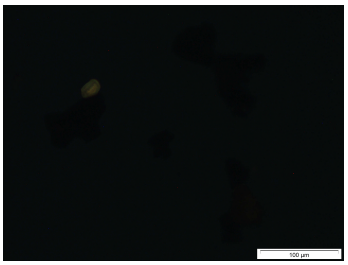
Extra note:

- Lot of spores compare to the previous samples

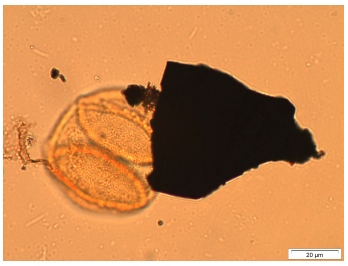




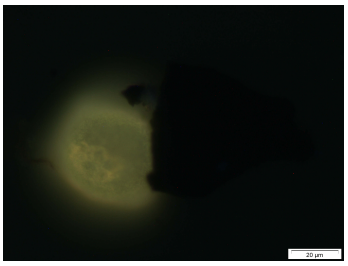
Phytoclasts opaque; spore; unidentified



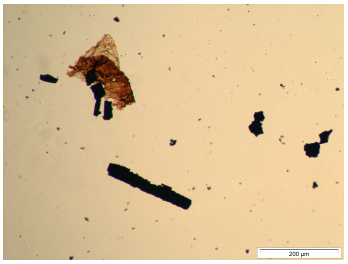
Phytoclasts opaque; spore; unidentified (UV fluorescence)



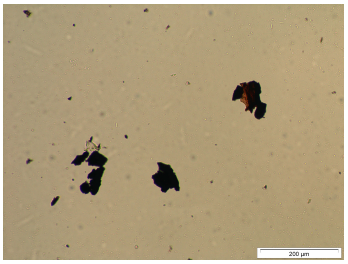
Pollen



Pollen (UV fluorescence)



Phytoclasts opaque and translucid



Phytoclasts opaque

Appendix 5.11 Palynology including palynofacies analysis — P071.1

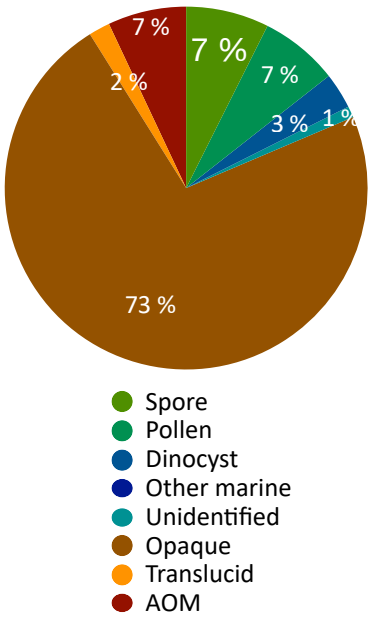
- **Height:** from the base of the sequence
- **Counts:** 250 particles were counted per sample (in %)
- **Pie Chart:** is based on each organic residue abundance

Layer n°	Height (m)	Sample code	Palynomorphe					Phytoclast		AOM
			Spore	Pollen	Dinocyst	Other marine	Unidentified	Opaque	Translucid	
59	70.85	**P071.1**	7,4	7,0	3,2	0,0	1,0	72,6	1,9	7,0
		Total %			18,6			74,5		7,0

Extra note:

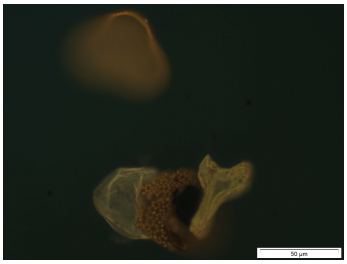
- Lot of spores compare to the previous samples

Detailed Pi Chart

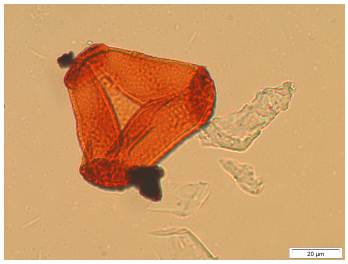




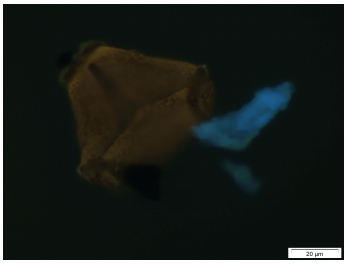
Spore; pollen



Spore; pollen (UV fluorescence)



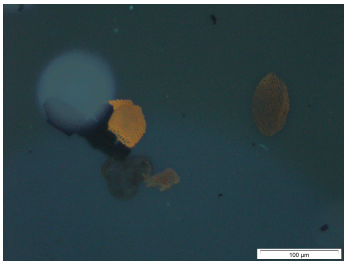
Spore



Spore (UV fluorescence)



Spore; pollen; Phytoclast opaque



Spore; pollen; Phytoclast opaque (UV fluorescence)

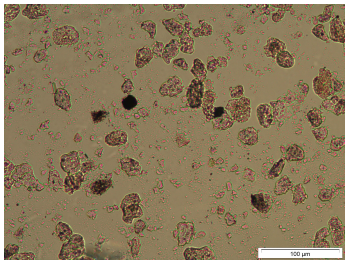
Appendix 5.12 Palynology including palynofacies analysis — P077.1

- **Height:** from the base of the sequence
- **Counts:** 250 particles were counted per sample (in %)
- **Pie Chart:** is based on each organic residue abundance

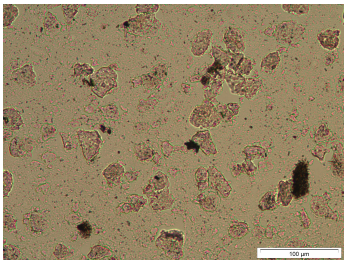
Layer n°	Height (m)	Sample code	Palynomorphe					Phytoclast		AOM
			Spore	Pollen	Dinocyst	Other marine	Unidentified	Opaque	Translucid	
66	77.45	**P077.1**	0,0	0,0	0,0	0,0	0,0	39,0	18,0	43,0
		Total %			0,0			57,0		43,0

Extra note:

- Not very clean, seems to have a lot of clay minerals

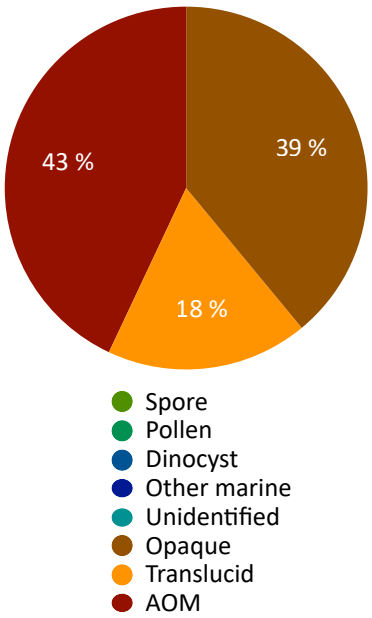


Overview



Overview

Detailed Pi Chart



Appendix 5.13 Palynology including palynofacies analysis — P081.1

- **Height:** from the base of the sequence
- **Counts:** 250 particles were counted per sample (in %)
- **Pie Chart:** is based on each organic residue abundance

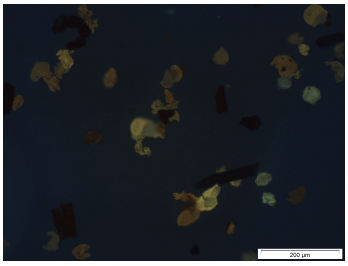
Layer n°	Height (m)	Sample code	Palynomorphe					Phytoclast		AOM
			Spore	Pollen	Dinocyst	Other marine	Unidentified	Opaque	Translucid	
71	79.85	**P081.1**	1,1	36,3	11,8	0,4	13,5	15,7	2,5	18,9
		Total %			63,1			18,2		18,9

Extra note:

- Lot of pollen,
- Pyrite in palynomorphs
- Some AOM
- Two types of dinocysts
- Some foraminifer innerlinings

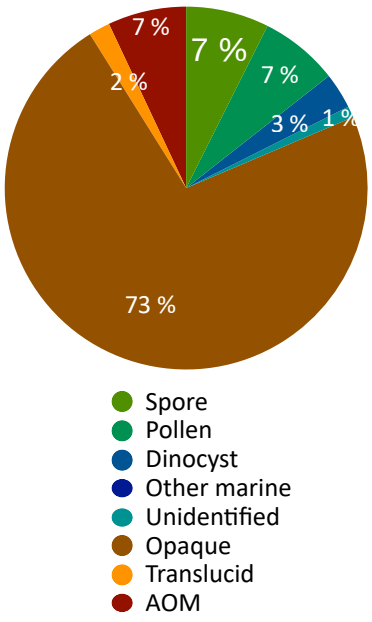


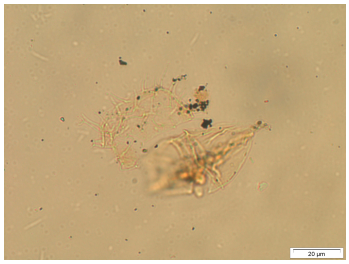
Overview



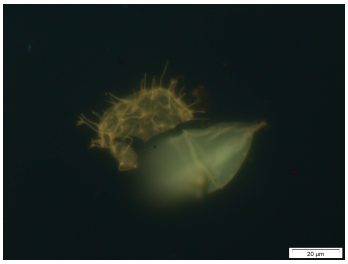
Overview (UV fluorescence)

Detailed Pi Chart

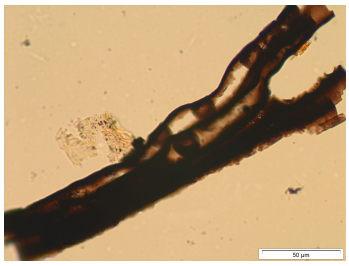




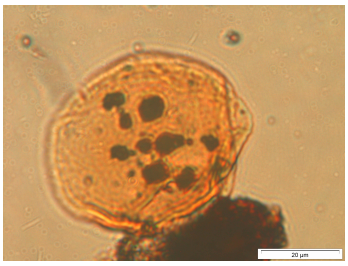
Dinocysts



Dinocysts (UV fluorescence)



Translucid phytoclast



Palynomorph with pyrite

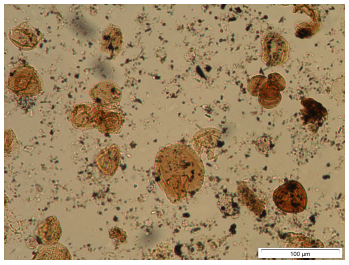
Appendix 5.14 Palynology including palynofacies analysis — P085.1

- **Height:** from the base of the sequence
- **Counts:** 250 particles were counted per sample (in %)
- **Pie Chart:** is based on each organic residue abundance

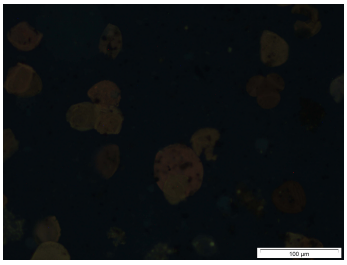
Layer n°	Height (m)	Sample code	Palynomorphe					Phytoclast		AOM
			Spore	Pollen	Dinocyst	Other marine	Unidentified	Opaque	Translucid	
76	81.95	**P085.1**	1,5	9,4	10,5	10,9	30,1	24,1	8,6	4,9
		Total %			62,4			32,7		4,9

Extra note:

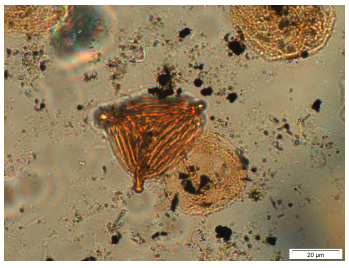
- Not clean, a lot of clay minerals
- Some algae
- Some foraminifer innerlinings



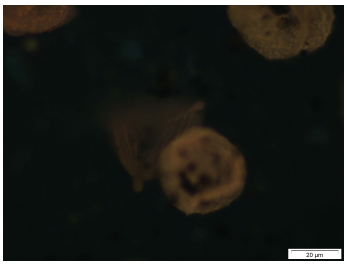
Overview



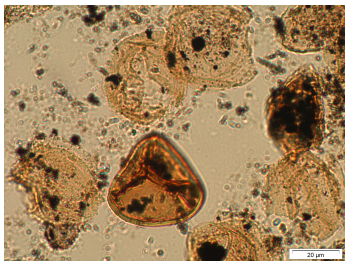
Overview (UV fluorescence)



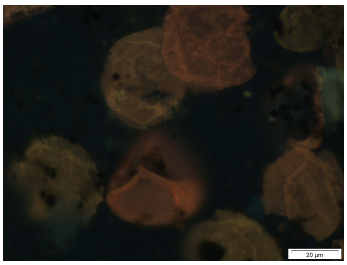
Spore



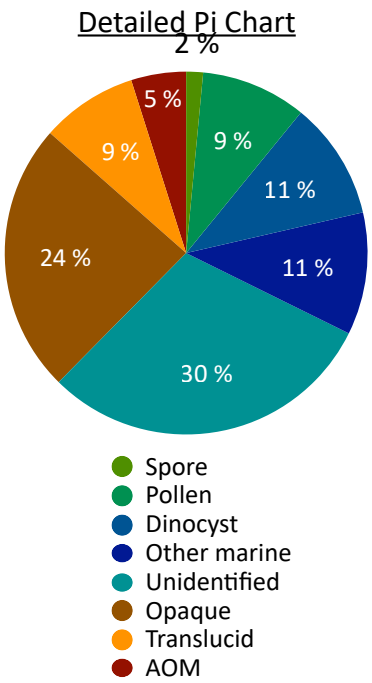
Spore (UV fluorescence)



Spore and algae



Spore and algae (UV fluorescence)



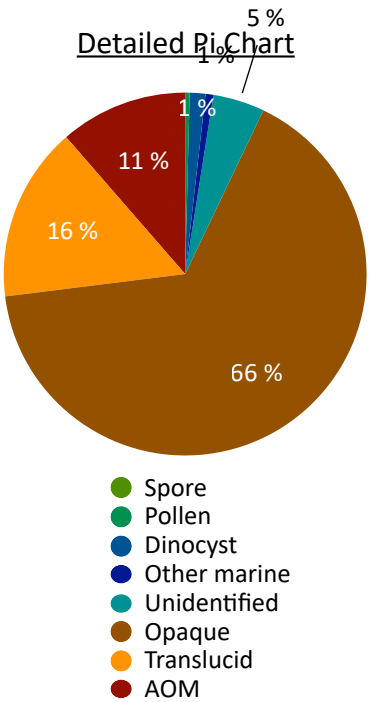
Appendix 5.15 Palynology including palynofacies analysis — P089.1

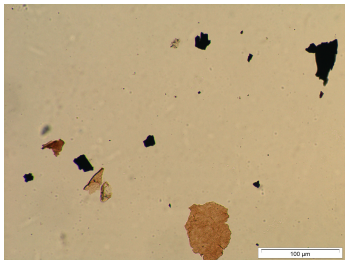
- **Height:** from the base of the sequence
- **Counts:** 250 particles were counted per sample (in %)
- **Pie Chart:** is based on each organic residue abundance

Layer n°	Height (m)	Sample code	Palynomorphe					Phytoclast		AOM
			Spore	Pollen	Dinocyst	Other marine	Unidentified	Opaque	Translucid	
89	87.1	**P089.1**	0,0	0,4	1,4	0,7	4,6	66,0	15,6	11,4
		Total %			7,1			81,6		11,4

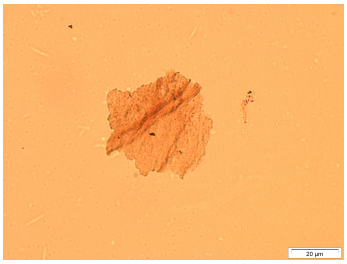
Extra note:

- Dinocysts
- Some algae





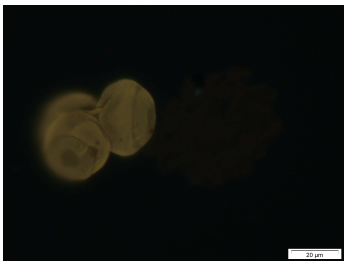
Overview



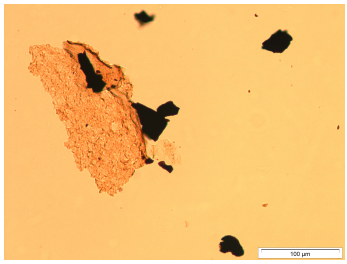
Translucid phytoclast



Classopolis pollen; phytoclasts opaque and translucid



Classopolis pollen; phytoclasts opaque and translucid (UV fluorescence)



Phytoclasts opaque and translucid

Appendix 5.16 Palynology including palynofacies analysis — P095.1

- **Height:** from the base of the sequence
- **Counts:** 250 particles were counted per sample (in %)
- **Pie Chart:** is based on each organic residue abundance

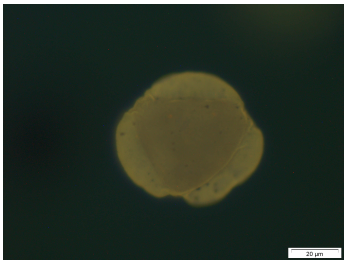
Layer n°	Height (m)	Sample code	Palynomorphe					Phytoclast		AOM
			Spore	Pollen	Dinocyst	Other marine	Unidentified	Opaque	Translucid	
95	91.95	**P095.1**	1,5	21,5	27,3	3,1	7,7	24,3	2,3	12,3
		Total %			61,1			26,6		12,3

Extra note:

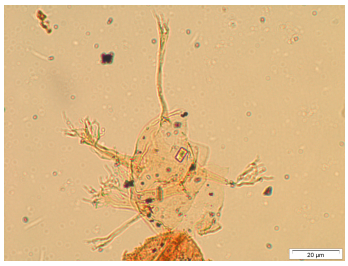
- Chorate dinocysts
- A lot of pyrite in palynomorphs
- Some of the palynomorphs are well preserved while other are very degraded



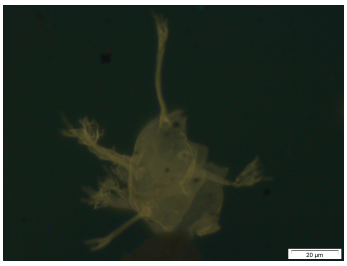
Pollen



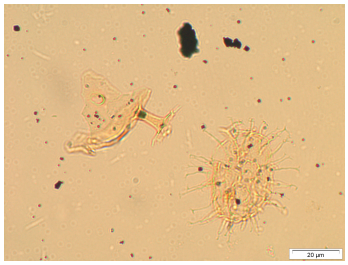
Pollen (UV fluorescence)



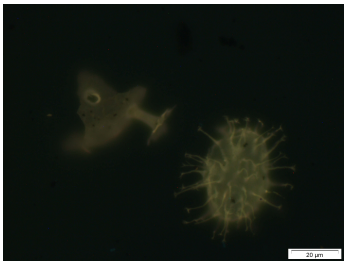
Chorate dinocyst



Chorate dinocyst (UV fluorescence)

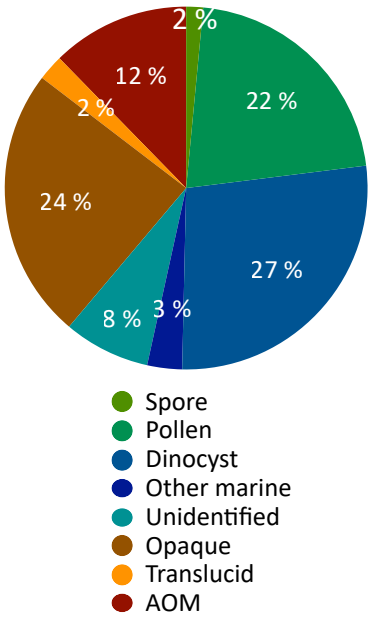


Chorate dinocyst



Chorate dinocyst (UV fluorescence)

Detailed Pi Chart



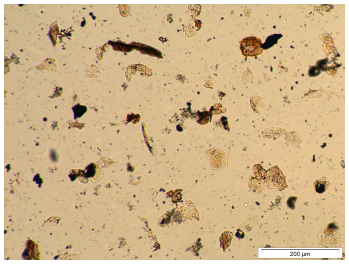
Appendix 5.17 Palynology including palynofacies analysis — P097.1

- **Height:** from the base of the sequence
- **Counts:** 250 particles were counted per sample (in %)
- **Pie Chart:** is based on each organic residue abundance

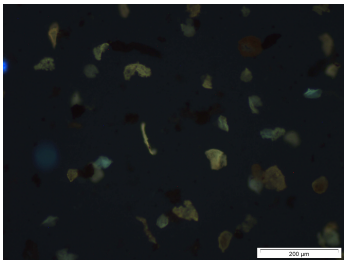
Layer n°	Height (m)	Sample code	Palynomorphe					Phytoclast		AOM
			Spore	Pollen	Dinocyst	Other marine	Unidentified	Opaque	Translucid	
97	93	**P097.1**	1,1	1,5	31,7	0,8	21,3	18,7	14,9	10,1
		Total %			56,4			33,6		10,1

Extra note:

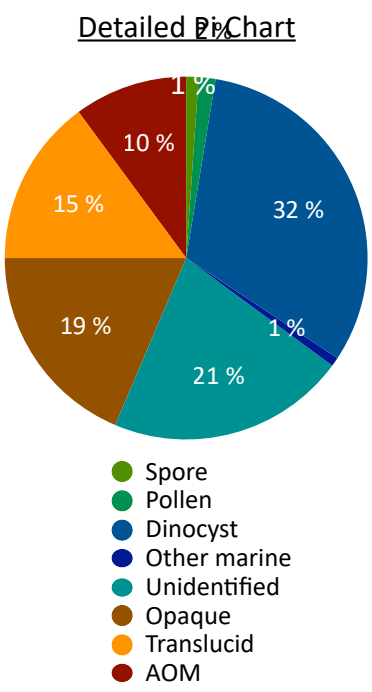
- Chorate dinocysts
- Some pyrite



Overview

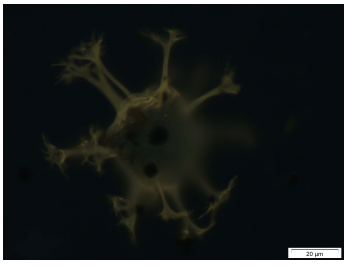


Overview (UV fluorescence)





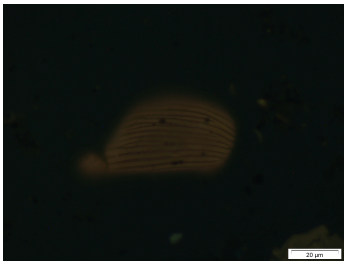
Chorate dinocyst with pyrite



Chorate dinocyst with pyrite (UV fluorescence)



Unidentified



Unidentified (UV fluorescence)

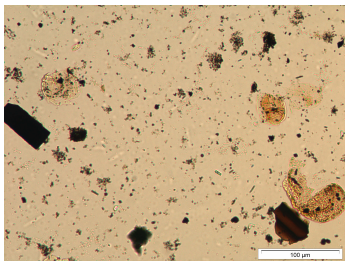
Appendix 5.18 Palynology including palynofacies analysis — P106.1

- **Height:** from the base of the sequence
- **Counts:** 250 particles were counted per sample (in %)
- **Pie Chart:** is based on each organic residue abundance

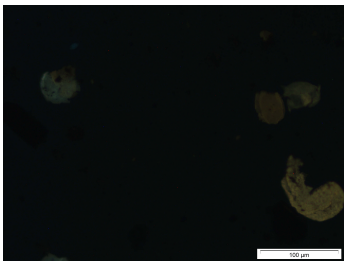
Layer n°	Height (m)	Sample code	Palynomorphe					Phytoclast		AOM
			Spore	Pollen	Dinocyst	Other marine	Unidentified	Opaque	Translucid	
106	103.15	**P106.1**	1,6	14,3	34,8	0,4	14,7	23,6	8,1	2,7
		Total %			65,8			31,7		2,7

Extra note:

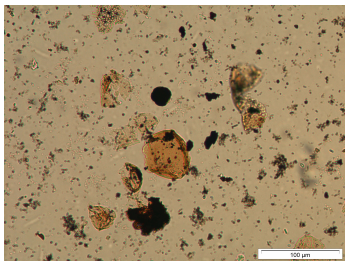
- Palynomorphs are degraded
- A lot of pyrite



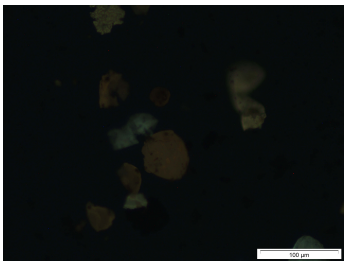
Overview



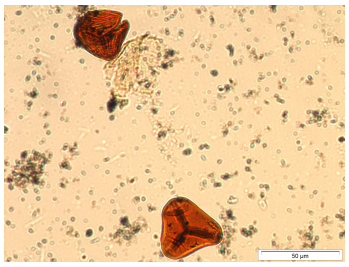
Overview (UV fluorescence)



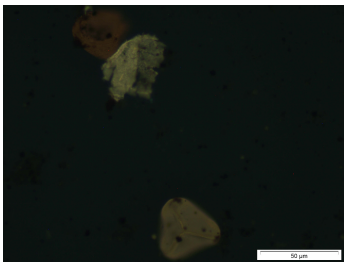
Overview



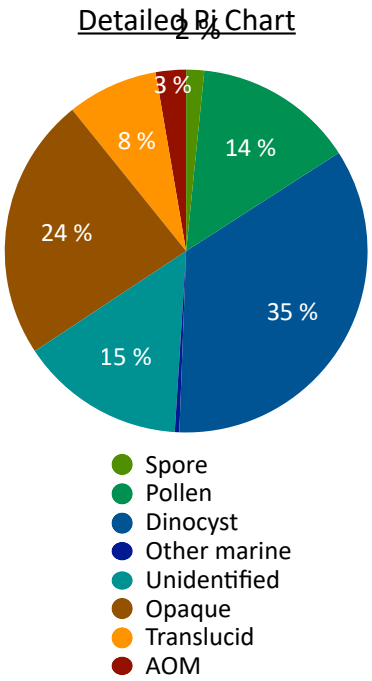
Overview (UV fluorescence)



Some spores



Some spores (UV fluorescence)



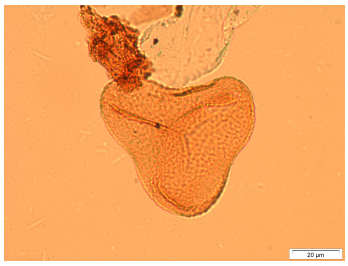
Appendix 5.19 Palynology including palynofacies analysis — P108.1

- **Height:** from the base of the sequence
- **Counts:** 250 particles were counted per sample (in %)
- **Pie Chart:** is based on each organic residue abundance

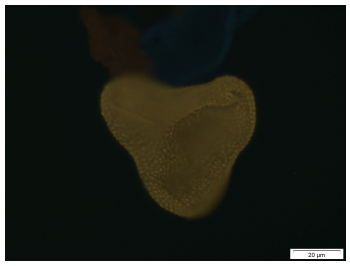
Layer n°	Height (m)	Sample code	Palynomorphe					Phytoclast		AOM
			Spore	Pollen	Dinocyst	Other marine	Unidentified	Opaque	Translucid	
108	105.2	**P108.1**	1,1	7,1	6,0	4,1	33,2	32,9	10,1	5,6
		Total %			51,5			43,0		5,6

Extra note:

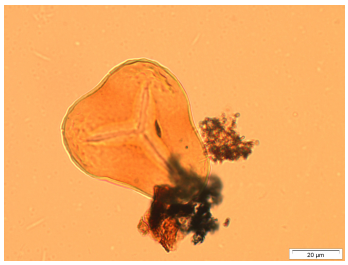
- Very poor sample, but clean
- Organic matter is very degraded, unidentified are a lot
- Chorate dinocysts
- Some algae



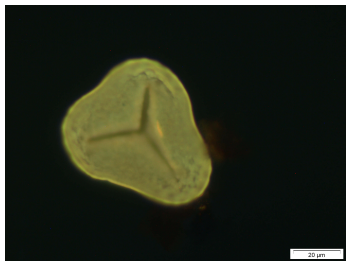
Spore



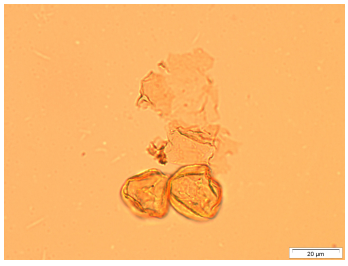
Spore (UV fluorescence)



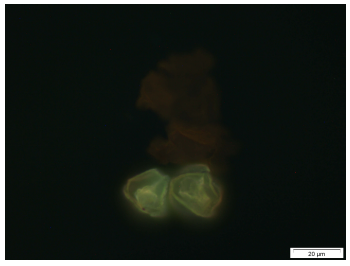
Spore



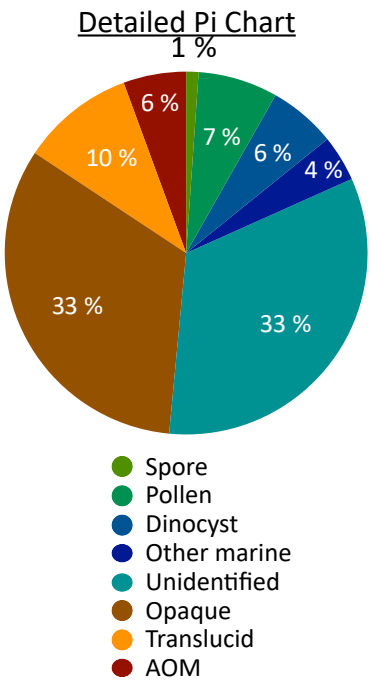
Spore (UV fluorescence)



Armored dinocyst; pollen



Armored dinocyst; pollen (UV fluorescence)



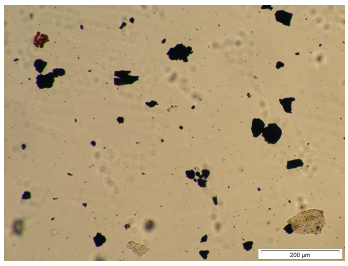
Appendix 5.20 Palynology including palynofacies analysis — P114.1

- **Height:** from the base of the sequence
- **Counts:** 250 particles were counted per sample (in %)
- **Pie Chart:** is based on each organic residue abundance

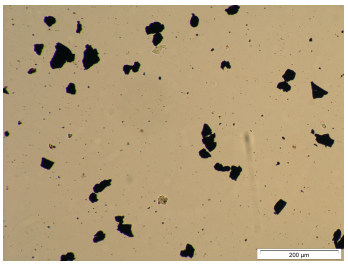
Layer n°	Height (m)	Sample code	Palynomorphe					Phytoclast		AOM
			Spore	Pollen	Dinocyst	Other marine	Unidentified	Opaque	Translucid	
114	110.4	**P114.1**	0,4	0,7	0,0	0,0	5,4	74,6	13,8	5,1
		Total %			6,5			88,4		5,1

Extra note:

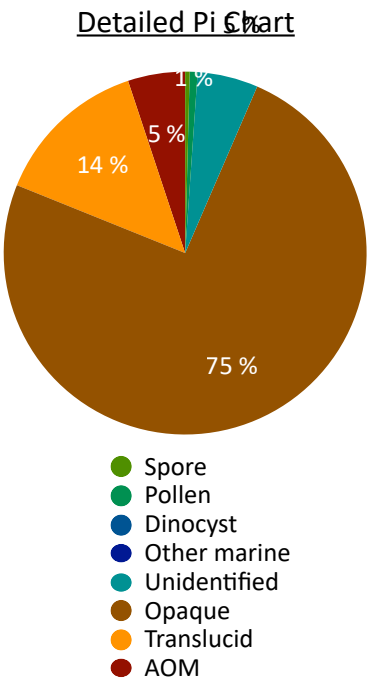
- A lot of phytoclasts, opaque one can be big while translucids are much more smaller
- Some AOM show no fluorescence
- Unidentified: membrane
- Some algal tissues

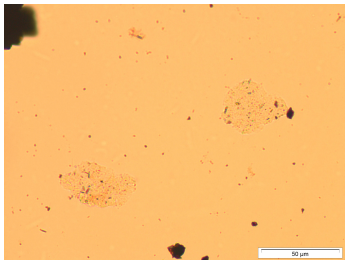


Overview

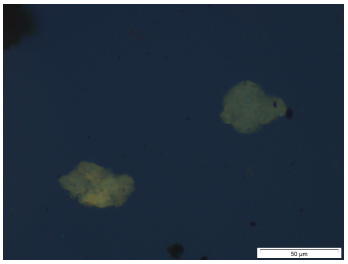


Overview

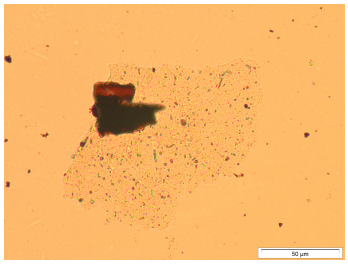




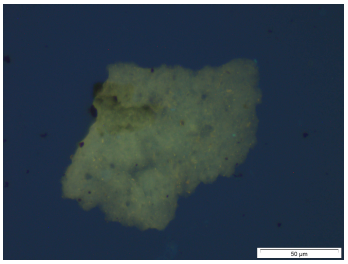
Membrane



Membrane (UV fluorescence)



Membrane



Membrane (UV fluorescence)

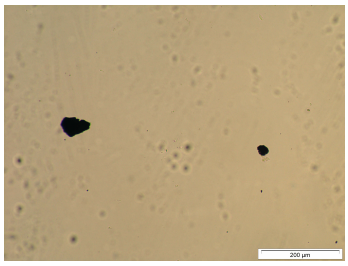
Appendix 5.21 Palynology including palynofacies analysis — P120.1

- **Height:** from the base of the sequence
- **Counts:** 250 particles were counted per sample (in %)
- **Pie Chart:** is based on each organic residue abundance

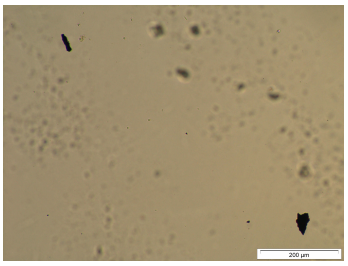
Layer n°	Height (m)	Sample code	Palynomorphe					Phytoclast		AOM
			Spore	Pollen	Dinocyst	Other marine	Unidentified	Opaque	Translucid	
118	112.35	**P120.1**	0,0	1,0	1,0	0,0	4,0	84,1	10,0	0,0
		Total %			6,0			94,1		0,0

Extra note:

- Very poor sample

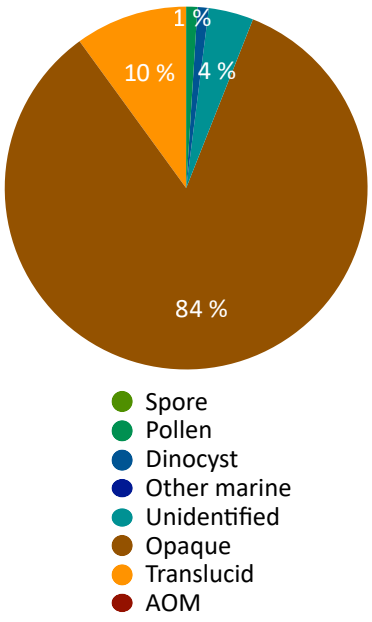


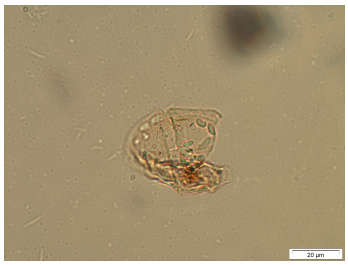
Overview



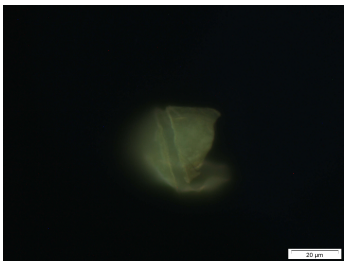
Overview

Detailed Pie Chart





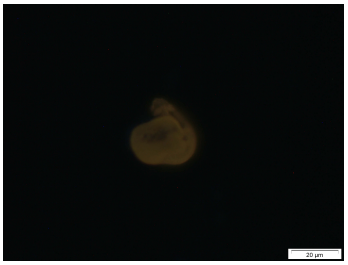
Armored dinocyst



Armored dinocyst (UV fluorescence)



Unidentified



Unidentified (UV fluorescence)

Appendix 5.22 Palynology including palynofacies analysis — P124.1

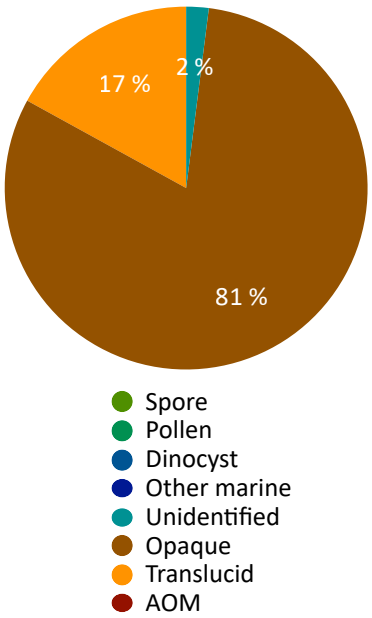
- **Height:** from the base of the sequence
- **Counts:** 250 particles were counted per sample (in %)
- **Pie Chart:** is based on each organic residue abundance

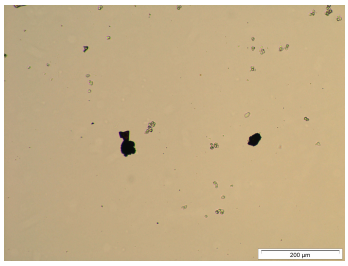
Layer n°	Height (m)	Sample code	Palynomorphe					Phytoclast		AOM
			Spore	Pollen	Dinocyst	Other marine	Unidentified	Opaque	Translucid	
124	124.6	**P124.1**	0,0	0,0	0,0	0,0	2,0	81,1	17,0	0,0
		Total %			2,0			98,1		0,0

Extra note:

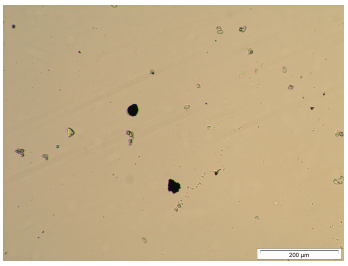
- Very poor sample

Detailed Pi Chart

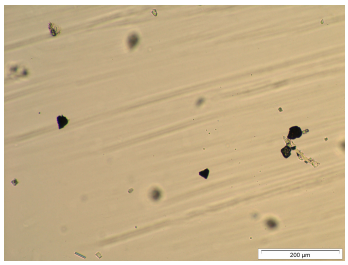




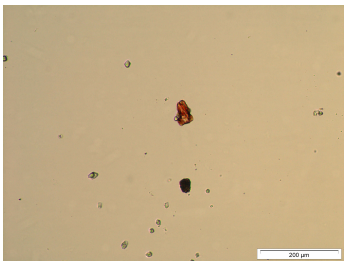
Opaque phytoclasts



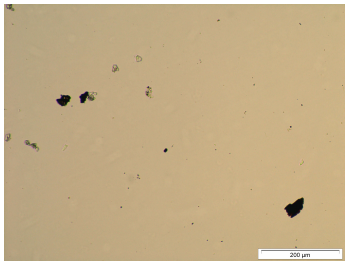
Opaque phytoclasts



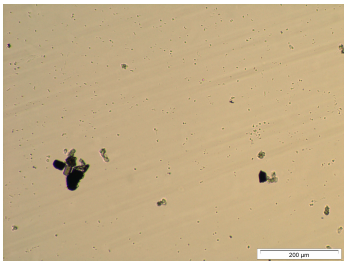
Opaque phytoclasts



Phytoclasts opaque and translucid



Opaque phytoclasts



Opaque phytoclasts

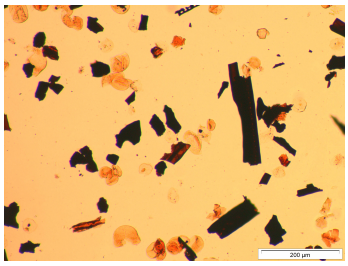
Appendix 5.23 Palynology including palynofacies analysis — P126.1

- **Height:** from the base of the sequence
- **Counts:** 250 particles were counted per sample (in %)
- **Pie Chart:** is based on each organic residue abundance

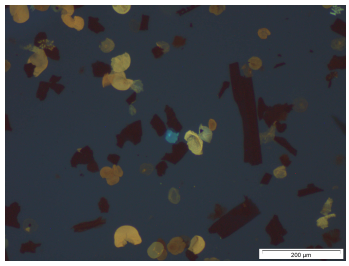
Layer n°	Height (m)	Sample code	Palynomorphe					Phytoclast		AOM
			Spore	Pollen	Dinocyst	Other marine	Unidentified	Opaque	Translucid	
126	126.4	**P126.1**	0,4	10,4	22,6	0,4	18,8	26,5	17,3	3,8
		Total %			52,6			43,8		3,8

Extra note:

- Good sample
- Chorate dinocysts
- Foraminifer innerlinings

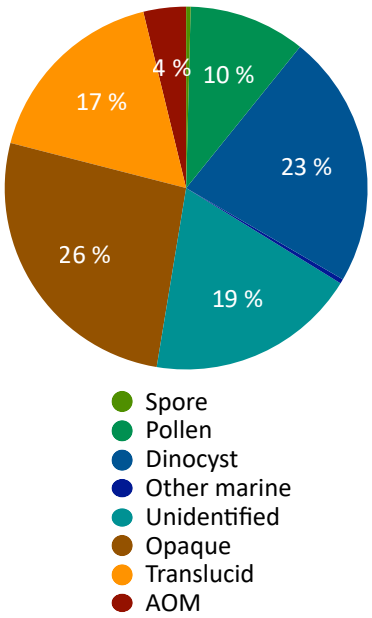


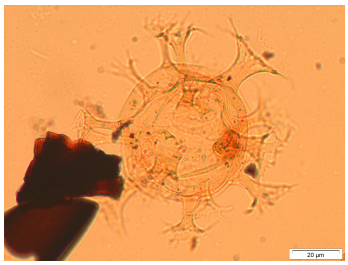
Overview



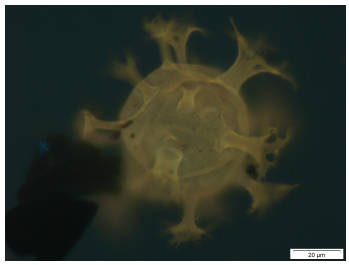
Overview (UV fluorescence)

Detailed Pi Chart





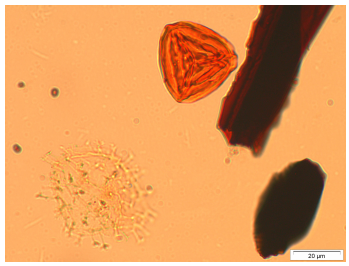
Chorate dinocyst; translucid phytoclast



Chorate dinocyst; translucid phytoclast (UV fluorescence)



Spore



Spore; chorate dinocyst; translucid phytoclasts

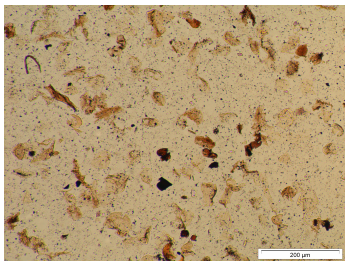
Appendix 5.24 Palynology including palynofacies analysis — P130.1

- **Height:** from the base of the sequence
- **Counts:** 250 particles were counted per sample (in %)
- **Pie Chart:** is based on each organic residue abundance

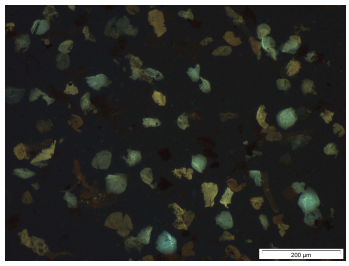
Layer n°	Height (m)	Sample code	Palynomorphe					Phytoclast		AOM
			Spore	Pollen	Dinocyst	Other marine	Unidentified	Opaque	Translucid	
130	127.85	**P130.1**	0,0	8,5	28,7	0,4	28,0	12,0	14,0	8,5
		Total %			65,6			26,0		8,5

Extra note:

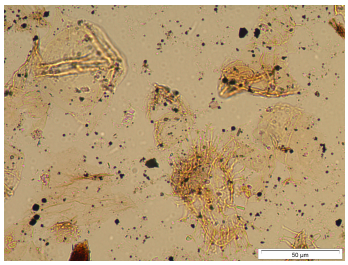
- Abundant sample
- Well preserved dinocysts
- Chorate dinocysts
- Foraminifer innerlinings



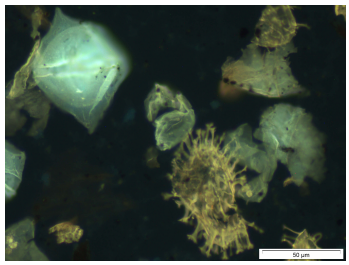
Overview



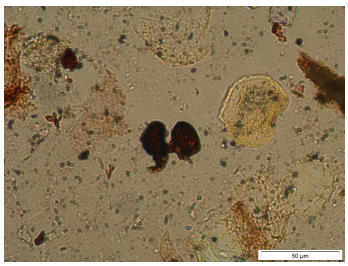
Overview (UV fluorescence)



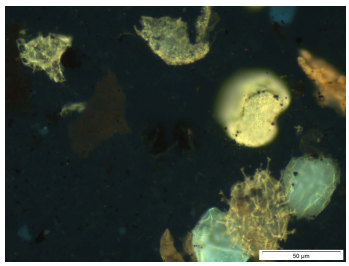
Dinocysts



Dinocysts (UV fluorescence)

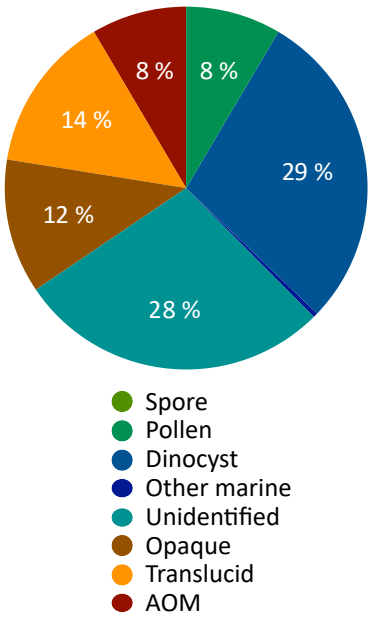


Dinocysts; foraminifer innerlinings



Dinocysts; foraminifer innerlinings (UV fluorescence)

Detailed Pi Chart



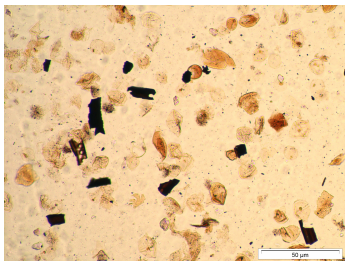
Appendix 5.25 Palynology including palynofacies analysis — P134.1

- **Height:** from the base of the sequence
- **Counts:** 250 particles were counted per sample (in %)
- **Pie Chart:** is based on each organic residue abundance

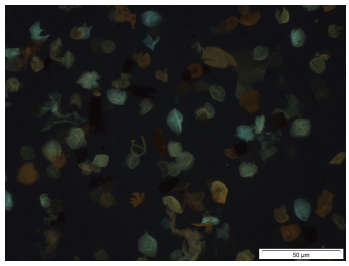
Layer n°	Height (m)	Sample code	Palynomorphe					Phytoclast		AOM
			Spore	Pollen	Dinocyst	Other marine	Unidentified	Opaque	Translucid	
134	132.05	**P134.1**	0,8	9,4	35,2	0,0	26,2	14,3	9,7	4,5
		Total %			71,6			24,0		4,5

Extra note:

- Abundant sample
- Well preserved dinocysts
- Chorate dinocysts



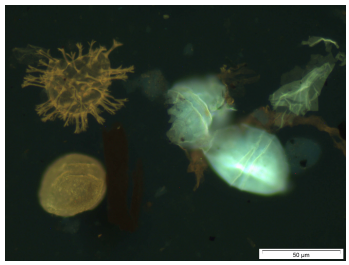
Overview



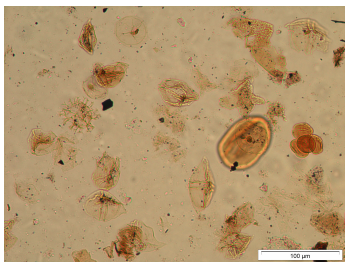
Overview (UV fluorescence)



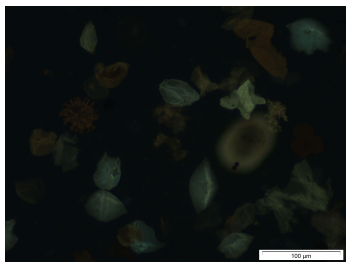
Overview



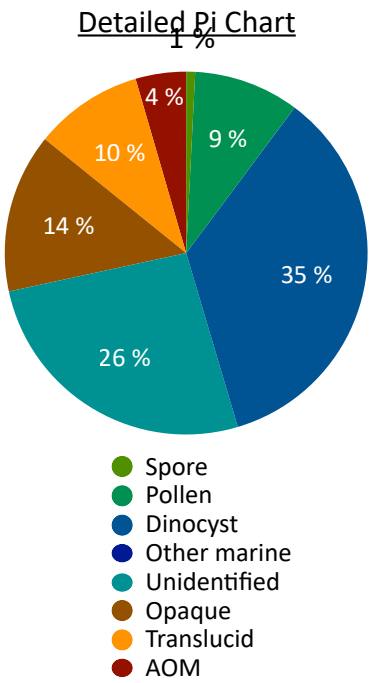
Overview (UV fluorescence)



Overview



Overview (UV fluorescence)



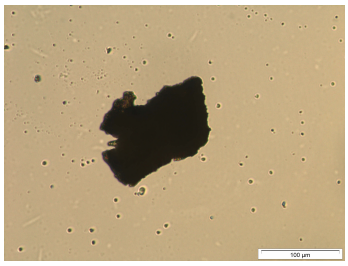
Appendix 5.26 Palynology including palynofacies analysis — P138.1

- **Height:** from the base of the sequence
- **Counts:** 250 particles were counted per sample (in %)
- **Pie Chart:** is based on each organic residue abundance

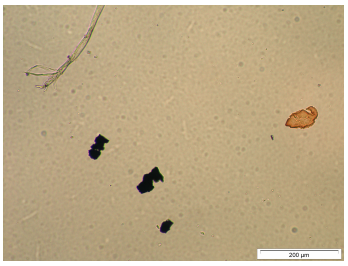
Layer n°	Height (m)	Sample code	Palynomorphe					Phytoclast		AOM
			Spore	Pollen	Dinocyst	Other marine	Unidentified	Opaque	Translucid	
138	138.25	**P138.1**	0,0	0,0	0,0	0,0	3,0	86,1	6,0	5,0
		Total %			3,0			92,1		5,0

Extra note:

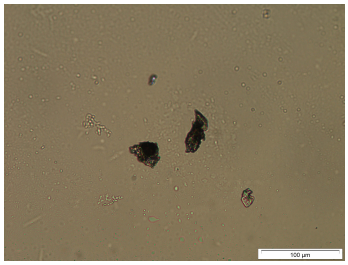
- Almost barren sample



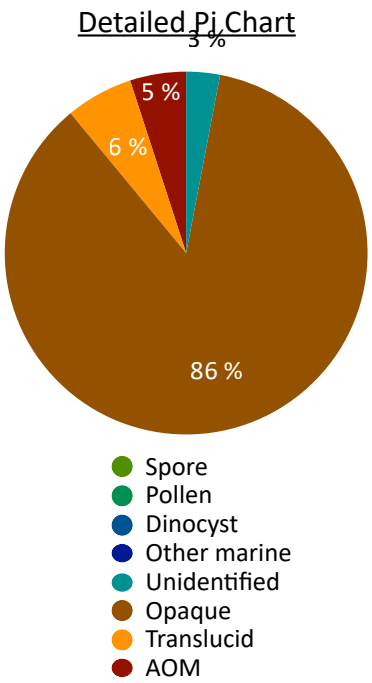
Opaque phytoclast



Phytoclasts opaque and translucid



Opaque phytoclasts



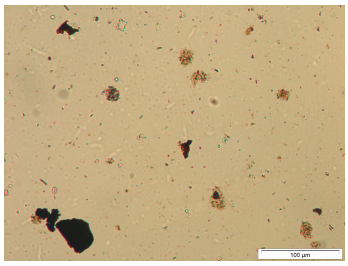
Appendix 5.27 Palynology including palynofacies analysis — P140.1

- **Height:** from the base of the sequence
- **Counts:** 250 particles were counted per sample (in %)
- **Pie Chart:** is based on each organic residue abundance

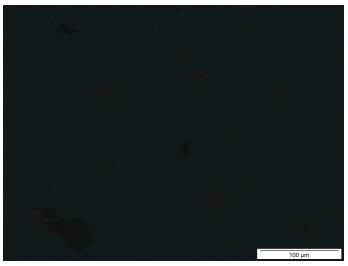
Layer n°	Height (m)	Sample code	Palynomorphe					Phytoclast		AOM
			Spore	Pollen	Dinocyst	Other marine	Unidentified	Opaque	Translucid	
140	140.25	**P140.1**	0,0	0,0	0,0	0,0	1,6	29,5	9,3	59,7
		Total %			1,6			38,8		59,7

Extra note:

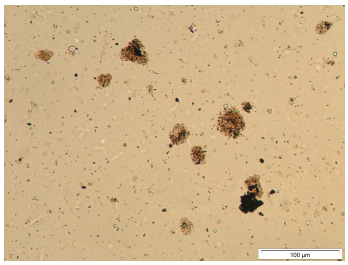
- Poor sample



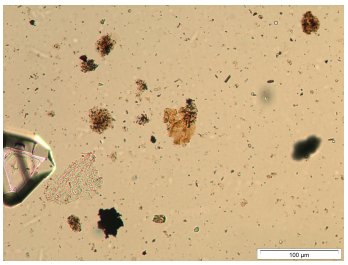
Overview



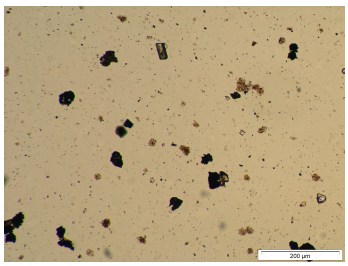
Overview (UV fluorescence)



Opaque phytoclasts; AOM

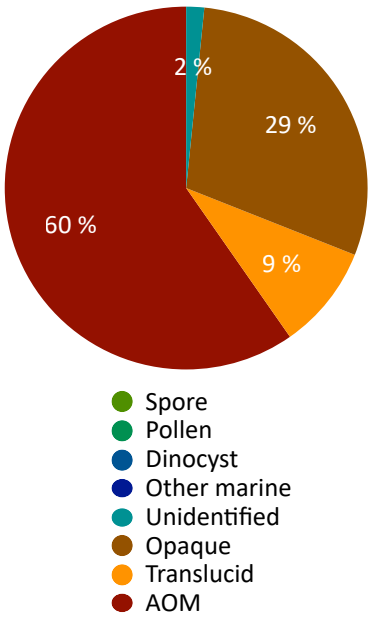


Opaque phytoclasts; AOM



Opaque phytoclasts; AOM

Detailed Pi Chart



Appendix 5.28 Palynology including palynofacies analysis — P153.1

- **Height:** from the base of the sequence
- **Counts:** 250 particles were counted per sample (in %)
- **Pie Chart:** is based on each organic residue abundance

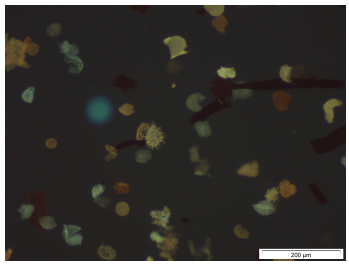
Layer n°	Height (m)	Sample code	Palynomorphe					Phytoclast		AOM
			Spore	Pollen	Dinocyst	Other marine	Unidentified	Opaque	Translucid	
143	143.7	**P153.1**	0,8	11,8	33,0	1,8	18,5	25,2	6,3	2,6
		Total %			65,9			31,5		2,6

Extra note:

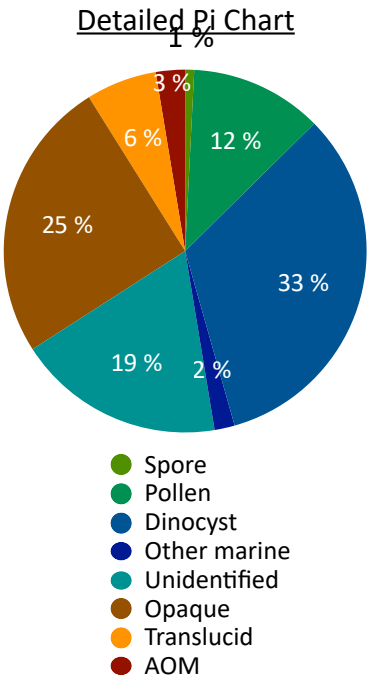
- Abundant sample
- Well preserved palynomorphs
- Chorate dinocysts

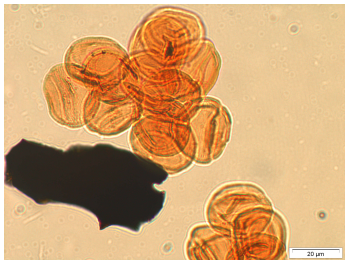


Overview

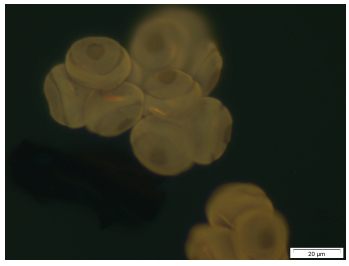


Overview (UV fluorescence)

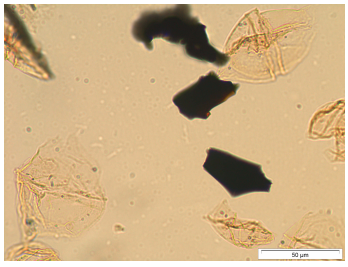




Classopolis pollen; opaque phytoclast



Classopolis pollen; opaque phytoclast (UV fluorescence)



Dinocysts; phytoclasts



Spore

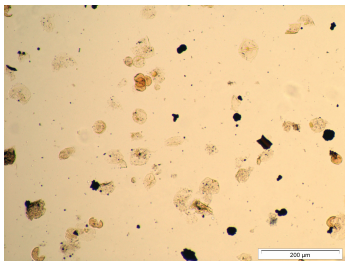
Appendix 5.29 Palynology including palynofacies analysis — P155.1

- **Height:** from the base of the sequence
- **Counts:** 250 particles were counted per sample (in %)
- **Pie Chart:** is based on each organic residue abundance

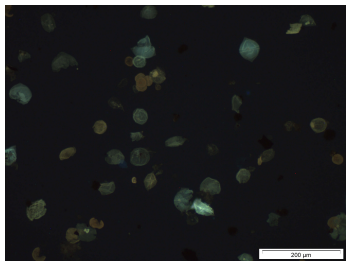
Layer n°	Height (m)	Sample code	Palynomorphe					Phytoclast		AOM
			Spore	Pollen	Dinocyst	Other marine	Unidentified	Opaque	Translucid	
145	147.1	**P155.1**	0,4	16,0	36,7	1,6	24,2	10,2	3,9	7,0
		Total %			78,9			14,1		7,0

Extra note:

- Abundant sample
- A lot of dinocysts
- Some algae
- A lot of pyrite in the sample and in the palynomorphs

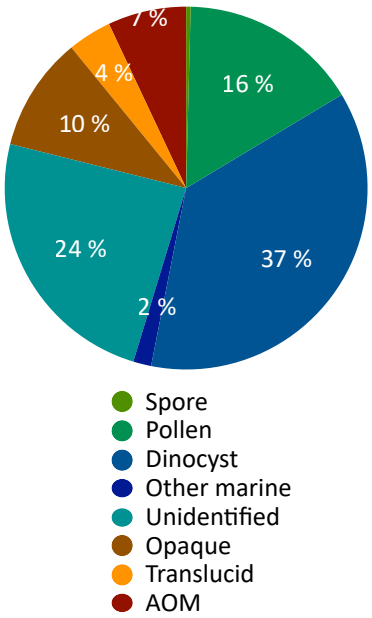


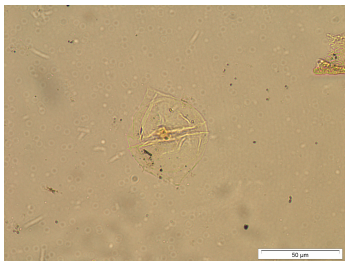
Overview



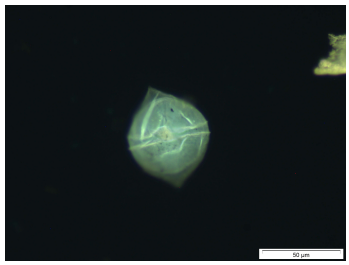
Overview (UV fluorescence)

Detailed Pi Chart

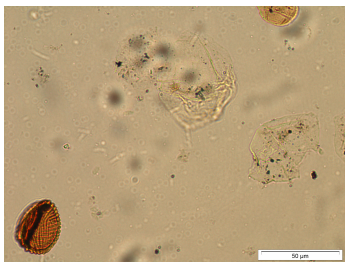




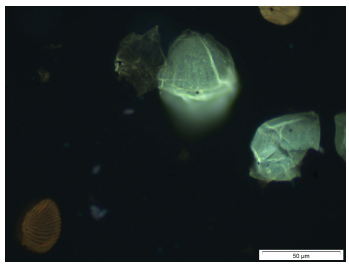
Dinocyst



Dinocyst (UV fluorescence)



Dinocysts; pollen



Dinocysts; pollen (UV fluorescence)

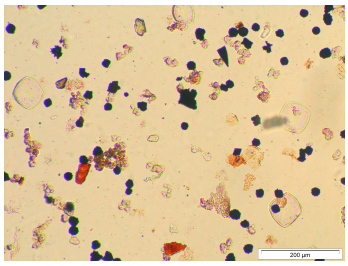
Appendix 5.30 Palynology including palynofacies analysis — P158.1

- **Height:** from the base of the sequence
- **Counts:** 250 particles were counted per sample (in %)
- **Pie Chart:** is based on each organic residue abundance

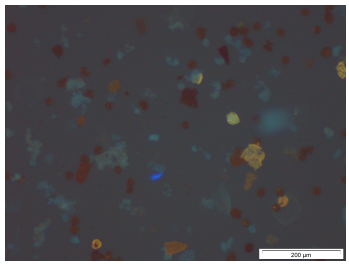
Layer n°	Height (m)	Sample code	Palynomorphe					Phytoclast		AOM
			Spore	Pollen	Dinocyst	Other marine	Unidentified	Opaque	Translucid	
148	149	**P158.1**	0,8	17,5	16,4	2,0	20,7	13,3	17,1	12,4
		Total %			57,4			30,4		12,4

Extra note:

- A lot of pyrite minerals
- Dinocyst (only saw one chorate dinocyst)
- Foraminifer innerlining

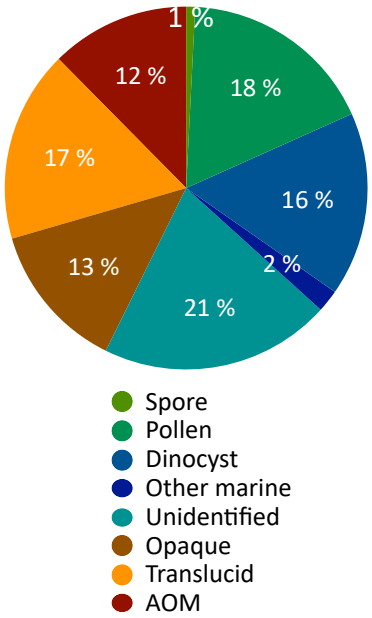


Overview



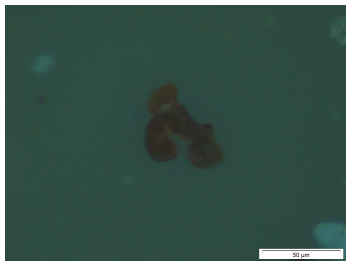
Overview (UV fluorescence)

Detailed Pi Chart

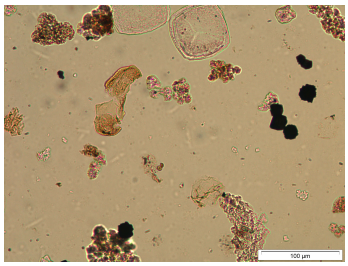




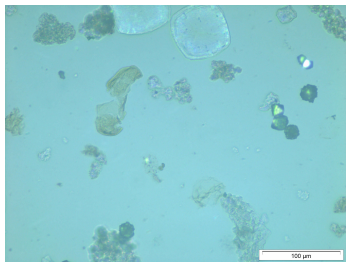
Foraminifer innerlinings



Foraminifer innerlinings (UV fluorescence)



Overview



Overview (LPNA: polarised light)

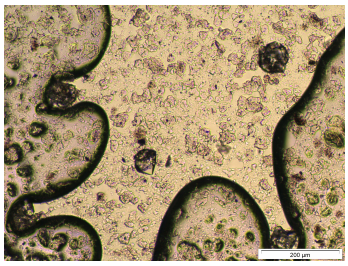
Appendix 5.31 Palynology including palynofacies analysis — P152.1

- **Height:** from the base of the sequence
- **Counts:** 250 particles were counted per sample (in %)
- **Pie Chart:** is based on each organic residue abundance

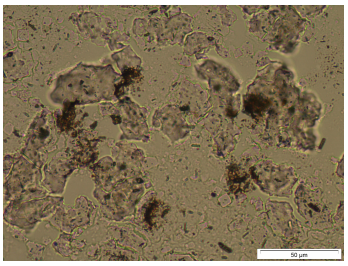
Layer n°	Height (m)	Sample code	Palynomorphe					Phytoclast		AOM
			Spore	Pollen	Dinocyst	Other marine	Unidentified	Opaque	Translucid	
152	152.4	**P152.1**	0,0	0,0	0,0	0,0	1,0	22,0	6,0	71,1
		Total %			1,0			28,0		71,1

Extra note:

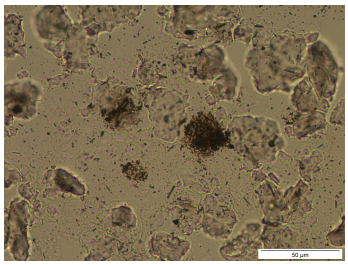
- Not clean sample (clay and other minerals)



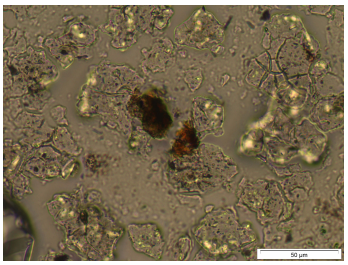
Overview



Overview

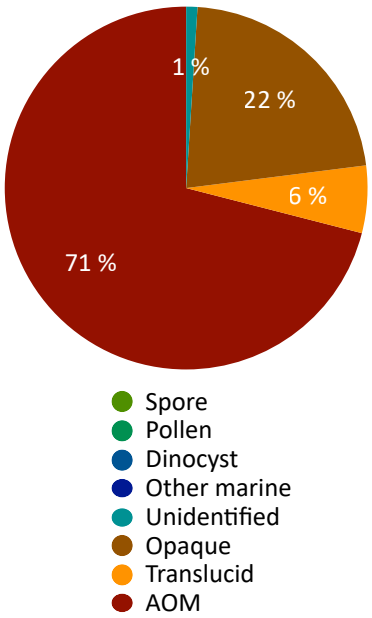


Overview



Overview

Detailed Pi Chart



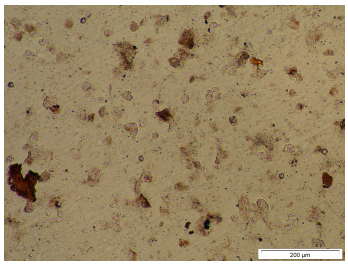
Appendix 5.32 Palynology including palynofacies analysis — P152.2

- **Height:** from the base of the sequence
- **Counts:** 250 particles were counted per sample (in %)
- **Pie Chart:** is based on each organic residue abundance

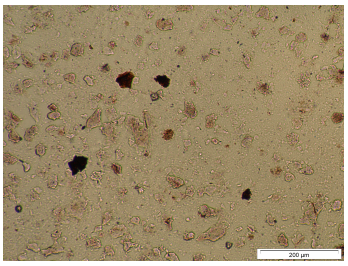
Layer n°	Height (m)	Sample code	Palynomorphe					Phytoclast		AOM
			Spore	Pollen	Dinocyst	Other marine	Unidentified	Opaque	Translucid	
152	152.9	**P152.2**	0,0	0,0	0,0	0,0	1,0	17,5	19,4	62,2
		Total %			1,0			36,9		62,2

Extra note:

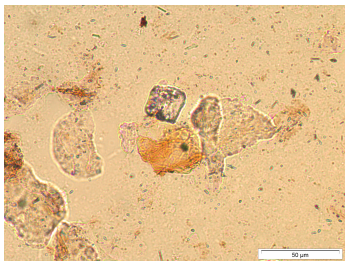
- Poor sample



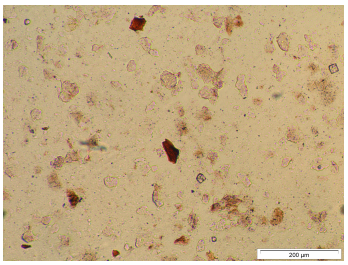
Overview



Overview

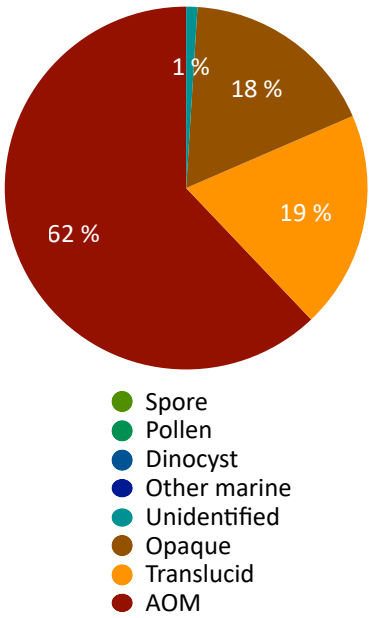


Overview



Overview

Detailed Pi Chart

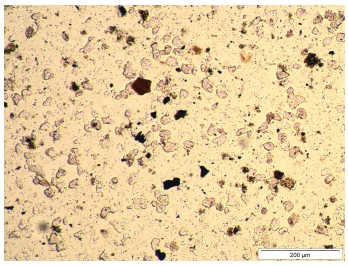


Appendix 5.33 Palynology including palynofacies analysis — P154.1

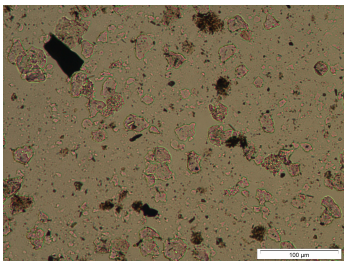
- **Height:** from the base of the sequence
- **Counts:** 250 particles were counted per sample (in %)
- **Pie Chart:** is based on each organic residue abundance

Layer n°	Height (m)	Sample code	Palynomorphe					Phytoclast		AOM
			Spore	Pollen	Dinocyst	Other marine	Unidentified	Opaque	Translucid	
154	154	**P154.1**	0,0	0,0	0,0	0,0	0,0	28,9	21,2	50,0
		Total %			0,0			50,1		50,0

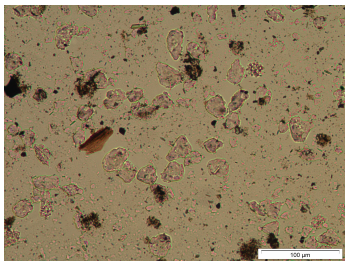
Extra note:



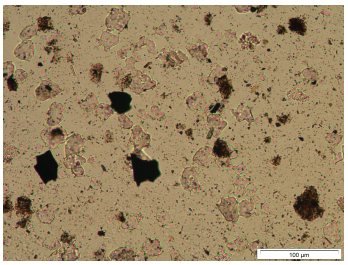
Overview



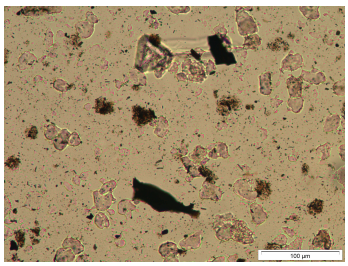
Overview



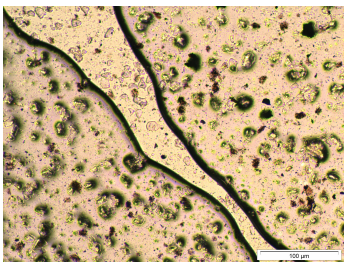
Overview



Overview

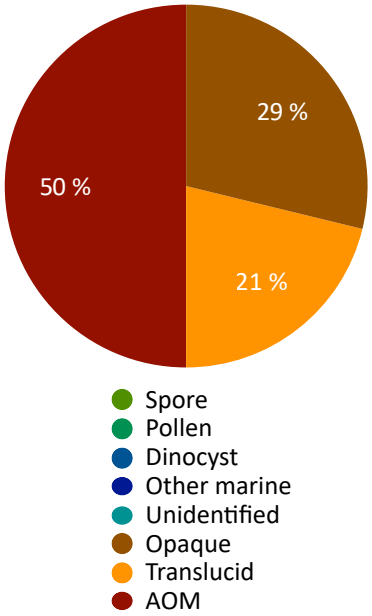


Overview



Overview

Detailed Pi Chart



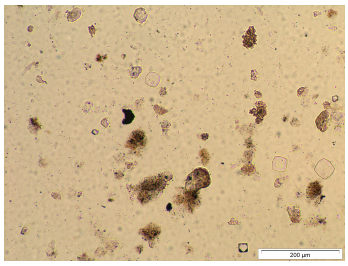
Appendix 5.34 Palynology including palynofacies analysis — P166.1

- **Height:** from the base of the sequence
- **Counts:** 250 particles were counted per sample (in %)
- **Pie Chart:** is based on each organic residue abundance

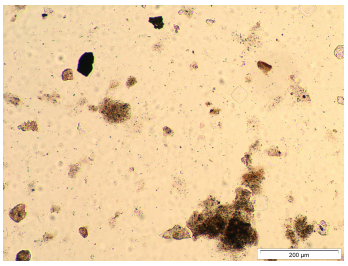
Layer n°	Height (m)	Sample code	Palynomorphe					Phytoclast		AOM
			Spore	Pollen	Dinocyst	Other marine	Unidentified	Opaque	Translucid	
156	155.9	**P166.1**	0,0	0,0	0,0	0,0	0,0	22,0	9,0	69,1
		Total %			0,0			31,0		69,1

Extra note:

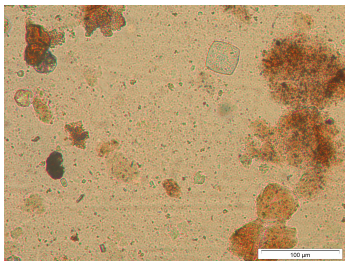
- Some AOM show no fluorescence
- Some AOM are large particles
- Few phytoclasts



Overview

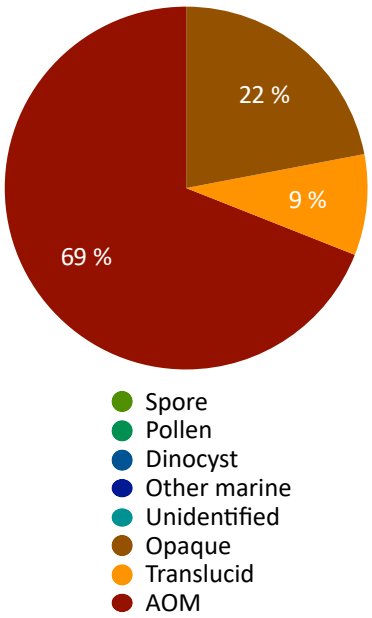


Overview



Overview

Detailed Pi Chart



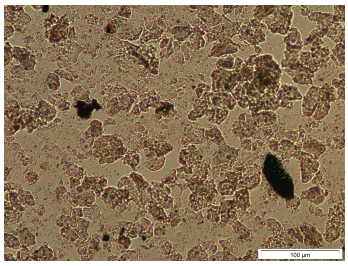
Appendix 5.35 Palynology including palynofacies analysis — P168.1

- **Height:** from the base of the sequence
- **Counts:** 250 particles were counted per sample (in %)
- **Pie Chart:** is based on each organic residue abundance

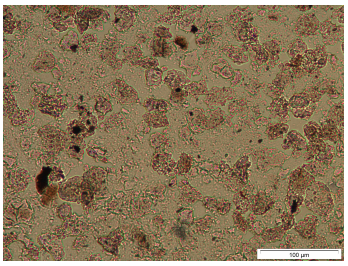
Layer n°	Height (m)	Sample code	Palynomorphe					Phytoclast		AOM
			Spore	Pollen	Dinocyst	Other marine	Unidentified	Opaque	Translucid	
158	157.1	**P168.1**	0,0	0,0	0,0	0,0	0,0	70,1	30,0	0,0
		Total %			0,0			100,1		0,0

Extra note:

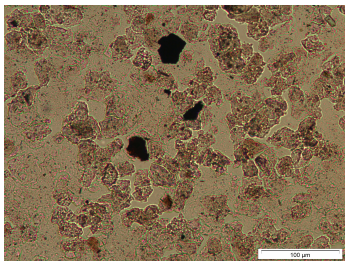
- Not clean sample



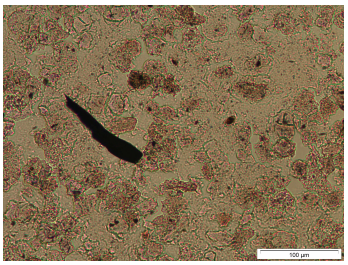
Overview



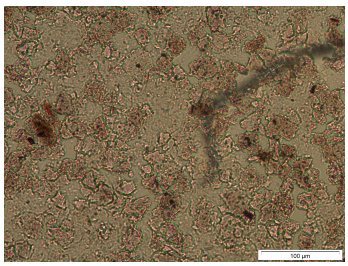
Overview



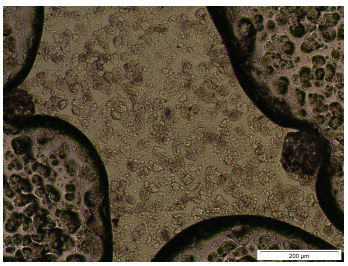
Overview



Overview

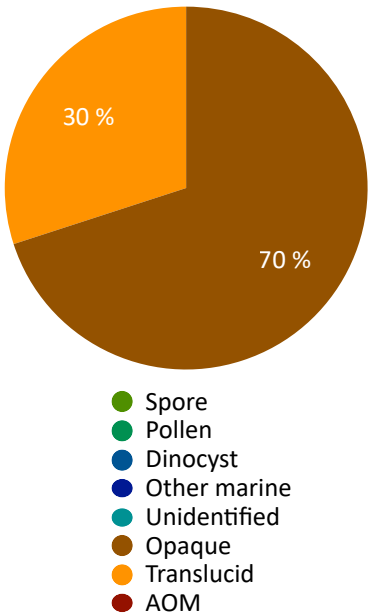


Overview



Overview

Detailed Pi Chart



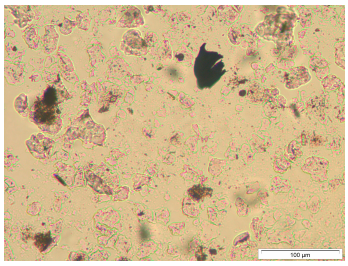
Appendix 5.36 Palynology including palynofacies analysis — P160.1

- **Height:** from the base of the sequence
- **Counts:** 250 particles were counted per sample (in %)
- **Pie Chart:** is based on each organic residue abundance

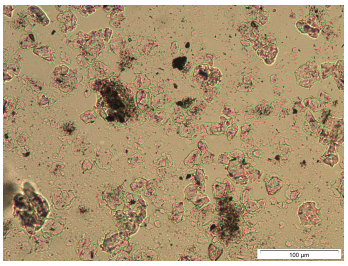
Layer n°	Height (m)	Sample code	Palynomorphe					Phytoclast		AOM
			Spore	Pollen	Dinocyst	Other marine	Unidentified	Opaque	Translucid	
160	159.9	**P160.1**	0,0	0,0	0,0	0,0	0,0	96,1	4,0	0,0
		Total %			0,0			100,1		0,0

Extra note:

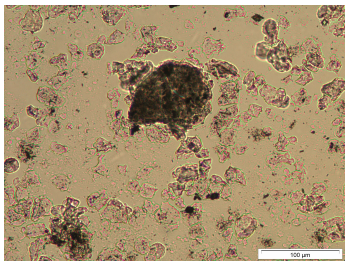
- Almost barren sample
- Not clean at all



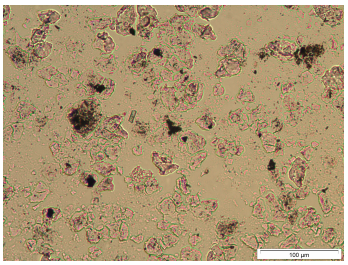
Overview



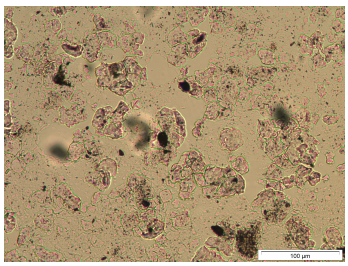
Overview



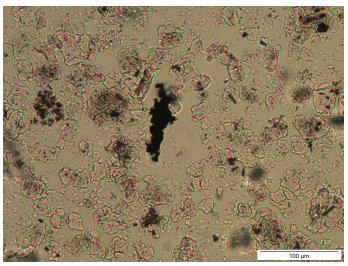
Overview



Overview

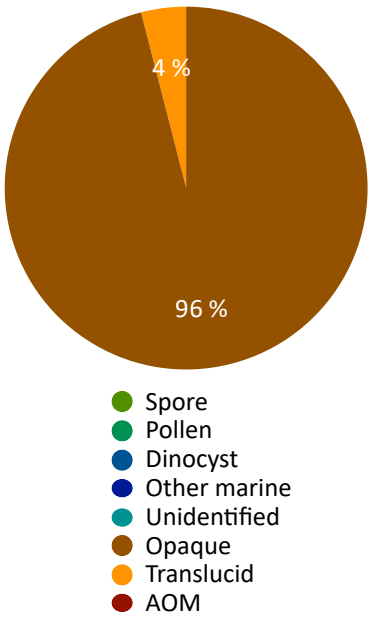


Overview



Overview

Detailed Pi Chart



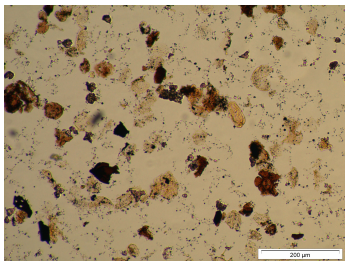
Appendix 5.37 Palynology including palynofacies analysis — P162.1

- **Height:** from the base of the sequence
- **Counts:** 250 particles were counted per sample (in %)
- **Pie Chart:** is based on each organic residue abundance

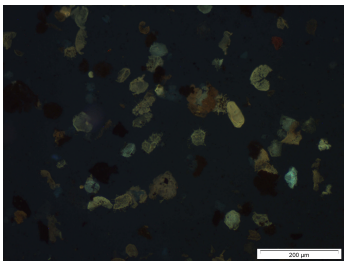
Layer n°	Height (m)	Sample code	Palynomorphe					Phytoclast		AOM
			Spore	Pollen	Dinocyst	Other marine	Unidentified	Opaque	Translucid	
162	161.3	**P162.1**	0,4	10,0	31,1	4,6	22,6	11,5	15,0	5,0
		Total %			68,7			26,5		5,0

Extra note:

- Abundant sample
- Foraminifer innerlinings

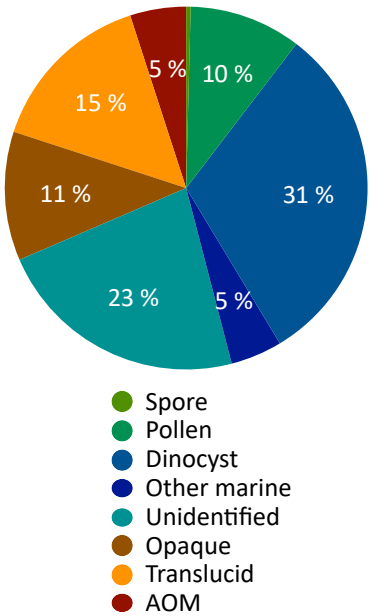


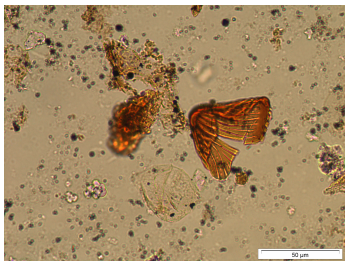
Overview



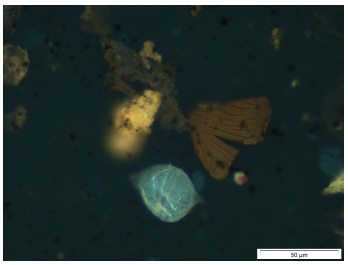
Overview (UV fluorescence)

Detailed Pi Chart

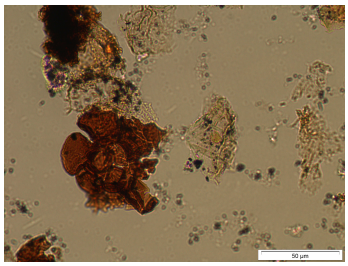




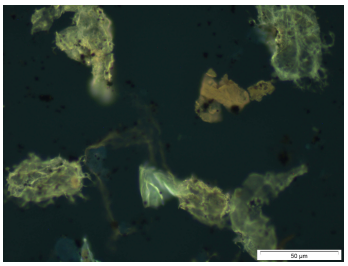
Spore; dinocyst; other



Spore; dinocyst; other (UV fluorescence)



Foraminifer innerlining; chorate dinocysts



Foraminifer innerlinings; chorate dinocysts (UV fluorescence)

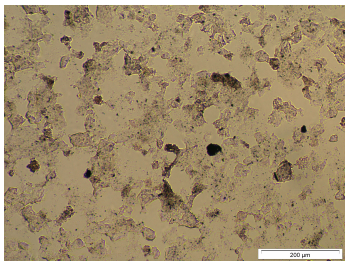
Appendix 5.38 Palynology including palynofacies analysis — P164.1

- **Height:** from the base of the sequence
- **Counts:** 250 particles were counted per sample (in %)
- **Pie Chart:** is based on each organic residue abundance

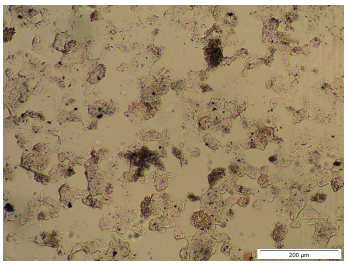
Layer n°	Height (m)	Sample code	Palynomorphe					Phytoclast		AOM
			Spore	Pollen	Dinocyst	Other marine	Unidentified	Opaque	Translucid	
164	162.4	**P164.1**	0,0	0,0	0,0	0,0	0,0	92,1	8,0	0,0
		Total %			0,0			100,1		0,0

Extra note:

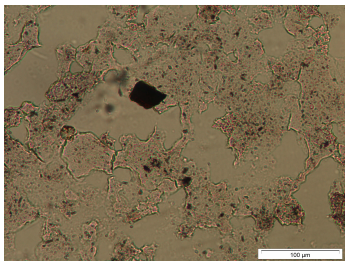
- Not clean sample



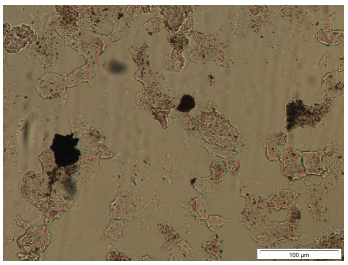
Overview



Overview

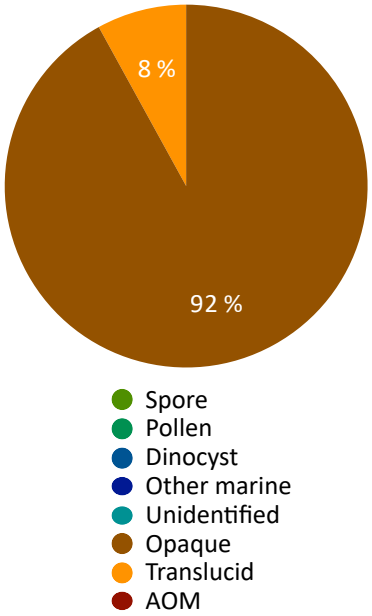


Overview



Overview

Detailed Pi Chart

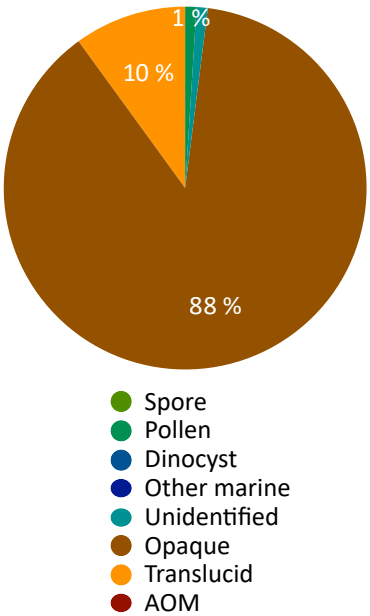


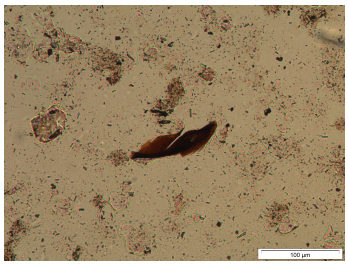
Appendix 5.39 Palynology including palynofacies analysis — P173.1

- **Height:** from the base of the sequence
- **Counts:** 250 particles were counted per sample (in %)
- **Pie Chart:** is based on each organic residue abundance

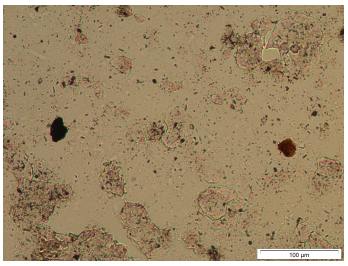
Layer n°	Height (m)	Sample code	Palynomorphe					Phytoclast		AOM
			Spore	Pollen	Dinocyst	Other marine	Unidentified	Opaque	Translucid	
171	168.6	**P173.1**	0,0	1,0	0,0	0,0	1,0	88,1	10,0	0,0
		Total %			2,0			98,1		0,0

Extra note:

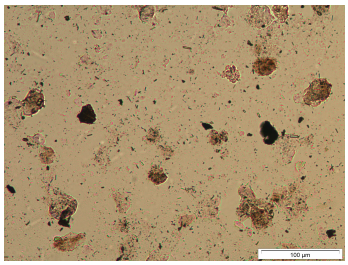




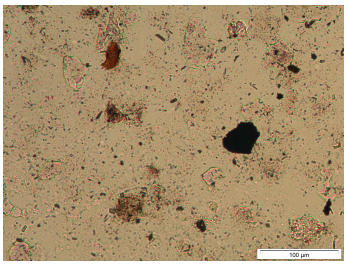
Overview



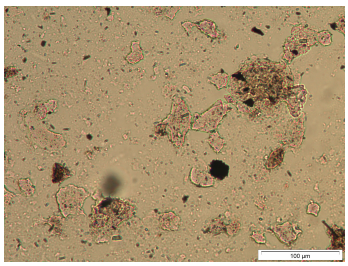
Overview



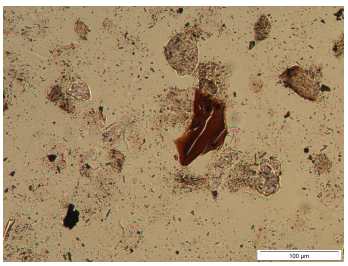
Overview



Overview



Overview



Overview

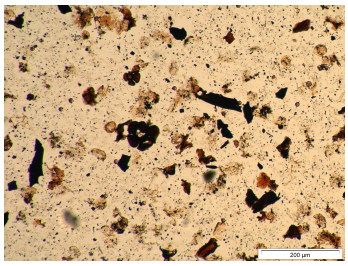
Appendix 5.40 Palynology including palynofacies analysis — P173.2

- **Height:** from the base of the sequence
- **Counts:** 250 particles were counted per sample (in %)
- **Pie Chart:** is based on each organic residue abundance

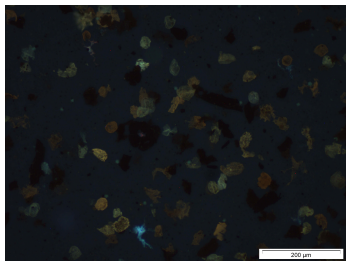
Layer n°	Height (m)	Sample code	Palynomorphe					Phytoclast		AOM
			Spore	Pollen	Dinocyst	Other marine	Unidentified	Opaque	Translucid	
172	170.3	**P173.2**	0,6	12,3	33,3	1,9	13,5	18,9	17,66	1,9
		Total %			61,6			36,6		1,9

Extra note:

- Abundant sample
- Chorate dinocysts
- A lot of phytoclasts, all sizes and colours
- Several foraminifer innerlinings
- Few pyrite in palynomorphs

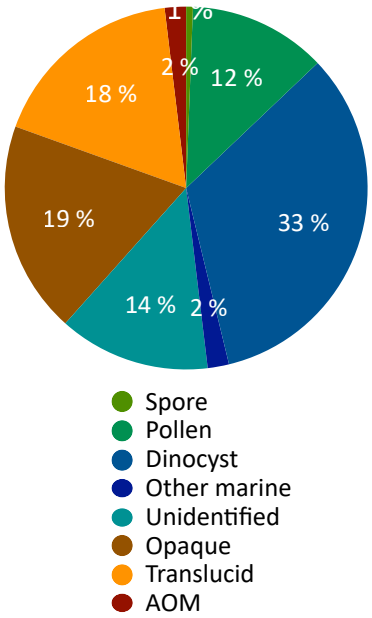


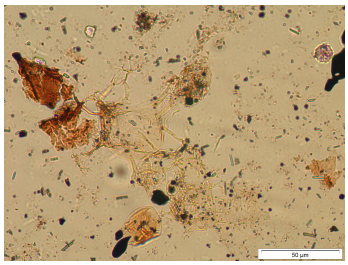
Overview



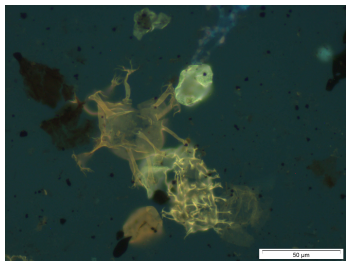
Overview (UV fluorescence)

Detailed Pi Chart

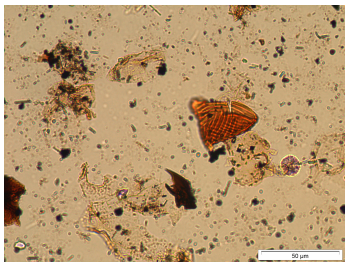




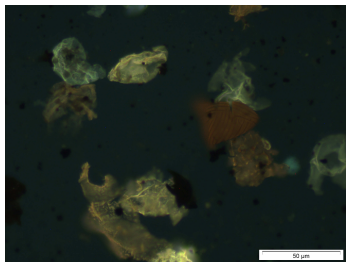
Chorate dinocysts; other



Chorate dinocysts; other (UV fluorescence)



Spore; dinocysts



Spore; dinocysts (UV fluorescence)

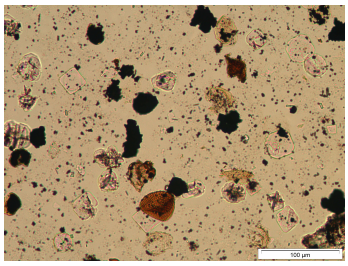
Appendix 5.41 Palynology including palynofacies analysis — P173.3

- **Height:** from the base of the sequence
- **Counts:** 250 particles were counted per sample (in %)
- **Pie Chart:** is based on each organic residue abundance

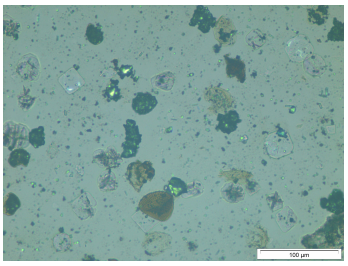
Layer n°	Height (m)	Sample code	Palynomorphe					Phytoclast		AOM
			Spore	Pollen	Dinocyst	Other marine	Unidentified	Opaque	Translucid	
173	171.2	**P173.3**	1,2	17,5	28,2	0,8	14,3	15,1	20,3	2,8
		Total %			62,0			35,4		2,8

Extra note:

- Chorate dinocysts
- A lot of phytoclasts, all sizes and colours
- Some algae
- A lot of pyrite in palynomorphs

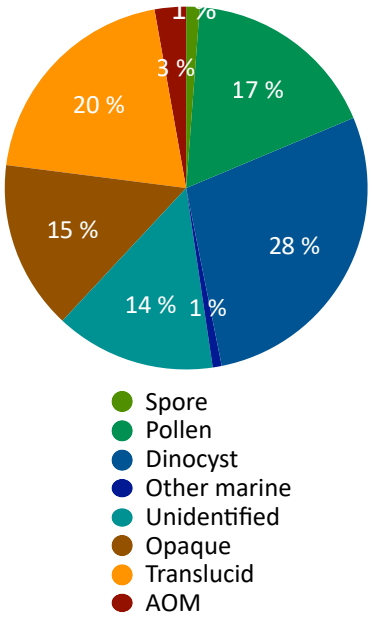


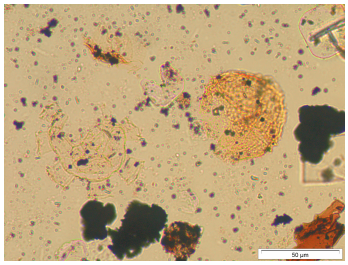
Overview



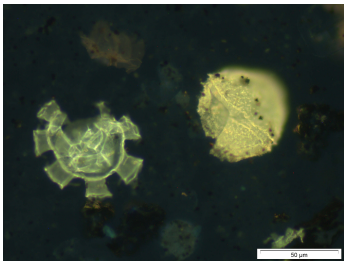
Overview (LPNA: polarised light)

Detailed Pi Chart

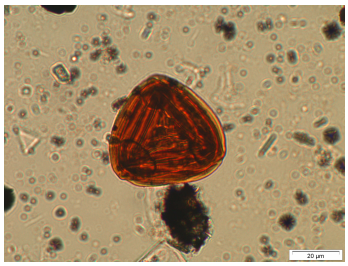




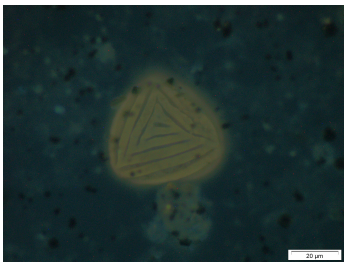
Dinocysts



Dinocysts (UV fluorescence)



Spore



Spore (UV fluorescence)

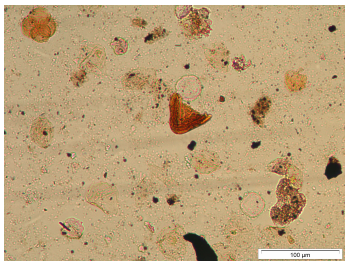
Appendix 5.42 Palynology including palynofacies analysis — P175.1

- **Height:** from the base of the sequence
- **Counts:** 250 particles were counted per sample (in %)
- **Pie Chart:** is based on each organic residue abundance

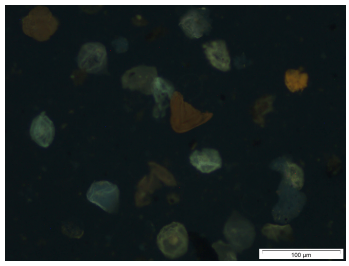
Layer n°	Height (m)	Sample code	Palynomorphe					Phytoclast		AOM
			Spore	Pollen	Dinocyst	Other marine	Unidentified	Opaque	Translucid	
175	173.4	**P175.1**	3,5	7,6	38,9	6,5	23,5	12,4	3,5	4,1
		Total %			80,0			15,9		4,1

Extra note:

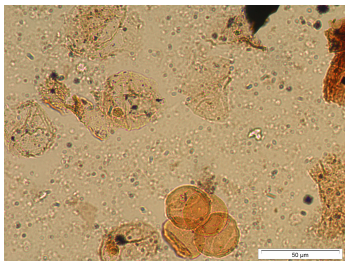
- Super abundant sample
- A lot of dinocysts
- *Classopolis* pollen
- Some algae
- Some foraminifer innerlinings



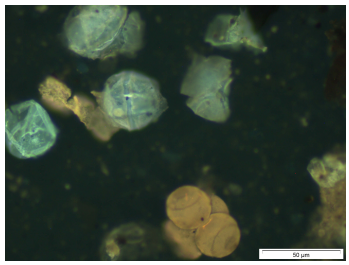
Overview



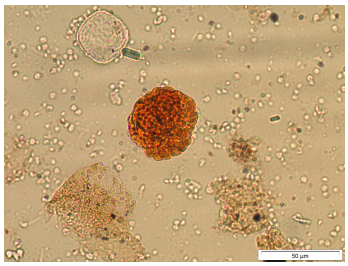
Overview (UV fluorescence)



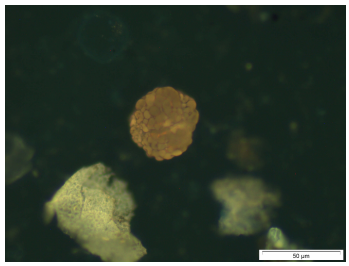
Classopolis pollen; dinocysts



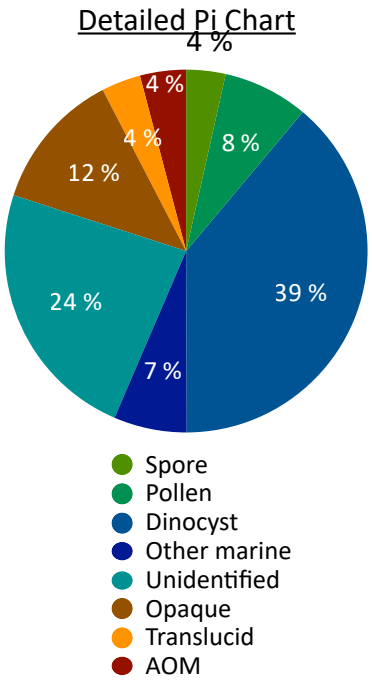
Classopolis pollen; dinocysts (UV fluorescence)



Spore; ''Mickey'' pollen membrane



Spore; ''Mickey'' pollen membrane (UV fluorescence)



Appendix 5.43 Palynology including palynofacies analysis — P175.2

- **Height:** from the base of the sequence
- **Counts:** 250 particles were counted per sample (in %)
- **Pie Chart:** is based on each organic residue abundance

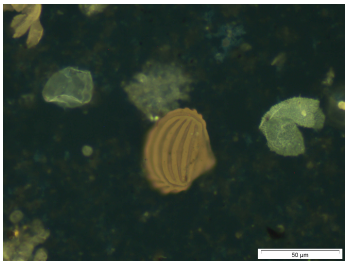
Layer n°	Height (m)	Sample code	Palynomorphe					Phytoclast		AOM
			Spore	Pollen	Dinocyst	Other marine	Unidentified	Opaque	Translucid	
175	174.4	**P175.2**	0,4	11,2	25,5	8,6	27,7	9,4	7,5	9,7
		Total %			73,4			16,9		9,7

Extra note:

- The residues are super degraded
- Some algae
- Some foraminifers innerlinings

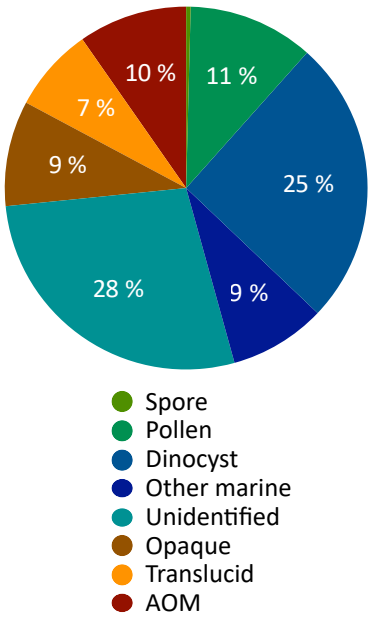


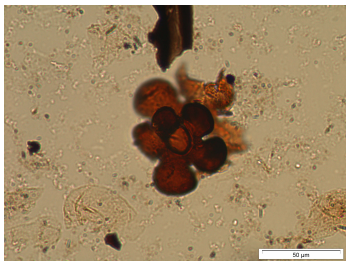
Spore; dinocysts



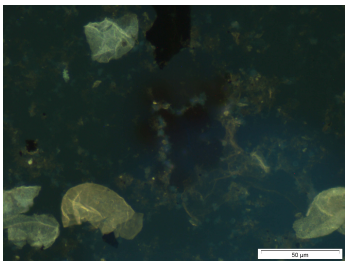
Spore; dinocysts (UV fluorescence)

Detailed Pi Chart

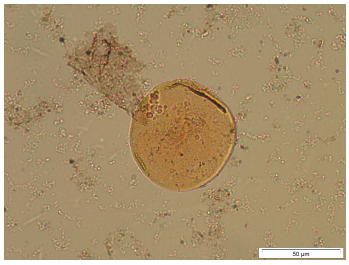




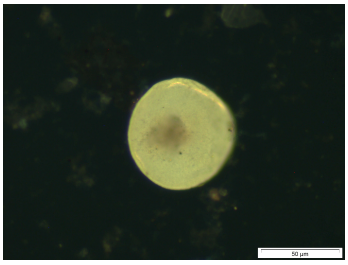
Foraminifer innerlining; dinocysts



Foraminifer innerlining; dinocysts (UV fluorescence)



Algae



Algae (UV fluorescence)

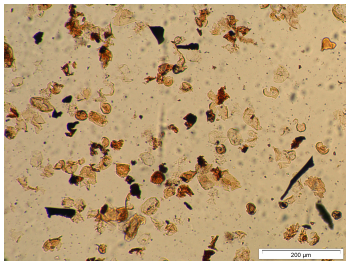
Appendix 5.44 Palynology including palynofacies analysis — P176.a

- **Height:** from the base of the sequence
- **Counts:** 250 particles were counted per sample (in %)
- **Pie Chart:** is based on each organic residue abundance

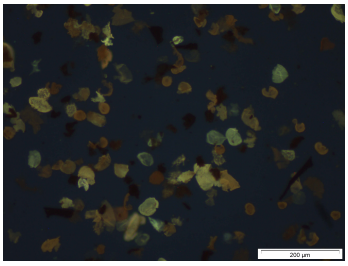
Layer n°	Height (m)	Sample code	Palynomorphe					Phytoclast		AOM
			Spore	Pollen	Dinocyst	Other marine	Unidentified	Opaque	Translucid	
176	175	**P176.a**	0,4	17,0	21,1	0,4	26,8	3,8	24,9	5,7
		Total %			65,7			28,7		5,7

Extra note:

- Abundant and clean sample
- Some pyrite in palynomorphs
- Some algae

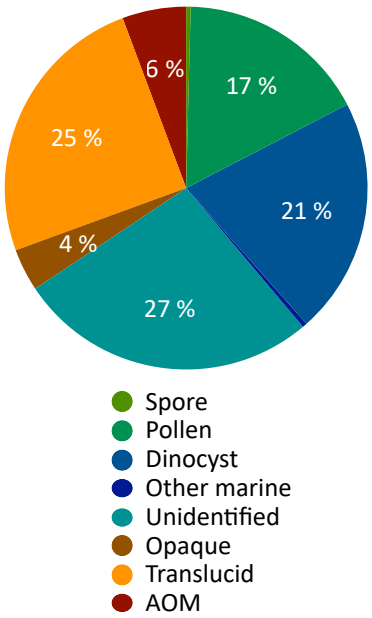


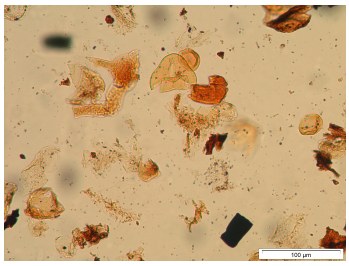
Overview



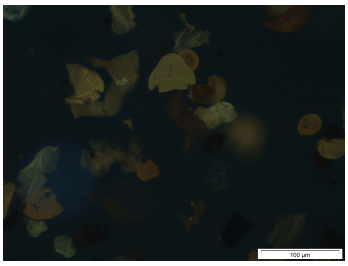
Overview (UV fluorescence)

Detailed Pi Chart

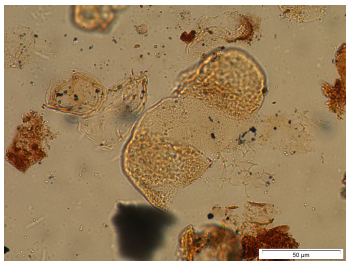




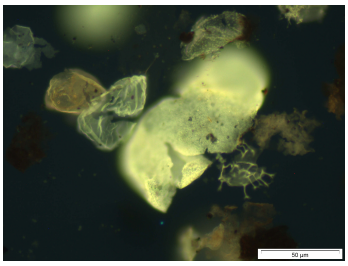
Overview



Overview (UV fluorescence)



Chorate dinocyst; pollen; other residues



Chorate dinocyst; pollen; other residues (UV fluorescence)

Appendix 5.45 Palynology including palynofacies analysis — P176.b

- **Height:** from the base of the sequence
- **Counts:** 250 particles were counted per sample (in %)
- **Pie Chart:** is based on each organic residue abundance

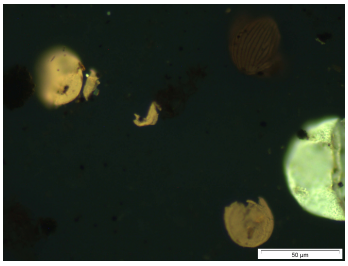
Layer n°	Height (m)	Sample code	Palynomorphe					Phytoclast		AOM
			Spore	Pollen	Dinocyst	Other marine	Unidentified	Opaque	Translucid	
176	175.7	**P176.b**	0,0	20,9	19,8	1,2	18,6	20,4	13,4	5,8
		Total %			60,5			33,8		5,8

Extra note:

- Normal sample
- Palynomorphs are broken
- Some pyrite in palynomorphs
- Some foraminifer innerlining

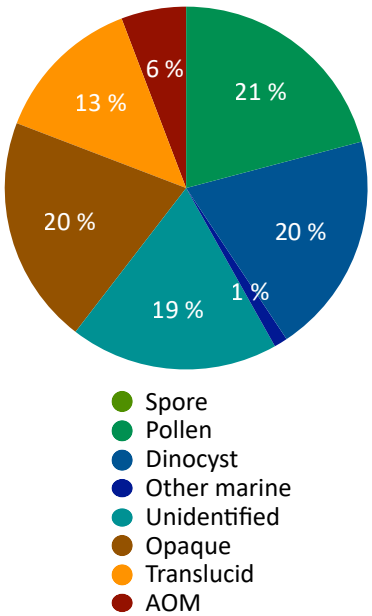


Overview



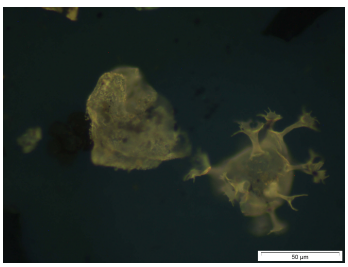
Overview (UV fluorescence)

Detailed Pi Chart

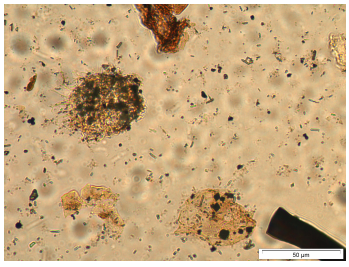




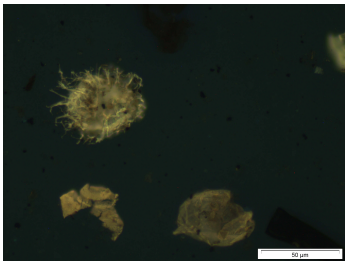
Foraminifer innerlining; chorate dinocysts



Foraminifer innerlining; chorate dinocysts (UV fluorescence)



Chorate dinocysts



Chorate dinocysts (UV fluorescence)

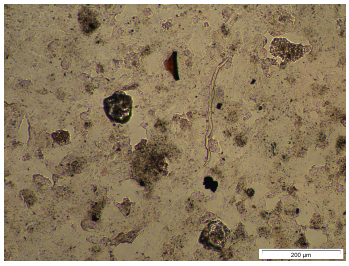
Appendix 5.46 Palynology including palynofacies analysis — P178.1

- **Height:** from the base of the sequence
- **Counts:** 250 particles were counted per sample (in %)
- **Pie Chart:** is based on each organic residue abundance

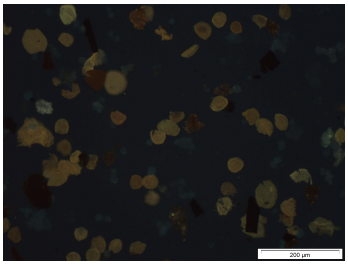
Layer n°	Height (m)	Sample code	Palynomorphe					Phytoclast		AOM
			Spore	Pollen	Dinocyst	Other marine	Unidentified	Opaque	Translucid	
178	177.2	**P178.1**	0,0	0,0	0,0	0,0	0,0	79,1	21,0	0,0
		Total %			0,0			100,1		0,0

Extra note:

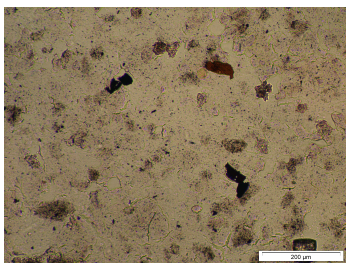
- Dirty sample



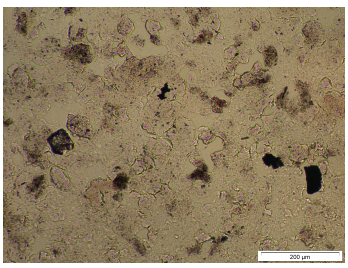
Overview



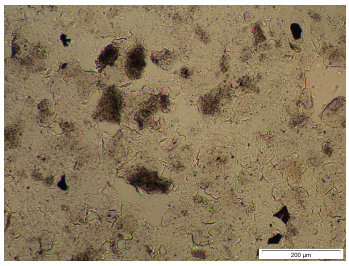
Overview



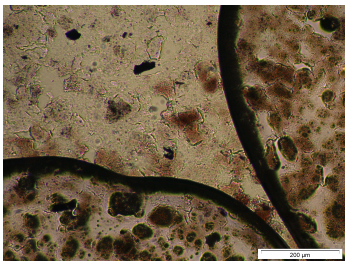
Overview



Overview

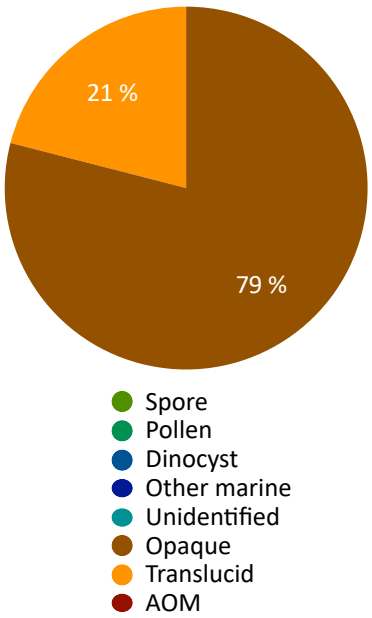


Overview



Overview

Detailed Pi Chart



Appendix 5.47 Palynology including palynofacies analysis — P181.1

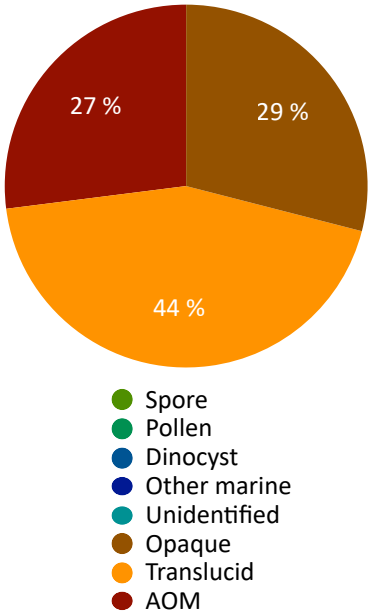
- **Height:** from the base of the sequence
- **Counts:** 250 particles were counted per sample (in %)
- **Pie Chart:** is based on each organic residue abundance

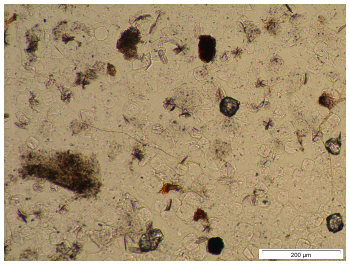
Layer n°	Height (m)	Sample code	Palynomorphe					Phytoclast		AOM
			Spore	Pollen	Dinocyst	Other marine	Unidentified	Opaque	Translucid	
181	180.9	**P181.1**	0,0	0,0	0,0	0,0	0,0	29,0	44,0	27,0
		Total %			0,0			73,0		27,0

Extra note:

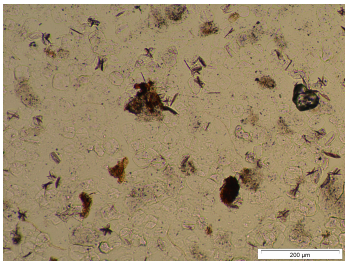
- Translucid phytoclasts are very big

Detailed Pi Chart

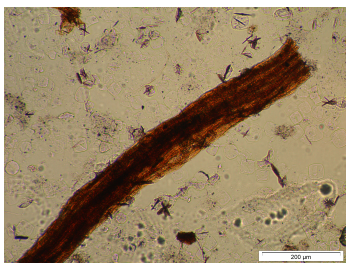




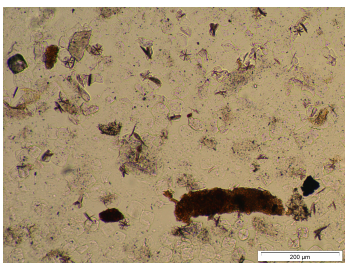
Overview



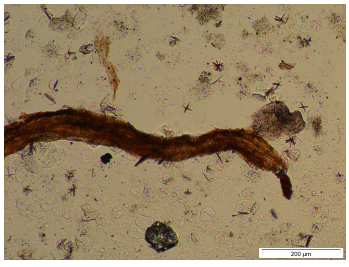
Overview



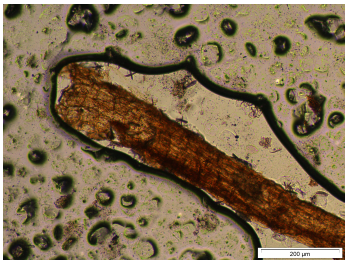
Overview; big translucid phytoclast



Overview



Overview; big translucid phytoclast



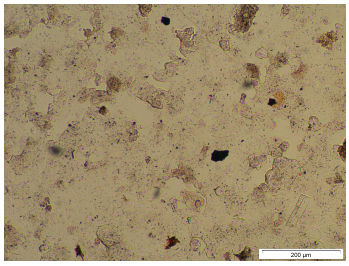
Overview; big translucid phytoclast

Appendix 5.48 Palynology including palynofacies analysis — P193.1

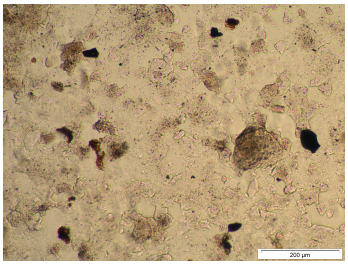
- **Height:** from the base of the sequence
- **Counts:** 250 particles were counted per sample (in %)
- **Pie Chart:** is based on each organic residue abundance

Layer n°	Height (m)	Sample code	Palynomorphe					Phytoclast		AOM
			Spore	Pollen	Dinocyst	Other marine	Unidentified	Opaque	Translucid	
193	193.5	**P193.1**	0,0	0,0	0,0	0,0	3,0	46,0	31,0	20,0
		Total %			3,0			77,0		20,0

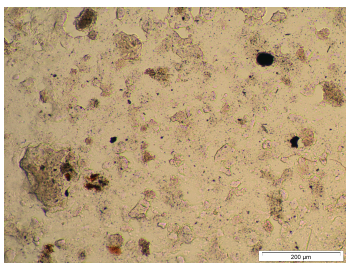
Extra note:



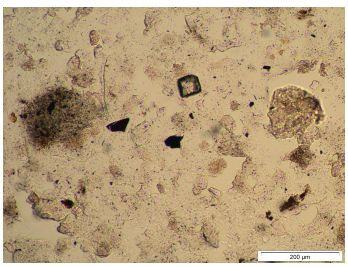
Overview



Overview

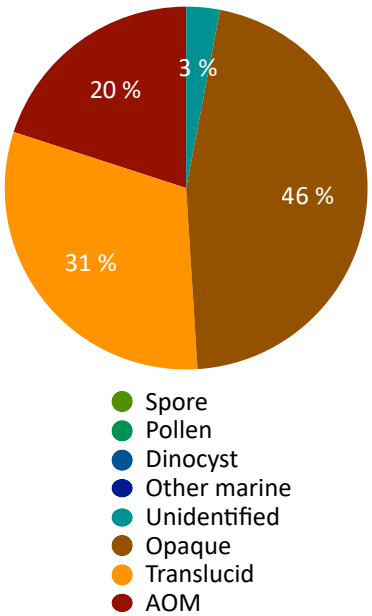


Overview



Overview

Detailed Pi Chart



Appendix 6.1 Whole-rock geochemistry results

For G1 and G2 (Arrifes stratigraphic sequence)

	Salema Formation (n=13) (Dinis et al. 2020)					**Barrancão Formation (n=4)** (Dinis et al. 2020)				
	Méd.	STD	Max.	Min.	X	Méd.	STD	Max.	Min.	X
SiO2	53,95	1,46	55,49	51,98	54,34	56,17	3,17	62,58	51,90	55,23
TiO2	1,04	0,03	1,10	0,99	1,04	1,01	0,08	1,14	0,81	1,02
Al2O3	19,04	1,61	21,73	17,40	19,20	19,30	1,92	22,60	16,08	19,29
Fe2O3(T)	6,84	1,07	9,04	5,88	6,53	6,31	1,15	8,71	3,55	6,11
MnO	0,03	0,01	0,05	0,02	0,02	0,02	0,01	0,03	0,01	0,02
MgO	2,12	0,25	2,47	1,71	2,13	1,75	0,32	2,22	0,95	1,75
CaO	0,40	0,39	1,26	0,10	0,31	0,31	0,15	0,76	0,16	0,28
Na2O	0,22	0,05	0,29	0,16	0,24	0,22	0,05	0,29	0,08	0,22
K2O	5,54	0,59	6,26	4,70	5,57	4,63	0,99	5,89	1,72	4,80
P2O5	0,04	0,01	0,06	0,04	0,04	0,04	0,02	0,08	0,02	0,04
S	0,43	0,63	1,75	0,01	0,15	1,30	1,39	3,74	0,01	1,11
LOI	9,67	1,20	11,25	8,11	9,73	9,81	1,40	12,11	7,61	10,07
Total	98,91	0,39	99,48	98,42	98,95	99,58	0,73	100,90	98,62	99,37
Sc	16,69	2,48	20,10	13,80	16,90	15,51	1,83	18,30	12,00	15,80
V	129,29	20,43	150,00	97,00	134,00	137,40	28,81	164,00	48,00	143,00
Cr	121,00	11,30	134,00	108,00	125,00	112,33	15,01	130,00	82,00	114,00
Co	15,57	3,51	20,00	11,00	15,00	13,07	5,90	30,00	5,00	12,00
Ni	41,00	7,90	57,00	33,00	39,00	38,20	8,35	60,00	26,00	37,00
Rb	226,43	30,18	268,00	194,00	212,00	192,80	38,53	241,00	87,00	198,00
Sr	54,00	9,20	66,00	37,00	56,00	48,60	9,72	62,00	20,00	50,00
Zr	186,43	27,76	240,00	162,00	179,00	202,07	52,10	304,00	156,00	181,00
Nb	17,74	1,92	21,60	15,80	17,30	16,26	0,86	17,40	14,40	16,20
Cs	8,66	0,94	10,40	7,60	8,60	8,61	1,38	10,20	5,10	8,90
Ba	312,43	70,95	386,00	193,00	342,00	302,47	75,25	394,00	79,00	312,00
Th	7,99	1,49	9,96	5,83	7,54	7,60	2,16	11,00	2,43	7,09
U	3,08	1,21	4,88	1,69	2,82	2,91	1,36	6,01	0,50	2,48
La	23,70	4,23	31,10	18,00	24,50	25,29	5,31	37,10	14,50	24,10
Ce	43,31	7,94	57,80	32,90	43,80	47,58	10,56	71,70	27,50	45,50
Pr	4,84	0,91	6,45	3,62	4,83	5,43	1,24	8,34	3,09	5,14
Nd	17,49	3,21	22,90	13,10	17,40	19,94	4,93	32,30	11,60	19,00
Sm	3,21	0,59	4,30	2,48	3,05	3,68	0,78	5,27	2,27	3,54
Eu	0,66	0,13	0,86	0,52	0,64	0,72	0,14	1,00	0,43	0,70
Gd	2,57	0,38	3,33	2,26	2,40	2,93	0,55	4,05	2,09	2,81
Tb	0,46	0,06	0,56	0,41	0,43	0,52	0,10	0,71	0,40	0,51
Dy	3,08	0,36	3,81	2,74	3,03	3,32	0,55	4,39	2,62	3,21
Ho	0,65	0,06	0,77	0,59	0,64	0,70	0,10	0,91	0,55	0,68
Er	1,98	0,20	2,37	1,79	1,92	2,18	0,31	2,82	1,76	2,14
Tm	0,31	0,03	0,37	0,28	0,30	0,33	0,04	0,41	0,27	0,33
Yb	2,14	0,25	2,64	1,90	2,04	2,29	0,28	2,83	1,91	2,21
Lu	0,34	0,04	0,42	0,30	0,32	0,36	0,04	0,45	0,32	0,34
CIA	72,78	2,87	78,39	68,88	72,33	76,47	3,63	87,57	72,81	75,92
CIX	74,91	2,44	79,75	72,83	73,91	78,27	4,05	90,96	73,83	77,78
CPA	98,13	0,32	98,51	97,64	98,07	98,15	0,39	99,35	97,67	98,09
K2O/Th*1000	7,14	1,53	9,55	5,06	6,72	7,11	4,53	22,18	1,69	6,57
NaO/Sm	690,92	87,46	852,46	594,41	674,42	614,28	171,33	938,51	352,42	637,81
α Na (Al)	22,67	3,92	27,88	17,45	21,43	24,45	11,27	64,32	17,66	21,67
α Ca (Al)	23,25	17,02	53,05	3,84	15,75	19,82	7,26	33,31	6,76	18,44
α Sr (Al)	8,28	1,23	10,83	6,89	8,10	9,74	3,75	23,12	7,41	8,89
α Mg (Al)	1,33	0,26	1,84	1,04	1,30	1,67	0,46	3,07	1,26	1,57
α K (Al)	0,77	0,12	1,03	0,69	0,71	1,00	0,45	2,59	0,73	0,90
α Ba (Al)	2,30	0,48	3,27	1,85	2,12	2,68	1,82	9,21	1,88	2,15
α Rb (Al)	0,63	0,11	0,83	0,52	0,63	0,78	0,27	1,70	0,60	0,69
α Cs (Al)	0,54	0,06	0,62	0,46	0,55	0,56	0,12	0,96	0,47	0,53
α Na*	12,67	1,50	14,54	10,14	12,82	15,25	4,69	24,53	9,21	13,55
α K *	1,56	0,36	2,15	1,11	1,54	2,05	0,97	5,26	0,85	1,90
SiO2/Al2O3	2,85	0,30	3,19	2,39	2,83	2,95	0,46	3,86	2,33	2,89
K2O/Al2O3	0,29	0,04	0,32	0,22	0,31	0,24	0,05	0,31	0,09	0,25
K2O/Na2O	25,88	5,71	33,94	18,08	23,92	21,21	2,52	24,57	14,90	21,33
TiO2/Al2O3	0,06	0,00	0,06	0,05	0,06	0,05	0,01	0,07	0,04	0,05
Zr/Al2O3	9,92	2,15	13,69	7,69	8,94	10,78	3,87	18,35	7,17	9,57
Fe/Ti	7,64	1,11	10,03	6,80	7,31	7,26	1,38	10,62	5,09	7,03
K/Cs	5329,72	479,91	5930,85	4536,59	5257,30	4449,26	714,65	5649,29	2799,55	4386,51
Rb/K	0,00	0,00	0,01	0,00	0,00	0,01	0,00	0,01	0,00	0,01
Rb/Cs	26,15	1,85	28,11	22,56	26,32	22,30	2,48	26,63	17,06	22,35
Zr/Sc	11,54	3,17	16,78	8,27	10,59	13,34	4,44	24,58	9,14	11,83
Ti/Zr	34,24	5,39	40,52	24,68	34,56	31,62	6,69	39,16	18,82	33,48
Th/U	3,00	1,51	5,89	1,92	2,15	3,13	1,46	6,80	1,18	2,85
Th/Sc	0,49	0,12	0,68	0,34	0,50	0,49	0,14	0,68	0,15	0,51
Cr/Th	15,65	3,57	21,44	11,05	15,06	17,24	10,77	53,50	8,04	16,08
∑REE	104,73	18,16	137,68	81,19	105,00	115,28	24,57	171,79	70,75	110,12
∑LREE	92,55	16,82	122,55	70,10	93,98	101,91	22,73	154,71	58,96	97,09
∑HREE	11,52	1,36	14,27	10,38	10,95	12,65	1,90	16,48	10,37	12,24
∑REE/Al2O3	5,49	0,77	6,97	4,67	5,38	6,12	1,89	10,58	3,53	5,67

Appendix 6.2 Whole-rock geochemistry results

For Salema and Barrancão Formations (Dinis et al., 2020)

	Salema Formation (n=13) (Dinis et al. 2020)					Barrancão Formation (n=4) (Dinis et al. 2020)				
	Méd.	STD	Max.	Min.	X	Méd.	STD	Max.	Min.	X
SiO2	51,32	8,45	57,46	24,32	54,07	62,57	1,48	64,52	61,09	62,33
TiO2	0,89	0,15	1,01	0,42	0,92	1,25	0,08	1,33	1,16	1,26
Al2O3	18,78	3,10	21,64	9,39	19,41	15,41	1,18	16,46	13,74	15,72
Fe2O3(T)	6,39	1,25	7,61	3,08	6,76	6,43	1,35	7,90	5,19	6,32
MnO	0,02	0,01	0,04	0,01	0,02	0,01	0,00	0,01	0,01	0,01
MgO	2,78	0,81	5,19	2,02	2,73	1,48	0,15	1,62	1,27	1,52
CaO	2,97	6,97	25,70	0,33	0,47	1,16	1,54	3,47	0,35	0,40
Na2O	0,22	0,02	0,25	0,17	0,22	0,15	0,03	0,17	0,11	0,16
K2O	5,19	0,91	6,09	2,61	5,30	4,30	0,48	4,80	3,64	4,38
P2O5	0,05	0,02	0,11	0,03	0,04	0,02	0,01	0,02	0,01	0,02
S										
LOI	11,20	5,63	28,90	8,50	9,10	7,03	0,79	8,20	6,50	6,70
Total	99,83	0,01	99,84	99,79	99,83	99,85	0,01	99,86	99,84	99,85
Sc	15,31	2,29	17,00	9,00	16,00	13,3	1,7	15,0	11,0	13,5
V	142,46	25,34	173,00	75,00	150,00	102,3	21,3	130,0	85,0	97,0
Cr	112,10	21,55	136,84	47,89	116,31	83,8	17,1	102,6	61,6	85,5
Co										
Ni	38,92	7,51	55,00	24,00	39,00	35,3	9,5	48,0	25,0	34,0
Rb	212,87	37,10	252,60	114,50	217,30	179,2	14,8	199,3	164,8	176,4
Sr	76,34	31,71	176,80	60,00	66,00	52,7	7,5	62,5	44,5	51,8
Zr	166,67	36,71	232,70	67,40	166,60	296,9	23,7	328,7	271,4	293,7
Nb										
Cs	10,23	2,18	13,40	4,40	10,70	7,5	0,2	7,7	7,3	7,5
Ba	358,15	73,02	497,00	176,00	359,00	249,0	25,9	278,0	217,0	250,5
Th	7,85	1,75	10,20	4,40	8,30	12,3	0,8	13,2	11,3	12,3
U	3,98	1,26	6,70	2,30	3,70	2,3	0,2	2,5	2,1	2,3
La	23,88	3,77	30,20	15,00	23,90	35,5	4,5	41,5	30,8	34,9
Ce	43,76	6,58	51,90	28,40	44,50	71,0	8,2	81,8	62,3	70,0
Pr	4,84	0,71	5,76	3,07	4,93	7,5	1,0	8,7	6,4	7,5
Nd	18,10	2,81	21,50	11,00	18,30	27,0	3,1	31,0	23,4	26,8
Sm	3,17	0,47	3,76	2,03	3,26	5,1	0,7	6,2	4,4	5,0
Eu	0,63	0,10	0,79	0,46	0,63	1,1	0,1	1,2	0,9	1,1
Gd	2,79	0,36	3,39	2,13	2,70	4,6	0,5	5,1	3,9	4,7
Tb	0,43	0,05	0,53	0,35	0,43	0,8	0,1	0,9	0,7	0,8
Dy	2,64	0,36	3,09	1,93	2,60	5,0	0,6	5,6	4,1	5,1
Ho	0,58	0,09	0,68	0,37	0,58	1,1	0,1	1,2	1,0	1,1
Er	1,89	0,34	2,43	1,09	1,92	3,3	0,4	3,7	2,7	3,4
Tm	0,29	0,05	0,38	0,16	0,28	0,5	0,1	0,5	0,4	0,5
Yb	1,88	0,32	2,34	1,03	1,96	3,2	0,2	3,5	3,0	3,2
Lu	0,29	0,05	0,35	0,16	0,30	0,5	0,1	0,5	0,4	0,5
CIA	66,54	16,27	76,31	15,86	71,87	69,11	8,19	73,53	56,84	73,03
CIX	75,78	1,79	78,14	72,89	75,91	75,94	0,73	76,92	75,15	75,84
CPA	98,05	0,30	98,41	97,11	98,12	98,46	0,20	98,70	98,23	98,45
K2O/Th*1000	6,73	1,00	9,32	5,64	6,49	3,51	0,39	3,81	2,94	3,65
NaO/Sm	710,03	81,25	837,44	584,96	674,85	292,18	75,23	383,75	220,44	282,26
α Na (Al)	21,55	2,58	26,03	14,16	22,04	27,27	3,72	32,03	23,39	26,83
α Ca (Al)	10,01	6,04	18,12	0,10	11,15	8,94	5,26	12,24	1,09	11,21
α Sr (Al)	6,36	1,93	8,19	1,22	6,87	6,88	1,29	8,03	5,06	7,21
α Mg (Al)	1,07	0,34	1,51	0,26	1,03	1,52	0,09	1,57	1,39	1,55
α K (Al)	0,81	0,08	0,92	0,68	0,81	0,80	0,03	0,84	0,76	0,80
α Ba (Al)	1,92	0,19	2,18	1,39	1,96	2,26	0,23	2,59	2,06	2,19
α Rb (Al)	0,65	0,06	0,77	0,57	0,65	0,63	0,03	0,66	0,61	0,63
α Cs (Al)	0,45	0,05	0,52	0,37	0,46	0,50	0,03	0,52	0,46	0,51
α Na*	12,32	1,37	14,78	10,32	12,81	31,07	7,73	39,21	22,53	31,26
α K *	1,57	0,21	2,01	1,22	1,51	1,59	0,13	1,79	1,49	1,54
SiO2/Al2O3	2,74	0,21	3,27	2,50	2,70	4,08	0,38	4,57	3,71	4,02
K2O/Al2O3	0,28	0,03	0,33	0,24	0,28	0,28	0,01	0,29	0,26	0,28
K2O/Na2O	23,26	3,27	27,68	15,35	23,42	29,55	3,62	33,09	25,35	29,88
TiO2/Al2O3	0,05	0,00	0,06	0,04	0,05	0,08	0,01	0,10	0,07	0,08
Zr/Al2O3	8,87	1,57	13,23	7,16	8,59	19,44	3,11	23,92	17,04	18,39
Fe/Ti	8,40	1,01	10,06	6,66	8,48	6,04	1,46	7,95	4,62	5,79
K/Cs	4311,30	733,58	5650,34	3278,19	4361,80	4765,69	442,21	5174,65	4139,13	4874,48
Rb/K	0,00	0,00	0,01	0,00	0,01	0,01	0,00	0,01	0,00	0,00
Rb/Cs	21,24	2,98	26,02	16,82	21,66	23,95	1,42	25,88	22,58	23,67
Zr/Sc	10,83	1,87	15,51	7,49	10,81	22,86	4,94	29,88	19,39	21,09
Ti/Zr	32,53	3,21	37,36	25,25	32,94	25,30	1,56	27,35	23,89	24,97
Th/U	2,16	0,86	4,09	0,90	1,98	5,42	0,61	6,29	4,96	5,21
Th/Sc	0,51	0,07	0,64	0,38	0,49	0,94	0,13	1,13	0,86	0,87
Cr/Th	14,65	3,44	21,89	10,89	14,32	6,81	1,16	8,28	5,45	6,76
∑REE	105,19	15,34	125,45	67,18	106,22	166,17	19,11	190,90	144,40	164,68
∑LREE	93,76	14,01	112,02	59,50	95,12	146,18	17,43	169,24	127,31	144,08
∑HREE	10,80	1,49	12,66	7,22	10,50	18,93	2,05	20,54	16,22	19,47
∑REE/Al2O3	5,68	0,73	7,15	4,34	5,58	10,80	1,17	11,86	9,31	11,02

Appendix 6.3 Whole-rock geochemistry results

For Burgau and Luz Formations (Dinis et al., 2020)

	Burgau Formation (n=3) (Dinis et al. 2020)					Luz Formation (n=16) (Dinis et al. 2020)				
	Méd.	STD	Max.	Min.	X	Méd.	STD	Max.	Min.	X
SiO2	66,87	7,01	74,93	62,20	63,48	47,52	11,87	69,27	30,89	45,04
TiO2	0,90	0,14	1,00	0,74	0,95	0,85	0,19	1,10	0,60	0,81
Al2O3	11,72	1,16	12,72	10,45	11,98	15,19	2,50	19,36	10,73	14,82
Fe2O3(T)	3,60	1,08	4,80	2,70	3,29	6,10	1,39	9,87	3,66	5,81
MnO	0,03	0,00	0,03	0,03	0,03	0,05	0,03	0,10	0,01	0,06
MgO	2,36	1,38	3,61	0,88	2,59	1,43	0,25	1,79	1,06	1,45
CaO	3,29	3,02	6,17	0,14	3,55	10,15	8,68	23,18	0,15	11,25
Na2O	0,12	0,01	0,13	0,11	0,11	0,18	0,03	0,23	0,13	0,18
K2O	2,31	0,13	2,46	2,21	2,25	3,78	0,77	4,95	2,23	3,65
P2O5	0,08	0,03	0,12	0,06	0,06	0,02	0,02	0,07	0,01	0,02
S										
LOI	8,57	3,30	11,50	5,00	9,20	14,58	5,62	23,20	6,20	15,50
Total	99,87	0,02	99,88	99,85	99,88	99,86	0,02	99,88	99,83	99,86
Sc	9,7	0,6	10,0	9,0	10,0	14,4	2,4	20,0	11,0	14,0
V	80,7	7,1	87,0	73,0	82,0	92,1	21,2	157,0	65,0	86,0
Cr	143,7	49,3	184,7	88,9	157,4	86,8	19,1	130,0	54,7	85,5
Co										
Ni	46,3	20,1	65,0	25,0	49,0	34,3	7,8	52,0	23,0	34,5
Rb	86,2	3,4	89,4	82,7	86,6	163,4	29,4	203,8	99,0	167,8
Sr	56,8	13,5	65,8	41,2	63,3	161,1	103,9	429,3	49,6	161,9
Zr	260,5	79,9	334,0	175,5	271,9	174,4	63,0	296,7	92,9	162,4
Nb										
Cs	3,6	0,3	3,9	3,4	3,6	7,1	0,9	8,7	5,8	7,0
Ba	168,3	15,5	184,0	153,0	168,0	270,9	83,5	492,0	174,0	260,5
Th	9,2	0,5	9,5	8,6	9,5	9,0	1,8	11,6	6,2	8,9
U	2,5	0,8	3,4	1,9	2,3	1,7	0,4	2,3	1,1	1,7
La	32,2	3,6	35,5	28,4	32,7	27,9	5,8	41,2	19,8	26,8
Ce	66,6	8,3	72,9	57,2	69,7	54,5	13,4	93,4	41,0	51,1
Pr	7,4	0,9	8,0	6,4	7,9	6,0	1,4	9,4	4,4	5,6
Nd	28,4	4,0	31,7	24,0	29,4	23,3	5,2	33,9	15,8	22,2
Sm	5,6	0,7	6,1	4,7	5,9	4,3	1,0	5,9	2,8	4,0
Eu	1,2	0,1	1,3	1,1	1,3	0,9	0,2	1,3	0,6	0,9
Gd	5,1	0,5	5,5	4,5	5,2	4,1	1,0	5,9	2,6	3,9
Tb	0,8	0,1	0,8	0,7	0,8	0,7	0,1	1,0	0,5	0,7
Dy	4,6	0,5	5,1	4,1	4,8	4,1	0,8	5,4	2,8	4,0
Ho	0,9	0,1	1,0	0,8	1,0	0,9	0,2	1,2	0,6	0,8
Er	2,7	0,3	2,9	2,4	2,9	2,7	0,7	3,9	1,7	2,7
Tm	0,4	0,0	0,4	0,4	0,4	0,4	0,1	0,6	0,3	0,4
Yb	2,7	0,3	2,9	2,3	2,8	2,7	0,7	3,8	1,8	2,5
Lu	0,4	0,1	0,4	0,3	0,4	0,4	0,1	0,6	0,3	0,4
CIA	60,28	18,25	79,45	43,11	58,28	47,63	23,52	81,07	19,31	37,79
CIX	81,27	1,32	82,76	80,24	80,81	77,54	2,69	83,76	73,90	76,87
CPA	98,39	0,11	98,51	98,30	98,35	98,02	0,44	98,82	97,24	98,02
K2O/Th*1000	2,99	0,97	3,81	0,39	3,22	4,36	1,29	7,48	2,59	4,23
NaO/Sm	254,66	86,34	383,75	75,23	237,49	435,24	99,79	719,42	304,57	417,49
α Na (Al)	25,79	1,88	27,92	24,36	25,09	22,01	5,38	35,23	14,85	20,89
α Ca (Al)	8,37	13,23	23,64	0,47	0,99	5,55	9,20	33,89	0,13	0,38
α Sr (Al)	4,99	1,52	6,70	3,80	4,45	3,40	2,41	6,93	0,75	2,24
α Mg (Al)	1,04	0,83	1,98	0,42	0,71	1,58	0,36	2,38	1,14	1,49
α K (Al)						0,91	0,16	1,32	0,72	0,86
α Ba (Al)	2,52	0,06	2,59	2,48	2,51	2,12	0,39	2,96	1,32	2,14
α Rb (Al)	1,00	0,08	1,08	0,93	0,99	0,69	0,10	0,92	0,59	0,66
α Cs (Al)						0,53	0,08	0,67	0,41	0,54
α Na*	41,44	5,73	47,94	37,09	39,30	20,72	4,18	28,38	12,02	20,71
α K *	2,30	0,19	2,44	2,09	2,37	1,88	0,50	2,61	1,01	1,92
SiO2/Al2O3	5,73	0,66	6,25	4,99	5,95	3,57	1,37	5,95	2,47	3,00
K2O/Al2O3	0,20	0,02	0,21	0,18	0,21	0,25	0,04	0,31	0,17	0,26
K2O/Na2O	19,92	2,53	22,36	17,31	20,09	21,55	3,25	27,50	16,00	20,82
TiO2/Al2O3	0,08	0,01	0,08	0,07	0,07	0,06	0,01	0,08	0,05	0,06
Zr/Al2O3	22,02	5,57	27,88	16,79	21,38	11,95	4,75	22,91	7,33	10,45
Fe/Ti	4,66	1,09	5,89	3,84	4,26	8,58	2,01	11,51	5,86	8,53
K/Cs	5296,98	632,92	6006,02	4789,04	5095,89	4443,70	763,28	5593,60	2938,29	4458,64
Rb/K	0,00	0,00	0,00	0,00	0,00	0,01	0,00	0,01	0,00	0,01
Rb/Cs	23,82	2,17	26,29	22,21	22,97	23,09	3,15	27,89	15,71	23,05
Zr/Sc	27,28	9,78	37,11	17,55	27,19	12,33	4,80	24,73	7,15	11,29
Ti/Zr	21,39	3,68	25,28	17,95	20,95	30,96	5,93	38,72	21,22	31,35
Th/U	3,89	1,25	5,00	2,53	4,13	5,60	1,13	7,09	2,82	5,41
Th/Sc	0,96	0,10	1,06	0,86	0,95	0,63	0,11	0,88	0,44	0,65
Cr/Th	15,70	5,52	19,45	9,36	18,30	9,99	3,38	20,97	6,49	9,59
∑REE	159,00	18,88	171,66	137,30	168,04	133,01	28,09	205,18	104,82	124,07
∑LREE	140,16	16,96	151,65	120,68	148,15	116,01	26,25	183,78	85,41	109,27
∑HREE	17,62	1,81	18,76	15,54	18,57	16,09	3,12	21,02	11,51	15,76
∑REE/Al2O3	13,55	0,45	14,03	13,14	13,50	8,98	2,34	13,66	5,61	8,77